Identification and functional characterization of nuclear receptors with roles in the reproductive development and approaches to establish genome editing in *Schistosoma mansoni*

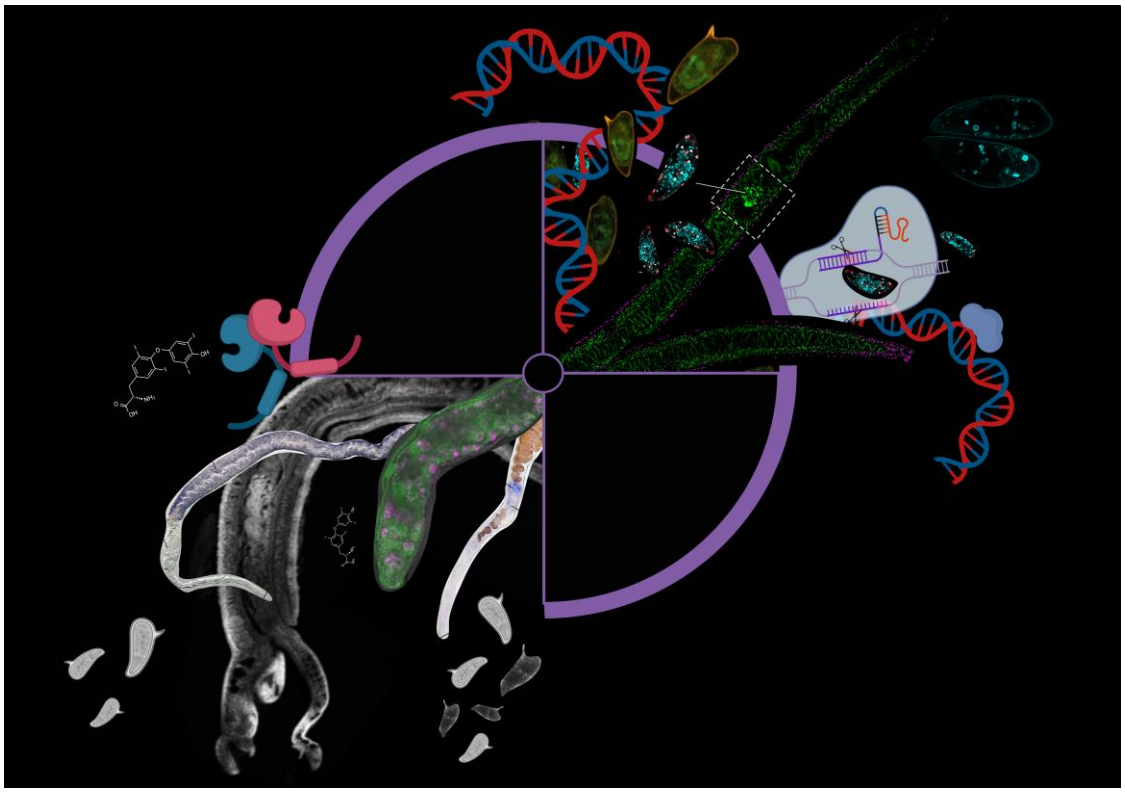

Inaugural-Dissertation

zur Erlangung des Doktorgrades der Naturwissenschaften

(Dr. rer. nat.)

im Fachbereich Biologie und Chemie der

Justus-Liebig-Universität Gießen

Max Frederik Möscheid

August 2024

The present work was carried out at the Institute of Parasitology (Faculty 10), Justus Liebig University Giessen between May 2020 and August 2024 under the supervision of Prof. Dr. Annette Becker and Prof. Dr. Christoph G. Grevelding.

First supervisor: **Prof. Dr. Annette Becker**

Institute of Botany, Developmental biology of plants, Justus Liebig University Giessen, Heinrich-Buff-Ring 38, 35392 Giessen, Germany.

Second supervisor: **Prof. Dr. Christoph G. Grevelding**

Institute of Parasitology, BFS, Justus Liebig University Giessen, Schubertstraße 81, 35392 Giessen, Germany.

„Hör auf dein Bauchgefühl und lasse dich von keinem Zweifel oder Zweifler zurückhalten”

-

Jens Voigt

Danksagung

Es gibt so viele, denen ich danken möchte, sodass ein Anfang schwer ist…
In den vergangenen Jahren haben mich viele Menschen wie Kollegen, Projektpartner, Studenten, Freunde und Familie begleitet, ohne die die Erstellung dieser Thesis nicht möglich gewesen wäre. Daher möchte ich mich zunächst bei all jenen bedanken, die mich in den letzten Jahren unterstützt haben, sei es nur für einen bestimmten Zeitraum oder die ganze Zeit über.

An erster Stelle möchte ich mich bei Herrn Prof. Dr. Christoph Grevelding bedanken, der mich als mein Doktorvater betreute und dessen Tür immer offenstand, um jegliche Probleme zu besprechen. Für sein persönliches Engagement, mit mir zusammen eine Doktorandenstelle zu schaffen und sein Vertrauen, mir dieses Projekt anzuvertrauen, möchte ich mich sehr herzlich bedanken. Ich bedanke mich auch für die Möglichkeiten, neben internationalen Konferenzen auch internationale Laborerfahrung sammeln zu können, die mir geholfen haben, mich sowohl wissenschaftlich als auch persönlich weiterzuentwickeln.

Vielen Dank an Frau Prof. Dr. Annette Becker für die Übernahme der Rolle als Betreuerin und der Prüfung dieser Arbeit. Weiterführend möchte ich Prof. Dr. Kai Thormann und Prof. Dr. Ivan Manzini für ihre Bereitschaft meiner Prüfung als Prüfer beizusitzen, bedanken.

Vielen Dank an Dr. Thomas Quack und Dr. Oliver Weth, welche mich zum einen während der Thesis, zum anderen während eines Praktikums betreuten und erst meine Faszination für die Parasitologie und die Schistosomen erweckten. Beiden möchte ich insbesondere für ihre große Leidenschaft für Wissenschaft und ihre Fähigkeit diese Leidenschaft an die nächste Generation zu vermitteln bedanken. Insbesondere danke ich Thomas, welcher als wandelnde Labor-Enzyklopädie für so ziemlich jedes Problem eine Lösung parat hatte und sich auch nicht zu schade war, jedes noch so kleine Stellschräubchen zu justieren.

Bezüglich der internationalen Laborerfahrung möchte ich mich besonders bei Prof. Paul Brindley, Victoria Mann und Wannaporn Ittiprasert Tanno für die herzliche Einladung in das Labor an der George Washington University, die viele Unterstützung und die gute wissenschaftliche und freundschaftliche Atmosphäre bedanken. Außerdem möchte ich mich bei Kota, Bell, Jom, Robin und Nahom bedanken, die mir mit Rat und Tat zur Seite standen und meinen Aufenthalt, auch in der Freizeit, zu einem unvergesslichen Erlebnis machten.

Ein sehr großer Dank gebührt Oliver Puckelwaldt, für seine Bereitschaft sich als zweites Hirn mit mir über so ziemlich jedes Problem auseinander zu setzen, kritisch Ergebnisse zu hinterfragen und den stetigen (verbalen) Tritt, wieder aufzustehen und weiterzumachen, wenn die Etablierung neuer Methoden widerspenstiger verlief, als gedacht. Oli, vielen Dank, dass ich *live* mitverfolgen durfte, wie sich aus Blumen- und Wal-artigen UMAP-Plots ein *single cell*

Atlas zusammenbaute, du Paper aus den Tiefen PubMeds ausgegraben hast, die sonst für immer dageblieben wären und dass du dir, wie auch immer, jedes Marker-Gen, was jemals in einer *in situ* untersucht wurde, gemerkt hast.

Vielen Dank an Dr. Pia Naujack für Ihre fachliche Unterstützung, ihre stetige Hilfsbereitschaft und vor allem für das zusammenschweißen unseres „Jahrgangs“.

Weiter möchte ich Dr. Simone Häberlein für Ihre Unterstützung bei diversen Problemen, besonders am CLSM und für die Unterstützung im Retinsäure-Projekt bedanken. Vielen Dank auch an Theresa Huber und Pauline Holzäpfel, die ich im Rahmen ihrer Abschlussarbeiten betreuen durfte, für ihr großes Engagement bei der Bearbeitung der jeweiligen Projekte, so dass mir die Betreuung sehr viel Spaß gemacht hat und alles andere als Arbeit war.

Ganz besonders möchte ich mich bei allen Mitgliedern des Institutes für eine unvergessliche Zeit bedanken. Insbesondere bedanke ich mich bei Oli, Xuesong, Sophie, Svenja, Monique, Sagar, Rashmi, Lisa, Gabo, Jonas und Martin, für ihre fachliche und freundschaftliche Unterstützung. Des Weiteren bedanke ich mich bei Tobi für sein stetiges Hilfsangebot, mich zu unterstützen, insbesondere bei der Infektion. Auch geht ein großer Dank an Tina, Bianca und Georgette. Ein weiterer großer Dank geht darüber hinaus an Anne Rognon, die mir die Transplantation von Sporocysten beibrachte und mir damit erheblich bei der Umsetzung der finalen Schritte des CRISPR/Cas Projektes geholfen hat.

Des Weiteren bedanke ich mich beim Graduiertenstipendium der Justus-Liebig-Universität Giessen und FUGI für die Förderung dieses Projekts. Darüber hinaus möchte ich mich auch bei der DGP für die Unterstützung im Zuge eines Reisestipendiums bedanken.

Vielen, vielen Dank an meine Freunde und Familie, die mir immer den Rücken gestärkt haben und nicht müde wurden, motivierende Worte zu finden. Ein besonderer Dank gilt meinen Eltern, die mich immer bedingungslos unterstützt haben.

Sabrina, vielen lieben Dank, dass du diesen Weg mit mir zusammengegangen bist, dass du nie müde wurdest, mit mir über mein Projekt, Probleme und Herausforderungen zu diskutieren und dass ich immer auf deinen Rat zählen kann. Vielen Dank für deine Unterstützung und dass du mit mir zusammen sowohl die Hochs als auch Tiefs während meiner Doktorarbeit durchgestanden hast.

List of abbreviations

Abbreviations	Full name
aa	Amino acid
ABAM	Antibiotic-antimycotic
ABC	Ascorbic acid / red blood cells/ cholersterol
AmpR	*E. coli* ampicillin resistance
BATT	β- alanyl-tryptamine
BLAST	Basic local alignment search tool
BMPG	Bone marrow protein glycan
bF	Female worms from couples obtained from mixed-sex infections
bM	Male worms from couples obtained from mixed-sex infections
bO	Ovaries isolated from bF
bp	Base pairs
bT	Testes isolated from bM
Cas	CRISPR-associated protein
CBSS	Chernins´ balanced salt solution
cDNA	Complementary DNA
CLSM	Confocal laser scanning microscopy
crRNA	CRISPR-RNA
CRISPR	Clustered regularly interspaced short palindromic repeats
d	Day
DARNT	*Drosophila melanogaster* aryl hydrocarbon receptor nuclear translocator
DBD	DNA binding domain
ddH2O	Double distilled water
DEPC	Diethylpyrocarbonate
dH2O	Distilled water
DIG	Digoxygenin
DIG-AP	Digoxigenin-alkaline phosphatase
DIG-dUTP	Digoxygenin-uridinetriphosphate
DNA	Desoxyribonucleic acid
DSB	Double-strand breaks
dsDNA	Double-stranded DNA
dsRED	*Discosoma spp.* red fluorescent protein
dsRNA	Double-stranded RNA
EdU	5-ethynyl-2'-deoxyuridine
eGFP	Enhanced green fluorescent protein
EPO	Electroporation
EtOH	Ethanol
FGFR	Fibroblast growth factor receptor

Abbreviations	Full name
FISH	Fluorescence *in situ* hybridization
FTZ	Fushi Tarazu protein
gDNA	Genomic DNA
GLI	Bifunctional glioma-associated oncogene transcription factor
GPCR	G-protein coupled receptor
gRNA	Guide RNA
GOI	Gene of interest
HA	Homology arms
HAT	Histone acetyl transferase
HEPES	2-4-(2-hydroxyethyl)-1-piperazinyl ethane sulfonic acid
HDAC	Histone deacetylase
HDR	Homology directed repair
Hoechst 33342	2'-[4-ethoxyphenyl]-5-[4-methyl-1-piperazinyl]-2,5'-bi-1H-benzimidazole trihydrochloride trihydrate
hs	Head sucker
HSP	Heat shock protein
InDel	Insertion/Deletion
iO	Immature ovary
iOo	Immature oocytes (oogonia)
KI	Knock-in
KD	Knock-down
KO	Knock-out
LBD	Ligand binding domain
Letm1	Leucine zipper-EF-hand-containing transmembrane protein 1
LDL	Low density lipoprotein
lssDNA	Long single stranded DNA
M199egg	*S. mansoni* egg-specific medium based on M199
M199sporo	*S. mansoni* sporocyst-specific medium based on M199
MEIOB	Meiosis-specific OB-domain containing protein
MEM	Minimal essential medium
MeOH	Methanol
min	Minute
mO	Mature ovary
mOo	Mature oocytes (primary oocytes)
mRNA	Messenger ribonucleic acid
NCoR	Nuclear receptor co-repressor
NGS	Next generation sequencing
NHEJ	Non-homologous directed repair
NR	Nuclear receptor
NCS	Newborn cattle serum

Abbreviations	Full name
ov	Ovary
PB	Particle bombardment
PBS	Phosphate-buffered saline
PBSTx	PBS/Triton X-100
PCR	Polymerase chain reaction
PEG10	Polyethylene glycol (10) ester
Phyre	Protein homology/ analogy recognition engine
p.i.	Post infection
PZQ	Praziquantel
RA	Retinoic acid
RAR	Retinoic acid receptor
RARE	Retinoic acid-response element
RT-qPCR	Quantitative real-time polymerase chain reaction
RNA	Ribonucleic acid
RNAi	RNA interference
RNA-Seq	RNA sequencing
RPA	Replication protein A
RT	Room temperature
RXR	Retinoid-X-receptor
scRNA-Seq	Single cell RNA sequencing
sF	Females obtained from single-sex infections
siRNA	Small interfering RNA
sM	Male worms obtained from single-sex infections
Smp_	*Schistosoma mansoni* protein (_number)
sO	Ovaries isolated from sF
sT	Testes isolated from sM
Stra	Steroidogenic acute regulatory protein
SMART	Simple Modular Architecture Research Tool
Suppl. Fig.	Supplemental Figure
T_3	Trijodthyronin
T_4	Thyroxin
TF	Transcription factor
TH	Thyroid hormone
THR	Thyroid hormone receptor
TIDE	Tracking of indels by decomposition
TGFβ	Transforming growth factor β
TNT	Tris/NaCl/Tween
Tricaine	Ethyl 3-aminobenzoate methanesulfonate
Tris	Tris(hydroxymethyl)aminomethane

Abbreviations	Full name
$TRPM_{PZQ}$	*S. mansoni* transient receptor potential melastatin channel
TSS	Transcription start site
Tyr2	Tyrosinase 2
UTR	Untranslated region
vit	Vitellarium
VF1	Vitellogenic factor 1
vs	Ventral sucker
Vtg	Vitellogenin
VtgR	Vitellogenin receptor
WHO	World-Health Organization
WISH	Whole mount *in situ* hybridization
Wnt	Wingless and Int-1

Abstract

Schistosoma mansoni is a parasite of humans and animals and causes the infectious disease schistosomiasis. Schistosomes are the only trematodes to have evolved separate sexes. Furthermore, females reach sexual maturity only if they are permanently paired with a male. Previous comparative transcriptomics studies of adult schistosomes and their isolated gonads have revealed that genes encoding type II nuclear receptors (NRs) are regulated in a pairing-dependent and tissue-specific manner with a preference for the female ovary. Members of the nuclear receptor superfamily are ligand-activated transcription factors that play diverse roles in cell differentiation, development, and proliferation. In vertebrate systems, type II NRs, such as retinoic acid receptors (RAR/RXR) and thyroid hormone receptors (THR) have been reported to be involved in spermatogenesis, embryogenesis, and tissue homeostasis.

In the course of this work, potential *S. mansoni* NRs orthologs were identified and assigned to different NR classes as RAR (Smp_144170, SmRAR), RXR (Smp_097700, SmRXR-1), THRα (Smp_134490, SmTHRα), and THRβ (Smp_174260, SmTHRβ) based on polygenetic and comparative domain analyses. In addition, whole mount *in situ* hybridization (WISH) and functional analyses using RNA interference (RNAi) were performed to characterize these previously uncharacterized *S. mansoni* NR orthologs. Using WISH, transcripts of these receptors were found in the posterior part of the ovary. In addition, transcripts of these receptors dominated in oocytes at the intermediate stage of development, which was recently discovered by a new scRNA-Seq atlas of isolated ovaries of paired females, work performed by Zhigang Lu, a former member of the Grevelding lab. In my work, functional analyses provided first evidence for the involvement of these receptors in early embryogenesis and tissue homeostasis in adult schistosomes. Morphological analyses following RNAi revealed changes in the cellular structure of the ovary of paired females. In particular, RNAi against SmRAR and SmRXR-1 as well as biologically associated molecules, such as SmMEIOB and SmGLI1, strongly suggested essential roles of these genes in oocyte maturation and meiotic progression. These results as well as subsequent analyses of the influence of 9cis-retinoic acid on egg production suggest a critical role for RA signaling in the reproductive biology of *S. mansoni*.

The second aim of this project was to establish a CRISPR/Cas-based editing method for *S. mansoni*. Knock-out models are commonly used to study the function of a gene of interest (GOI). However, in the post-genomic era of schistosome research, there is no established protocol for stable transformation of this and other platyhelminth parasites. To date, RNAi has been the most appropriate method for functional gene characterization. Though, RNAi efficiency is variable and can lead to ectopic effects. CRISPR/Cas-based editing is a powerful tool for gene characterization. To make this technique accessible for trematode research, a

protocol was established to edit a genomic safe harbor (GSH) site of *S. mansoni*, which was bioinformatically predicted before by our collaboration partner Professor Christoph Grunau (Perpignan) and named GSH1. GSHs represent distinct sites in the genome that tolerate the integration of new genetic material without compromising genome integrity or gene expression. Thus, GSHs should allow the constitutive expression of reporter-genes. In order to edit the identified candidate GSH1, a 5'C6-PEG10 modified construct encoding an eGFP reporter-gene under a strong native *S. mansoni* promoter was used as a donor repair template. Cas-mediated integration of the transgene was achieved by electroporation of eggs. To this end, Cas9 and Cas12a were used in a comparative approach. Sequence analyses post editing showed differences in the reporter gene-integration efficiencies between the two enzymes with a bias for Cas12a. Nonetheless, integration of the reporter-gene into GSH1 was demonstrated by PCR for both ribonucleoprotein complexes formed by Cas9 or Cas12a. Moreover, this work succeeded in transferring transgenic larvae into the parasitic life cycle. Finally, eGFP signals were detected in eggs and adult worms, which demonstrated reporter-gene activity at GSH1.

In summary, strong evidence was found for SmRAR and SmRXR-1 as key factors in the regulation of meiosis in *S. mansoni*. In addition, SmTHRβ and SmRXR-1 were shown to be critical for tissue homeostasis and oocyte formation. These findings suggest that these receptors and their ligands play a vital role in schistosome reproduction and indicating that the sexual maturation of females is not only influenced by pairing, but also by the host environment and thus by host derived molecules (e.g. RA and TH). Furthermore, the successful editing of the schistosomal GSH1 by transgene knock-in and the expression of the integrated eGFP reporter gene was achieved. By analyzing transgenic worms, strong evidence was found for transgene integration into germline cells. For the first time in schistosome research, these results provided proof of concept for a new genome editing approach in *S. mansoni*. This opens new perspectives to fill one of the existing technical gaps in schistosome research.

Zusammenfassung

Schistosoma mansoni ist ein Parasit, der sowohl Menschen als auch Tiere befällt. Im Zuge der Infektion verursachen Schistosomen die Infektionskrankheit Schistosomiasis. Ein Alleinstellungsmerkmal der Schistosomen innerhalb der Trematoden ist die Ausbildung von zwei separaten Geschlechtern. Darüber hinaus erreichen die Weibchen nur dann die Geschlechtsreife, wenn sie sich in einem konstanten Paarungskontakt mit einem Männchen befinden. Vergleichende RNA-Sequenzierungsstudien, welche die Transkriptome adulter Schistosomen und ihrer isolierten Gonaden analysierten, zeigten, dass eine Vielzahl der Gene im Weibchen paarungsabhängig reguliert sind. Darunter befanden sich auch Gene, die für nukleäre Rezeptoren (NRs) kodieren. Für diese NRs konnte eine paarungsabhängige und Ovar-präferenzielle Regulation gezeigt werden. Mitglieder der NR-Superfamilie sind Liganden-aktivierte Transkriptionsfaktoren, für die verschiedenste Rollen bei der Zelldifferenzierung, -proliferation und Embryogenese beschrieben worden sind. Des Weiteren wurde für Vertebraten-NRs des Typs II gezeigt, dass die Klassen der Retinsäurerezeptoren (RAR/RXR) und die Thyroidhormonrezeptoren (THR) essenzielle Rollen in der Spermatogenese, der Embryogenese und der Gewebehomöostase spielen.

Im Rahmen dieser Arbeit wurden potenzielle *S. mansoni* NRs identifiziert und durch polygenetische und vergleichende Domänenanalysen den Klassen RAR (Smp_144170, SmRAR), RXR (Smp_097700, SmRXR-1), THRα (Smp_134490, SmTHRα) und THRβ (Smp_174260, SmTHRβ) zugeordnet. Zusätzlich wurden die Transkripte dieser Rezeptoren mittels *in situ* Hybridisierung ganzer Würmer (WISH) im posterioren Teil des Ovars, welcher mature Oozyten beinhaltet, lokalisiert. Darüber hinaus wurden die Transkripte dieser Rezeptoren mit Hilfe des kürzlich von Zhigang Lu*,* einem ehemaligen Mitarbeiter der AG Grevelding, erstellten scRNA-Seq-Atlas von isolierten maturen Ovarien vor allem in Oozyten des intermediären Entwicklungsstadiums gefunden. Dieses Ergebnis deutete auf eine Beteiligung dieser Rezeptoren an der Regulation meiotischer Prozesse hin.

Funktionelle Gen-Charakterisierungen mittels RNA-Interferenz (RNAi) lieferten eindeutige Beweise für die Beteiligung dieser Rezeptoren an der frühen Embryogenese und der Gewebehomöostase in adulten Schistosomen. Vor allem die morphologischen Analysen der Ovare paarungserfahrender Weibchen post RNAi zeigten starke Veränderungen in der zellulären Struktur. Insbesondere die funktionelle Charakterisierung von SmRAR und SmRXR-1 sowie biologisch assoziierter Moleküle wie SmMEIOB und SmGLI1 deutete auf eine zentrale Rolle dieser Gene bei der Maturation der Oozyten und der Progression der Meiose hin. Diese Ergebnisse sowie die anschließende Analyse des positiven Einflusses von 9cis-Retinsäure auf die Eiproduktion deuten auf eine entscheidende Rolle der RA-Signaltransduktion in der Reproduktionsbiologie von *S. mansoni* hin.

Das zweite Ziel dieser Arbeit stellte die Etablierung einer CRISPR/Cas-basierten Editiermethode für *S. mansoni* dar. In Modellorganismen wird die funktionelle Charakterisierung von Genen meist mit Hilfe von *Knock-out*-Modellen durchgeführt. In der post-genomischen Ära der Schistosomenforschung gibt es jedoch bislang kein etabliertes Protokoll, um diesen Parasiten und andere parasitische Plathelminthen stabil zu transformieren. Bisher beruhte die funktionelle Gen-Charakterisierung auf der Nutzung von RNAi. Jedoch ist die Effizienz eines RNAi-vermittelten Gen-*Knock-downs* variabel, abhängig von der Ziel-Sequenz und kann zu ektopischen Effekten führen. Um diese Effekte und deren Auswirkungen auf die Auswertung experimenteller Daten zu vermeiden, ist die Entwicklung alternativer Methoden unumgänglich. Die CRISPR/Cas-basierte Genom-Editierung ist ein potentes Werkzeug zur Gencharakterisierung und konnte in den letzten Jahren für eine Vielzahl an Organsimen etabliert werden. Um diese Technik für die Trematoden-Forschung zugänglich zu machen, wurde ein Protokoll zur Editierung einer genomischen *Safe Harbors* (GSH)-Stelle in *S. mansoni*, die unser Kollaborationspartner, Professor Christoph Grunau (Perpignang), bioinformatisch vorhergesagt und mit GSH1 benannt hatte, entwickelt. GSHs sind spezielle Stellen im Genom, die die Integration neuen genetischen Materials ermöglichen, ohne die Integrität des Genoms oder die Genexpression zu beeinträchtigen. GSHs sollten daher die konstitutive Expression von Reportergenen ermöglichen. Zur Editierung der GSH1 wurde ein 5'C6-PEG10-modifiziertes Konstrukt, das ein eGFP-Reportergen unter einem starken nativen *S. mansoni*-Promotor kodiert, als Reparatur-DNA-Template verwendet.

Die Cas-vermittelte Integration des eGFP-Transgens konnte durch Co-Elektroporation von Schistosomen-Eiern erreicht werden. Zusätzlich wurden in einem vergleichenden Ansatz Cas9 und Cas12a für die Editierung der GSH1 verwendet. Dabei wurden signifikante Unterschiede in der Editierungs-Effizienz der beiden Enzyme festgestellt mit einer leicht höheren Effizienz von Cas12a. Weiterhin konnte die Integration des Reportergens in die GSH1 durch Ribonukleoproteinkomplexe, die durch Cas9 oder Cas12a gebildet wurden, nachgewiesen werden. Ferner gelang es, transgene Larven in den *S. mansoni* Lebenszyklus zu überführen und diesen zu schließen. Schlussendlich wurde die Aktivität des Reportergens in GSH durch die Detektion von eGFP-Signalen in Eiern, sich entwickelnden Miracidien und adulten Würmern nachgewiesen.

Zusammenfassend konnten SmRAR und SmRXR-1 als Schlüsselfaktoren bei der Regulation der Meiose in *S. mansoni* identifiziert werden. Darüber wurde gezeigt, dass SmTHRβ und SmRXR-1 entscheidende Rollen in der Gewebehomöostase und Oozytenbildung einnehmen. Diese Ergebnisse legen nahe, dass diese Rezeptoren und ihre Liganden eine wesentliche Rolle in der Reproduktionsbiologie der Schistosomen spielen. Des Weiteren deuten diese Ergebnisse darauf hin, dass die sexuelle Reifung des Weibchens nicht nur durch die Paarung mit einem Männchen, sondern auch durch die Wirtsumgebung und somit durch Wirtsmoleküle

(z.B. RA und TH) beeinflusst wird. Weiterhin konnten die gRNA-programmierte Editierung einer vorhergesagten schistosomalen GSH, die Integration eines Transgens sowie die Expression eines Reportergens nachgewiesen werden. Darüber hinaus belegte die fluoreszenzmikroskopische Analyse potenzieller transgener Würmer eine Integration des Transgens in Zellen der Keimbahn. Zum ersten Mal in der Schistosomenforschung wurde die Möglichkeit aufgezeigt, das Genom von *S. mansoni* zu editieren und somit das Potential, funktionelle Genanalysen in Schistosomen durchführen zu können. Diese Ergebnisse eröffnen neue Perspektiven, um bestehende technische Lücken in der Forschung an Schistosomen und darüber hinaus zu schließen.

List of Contents

List of Figures

List of Tables

List of Equations

1 Introduction

1.1 Schistosome life cycle

Schistosoma mansoni, a member of the parasitic genus Schistosomatidae, is the cause of the widespread infectious disease schistosomiasis, which is one of the most emerging parasitic diseases worldwide. Schistosomiasis has been classified as a neglected tropical disease (NTD) by the World Health Organization (WHO (1)). NTDs primarily affect people in impoverished countries with limited access to healthcare and suitable sanitary infrastructure (2–5). Schistosomiasis is prevalent in subtropical and tropical regions such as Asia, South America, and sub-Saharan Africa, and has been reported in 78 countries. Furthermore, estimates indicate more than 237 million people requiring preventive treatment. More than 20 million are severely affected by this disease, resulting in up to 200,000 deaths each year (6, 7). Recently, outbreaks of urogenital schistosomiasis have been reported also in Corsica (France) (8) and Almeria (Spain) (9), indicating that this disease can also spread to moderate climate zones. This reflects a worrying trend, especially given global warming and the resultant shifting of habitats for different animals and their parasites (10). Moreover, this zoonotic disease is of immense veterinary and economic importance, as some *Schistosoma* species are capable to infect not only humans but also livestock as final hosts (11). Furthermore, wild animals such as rodents can serve as reservoir hosts (12).

Figure 1. Fine structure of a *S. mansoni* couple. Representative image of the fine structure of an adult *S. mansoni* couple, which was stained by carmine red and analysed by CLSM. The larger, muscular male embraces the smaller, longer female in the *canalis gynecophoris.* Picture taken from Moescheid and Puckelwaldt *et al.* 2023 (152)**.** Scale bar: 200 µm

Schistosomes are the only dioecious representatives of the obligate parasitic trematodes, of which all other species are hermaphrodites (Figure 1). They have a complex life cycle (Figure 2), which is typical for trematode parasites. This comprises an obligatory change of hosts and free-living as well as intermediate host-associated (sporocysts) larval stages. In the definitive human host, adult *S. mansoni* colonizes the mesenteric veins of the intestine. Mature

females can produce approximately 300 eggs per day (13, 14). These eggs migrate from the endothelium of the mesenterial vessels through the intestinal wall, secrete proteolytic enzymes, and are excreted with faeces into water. During the migration of eggs into the intestinal tissue, the first larval form, the ciliated miracidium, develops inside the egg. Upon contact with fresh water and sunlight, miracidia hatch from the eggs and actively infect an intermediate snail host of the genus *Biomphalaria* (4, 15). Inside the snail, the miracidium first transforms into a mother sporocyst and reproduce asexually in daughter sporocysts. Finally, daughter sporocysts migrate into the midintestinal gland of the snail, where they develop within three to seven weeks post infection (p.i.) into the second free-living larval form, known as cercaria. These larvae actively leave the snail as the infectious stage of this parasite aiming to find a final host by swimming through the water. Following contact, infection occurs via penetration of the skin supported by the secretion of proteolytic enzymes (16, 17). Once the cercariae have entered the skin, they undergo a morphological transformation. While penetrating the skin, cercariae lose their tails. Next, they develop a double-layered membrane called the tegument and transform into schistosomula, which represents the juvenile stage of schistsosomes. Within approximately 24 h, schistosomula migrate through the dermis and reach the blood vessels, and finally migrate through the lung capillaries. Here, they continue to develop for 3 to 10 days before migrating to the portal vein of the liver, where they complete their development and mate. Pairing occurs when the female is placed in the ventral grove, called the *canalis gynecophorus,* which is formed by the male upon physical contact with a female(18). After pairing, the *Schistosome* couples move to their final destinations and remain permanently paired. This led to the German designation for schistosomes: “Pärchenegel”. Adult *S. mansoni* and *S. japonicum* reside in the mesenteric veins, while *S. haematobium*, another relevant species for humans, resides in the vesical vein plexus of the urogenital system (4, 19).

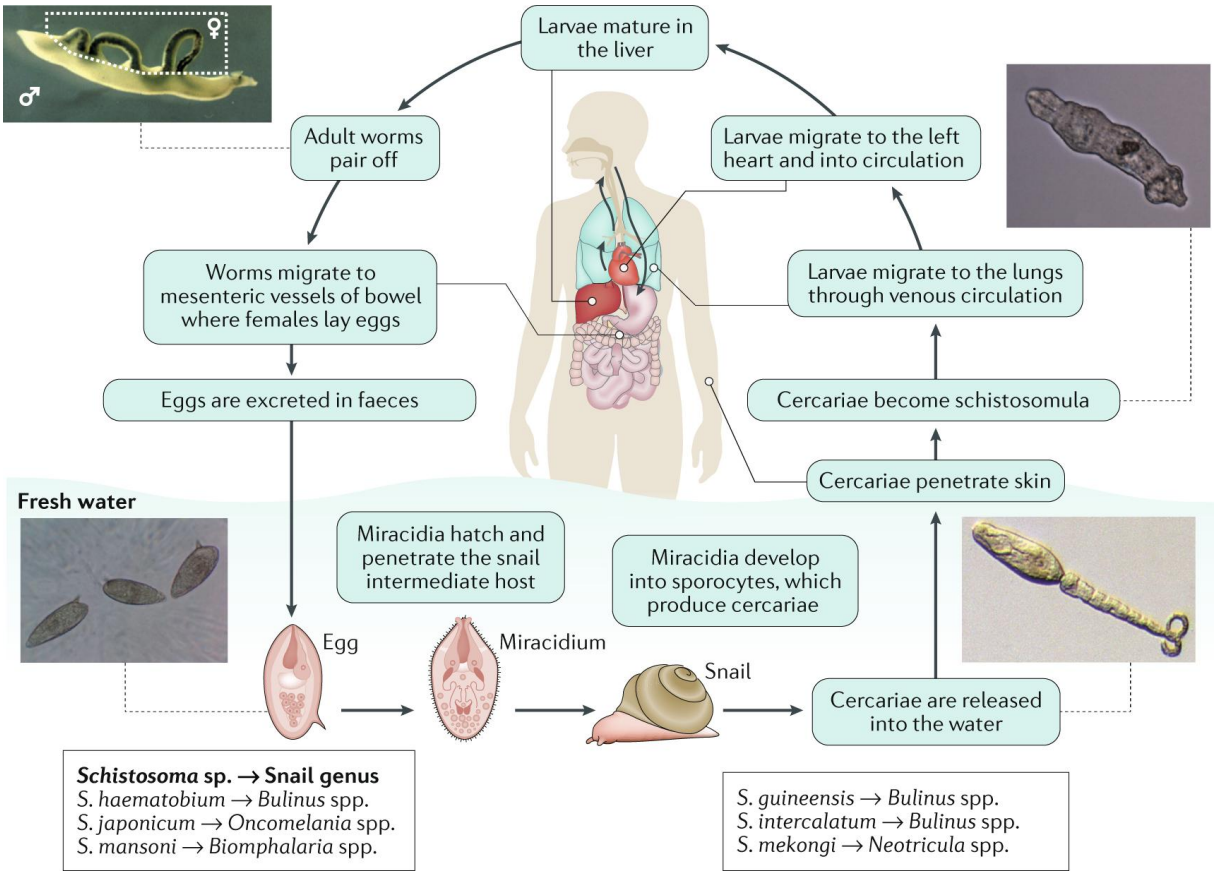

Figure 2. Life cycle of *Schistosoma mansoni.*

Schistosomes have a complex life cycle involving a freshwater snail (*Biomphalaria spp.*) as intermediate host and the human as definitive host. Eggs are excreted with the human faeces and hatch phototactically induced by light and upon contact with water. Subsequently, miracidia hatch from these eggs and invade the intermediate snail host. Here, miracidia develop into mother and daughter sporocysts, which then reproduce asexually, finally producing numerous cercariae. After approximately 30 days, cercariae emerge from the snail in response to light, swim through the water and, following contact, penetrate the skin of the final host, such as a human. During penetration, the tails of cercariae are shed, and the larvae transform into schistosomula within the skin. These schistosomula then enter the bloodstream and travel to the lungs and further to the portal vein system, where they mature into adult worms. The male worm then grasps the female worm in the gynaecophoral canal, and as couples they migrate to the mesenteric vein system of the gut. Following pairing, female have matured and start the production of eggs, of which a part is excreted by the faeces of human hosts to continue the life cycle. Image was adapted from McManus *et al.* 2018 (4).

The most serious pathological consequences of schistosomiasis are not caused by the worms, but by their deposited eggs. Only about half of the eggs are excreted, whereas the other half of eggs are transported in the intestinal tissue or through the bloodstream to various organs (13), with the majority of eggs ending up in liver and spleen. This can lead to blockage of blood vessels and local inflammation, one of the clinical hallmarks of chronical schistosomiasis (20,

21). In addition to damage to the intestinal tissue, there is often pathological enlargement of the liver and spleen (hepatosplenomegaly) and ascites. Damage to the liver, can lead to fibrosis and ultimately to death of patients, if left untreated (22, 23). Schistosomiasis can also cause urogenital or colorectal cancer (24–26). Most recently, a study using bulk RNA-Seq showed that the transcription of pathogenicity factors is highly upregulated in eggs trapped in the liver of the final host (27). Especially for *S. haematobium*, its potential as carcinogen has been shown (24), whereas for *S. mansoni* first evidence exist for a potential participation in liver cancer development (26). In both cases, eggs and their antigens are triggering carcinogenesis. Furthermore, infections with *S. haematobium* manifests pathogenesis within the human genital tract, which in females may lead to impairment of the reproductive system, eventually leading to infertility and other clinical consequences (28, 29). Until now, no protective vaccines against the parasite itself or the egg-released pathogenicity-mediating proteins such as IPSE (30) or omega (31–33), are available. The only effective drug currently used against schistosomiasis (praziquantel) is not uniformly effective (34). Moreover, first signs of resistance to this drug have already been observed (35, 36). Therefore, further research into the unique biology of *Schistosoma* is needed to identify future targets for the development of preventive measures, such as appropriate vaccination, and/or drugs to interrupt the parasitic life cycle.

1.2 Reproductive biology of schistosomes

1.2.1 Pairing-dependent sexual maturation of *S. mansoni* females

The complex life cycle of *S. mansoni*, provides a broad basis for basic parasitological research. The reproductive biology of adult schistosomes, which is almost unique in the animal kingdom, has become a main focus of scientific research. The fact that schistosomes are the only members of the Trematoda that have evolved separate sexes (Figure 1), and that both sexes live in permanent mating contact, which is necessary to maintain the sexual maturation status of the females and its reproduction capacity (18), is seemingly of great interest. This phenomenon is particularly significant because the eggs are the cause of the pathological consequences of schistosomiasis (22, 23, 26).

A female worm has to be continuously paired with a male to mature sexually. Pairing-inexperienced females (sF, single-sex females) are characterized by an underdeveloped ovary with undifferentiated, stem cell-like oogonia (immature oocytes) and precursor vitellocytes (Figure 3 A) (37–40). Pairing initiates mitogenic process (41) and subsequently the complete differentiation of the female reproductive organs (18). The ovary of paired, mature females (bF, bisex females) is represented by a typical oval structure containing small stem cell-like oogonia in the anterior part of the ovary and large mature oocytes (primary oocytes) in its posterior part

(Figure 3) (38, 42). Moreover, only the vitellarium of bF contains stem-cell like S1 cells, differentiating S2 and S3 cells, and terminally differentiated S4 cells. Both cell types – mature oocytes and S4 vitellocytes – are required for egg production (18, 43, 44). However, only undifferentiated S1 cells with stem-cell characteristics have been identified in immature females (37, 45, 46). In contrast to females, the influence of mating on the morphology of male schistosomes is less significant. Pairing-inexperienced males (sM, single-sex males) have the same body size compared to paired males (bM, bisex males). Moreover, pairing-independent development of testes that are capable of sperm production has been demonstrated (47).

Another fascinating aspect of schistosome reproductive biology is that female maturation is reversible. Separation of couples results in a decline in the reproductive capabilities of the female. This process includes a decrease in and final stop of egg production, which is paralleled by the dedifferentiation of the reproductive organs in separated females that finally resemble sF. Previous studies demonstrated a decline in the grade of female maturation within 35 d of separation. During that period females revert to an immature status (39, 48). However, ovary and vitellarium re-differentiate and egg production resumes when previously separated females are re-paired with males (18, 48–50).

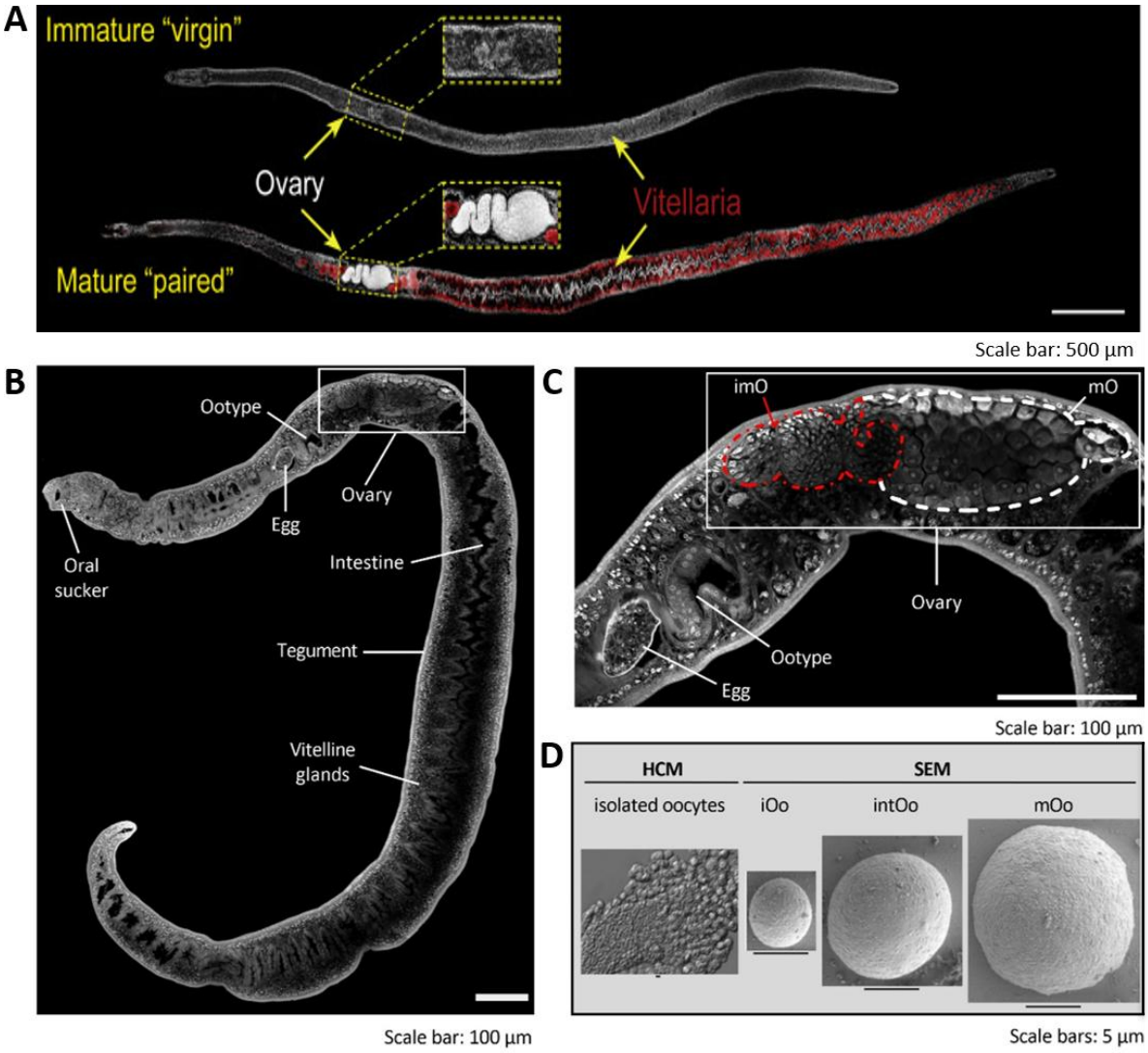

Figure 3. Microscopic analyses of the pairing-induced sexual maturation of female schistosomes and different stages of oocyte differentiation.

A, Analysis of the fine structure of immature (pairing-inexperienced) and mature (pairing-experienced) female schistosomes by DAPI (grey) and Fast Blue BB (red) labelling. Fast Blue BB (orange-red) labelled the lipid containing vitelline droplets in mature vitellocytes, Chen *et al.* 2022 (51). **B**, representative image of a sexually mature female of *S. mansoni*, which had been separated from the male partner for confocal laser scanning microscopy (CLSM). The image depicts various organs and tissues, and the position of the ovary is highlighted. **C**, close-up section of the detailed structure of the fully mature ovary. A pear-like shape, with two distinct areas, characterizes the ovary: a smaller, anterior part containing immature oocytes (imO, outlined in red) and a larger, posterior part containing mature oocytes (mO, outlined in white). The ootype, responsible for egg formation (52), as well as an egg within the uterus, are indicated. **D**, Images of oocytes at different developmental stages were obtained using Hoffman modulation contrast microscopy (HCM) and scanning electron microscopy (SEM) after trypsinization of an ovary from a paired female. The images show an immature oocyte (iOo, oogonia, about 5 µm in size), a differentiating intermediate-stage oocyte (intOo, 8 – 12 µm in size), and a mature oocyte (mOo, primary oocytes, about 15 µm).

Several studies have been conducted to understand the mechanisms of how male worms stimulate female development (48, 49, 51, 53–58). First evidence for the male induced maturation were collected by physiological experiments. For this purpose, sexually undifferentiated females were paired with males that had been cut in half without being fertilized. Here, the interaction between the male worm fragments and females resulted in the maturation of the female reproductive organs exactly at the location that had been covered (48).These females produced eggs containing haploid embryos (48, 49). However, the diploid karyotype of embryos produced by paired schistosomes (2 n) has 16 chromosomes, whereas the mitotic cells in eggs produced by females paired with castrated males were haploid (49). Moreover, some works have focused on identifying the "molecular/chemical components" that are transported from males to females during initial pairing contact, thereby inducing female sexual maturation (51, 55–58). Most recently, a first key factor for the male- induced female maturation was identified, a β-alanyl-tryptamine (BATT). BATT is generated by a non-ribosomal peptide synthetase (Smp_158480, SmNRPs) and is released by ciliated sensory neurons into the gynecophoric canal. Even in the complete absence of a male, a synthetic BATT version was found to partially induce sexual maturation in immature females (51). Furthermore, two genes were found to act as key factors in female maturation. First, the Vitellogenic Factor 1 (VF1), a pairing-specific transcription factor (55), which belongs to the nuclear receptor (NR) superfamily (49). RNA interference (RNAi) experiments targeting *vf1* transcripts demonstrated a critical role for VF1 in vitellarium maturation. Second, SmGli1 an ortholog of the *C. elegans* Ci/Gli, which is known to orchestrate the formation of female and male gonads during larval development (59). Both have been shown to be one of the male driven key factors of female maturation (51, 60). In addition, a recent study provided strong evidence that the male-derived competence factors SmTDC-1 and SmDDC-1 and their metabolites, biogenic amines such as dopamine, are important key factors in the induced maturation of female schistosomes (57). Both genes, Sm*tdc-1* and Sm*ddc-1* pairing-dependent regulated in male schistosomes (55, 57). Functional characterization of these factors in sM by RNAi caused maturation deficiency in female schistosomes during pairing experiments (57). New techniques, particularly high-resolution RNA-Seq techniques (55, 61, 62), make it possible to decipher specific factors responsible for the reproductive biology of schistosomes, which may cover a greater variety of molecules as thought before (46, 51, 53, 57, 63).

1.2.2 Transcriptomics - decoding the maturation of female schistosomes

In addition to the morphologically visible changes in the female reproductive organs, the effects of its pairing-induced sexual maturation were also demonstrated at the level of gene expression. The influence of pairing on transcription processes in females, which was initially shown for individual genes such as the eggshell precursor proteins p14, p19 and p48 (64–67), has now been confirmed for a large number of other genes (55, 61), also in *S. japonicum* (68). First datasets were obtained by SAGE and microarray analyses, confirming the pairing-dependent expression of many different genes and gene families (69–71). With respect to transcript profiling of genes in different life stages and upon pairing, some genes, such as follistatin, have been shown to play important roles in the TGFβ-pathway (71). With the help of yeast-two-hybrid analysis, a TGFβ-receptor orthologue from *S. mansoni* was found to interact with the TGFβ-receptor agonists inhibin/activin (SmInAct) and bone morphogenic protein (SmBMP) (71). This study also highlighted a previously unknown role of neurotransmitters in male development. Nevertheless, these methods failed in assessing the whole transcriptome. After RNA-Seq methods were available and more feasible, bulk RNA-Seq was performed to assess pairing dependent global changes in the transcriptome of both sexes. In order to obtain a better understanding of the sexual biology of schistosomes, comparative transcriptomics of adult schistosomes (pairing-experienced and -inexperienced) and their (isolated) gonads were conducted (55). This analysis uncovered a significant difference in the transcription of > 3,600 genes between ovaries of immature (= unpaired) and mature (= paired) females. Here, 243 genes occurred to be pairing-dependently regulated within the male gonads, which is a remarkable number against the background of the absence of phenotypic differences between sM and bM.

Transcriptomic data obtained from various studies assembled the transcriptomic profiles of *S.mansoni* throughout the life cycle, including different larval stages such as egg, miracidium, sporocyst, cercaria, schistosomulum, juvenile (21-28 d), and adult (42 d) worms stages (62). Additionally, pairing-dependent effects on the transcriptome were investigated by comparing bM, sM, bF, and sF (55, 68, 69, 72). However, these bulk RNA-Seq approaches failed to distinguish differences in gene expression among diverse tissues. To overcome this hurdle, Wendt *et al*. (61) established the first whole worm single cell RNA-Seq (scRNA-Seq) atlas. This groundbreaking work identified cell populations of female and male *S. mansoni* including gonadal cells (61). Using this atlas data, a recent study identified several key regulators of male-derived female maturation, such as the transcription factor SmGli1 (51), as well as the potential key regulator of female maturation SmNRPs, which is preferentially expressed in bM (51, 55). SmNRP is responsible for the production of BATT, which is released by ciliated sensory neurons into the gynaecophoric canal. BATT can partially induce sexual maturation in

sF, even in the absence of a pairing contact with a male. Interestingly, egg number and quality as well as ovary differentiation were found to be inferior in BATT-treated sF compared to naturally paired females (51, 57).

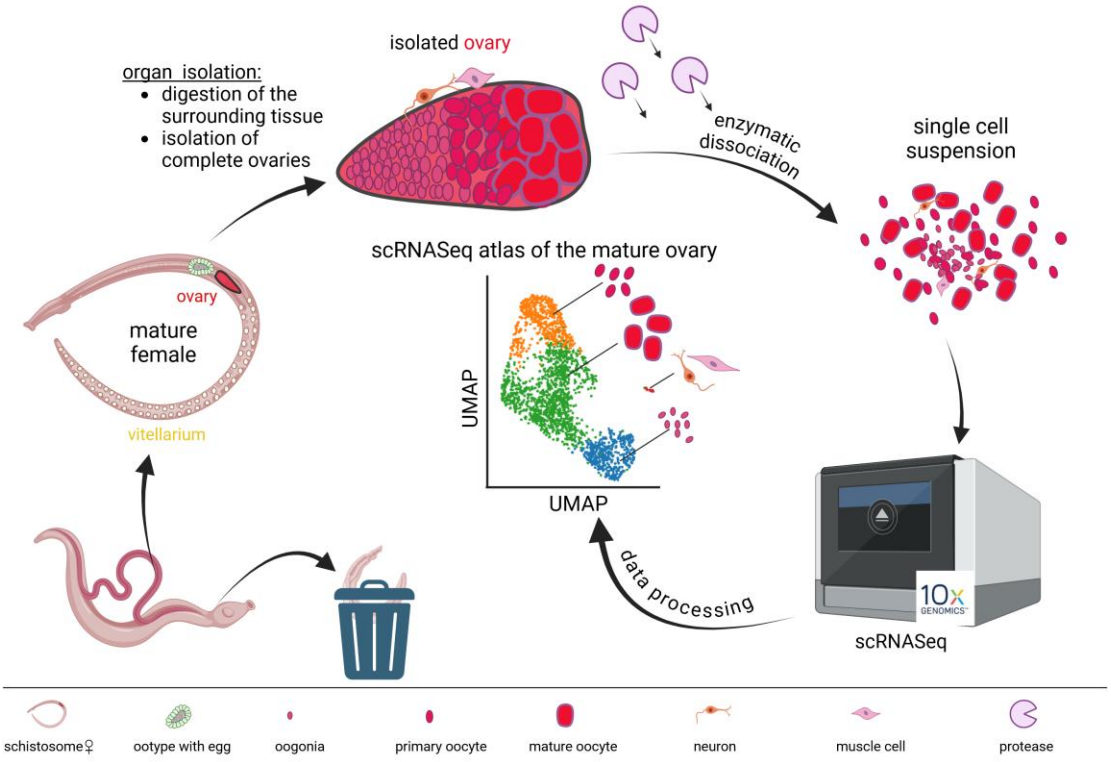

Figure 4. Creation of the first ovarian scRNA-Seq atlas of mature *S. mansoni*.
Stable couples were separated and the established approach for isolating vital *S. mansoni* gonads (73) was used to extract ovaries from sexually mature females. To study the ovary transcriptome at the single-cell level, 10X Chromium scRNA-Seq technology was utilized (74), Moescheid and Lu *et al.,* submitted.

In the past, RNA-Seq approaches failed to achieve high-resolution gene expression profiles among and within sub-populations of cells, including cells of gonad tissues. Since whole worms were used as starting material to generate the first scRNA-Seq atlas of *S. mansoni*, only small cell numbers belonging to certain clusters (e.g. 20-79 cells in late female germ cell clusters) were captured, such as oogonia and oocysts (61). To overcome this problem, the organ isolation approach previously established in our lab for *S. mansoni* (73) to isolate ovaries from sexually mature females was used to enrich cells underrepresented in the previous scRNA-Seq study (Figure 4). Based on this approach, and by further applying the Chromium 10X method, the first scRNA-Seq atlas of the ovary of *S. mansoni* bF was assembled (Figure 4, Moescheid and Lu *et al*., in revision; scRNA-Seq atlas data are available at gonadsc.schisto.xyz). Since the ovary of a paired female contains both mitotic, immature oogonia, and meiotic, mature oocytes, part of this thesis was to identify genes contributing to

developmental processes from the oogonia (gonadal stem cell-like) stage to mature oocytes. Bioinformatics analyses uncovered distinct cell clusters and associated marker genes for different developmental stages of oocytes. To this end, the combined analysis of these comparative transcriptome studies revealed among others pairing-dependent and ovary-preferentially transcribed nuclear receptors (NRs), for which I assumed a potential role in ovary development.

1.2.3 Egg formation and miracidia development

In paired female schistosomes, oocytes are formed in the ovary. They leave the ovary at its posterior end to enter the oviduct. Here, they migrate along the sperm reservoir (*receptaculum seminis*), which is a dilated region close to the ovary exit and within the oviduct. After fertilization, the oocyte moves forward to the oviduct, which is also connected to the vitelline duct. Thus, also S4 vitellocytes, originating from the vitellarium, end up in the ootype, which is the egg-forming organ in trematodes. Within the ootype, the fertilized oocyte reaches the zygote stage and is surrounded by 30-40 S4 cells that provide energy resources and egg-shell precursor proteins for egg-shell formation (18, 43, 64, 75, 76). This process is supported by excretion products from the Mehlis' gland that surrounds the ootype (52). Within the ootype, vitellocytes release their granules contents, which are essential for egg-shell formation and embryogenesis (64, 77, 78). The egg-shell is finally formed through biochemical cross-linking processes of these precursor proteins and two developmentally regulated tyrosinases (SmTYR1 and SmTYR2) (49, 79, 80). Following egg formation, the egg passes through the uterus to be released into the environment through a pore near the ventral sucker. Embryonic development occurs externally while the egg migrates from the host´s intestine into the faeces (76, 80). In the external environment, Jurberg *et al.* (76) identified eight embryonic stages based on Vogel and Prata´s staging system (Figure 5) (81, 82). Stage 1 is characterized by a single, yet undeveloped zygote and surrounding vitellocytes (yolk). In stage 2, the zygote starts to form the multicellular stages of a stereoblastula and the initiation of outer envelope differentiation (von Lichtenberg´s envelope (83)). Stage 3 includes the elongation of the embryonic primordium and the onset of inner envelope formation. At stage 4, the primordia of the first organ arise. During stages 5–7, tissue and organ differentiation occurs (neural mass, epidermis, terebratorium, musculature, and miracidial glands). Stage 7 is characterized by the nuclear condensation of neurons in the central neural mass. Stage 8 refers to the fully formed miracidium, which exhibits muscular contraction, cilia, and flame cell activity. Part of the developed eggs are released by the faeces into fresh water. Induced by the changes of osmotic pressure and by light (15), the miracidium hatches from the egg to actively search for the intermediate host, in case of *S. mansoni* the freshwater snail *Biomphalaria glabrata*.

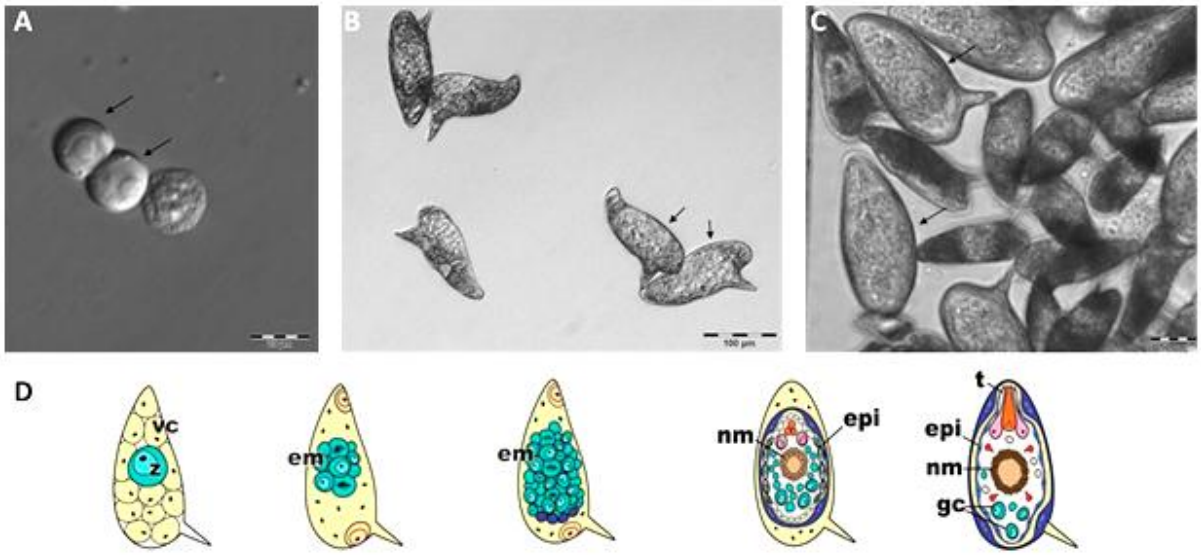

Figure 5. Development of *Schistosoma mansoni* eggs from the fertilized zygote to the mature miracidium.

A, fertilized oocytes (zygotes), phase-I eggs according to Vogel and Prata's classification, obtained as individual cells separated from the surrounding vitellocytes (scale bar 20 µm) (76, 81, 82). **B**, phase III eggs, which are characterized by the increase in size of the embryo compared to the egg itself (scale bar: 100 µm). **C**, phase V eggs (arrows) in comparison to phase III eggs (scale bar: 50 µm). Stage V eggs contain the mature miracidium. In **D**, the different developmental stages of the *S. mansoni* egg are shown, modified according to Jurberg *et al.* 2009 (76, 84). The development of the egg, according to Vogel and Prata's phase I to V, is shown (from left to right). Abbreviations: *vc*, vitellocytes; *z*, zygote; *em*, embryo; nM, neural cells; *epi*, epidermis; *t*, terebratorium; *gc*, terminal cells.

1.3 Nuclear receptors

Members of the nuclear receptors (NR) superfamily are ligand-activated transcription factors (TF) that play diverse roles in cell differentiation, proliferation, and metabolism, emphasizing their biological importance (85–88). NRs are activated by lipophilic steroid hormones, such as estrogen, cortisol, vitamin-D, retinoic acids, and/or thyroid hormones (85, 88–90). NRs share a general characteristic domain structure (Figure 6) consisting of (i) a highly variable amino-terminal domain comprising several distinct transactivation regions (A/B domain), (ii) a conserved DNA-binding domain, which features two Zn-fingers (C domain), (iii) a nuclear localization (D domain), and (iV) a highly conserved carboxy-terminal ligand-binding domain (E domain) (88, 91). The binding of the ligand to its corresponding NR results in dimerization of certain receptors and finally in the transactivation of specific genes within a target tissue (92).

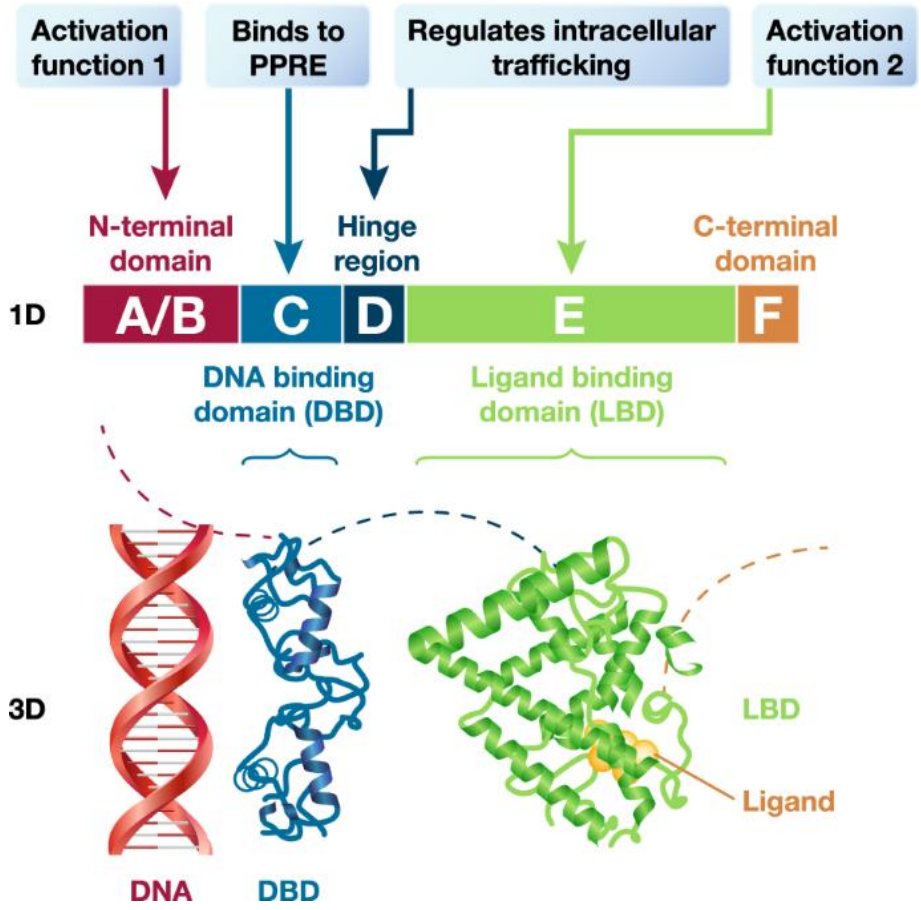

Figure 6. Structural characteristics of nuclear receptors.

Nuclear receptors are characterized by a N-terminal A/B-domain and a DNA binding (zinc finger) domain, which is connected by a hinge region to the C-terminal ligand binding domain, Fruchart *et al.* 2019 (91).

Unlike most other intercellular messenger molecules, ligands of NRs can cross the cell membrane without the necessity to interact with receptors located at the cell surface (85). NRs are categorized into four distinct classes, each characterized by its unique mode of action. Accordingly, they can act as monomers, heterodimers, or homodimers. These receptors modulate gene transcription by recognizing a specific DNA hormone response element (HREs), which is associated with chromatin remodeling (93). In mammalian model organisms, the HRE is derived from pairs of the consensus sequence RGGTCA (R, purine base) (85, 94).

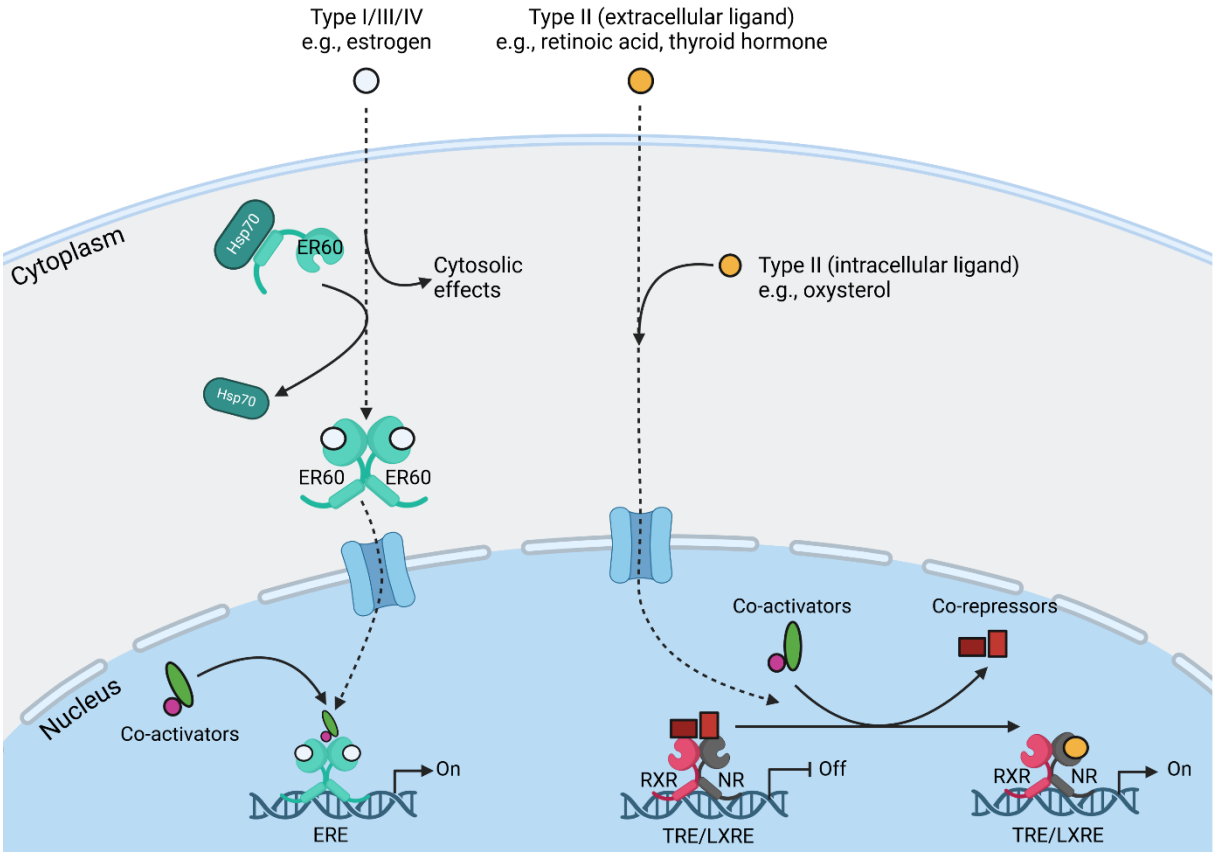

Figure 7. Nuclear receptor-mediated transcriptional regulation.

The different types of nuclear receptors (NRs) can be divided into two classes based on their ligand-dependent activation. The first class is characterized by ligand-mediated activation of the NR in the cytoplasm (Type I, III, and IV NRs), followed by the recruitment of transcriptional co-activators in the nucleus. This leads to stimulation of transcription. In contrast, receptors belonging to the second class of NRs (Type II NRs) are already bound as heterodimers to the target hormone response element (HRE) of the promoter as a complex with transcriptional co-repressors. Ligand-dependent stimulation of the heterodimer recruits co-activators, which are ultimately involved in the transcriptional upregulation of controlled genes. Modified illustration from Sever and Glass 2013 (85).

Depending on their roles and according classification, ligand binding cause either dimerization and HRE-binding or the disassembly of the NR-complexes bound to DNA (85, 93). Type I receptors, such as the estrogen receptor, are activated upon ligand binding in the cytoplasm. The inactive Type I NR (Figure 7) is bound to a chaperon of the heat shock protein (HSP) superfamily (95). Activation of the NR by the ligand causes the disassembly of the NR/HSP complexes and NR homodimerization, which ultimately ends in exposure of the nuclear localization sequence and entry into the nucleus (85). Within the nucleus, the ligand-activated NR-complex binds to NR-associated transcriptional co-activators promoting transcription of target genes (96). Most NR binding sites of Type I were found in enhancer elements in great distance to the transcriptional start site (97). Type III and IV NRs exhibit similarities to Type I

NRs, albeit with variations in the arrangement of hormone response elements (HREs). Additionally, Type IV NRs employ monomeric behavior, binding to half-occupied HREs upon activation by specific ligands (85, 88, 93).

Type II receptors, such as retinoic acid receptors (RAR/RXR) and thyroid hormone receptors (THR), show distinct characteristics compared to Type I, III and IV NRs (Figure 7). The main differences can be found in their location, whereby type II receptors are found to bind DNA within the nucleus, in the absence of specific ligands (85, 98). The latter can be of both intercellular and intracellular origin (85). Retinoic acid (RA), as well as thyroid hormones (TH), belong to ligands of the type II NRs. They typically form heterodimers with a retinoid-X-receptor (RXR) and, in the absence of a ligand, exert active repressive functions through interactions with NCoR (Nuclear co-repressor) and SMRT co-repressor complexes (99–102). Hereby, heterodimerization of retinoic acid receptors (RARs) with THRs was demonstrated as well (103). These co-repressor complexes are linked to histone deacetylases (HDACs), which causes heterochromatization of the target locus and thus leads to transcriptional suppression (104–106). Upon binding of a ligand to the LBD, co-repressors are released and replaced with co-activator complexes. Co-activator complexes generally comprise histone-interacting proteins, including histone acetyltransferases (HATs) and other activator proteins (104, 106), which results in the remodeling of the chromatin, and which promotes transcription of target genes (96). Furthermore, in vertebrate systems members of this NR-subfamily are associated with post-embryonic development, lipid metabolism, immune modulation, and adult homeostasis (85, 98, 107).Recent studies have also shown that RA and TH are indispensable hormones in embryogenesis. For example, an essential role of RA in the development of the central nervous system was demonstrated (107–109). In line with that, several studies provided evidence for the involvement of THs at early embryogenesis and development of the central nervous system (108, 110).

1.3.1 Retinoic acid receptors and their role in germ cell development

RA is the metabolic active isoform of vitamin A. It is known to act as ligand of RAR and RXR receptors and for its involvement in various biological processes. In this context, heterodimerization of RAR with RXR plays a critical role in gene regulation (85, 98). As type II NRs, RAR/RXR heterodimers bind to specific RA-response elements (RAREs) that are located in the promoter sequence of target genes (98). The consensus sequence of RARE bears a direct repeat of AGGTCA with a gap of 1-5 nucleotides (98). Both RARs and RXRs can be classified in three isotypes: i) -α, ii) -β and iii) -γ, which share 90% identity in their DNA binding domains (DBD) and 85% identity in their ligand binding domains (LBD). Although the isotypes within the different receptor classes show a high degree of similarity, there are significant

differences between the two receptor classes. RARs and RXRs share only 60% identity in their DBD and only 27% in their LBD (111). Nevertheless, RA and its metabolites can activate both receptors. For instance, by employing *in vitro* ligand binding assays, affinities of all-trans RA (atRA), 9cis-RA, and 13-cis RA for RARs, were shown (112, 113). Even though some studies provided first evidence that that 9cis-RA (111, 114) and polyunsaturated fatty acids (PFUA) (115, 116) are RXR ligands, the exact ligand have not been identified, yet. Furthermore, the involvement of RAR/RXR in various cellular processes was confirmed, including major roles in the regulation of lipid metabolism (98), inflammatory processes (117), neuronal development (107–109), and germ cell proliferation (118–120). In mammalian model organisms, meiosis is regulated by several signals. Among these, RA has been found to orchestrate meiotic entry and maintenance in spermatogenesis (121).

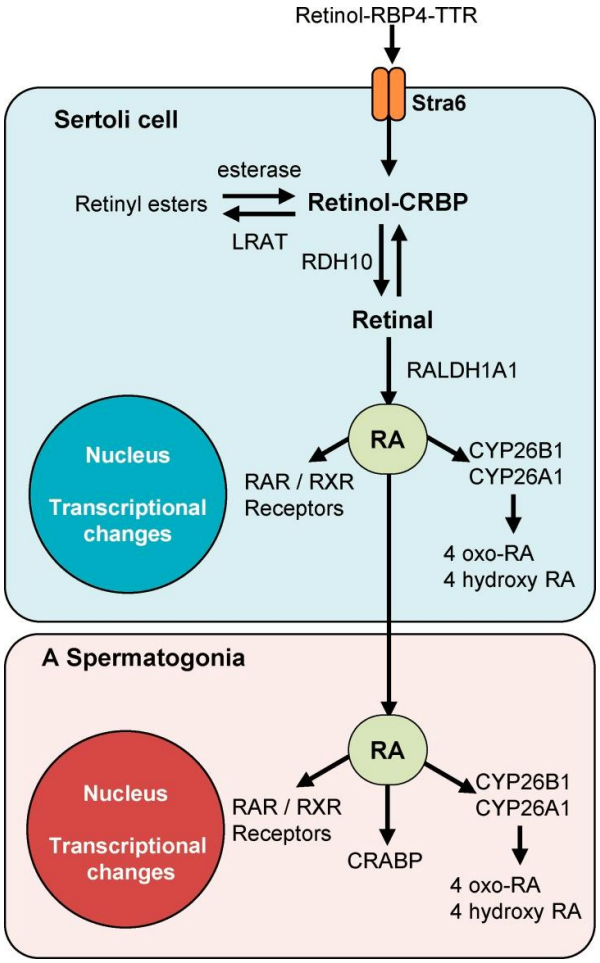

Figure 8. Retinoic acid signaling and metabolism during spermatogenesis.
Vitamin A is transported to target tissues by serum retinoid binding proteins. Upon arrival, specific retinol binding proteins facilitate retinol incorporation into surrounding cells (Sertoli cells). Retinol is then converted to its biologically active metabolite, RA, by alcohol dehydrogenases and retinaldehyde dehydrogenases. RA then binds to RAR/RXR heterodimers, leading to the upregulation of target genes through co-activator recruitment. Additionally, the cytochrome P-450 enzymes CYP26A1, CYP26B1, and CYP26C1 are crucial for maintaining the balance between active and inactive RA isoforms. Illustration by Griswold 2016 (122).

Vitamin A, particularly in the form of RA, has been found to initiate meiotic processes, as demonstrated in various studies by investigating meiotic regulation in mammalian model organisms (123, 124). Vitamin A originates from retinol by nutritional intake or from the liver. Bound to serum retinoid binding proteins, vitamin A can be transported to target tissues, such as the testes. Here, retinol is bound by retinol-binding protein 4 (RBP4), as well as the transthyretin-retinol-binding complex (TTR, Figure 8) (125–127). When bound to the Stra6 receptor, retinol, which is complexed to RBP4-TTR, can be detected by Sertoli cells (128, 129). By playing an important role in cellular retinol uptake, the Stra6 receptor has been shown to be important in maintaining vitamin A homeostasis (122).

In the Sertoli cells, the conversation of retinol to the biological active metabolite RA is catalyzed by the retinol dehydrogenase 10 (RDH10) and retinaldehyde dehydrogenases (ALDH1A1, ALDH1A2, and ALDH1A3) (122, 130). Once activated, RA binds to RAR/RXR heterodimers, which eventually enables the upregulation of meiosis associated genes like *stra8* and *meiosin* that play critical roles in meiosis initiation (131, 132). In addition, three different cytochrome P-450 enzymes, CYP26A1, CYP26B1, and CYP26C1, are involved in RA degradation, thus regulating the precise balance between biologically active and inactive RA isoforms (133). Additionally, the precise degradation of RA is known to be essential for regulating proper spermatogonial differentiation. In context with that, CYP26B1, which is expressed in immature Sertoli cells, degrades RA and prevents premature meiosis in germ cells (118, 134). This was shown in Cyp26b1 knock-out (KO) mice (135, 136). Upon Cyp26b1 KO, germ cells entered meiosis prematurely and underwent apoptosis. Additionally, inhibitor experiments, in which testes were treated with a CYP26 inhibitor, demonstrated an increase in the number of germ cells expressing the meiosis associated transcription factor STRA8 (137). In the past, it has also been shown that RA plays a critical role not only in the regulation of the RA-dependent pre-meiotic transition to meiosis, but also in the regulation of post-meiotic germ-cell differentiation (138). Moreover, the levels of RA fluctuate periodically. It was demonstrated that post-meiotic development depends on RA originating from meiotic cells, whereas the pre-meiotic transitions require RA from somatic cells.

1.3.2 Nuclear hormone receptors in *S. mansoni*

The current knowledge about NRs and RA-dependent gene regulation in *S. mansoni* and other trematode species is rather limited (139). Over the last decades, efforts have been made to fill these gaps of knowledge by identifying orthologous receptors and describing the effect of their potential ligands on schistosome physiology (87, 140–142). Recently, several yet uncharacterized NRs have been identified (87). This was mainly achieved by the availability of the *S. mansoni* genome sequence (143) and increasingly accurate RNA-Seq datasets (55, 61,

62). Several studies confirmed the existence of respective members of the NR superfamily in *S. mansoni*. These include for instance the retinoid-X receptor (RXR) orthologs binding to the promoter of the p14 egg-shell precursor protein (104, 141, 142), an androstane receptor homologue (144), two thyroid hormone receptors (145), the vitellogenic factor 1 (VF1) regulating the pairing induced development of the female vitellarium (49), and the fushi tarazu ortholog SmFTZ-F1 as one key regulator of oesophageal tissue homeostasis (87).

The best characterized NRs in schistosome species are the orthologues of the RXR subfamily, for which two putative *S. mansoni* RXR, SmRXR1 and SmRXR2, have been identified (104, 140, 140–142, 146). By performing co-immunoprecipitation (CoIP) experiments, heteromidimazation with a putative RAR receptor in case of SmRXR1 was described (104). An interaction between RXR/RAR heterodimers with chromatin remodeling enzymes, like histone deacetylases (HDACs) and histone acetyl transferases (HAT), is known (85, 98, 147). In addition to these findings, SmRXR/SmRAR-mediated recruitment of *S. mansoni* HATs, SmCBP1 and SmGCN5, has been described (104). Targeting these HATs by specific inhibitors led to effects on female reproductive organs (104). Inhibitor treatment resulted in malformed, smaller eggs, proliferation deficiency of cells of the vitellarium, and a reduced number of mature oocytes. Furthermore, CoIP experiments demonstrated binding of the p14 promoter by the heterodimer complexes (104, 148). Interestingly, 9cis-RA was identified as a potential ligand of the *S. japonicum* SjRXR ortholog (140), whereby the ligands of *S. mansoni* RAR and RXRs have not yet been identified. Moreover, cytochromes play an important role in the regulation of cellular RA levels (122). Functional characterization of the *S. mansoni* cytochrome P450 orthologue (SmCYP450) by RNAi and inhibitor treatment resulted in arrest of embryogenesis in developing eggs and reduced vitality of schistosomula and adult worms (149). These findings highlight the important role of RA receptors in schistosome reproductive biology.

1.4 The road to transgenic schistosomes

Compared with other model organisms, the scope of gene characterization in *S. mansoni* is limited. For years, RNAi interference (RNAi) has been proven as the most suitable tool for functional gene characterization at a gene KO like level (150, 151). Notably, the use of RNAi harbors risks, such as the unintentional deregulation of off-target genes or the occupation of the cell's own RISC through the use of an excess of dsRNA/siRNA (152–154). This can lead to unintended deregulation of various genes. Therefore, many efforts have been made to edit the genome of *S. mansoni* in order to overcome existing limitations in gene characterization.
The main reason for these limitations is the complexity of the parasitic cycle. The life cycle of *S. mansoni* involves two different hosts (Figure 2), which makes it challenging to access the

organism during critical developmental phases, such as asexual reproduction of sporocysts in the snail intermediate host and prohibits the use of defined culture conditions. The absence of *S. mansoni* embryonic cell lines necessitates the use of heterologous systems, such as HEK or yeast cells, for expression studies (155, 156). Owing to the massive, multicellular body structure of adult *S. mansoni* that is surrounded by a resistant tegument, the access to defined cell and tissue types is highly restricted. This is a fundamental prerequisite for cell-specific genetic analyses and access to stem cells (155, 157). Another limiting factor is that most gene-editing approaches are based on the modification of zygotes at a single cell stage (158). Compared to other organisms, a striking characteristic of trematodes is the production of composed eggs surrounded by a resistant egg shell (64, 76). These factors make it challenging to set up efficient transfection protocols for the establishment of transgenic *S. mansoni*. Besides dsRNA soaking for RNAi, various further methods to introduce DNA such as lipofection, electroporation (EPO), and particle bombardment (PB) have been used and different *S. mansoni* life stages (159–161). Using PB, it was possible to introduce GFP, driven either by the native heat shock protein 70 (HSP70) or the actin promoter, or the promoter of E210 (a cysteine protease) into *S. mansoni* life stages (159, 160, 162, 163). The activity of these reporter-gene constructs has been demonstrated by transcriptional analysis, fluorescence microscopy to visualize GFP expression, and western blot analysis (159, 160); noteworthy, a stable germline transfection of *S. mansoni* has not been achieved probably due to the fact that the plasmid vector-based constructs failed to integrate in the schistosome genome but instead remained extra-chromosomally in the nucleus (159).

Furthermore, various strategies for chromosomal integration, such as the use of a transgene-like viral system (164–166) and/or the use of transposons, such as *piggyback* (167), have been tested. By the use of a Murine Leukemia Virus-based approach, an undirected transmutation of the germline was possible (165). However, this approach was not feasible for targeted gene characterization. Based on viral systems and the availability of the *S. mansoni* genome sequence (143, 168), a further approach involving a lentiviral system, carrying the CRISPR/Cas9 system, successfully catalyzed a target-directed gene KO (33). The functionality of this method was demonstrated by knocking-out the pathogenic factor *omega-1* in a significant number of cells of liver eggs (LEs), (33). The work of Paul Brindley (Washington University) pioneered the demonstration of the power of CRISPR/Cas for functional analysis in schistosome research (33). Furthermore, other CRISPR/Cas delivery strategies, such as the transfection of parasitic life stages with CRISPR/Cas ribonucleic complexes, have been increasing (169–172). However, these approaches were not able to show edited cells of the germline or to reintroduce edited life stages into the parasite life cycle.

1.5 CRISPR/Cas

Genome editing using CRISPR/Cas technology has greatly impacted research in the fields of biomedicine and life sciences (173–175). A wide range of Cas homologues were identified, such as the bacterial CRISPR/Cas9, Cas12a (169, 176), dCas13 (177, 178), or the phage exclusive CasΦ (179). Each of these Cas-enzymes possess a unique programmed nuclease activity, such as alternative PAMs (Protospacer Adjacent Motifs), selectivity for different nucleic acid substrates, and sensitivity to various factors such as metal ions and temperature (176–178, 180, 181). The best characterized enzymes and now indispensable tools for highly accurate genome editing (182, 183), marking of target loci (175) or gene silencing (184, 185), are CRISPR/Cas 9, Cas12a (176), and dCas13 (177).

The most frequently and best studied system is CRISPR/Cas9, for which its precise and programmable editing capacity was first described by Doudna and Charpentier (183). Since then, this system has been optimized multiple times and found to be a suitable tool, not only for basic research, but also for advanced biomedicine (173, 174). The CRISPR/Cas9 system comprises two components: a guide RNA (gRNA) and a Cas9 nuclease (183, 186, 187). This nuclease creates blunt end-DSBs at specific locations in the genome and can be repaired through genome maintenance mechanisms, such as non-homologous end joining (NHEJ) and homology-directed repair (HDR). These native cellular mechanisms can be used for either KO of a target locus by provoking indels (insertion-deletions) that are caused by NHEJ or the precise integration of a fragment harboring homologous sequence regions by HDR (Figure 9) (188). Essential proteins of the NHEJ and HDR machinery have also been found in *S. mansoni* (189). In contrast, the CRISPR/Cas12a system includes a single crRNA, which guides the Cas12a nuclease to target the DNA sequence, generating sticky end DSBs (190).

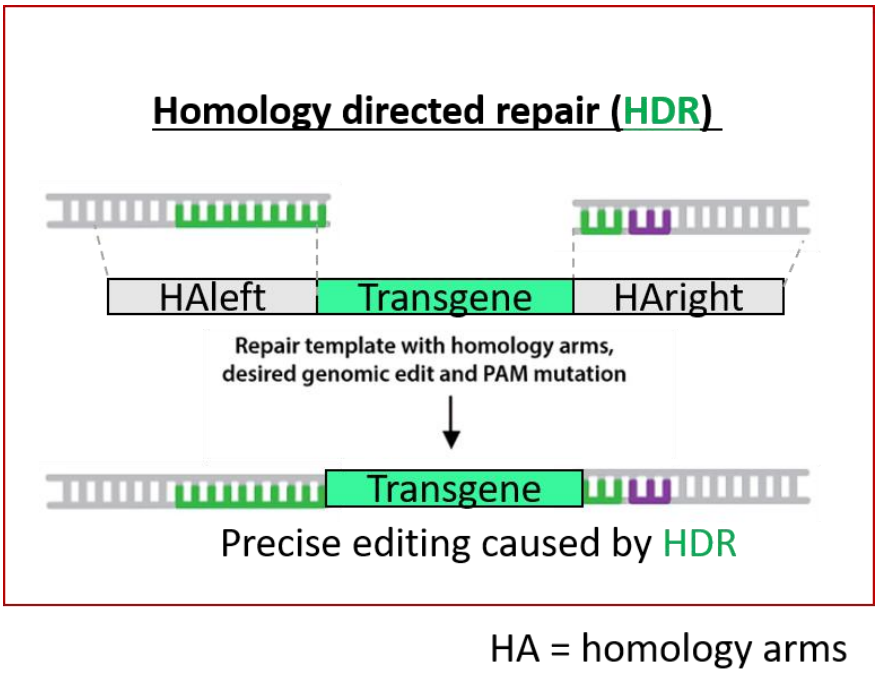

Figure 9. Integration of a transgene into target locus by homology directed repair (HDR). Integration of a donor DNA carrying a transgene, which is flanked by homologous sequences (homology arms, HA). These HAs are homologue to proposed CRISPR/Cas cleavage site. The donor DNA serves as a template for HDR in dividing (S and G2 phase) cells after CRISPR/Cas-induced DSB (182).

Besides differences in the architecture of the guide RNAs, the CRISPR/Cas9 system recognizes 3´-NGG-5´ as binding site to create DSBs upstream of the PAM, while the CRISPR/Cas12a system recognizes a T-rich PAM, 3´-TTTV-5´, and generates DSBs downstream of its PAM (Figure 10) (190, 191). Both nucleases are powerful tools for genome editing in specific genomic contexts. Whereas Cas9 may be better suited for editing GC-rich regions, Cas12a might be more effective for editing AT-rich regions (Figure 10) (169, 176, 192–194). Since there are different ways to introduce the CRISPR/Cas system into target cells or organisms, e.g. as riboprotein complexes (RNPs) (195), as plasmid (196), or as part of a lentiviral system (33), the consequences of each of these systems for target organisms have to be considered. Furthermore, systems have been established for *C. elegans*, as CRISPR/Cas9 has been integrated into the genome. In those systems, Cas9 is expressed under the control of either a constitutively active or inducible promoter (196). Nevertheless, the use of lentiviral-mediated genomically integrated Cas12a systems should be carefully considered as they can cause off-target effects (172, 197).

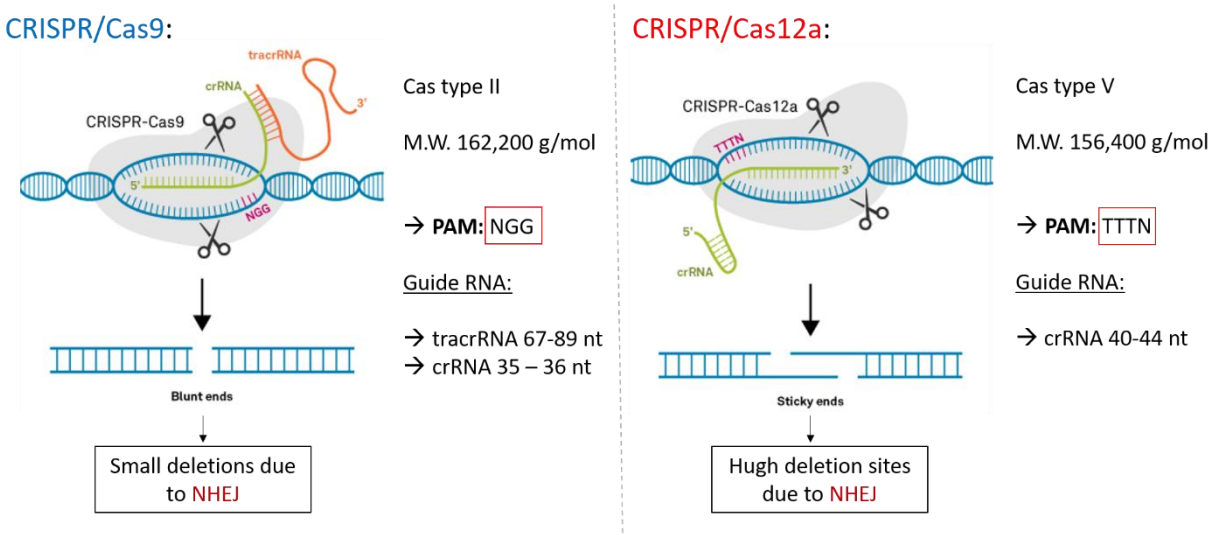

Figure 10. Functional comparison between the CRISPR/Cas9 and CRISPR/Cas12a systems. The CRISPR/Cas9 system is composed of a crRNA specific for a target DNA sequence. Here, binding of crRNA by a tracrRNA is indispensable for the enzymatic activity of the Cas9 endonuclease. On the other hand, the CRISPR/Cas12a system is composed of a single crRNA guiding the Cas12a endonuclease to target sequence. Here, the crRNA acts as guide but also as tracrRNA. The crRNA is processed by Cas12a itself without the binding of a tracrRNA, which compared to Cas9 is a unique feature of the CRISPR/Cas12a system. Illustration modified according to Wey 2018 (198).

Recent studies have demonstrated the effectiveness of CRISPR/Cas in editing the genome of *S. mansoni* (169–172), making it a compelling tool to overcome previous technical limitations and thus achieve precise transgene integration. One of the most promising candidates is a previously characterized schistosomal genomic safe harbor site (GSH), for which facilitating constitutive expression of a transgene during the parasitic lifecycle without affecting the genome integrity was demonstrated (172). Based on an approach applying the CRSIPR/Cas9 system and using three overlapping gRNA sequences that target a schistosomal GSH, the integration, as well the expression of a reporter-gene , was achieved (172). However, this work failed in introducing these edited life stages into the parasitic life cycle. Nevertheless, based on these promising data, the establishment of a transgenic *S. mansoni* has become feasible.

1.6 Aims

Comparative transcriptome studies of adult *S. mansoni* and their isolated gonads revealed the pairing-dependent and ovary-specific transcription of several NRs (55, 61, 62). Recent studies highlighted the essential role of NRs in schistosome maturation and tissue homeostasis (49, 87, 104). This thesis aimed to elucidate the function of yet uncharacterized type II NRs, including retinoic acid receptors (Smp_097700, SmRXR1) and Smp_144170, SmRAR) and thyroid hormone receptors (Smp_134490, SmTHRα and Smp_174260, SmTHRβ) in *S. mansoni* reproductive biology, given their known potential roles in tissue homeostasis, germ cell development, and fertility in vertebrate models (85, 98, 107–109, 122). The project also aimed to establish a CRISPR/Cas-based editing method to generate stably transformed *S. mansoni*. To provide an alternative, my plan was to find ways to chromosomally introduce a reporter-gene into the previously identified GSH1 of *S. mansoni* (172), and to reintegrate edited life stages back into the life cycle as a prerequisite for the first transgenic schistosome line. In detail, objectives of this study were:

1) To verify the annotations of NRs by *in silico* analyses, such as phylogenetic, domain and protein structure studies.
2) To verify the bioinformatics data with respect to NRs potentially involved in oocyte development, to confirm the RNA-Seq-based transcript profiles of the receptor-coding genes by RT-qPCR, and to localize transcript occurrence by whole mount *in situ* hybridizations (WISH).
3) To functional characterize selected NRs by RNAi in adult *S. mansoni*. Phenotype analyses included physiological assays (worm viability, pairing stability, and egg production), cell biological assays (stem cell proliferation, EdU assays), and morphological analyses (bright-field and confocal microscopy with a focus on the female gonads and eggs). In addition, the influence on the sexual maturity of female schistosomes should be determined by analyzing the transcript profiles of meiosis-associated marker genes and genes that were predicted *in silico* as protein-protein interaction partners. Finally, first-time pairing experiments were done *in vitro* to investigate RNAi effects on sexual maturation in virgin females and couples.
4) The establishment of the CRISPR/Cas method in combination with multiple transformation methods for stable integration of an eGFP reporter-gene construct into GSH1. For this, I aimed to identify a native promoter and terminator, which was able to ensure constitutive reporter-gene expression in all parasitic life stages and among all tissue types.
5) In this context, the efficiencies of different Cas enzymes should be tested as well as various ways to reintegrate the edited life stage(s) into the life cycle to generate a transgenic *S. mansoni* line.

2 Material

2.1 List of chemicals

Chemicals used in this work are listed in Table 1.

Table 1. Chemicals used in this work

Chemical	Manufacturer	Reference
Acetic acid	Roth	3738.5
Agarose	Roth	2267.3
Bovine serum albumin (BSA)	Roth	8076.1
Blocking reagent	Roche	11096176001
5-bromo-4-chloro-3-indolylphosphate (BCIP)	Roche	11681451001
Brij35	Roth	9002-92-0
Calcium chloride ($CaCl_2$)	Roth	CN93.1
Carmin powder, CertistainH	Sigma-Aldrich / Merck	C1022
CH 55 (4-[(1E)-3-[3,5-bis(1,1-dimethyletyl)phenyl]-3-oxo-1propen-1-yl]-benzoic acid	Cayman	110368-33-7
Deionized formamide	Roth	P040.2
Diethylpyrocarbonate (DEPC)	Roth	K028.3
Dextran sulfate	Roth	5956.4
3,5-Diiod-L-Thyronon	Sigma-Aldrich	D0629
Dimethyl sulfoxide (DMSO)	Roth	A994.1
Dithiothreitol (DTT)	Roth	6908.1
5-ethynyl 2´-deoxyuridine (EdU)	Invitrogen	A10044
Ethanol	Roth	9065.4
Euparal	Roth	7356.1
FluorCare ROTIMount	Roth	HP19.1

Chemical	Manufacturer	Reference
Formaldehyde	Roth	4979.1
Formamide	Roth	6749.1
Glycerol	Roth	7530.1
HCl	Roth	T134.1
2-4-(2-hydroxyethyl)-1-piperazinyl ethane sulfonic acid (HEPES)	Roth	6763.3
Isopropanol (2-Propanol)	Roth	9781.1
Lithium chloride (LiCl)	Roth	P007.1
Magnesium chloride ($MgCl_2$)	Roth	KK36.3
Methanol	Roth	4627.1
MES (2-morpholinoethanesulfonic acid)	Sigma-Aldrich	M3671
Nonident-P40 substrate/substitute	Sigma-Aldrich	74385
Orange G	Roth	0318.2
Oil Red O	Merck	1320-06-5
PEG10 (Bis-PEG10-NHS ester)	BroadPharm	BP-22588
Percoll	Sigma-Aldrich	P1644
Polyvinyl alcohol, 30-70 kDa (PVA)	Sigma-Aldrich	341584
Propane 1,2-diol (Proylenglycol)	Sigma-Aldrich	614416
RA 9cis-retionoic acid	Sigma-Aldrich	19643
Spermidin	Sigma-Aldrich	85558
Sodium hypochloride	Roth	9062.3
Sodium chloride (NaCl)	Roth	3957.1
Sucrose	Sigma-Aldrich	S0389
Trehalose (α,α-Trehalose)	Sigma-Aldrich	T9449

Chemical	Manufacturer	Reference
Tricain (ethyl 3-aminobenzoate methanesulfonate	Sigma-Aldrich	A5040
Triton X-100	Roth	3051.3
TritonX-405	Merck	X405
Trisodium citrate 2-hydrate	Roth	3580.3
Tween20	Roth	9127.2
Tween80	Sigma-Aldrich	P1754
Yeast RNA	Roche	10109223001

2.2 Buffers

Buffers and solutions used in this work are listed in Table 2.

Table 2. Buffers and solutions

Name	Composition	Application
AFA	2% (v/v) Acetic acid 1.1% (v/v) PFA 66.7% (v/v) Ethanol in DEPC-water	Carmine red staining
AP buffer	100 mM Tris (pH=9.5) 100 mM NaCl 50 mM MgCl2 0.1% (v/v) Tween20 in PVA solution	WISH
Bleaching solution	5% (v/v) Deionized formamide 0.5x SSC 1.2% (v/v) H_2O_2 in DEPC-water	EdU staining, WISH
$CaCl_2$	2.5 M in nuclease free water (NEB) 0.2 µm filter sterilized	Particle bombardment
Carmine red solution	2.5% (w/v) Carmine red 2.5% (v/v) HCl (37%) 92.5% (v/v) Ethanol (90%) in H_2O	Carmine red staining
CBSS+T	NaCl 2.8 g/l KCl 0.15 g/l Na_2HPO_4 0.07 g/l $MgSO_4$*7xH2O 0.45 g/l $CaCl_2$*2xH2O 0.53 g/l $NaHCO_3$ 0.05 g/l Glucose 1 g/l Trehalose 1 g/l Abam 1% (v/v) In H2O	*In vitro* culture of sporocyts
10x CRISPR/Cas reaction buffer	200 mM HEPES 1 M NaCl 50 mM $MgCl_2$ 1 mM EDTA pH=6.5	Cas9/Cas12a activity assay
Colorimetric block solution	7.5% (v/v) Horse serum in TNT buffer	WISH
Developing buffer	450 µg mL^{-1} NBT 175 µg mL^{-1} BCIP in AP-buffer	WISH

Name	Composition	Application
10x DNA loading buffer	25% (v/v) Glycerol 0.2% (w/v) Orange G in TAE buffer	Agarose gel electrophoresis
Heparin	25,000 U mL−1 Heparin sodium in H_2O	Perfusion medium
Hybridization buffer	50% (v/v) Deionized formamide 10% (w/v) Dextran sulfate 5 x SSC 1 mg mL^{-1} Yeast t-RNA 1% (v/v) Tween20 in DEPC-water	WISH
WISH $MgCl_2$ solution	0.6 M $MgCl_2$ Add DEPC-water or in 100 mM Tris (pH=7.4)	WISH
Narcotics	1.9% (v/v) Ketamine 6.2% (v/v) Xylavet 0.9% (v/v) NaCl in H_2O	Perfusion
10x PBS (phosphate buffered saline)	1.37 M NaCl 27 mM KCl 100 mM Disodium hydrogen phosphate 17.5 mM Potassium dihydrogen phosphate in DEPC-water pH=7.0 – 7.2	WISH, washing of *S. mansoni*
PBSTx (PBS/Triton X-100)	0.3% (v/v) Triton X-100 in DEPC-PBS	EdU staining, WISH, lipid staining
PEG solution	20% (w/v) PEG 8000 20 mM $MgCl_2$ in DEPC-water	DNA clean up
Prehybridization buffer	50% (v/v) Deionized formamide 5x SSC 1 mg mL^{-1} Yeast t-RNA 1% (v/v) Tween20 in DEPC-water	WISH
PVA	10% (w/v) PVA In DEPC-water filter sterile	WISH
Sodium acetate	3 M Sodium acetate in DEPC-water pH=5.2	WISH
Snail water	0.3% (v/v) Snail water solution I 0.2% (v/v) Snail water solution II 0.04% (v/v) Snail water solution III in H_2O	Culture of *Biomphalaria glabrata* (*B. glabrata*)
Snail water solution I	1 M CaCl2 0.35 M $MgCl_2$ in H_2O	Culture of *B. glabrata*

Name	Composition	Application
Snail water solution II	21.71 M Potassium carbonate 273.78 M Sodium hydrogen carbonate in H_2O	Culture of *B. glabrata*
Snail water solution III	0.6 M NaOH in H_2O	Culture of *B. glabrata*
20x SSC (saline-sodium citrate)	3 M NaCl 0.3 M Trisodium citrate 2-hydrate in DEPC-water pH=7.0	WISH
50x TAE (Tris/acetate/EDTA) buffer	50 mM EDTA 2 M Tris 1 M Glacial acetic acid in H_2O pH=8.0	Agarose gel electrophoresis
TNT (Tris/NaCl/Tween) buffer	0.1 M Tris 150 mM NaCl 0.1% (v/v) Tween20 in DEPC-water pH=7.5	WISH
10x transcription buffer	0.4 M Tris (pH 8.0) 0.1 M MgCl2 20 mM Spermidine 0.1 mM DTT in DEPC-water	Synthesis of dsRNA and riboprobes
Tricain	0.25% Tricain in PBS	Separation of *S. mansoni* couples
Tris buffer	100 mM Tris in H_2O pH=7.4	DNA isolation
TS-solutiuon	0.5 g Brij35 0.5 g Nonident P-40 0.5 g Tween80 0.5 g TritonX-405 In 100 mL RNase free PBS	Organ isolation
Yeast t-RNA	1% (w/v) Yeast t-RNA in deionized formamide	WISH

2.3 Media

The media for the *in vitro* cultivation of *S. mansoni* and *E. coli* are listed in Table 3.

Table 3. Medium and additives

Name	Working concentration
Perfusion Medium	
M199 (powder, Gibco)	1% (w/v)
HEPES buffer (pH=7.4)	12.5 mM
Tris buffer (pH=7.4)	20 mM
Glucose	0.1% (w/v)
Heparin	0.01% (v/v)
In H_2O	
Medium for *in vitro* culture of adult *S. mansoni*	
M199^{+++}	
In M199 (liquid, Gibco)	
Antibiotic-antimycotic solution (Abam)	1% (v/v)
HEPES buffer (pH=7.4)	1% (v/v)
NCS	10% (v/v)
pH=7.3 – 7.4	
Basch ABC/LDL	
In Basal Medium Eagle (powder, BME, Sigma-Aldrich)	
D-Glucose	1% (w/v)
HEPES buffer (pH=7.4)	1% (v/v)
Lactalbumin	1% (w/v)
$NaHCO_3$	2.2 (w/v)
Hypoxanthine (100 mM stock solution)	0.5% (v/v)

Name	Working concentration
Hydrocortison (100 mM stock solution)	0.1% (v/v)
Triiodothronin (20 mM stock solution)	0.1% (v/v)
Insulin (8 mg/ml stock solution)	0.1% (v/v)
Schneiders´ medium	5% (v/v)
100x MEM vitamins	0.5% (v/v)
Ascorbic acid	200 µM
Human washed red blood cells (RBCs; (10% suspension in M199)	0.2% (v/v)
Human low-density lipoprotein (LDL; TRINA, Switzerland)	2.5% (v/v)
NCS	10%
Antibiotic-antimycotic solution (Abam)	1% (v/v)
pH=7.3 – 7.4	
M199egg - Medium for *in vitro* culture of *S. mansoni* eggs	
In M199 (liquid)	
Human low-density lipoprotein (LDL; TRINA, Switzerland)	0.25% (v/v)
NCS	20%
Antibiotic-antimycotic solution (Abam)	1% (v/v)
pH=7.0	
M199sporo - Medium for the *in vitro* culture of *S. mansoni* sporocyts	
M199 (liquid)	48% (v/v)
CBSS+T	48% (v/v)
7d Bge-cell conditioned StemMACS iPS-Brew XF medium (Miltenyi)	5% (v/v)
Antibiotic-antimycotic solution (Abam)	1% (v/v)
pH=7.0	

Name	Working concentration
Bge-medium - Medium for *in vitro* culture of *B. glabrata* embryonic cells (Bge-cells)	
Schneiders´ medium (liquid, Gibco)	22% (v/v)
Lactalbumin	1% (w/v)
FCS	10% (v/v)
Antibiotic-antimycotic solution (Abam)	1% (v/v)
in H_2O	
pH=7.0	
LB-medium – cultivation of *E. coli*	
Trypton	1% (w/v)
Yeast extract	0.5% (w/v)
NaCl	0.5% (w/v)
in H_2O	
pH=7.0	

2.4 Dyes and conjugates

Dyes used in this study with their working concentration are listed in Table 4.

Table 4. Dyes used in this study

Dye	Manufacturer	Reference	Concentration/Dilution
Calcein AM	Invitrogen	65-0853-39	5 - 25 nM
GelRed nucleic acid gel stain	Biotium	41003	1: 40 000
Hoechst 33342	Thermo Fisher Scientific	62249	2 µM
SYTOX Orange	Thermo Fisher Scientific	S11368	5 µM

2.5 Enzymes

The Enzymes used in this work are listed in Table 5.

Table 5. List of enzymes used in this work

Enzyme	Manufacturer	Reference	Application
AccuPrime Taq DNA-Polymerase	Invitrogen	12346086	PCR
AdHI	NEB	R0584S	Cloning
Alt-R S.p. Cas9 Nuclease V3	IDT	1081058	Genome editing
Alt-R A.s. Cas12a (Cpf1) V3	IDT	1081068	Genome editing
Alt-R L.b. Cas12a (Cpf1) Ultra	IDT	10007922	Genome editing
Collagenase Type II	Sigma-Aldrich	C2-22-1G	Egg isolation
Dispase II	Roche	04942078001	Egg isolation
DNase I (RNase-free)	NEB	M0303L	dsRNA/probe synthesis
DNAse I	Sigma-Aldrich	DN25-100MG	dsRNA synthesis
Elastase Type IV	Sigma-Aldrich	E0258	Organ isolation
FirePol DNA Polymerase	Solis Biodyne	01-01-00500	PCR
Hyaluronidase	Sigma-Aldrich	H3506-5G	Egg isolation
Proteinase K	Roche	03115801001	*in situ* hybridization
Q5 High Fidelity DNA Polymerase	NEB	M0491S	PCR
SP6 RNA Polymerase	Roche	RPOLSP6-RO	*in situ* hybridization
T3 RNA Polymerase	Roche	RPOLT3-RO	*in situ* hybridization
T7 RNA Polymerase	Selfmade	**-**	dsRNA synthesis
Trypsin-EDTA	Corning	25-053-CI	egg permeabilization
T4 DNA Ligase	NEB	M0202L	Cloning
RNase inhibitor	NEB	M0314S	dsRNA/probe synthesis

2.6 Kits

Kits used in this work are listed in Table 6.

Table 6. Kits for molecular biological applications

Product	Manufacturer	Reference	Application
Agilent RNA 6000 Nano Kit	Agilent Technologies	5067-1511	RNA Isolation
Agilent RNA 6000 Pico Kit	Agilent Technologies	5067-1513	RNA Isolation
Agilent DNA 1000 Kit	Agilent Technologies	5067-1504	Next generation sequencing (NGS)
Bio-Spin 30 column	BioRad	7326223	DNA purification
Click-iT Plus EdU Alexa 488 Imaging Kit	Invitrogen	C10637	Imaging of proliferating cells
DNAzol	Thermo Fisher Scientific	10503027	Isolation of gDNA
GoTaq Green Master Mix DNA Polymerase Kit	Promega	M7122	PCR
Q5® High-Fidelity DNA Polymerase Kit	NEB	M0515	PCR
Monarch DNA Gel Extraction Kit	NEB	T1020	Isolation of DNA fragments
Monarch PCR & DNA Cleanup Kit	NEB	T1030	Isolation of DNA fragments
Monarch Plasmid Miniprep Kit	NEB	T1010	Isolation of plasmid DNA
Label IT Nucleic Acid Labeling Kit, CX-Rhodamine	Mirusbio	MIR 3125	sgRNA labelling
RNAzol RT	Sigma-Aldrich	19533	Isolation of RNA
QuantiTec Reverse Transcription Kit	Qiagen	205313	cDNA synthesis
SuperScript IV Reverse Transcriptase Kit	Invitrogen	18090010	cDNA synthesis

2.7 Antibodies

Antibody for the execution of whole *in situ* hybridization (WISH) are listed in Table 7.

Table 7. Anti-Digoxigenin-POD antibody used in this work

Antibody	Supplier	Reference	Source
Anti-Digoxigenin-POD, Fab fragments	Roche	11207733910	Sheep

2.8 Molecular weight standards

DNA ladders used for DNA gel electrophoresis can be found in Table 8.

Table 8. DNA ladders used in this work

Ladder	Supplier	Reference
HyperLadder 50 bp	meridian bioscience	BIO-33054

2.9 Plasmids and plasmid backbones

Plasmid backbones used for cloning for WISH/RNAi and reporter-gene constructs are listed in Table 9.

Table 9. Plasmid backbones

Name	Application
pJC53.2	Riboprobe/dsRNA synthesis/cloning vector
pBluescript	Cloning vector
pET30a	Protein expression / cloning template

2.10 Primer sequences

Primer sequences for amplification of PCR fragments for cloning WISH/RNAi plasmids are listed in Table 10.

Table 10. Primers for WISH/RNAi constructs

Name	Sequence 5´- 3´
WISH Smp_144170 SmRAR fw	TAT TGA GTT CCT TTA TCT TAC CAG A
WISH Smp_144170 SmRAR rev	AGC GAC AAA CAC TCG ATC CA
WISH Smp_097700 fw	CAA TCC AAA CCA TAG CGA ATT CC
WISH Smp_097700 rev	GAC TGA GAA ACA GTA AGA GAA TT
WISH Smp_134490 fw	GTA AAC GTG CTG AAT CTG ATA AT
WISH Smp_134490 rev	GAT GAT GTG GTT GAT GAT GAT TAG TAC TT
WISH Smp_174260 Fw	CGT ACT TGA TGA AGA TAA ACG TTT A
WISH Smp_174260 Rev	ACA ACT GAA TTC TAT TGA TGG ATT C
WISH Smp_333540 SmMeiob fw	TTT GCA GTT GTT TCA GAA ATA AAG CAC CC
WISH Smp_333540 SmMeiob rev	GAC TTT GTA GAT CTC TGG TTG GGC TG
WISH Smp_163290 SmNcor fw	TTT CTA TCT AAT ATG TGT GAT ACA ATA TCC C
WISH Smp_163290 SmNcor rev	AGG GGG GCG TTT TTG GTT CCC TT
WISH Smp_266960 SmGli1 fw	AAT ACC ACT ACT CTT ACT ACT ACT ACT ACC ATT A
WISH Smp_266960 SmGli1 rev	CTG CCG TAT TGT TGG ATT TGA AAT TAT AAT TAT TAT TG
WISH Smp_165360 SmMyst4 fw	CAT CCA ACT CAC ATA ATT ATA AAC CA
WISH Smp_165360 SmMyst4 rev	CCA TCT TTT TTA ACA GGC GG
WISH Smp_013540 SmTYR2 fw (49)	CGA TAT AAT ATA TTA TCA TTT TCT CC
WISH Smp_013540 SmTYR2 rev (49)	GTC AAT ACT CGA AAG TTT GGC C
WISH Smp_055740 SmNanos-1 fw (199)	TGA TAT CGA AAT CGT CCA GAC A
WISH Smp_055740 SmNanos-1 rev (199)	TTG TAT CGG TTC CAA CAA ACC
Ampicillin fw (152)	GAG TAT TCA ACA TTT CCG TGT CGC
Ampicillin rev (152)	CGG TTC CCA ACG ATC AAG GC
GFP-RNAi fw (152)	GCA ACA TAC GGA AAA CTT ACC C
GFP-RNAi rev (152)	CGT TGG GAT CTT TCG AAA GGG
Neomycin fw (152)	TAA TAC GAC TCA CTA TAG GGA GA G TGG AGA GGC TAT TCG GCT
Neomycin rev (152)	TAA TAC GAC TCA CTA TAG GGA GA C ATC CTG ATC GAC AAG ACC
T7_extended (152)	CCT AAT ACG ACT CAC TAT AGG GAG

Primers for performing quantitative RT-PCRs are listed in Table 11.

Table 11. List of RT-qPCR Primers

Name	Sequence 5´- 3´
qRT Smp_144170 SmRAR fw	ACA TAT GAC TTG TGA TAG TAT AAC TGC TC
qRT Smp_144170 SmRAR rev	CAC AAT AAC GAC GTA ATA ATT CAG CCC
qRT smp174260 THRb 1 fw	GAT GCA GAG CTT CAC GTT CA
qRT smp174260 THRb 1 rev	GCA TTC GGT CGG AGG TAA TA
qRT smp097700 RXR 2 fw	GTC GGC TGA ATT AAG CAT GG
qRT smp097700 RXR 2 rev	AAA ACA CTG GCA ACT GAC GAG
qRT smp134490 THRa 1 fw	AAC AAC AGC GAC AAC ACC AC
qRT smp134490 THRa 1 rev	CTG CCA TCA TTG CAA CAT CT
qRT Smp_013540 SmTYR2 Fw (49)	ACA GCA TTC CCA ACA ACT CA
qRT Smp_013540 SmTYR2 Rev (49)	CAC CGG GAA AAG AAC AAA AT
Smp_131110 (Smp14) _qPCR_for (57)	CCT ATG GCG GTG ATT ATG G
Smp_131110 (Smp14) _qPCR_rev (57)	GGC TGG GTT TGT AAG TGC
Smp_333540 SmMeiob fw	TGC TGG ATA TGC CTG TAC ATT CGC C
Smp_333540 SmMeiob rev	ACC TGG AGT AGC GCA CAT TGC AAA C
qRT Smp_163290 SmNcor fw	CAG TCA CAA CTC AAC GCT CTG GCA G
qRT Smp_163290 SmNcor rev	GTC AGT CAC AAC TCA ACG CTC TGG C
qRT Smp_123420 SmDarnt fw	GCG CTT CCC AAC GCC ATA ATT CTC C
qRT Smp_123420 SmDarnt rev	ACA CTG GAT AGC TGA ACC TAG GCG C
qRT Smp_078720 SmBmpg fw	GGC GCT CTT GGA CCT CGC ATT TTT A
qRT Smp_078720 SmBmpg rev	GCA AGG GAA GTT CGT AGG ACC ATG C
qRT Smp_266960 SmGli1 qRT fw	GGA ACC AGG CCA TTC AAG GCT CAG TAC
qRT Smp_266960 SmGli1 qRT rev	ATT CTG ATG TTT AGC TCT GTC GGA TGC ATT AC
SmFGFR-A Smp_175590 qrt fw (200)	TGC ATG TAC CCA AGA GGA ATC A
SmFGFR-A Smp_175590 qrt rev (200)	GAT ATG GTG AAT TGC CCA AAC TG
SmFGFR-B Smp_157300 qrt fw (200)	CAC AGA AGG AGA TGT GTC TGA A
SmFGFR-B Smp_157300 qrt rev (200)	TTC CCG TAA GGA GCA TAT TCC A
qRT GFP-Analysis Pr (180) fw	CAACAGCCACAACGTCTATATCA
qRT GFP-Analysis Pr (180) rev	ACTGGGTGCTCAGGTAGTGGT
eGFP-2021-5´	CAA GGA CGA CGG CAA CTA CA
eGFP-2021-3´	GAC TGG GTG CTC AGG TAG TG
SmLETM_qPCR2_fw (201)	CGT GGA ATG CGT TCA GTT GG
SmLETM_qPCR2_rev (201)	GAA GCT GAT GGA GGT AAT TGAG
RT-PCR Smp_056970 SmGAPDH_fw (189)	ATG GGA CAT TTC CAG GCG AG
RT-PCR Smp_056970 SmGAPDH rev (189)	CCA ACA ACG AAC ATG GGT

Primers for the amplification of fragments for downstream analysis of Cas9 or Cas12a induced editing of the GSH1 or Smp_174260 locus are listed in Table 12. These fragments were analyzed using either Sanger direct sequencing or next generation sequencing.

Table 12. Primers for the generation of DNA libraries to analyze the Cas-mediated knock-out efficiency of target locus

Name	Sequence 5´- 3´
TIDE analysis (202)	
GSH3757 (GSH1) TIDE Fw	GAT GAG TGC ATC GAT CGA TTA CTA AGG AAT TG
GSH3757 (GSH1) TIDE Rev	GAC TCC TGA TTG AGG GTT GCA GGT G
Smp_174260 thr-β 1 TIDE fw	ATC TTC TCG GTA CTG TTT TAT TTT ACT TTA GTT C
Smp_174260 thr-β 1 TIDE rev	AGT TAC GTG ATG GTG ATG ATA ATA ATT GTG
Illumina sequencing (NGS) (203)	
NGS GSH3757 (GSH1) fw	ACA CTC TTT CCC TAC ACG ACG CTC TTC CGA TCt cct tt agt tat ggc taa ttt tta aca acc g
NGS GSH3757 (GSH1) rev	GAC TGG AGT TCA GAC GTG TGC TCT TCC GAT CT tgt at tta att ttg agg tag tag gtc aaa c

NGS, next generation sequencing; capital letters, Illumina adapters; small letters, GSH1-specific primer sequence

Primer sequences for the amplification of PCR fragments for the cloning of reporter-gene constructs using Gibson assembly are listed in Table 13.

Table 13. Primers to assemble reporter-gene constructs

Name	Sequence 5´- 3´
Promoter Smp_335990 fw	CCT TTC CAG ATT GTC TCC GA
Promoter Smp_335990 rev	CGT AAG GTC TAT CGT TTA CAC T
Terminator Smp_335990 fw	TGG AGG TTA ACT TTA ATT TTG
Terminator Smp_335990 rev	CCA AAG GTA TTG CGA ACT
eGFP (start codon) fw	ATG GTG AGC AAG GGC GAG
eGFP rev	CTT GTA CAG CTC GTC CAT
Gibson pJC53.2 x SmUbiProm fw	GGA GAA TTA ACC CTC ACT AAA GGG AGA CCT TCC TTT CCA GAT TGT CTC CGA
Gibson SmUbiProm fw x eGFP rev	GGA GAA TTA ACC CTC ACT AAA GGG AGA CCT TCC TTT CCA GAT TGT CTC CGA
Gibson eGFP x SmUbiTer fw	GCA TGG ACG AGC TGT ACA AGT GGA GGT TAA CTT TAA TTT TG
Gibson SmUbiTer x pJC53.2 fw	GGG AGA TTT AGG TGA CAC TAT AGA AGT GAC CTT CCA AAG GTA TTG CGA ACT AC

5'-modified primer sequences for amplifying the dsDNA donor for transgene integration into the *S. mansoni* GSH1 are listed in Table 14.

Table 14. Primers to generate the 50 bp HA containing knock-in dsDNA donor

Name	Sequence 5´- 3´
5´(C6)amin-donor SmUbi-eGFP fw	5´(C6)amin - ATG CCA CAA GTG TTT ACA AGG AAA ATG ATA CCT CGA GAT CAA TTA TCT GA cct ttc cag att gtc tcc g
5´(C6)amin-donor SmUbi-eGFP rev	5´(C6)amin - ACA CCA TCC CAA TTC CAG CTA TTG AAC CAG CCT TCA TCT ACC GAG TTC CA cat agc gac gca tac cac aca caa g

Capital letters, 50 bp GSH1 homology arms (HA); small letters: donor-specific-primer sequence

Primers for the amplification of the CRISPR/Cas-mediated integration of a reporter-gene into the *S. mansoni* GSH1 by homologous-directed repair are listed in Table 15.

Table 15. Primers for the amplification of a transgene after HDR induced incorporation into the target locus

Name	Sequence 5´- 3´
GSH1 primer fw	GTG TAT TTC CTA TGC TAT GAA AAT ACC T
Ubi-Prom HA left rev	ATT GAG GAC CGT TCA GAT CGT GTC
eGFP-Ubi-Ter fw	CAT GGA CGA GCT GTA CAA GTG AGA GGT TAAC
GSH1 primer rev	GGT TCC ATA CTA TGC AGT TTC CTT AAA C
eGFP-2021-5'	CAA GGA CGA CGG CAAC TAC A
eGFP-2021-3'	GAC TGG GTG CTC AGG TAGT G

2.11 Single guide RNA sequences

The single guided RNAs (sgRNA) used for the assembly of CRISPR/Cas riboprotein complexes and the RNA guided editing of the GSH1 or the Smp_174260 are listed in Table 16 or 17, respectively.

Table 16. Single guide RNAs for editing the *S. mansoni* GSH1

Name	Enzyme	Target locus	Sequence 5´- 3´
sgRNA GSH1 Cas9	Cas9	*S. mansoni* GSH1	GAG AUC AAU UAU CUG ACA AU
sgRNA GSH1 Cas12a	Cas12a	*S. mansoni* GSH1	GAG AUC AAU UAU CUG ACA AUG GAA
control sgRNA	Cas9/ Cas12a	scrambled sequence	GCA CUA CCA GAG CUA ACU CA

Table 17. Single guide RNAs sharing overlapping sequences for the knock-out of the potential thyroid hormone receptor Smp_174260

Name	Enzyme	Target locus	Sequence 5´- 3´
sgRNAthr-β 1	Cas12a	Start codon Smp_174260	GUA CUA GCA UUA UCU CAA UAU AUU
sgRNAthr-β 2	Cas12a	Start codon Smp_174260	UUU CGU ACU AGC AUU AUC UCA AUA
sgRNAthr-β 3	Cas12a	Start codon Smp_174260	UGU AAA UAA UUU UGU UUC GUA CU

2.12 WISH, RNAi, and reporter-gene constructs

The sequences cloned into the pJC53.2 backbone and used to synthesize WISH ribo-probes and dsRNA to perform RNAi experiments are listed in Table 18.

Table 18. Sequence information of the pJC53.2 based *in vitro* transcription constructs for WISH-probe and dsRNA synthesis

Smp_144170 Sm*rar* WISH probe / dsRNA sequence 5´- 3´
TATTGAGTTCCTTTATCTTACCAGATGAGCCATTGTCCTGTAGAATATTCAAATCCTAATTCCCAGAATACTATATCTTATA TTACCTCAGATTCTGTGATTAGTGTCTCATTCGCAGATTGTCAGTCGTCTAGTCCTTCATACCACTCTCTGTCATCAAGTA CAGCCCTTCCTGGTGTTGGCTCTTTCTTAGATAAATCAAATCACCTTCCCCACTATTCTCCTAATAAATATTATGATACAGA ACCTACTGCAATTCCGGGACACTCTTATGTTGAAAACACTGACGTTTTCGACAACAATCTTCCTTATCCAATAAAATCGGA GGCCATTCATGAAACAGTATCTGGGACGTTTATTACTCCAGATGCACACAACGAATCATGTTTTACATCTCCTTTACAACC TCTAAAATCATTAAACCCAAGTCTTCCTGTCCAATCTAGTGAATCTTTGTTAAGTGGTTTCACTCATCCACTTTCTATGGAC CATACCGTTTTAGAAGACGGTGGATTAGATTTGGATCGAGTGTTTGTCGCT
Smp_097700 Sm*rxr-1* WISH probe / dsRNA sequence 5´- 3
CTAATAATGTACTACTATCCGACGAAACAGATCTACCTAATTTAACATTACGATGTTTACTGTCGGCTGAATTAAGCATGG ATCCTAAATTGGCTGTATCAGAAAGAGGTGAAGCAATTTATGAAGATATACCTGGTGATGATGATACTGGTTTACATCCAT TGACCATAATCTGTCAGTCTATTGAACAACAATTACCTCGAATAGTTAATTGGGCTCGTCAGTTGCCAGTGTTTTCATCTG TCTATCTTAGTTTTGATGATCAATTTTGTTTAATAAAAGCTGCTTGGCCTGAATTAGTTTTAATCAGCTCAGCGTATCATTC AACTGTTATTAGAGACGGTTTGCTTTTATCGATTGGACGTCATCTTGGTAGAGAGGTGGCTAAATCACATGGTCTAGGTC CTCTTGTTGATAGAATTCTTCATGAACTTGTTGCACGTTTTCGTGATTTATCGTTACAAAGAACTGAATTAGCTTTACTACG TGCTATTATTCTTTTTAATCCTGATGCTAATGGCTTGTCATCACGTCATCGCGTGGAAGCTGTCAGGGAGCAGCTTTATTC AG
Smp_134490 Sm*thrα* WISH probe / dsRNA sequence 5´- 3´
CACATTTATCACCAACTGATGGTAATTCAACTCAATTACATATATCTACAAATCTTAGTCCAACAATACAATCCTACTAATA ATCTTGATCAACATAATTCAACATCAATTCAACCAACAATATATGATCCAAATTGTGCTATGCTTCCATTATTACAAACATC ACCAACAAGAAATAATCTTATCTATTCCGATGGAAATTCTCCTATAAATCAACATAGTCCTATGTAAGTACTAATCATCATC AACCACATCATCATCAACATCATCAACATCATCATCAACAACATCCTACTGGCATCCACTTCAAGTACCAACAACAGATTT AATGCCAAATAATACACTTCATTCAAGTTCATTAGTGAATATATCTTCCAGTATTCCGTTAGATGAATCCAATCAACTATAT TGGTCAAATAATTCAACAATTGAGAATACATTTCATCATATCATCCATTAACTACTATACATAGTGGTATCAATCCAATTCA TCAACATCATC
Smp_174260 Sm*thrβ* WISH probe / dsRNA sequence 5´- 3´
TCGTACTTGATGAAGATAAACGTTTAGCTAAACGTCGTCTAATCGAAGCAAATCGAGCACGTAAAAGAGCTGAAGCTATA GAAGCCTCCACTGCTGTATATGTTACAGATCCATCAATTAATATCCCTAATATTACAAATCCTAATTCAGTATCAAAATATC ATATTATACACAATCAACCCATCTCTACATCGAACACCATCTCTAGTACACCTGTTATTATGTCGACGATTCCTTATCATTC TACAATCCATTCTAATATTCATTTTACTAATCAATTTGCACTCAATTCAACAACTAGAAGTCAGTTTAACTGTAATCCTATTC AAACACGTTATTTGGAGGTAACCAACAATGATATCCATTCATTTGTTAATCCAAAAACTCCAGATGCAACATATTCACCTG CAAATGAAGCAAAATTAATTGTACAACCTATTCAAACAATCGATAAATTACAACCAACTACTATGCCCAACAATATGTGCT GGAATCCTATATGCGGAGCTCCGTATACACAGTGCTTTATGAATGATGCTAGTAATCATGATAACCATAATTCTAAAACCC CACTTTCATTTAAAGAATCCATCAATAGAATTCAGTTGTCT
Smp_333540 Sm*meiob* WISH probe / dsRNA sequence 5´- 3´
TTTGCAGTTGTTTCAGAAATAAAGCACCCAAAAACCTTGATAATGTCTCAAAAAAAACCAAAGTGTGAGGAAGACGAGGA ATTTACAATACAAAATGGGAGTCTAACTAGCAAATCCAAGTCAATTCAGTCGATTGAAACAGTTCAAACGGTACTTCAGCT GTGTGAAGTTATGCTTTTTGATGATTCATGTAGCTGTCTTCCGCTAATCTTTTGGAATGAAGACTGGATTCACATTGCATT AACAGCTTTTATACCATATTCTACCGTTTTATCGATTGTGAACTGTCCAGTTCGTTACGATCGTTACCGCAAAGGTGTGGT TGCCTCTCCAAACTCAAAAACCCTAATTATTATCTCACCTGACTGTGCTGAGGCCAATCGTTTAAGTCAACACTCTAAACA TCAGACTCAAAGCATGAATATTTTGGAAAGTGGCCATACTTCTTTTGCTGTTGAGAATGTGGATGACAGACTATTACAACC TTTACCGATAGGATATAAAACAGCCCAACCAGAGATCTACAAAGTC
Smp_163290 Sm*ncor* WISH probe / dsRNA sequence 5´- 3´
TTTCTATCTAATATGTGTGATACAATATCCCGCTTACAATCCGAAAGCCATTTACCTTCGAATGCCCCACCACCAGGTTTG CGGATTGCCCCCAGCCCTGAGCAGGGTTATGCCAGTAGTATCAATCGGAATGGGAGGTCTGAAAGTTTTCCAAGTGGA GGTCCGGTTCTCACAACTGGGCCTCATGCAGGGTTGTTGACTCCGGAAGACATGCTTGCTGCAGCACAAATTTGTAGCC ATCTAAGTCAGTCACAACTCAACGCTCTGGCAGCTGCTTACCATCAACAGCAGCAACAAATTCAACGTTCTGTTGGCCCA ACTGCTTCAGGAACTTCAACTCTTGGTCACGTACCAGGAATTACATTTGCGCAGGCTCTAGCAGCCGTTACATCTGTATC GAAGTCATCATCTCCTACAATTCCTCTGGGTGTTCACAGCTCTCAACAGTCACCTCGATTGCCGGTTCACTCAGTCCAAA CACCTGTGCATCAAGGGAACCAAAAACGCCCCCC

Smp_266960 Sm*gli1* WISH probe / dsRNA sequence 5´- 3´
AATACCACTACTCTTACTACTACTACTACCATTAATAATCATATTAACACAACTTCTACTAATAATTATCAACAACAAAATGA CACTATGTATGACAATAATAATAATAATGTTGATAATGATATGAAAGTCAAATCATCTATGAATGATTGTATTAATGACAAT ACTATAAATGATACACATTCTACCACTGTTATCCACGCGGAGAATGAAAATCCTAGAAGACCAATACCGTTGACGAATAC ATCAAATTTGGAAGGTTCAACATCTAATGTCGGTGGTAACAGTAATTTCCAAACAATGTCTGGAAATACAATTCCATTTCT GCCAATTTCCGCTACAAATGATGGTCGTTATGAATGGCCACCTTCAATGAGGTATTCATCAGCTAATACTGATCGATTCAT TCAAGGAATTAACACAAACACTGATAACAGACAAGAAGATTTTAGAAATCAACTAACAAGTAATAACAATAATAATTATAAT TTCAAATCCAACAATACGGCAG
Smp_165360 Sm*myst4* WISH probe sequence 5´- 3´
CATAATGAAAACCCAACTCACAAGAAACAACCTATTAAATCATCTGACCATTCATATACAAAAGATCAAACTCAATTACCAA CATCAAATTTGGAGAATAAACCATCTAGTAGACAAAATTATAAAGAAAACAGAAACAATGAACATTCAATTCATAAATCATC CAACTCACATAATTATAAACCACATGAACATAATGAATATAAAAAACATATTGATTCAAATAAACAAGAATCAAAAACAGAA GTGAAGGAATATTCAACAAAAAGAAATGAAGAGTCCTCTTTGTCAAATGAACCGAATAGTAATAATAATAATGAGAAGAAT ACCGGTAAGAATGATAATAAATTGAGTTATTACACAAAAACTAGTGAATATAAAACCGAGAATAAAAATGATGAGCTTATTT CATCAAGTCAACCAACTGTTACTCAAAGCCTTACATCAGTATCGTTTGTTTCCGGTAGTAATAAATATGATTCAACTAAGT CAAATGAATATAAAACATCATCTCAGAGTACAGTCAGTAAACCTGTATCAGAGGATGAGATTAAAACTCAAATAGAAAAAT TATTAAAGGACAATTTAAACAATCTGATT
Smp_013540 Sm*tyr2* WISH probe sequence 5´- 3´ (49)
CGATATAATATATTATCATTTTCTCCAAAAAAAAGAAAAATGTTTGTTAATGTTGTAACAAGAATGCTTACTACTCCAACGG ATTATTTGATATTATTTGAAAAAGATGCTATACATTCTGATCCATTATGGAAACCTAAATTTTTAGATGTAGATGTACAATAT TTATTCTCTTTTATACATCGTTATGCAAGCAGAGCTACATTATTTCATGATAATATAGATTGTATAATACGTAGACATTTGG ATAATAATCATGAAGTAGTTGGATTTTTAACTTGGCATAGATATTATATGTTATTTTGGGAAAGACATCTACGTAAAATTGC AATTCGACTGTATGGTTGGACAGATTTCACAATACCTTATTGGGATTGGGTTGATTCTAAAAGGTGTGATGTTTGTGTTAA TAGTTTATTAGGTGGTTATGGACAATGGGTTGGGCAAACTCGTTTAATAGACCCTAGAAGTCCATTTTACATGTGGCCGG AATACTGTTCTCCCCCAACTACGGGAAGTAATTGTTATAGTTGTCATGCTGGTTGGCCAAACTTTCGAGTATTGAC
***E. coli ampR* dsRNA control sequence 5´- 3´** (152)
GAGTATTCAACATTTCCGTGTCGCCCTTATTCCCTTTTTTGCGGCATTTTGCCTTCCTGTTTTTGCTCACCCAGAAACGCT GGTGAAAGTAAAAGATGCTGAAGATCAGTTGGGTGCACGAGTGGGTTACATCGAACTGGATCTCAACAGCGGTAAGATC CTTGAGAGTTTTCGCCCCGAAGAACGTTTTCCAATGATGAGCACTTTTAAAGTTCTGCTATGTGGCGCGGTATTATCCCG TATTGACGCCGGGCAAGAGCAACTCGGTCGCCGCATACACTATTCTCAGAATGACTTGGTTGAGTACTCACCAGTCACA GAAAAGCATCTTACGGATGGCATGACAGTAAGAGAATTATGCAGTGCTGCCATAACCATGAGTGATAACACTGCGGCCA ACTTACTTCTGACAACGATCGGAGGACCGAAGGAGCTAACCGCTTTTTTGCACAACATGGGGGATCATGTAACTCGCCT TGATCGTTGGGAACCG

The sequences information of the *S. mansoni* ubiquitin (SmUbi) promoter and terminator as well as the eGFP used for the assembly of a reporter- gene construct are listed in Table 19.

Table 19. Sequence information of the SmUbi promoter and terminator, and the reporter-gene eGFP

Sequence of the Smp_335990 (SmUbi) promoter 5´- 3´ (189)
CCTTTCCAGATTGTCTCCGATTGATTTCACTTATCTCAATCACCACCAGATTGTGTCTTCTCACTTGGACACGATCTGAAC GGTCCTCAATTGTGTGCGAACACTTCACTTTCCGATATTGGCTGCCATTCTGGTCATTGTGAAGGTCTACGTTTTTGTGG CTCATAAAAAGTCCCAGCTTTCGGCACAAGTAATTGTAAGACTGCCAAACTACCAAGGAAGAGGTTAAATGACTTATCTG GTAAGTGTTTTTCGGAAATATTTTGCTGTATGGAGTCACTAACCACACACGACCTGTTTTCTCTACTCGAGCTTGAGAAAG TCACTAACCCAAGAAAATTGAAGCCTGTAATGTTCGTCATCCCTTCTCTTAGCGTTTATCAAGCCCACGAATACGTCCAG CCAAAAGAGAATTATTGCTGCCGGAATAGCGGAGGTGAGTGCTTCTAAGTCACTGAGGTTGTCAACATGGTCAATGTAA GGAAACTTCTGACTGTTCCTTCTCTCAGAATCGAGGTAGATAATATGTGGACCAAGAAATGTGTTTTGTAGACAGCGTAT TTTCTGGTGTGTTAGCCTCGTACATAAGCTAACATCAGAGATTCATGGGAAACCGGTGTTGATGTTATCACTAGTGTGAA TACTAGGGAATGATCTGGGGTTTGGAAAGTATTAGTTGGTCCCATCATTATTCTTCACACTCGGAGCATCAGGGCTTGAT GACTTGAAAACGCCATCTTGTGTCTCCGTGTAAGTGGAAATATAACATAAAATAAGCTTTTTACGTTCGAGACACATATCG ACCAGCTTAGTTGGGCAATGAATGCAATCTTCTCTTTGGGATTCAGTCTAGGAATTTCCCATTTTTAAAGGAGAAAGTTCC TTTAAAATCTTTTTAAGAGTCTAATTTCGAGAAACTACATTAAACAGTGTGCGATTTTATCCTCATGTGTTCGATGAAGGAG CTAGAAAAACATTACTCGGCAGTCATCCTTCCGCAAAGAAACCATAGTGAGAGGTTGTTGGCGAAAACGTTTTTGCCAGT AAAGATATAATATTAGCAGACCTGTGACTGGATGCTGATCCCACATTGCAGAATAACTTGACTTCTCCGGACTTGAATTGT CCCTATTAATGAACTCATCTCCTCCACTATATGTGTTCTGAAAAATTAACCTAGAAAATATTCAAATATCTTCAGGCTATAA TATGAAGTTTCATAGTCTAAGAAAAGAGATTATTCCATCCAAAACCAGATTTTCACGCTCAATTTCAGAACCGTAGTTCTT GTCAACATTTCTGATGAGTGCTAGTTAGTTTCTGACAAATTGAAGTGATAAGAAAGTAAGAAGTGATGTCGGAAAGAAGA TGAGGGTGGTGACAAGCAGTCGAAATCCAGGAGTCACGGCTAATCCAATGGTCGCACCACTTTGTAAGTCGGAATTCTT ATAACCTTCGTGGACAGTCGTGTTATTTTCACGCTCAATTGTTGTGAACTGGGTCTTCCAATTTAGCGTCTGCAGAAGTAT CTGAACGTCTCTTACTCGCTTAAGTCAGAGACAAACTAGTGAGACATTTTCAAGGTCTTCACAATTGTTTTCTGTTGATTT AGATGTGAAAAATCATTCATATGATGCACTTGGAGATGTTTAAGTTCCGATCTAACGAAGCATATCTCCAACAGTTAACTG CTCTAATAAATTGATGACTTCACGTGAACTAAAACCCATAAAGATAAAATGGCAAACTTTATTTTACATTATTACCTAAACT TTTGTCATCTTGAAACTCGAAAAATGTGGCACTTGAATGAGAAGTTGCTGACTAACAAAAACGTTTCATAATGAATTAGGA GGTTCAGACTGTAACAAGTTATTTTCTGAAAGTAAATGTGACTAGAATGTGGTTTGAGTAAGTAACAATCACCTCGACGAA TACCTTGTTTTACTGCCCTGAATTGAAGGTAGCGCTAAATAAACGTAGTATAGACTATATATAGCCAGCAAAATCGAAAGG CTGCCATACTTGTTCGTTAGTGTAAACGATAGACCTTACG

Sequence of the eGFP reporter-gene 5´- 3´

ATGGTGAGCAAGGGCGAGGAGCTGTTCACCGGGGTGGTGCCCATCCTGGTCGAGCTGGACGGCGACGTAAACGGCCA
CAAGTTCAGCGTGTCCGGCGAGGGCGAGGGCGATGCCACCTACGGCAAGCTGACCCTGAAGTTCATCTGCACCACCG
GCAAGCTGCCCGTGCCCTGGCCCACCCTCGTGACCACCCTGACCTACGGCGTGCAGTGCTTCAGCCGCTACCCCGAC
CACATGAAGCAGCACGACTTCTTCAAGTCCGCCATGCCCGAAGGCTACGTCCAGGAGCGCACCATCTTCTTCAAGGAC
GACGGCAACTACAAGACCCGCGCCGAGGTGAAGTTCGAGGGCGACACCCTGGTGAACCGCATCGAGCTGAAGGGCAT
CGACTTCAAGGAGGACGGCAACATCCTGGGGCACAAGCTGGAGTACAACTACAACAGCCACAACGTCTATATCATGGC
CGACAAGCAGAAGAACGGCATCAAGGTGAACTTCAAGATCCGCCACAACATCGAGGACGGCAGCGTGCAGCTCGCCGA
CCACTACCAGCAGAACACCCCCATCGGCGACGGCCCCGTGCTGCTGCCCGACAACCACTACCTGAGCACCCAGTCCG
CCCTGAGCAAAGACCCCAACGAGAAGCGCGATCACATGGTCCTGCTGGAGTTCGTGACCGCCGCCGGGATCACTCTCG
GCATGGACGAGCTgtacAAGTG

Sequence of the Smp_335990 (SmUbi) terminator 5´- 3´ (189)

GAGGTTAACTTTAATTTTGTTCATTTAACTTAATAAACGTTTAATTTAACTTATTAAAATGTTTTCTTCCTAATTTGTAGCGTA
TCTTAGTGTAACTGTGCTTCCTATTAGATTGAAATTCTATCGTAATCTGCAATTAGGCTCATGGGGATATGTTATGCCAAT
TTTCCGAAAATTGTTAGCACTTAGGTTTCGGTGTTTTTTTACTAGGATGTCATGTTTTATTCATATTTGCGTCCTTGCTCTT
GTGTGTGGTATGCGTCGCTATGGTCTCAGCTTTGGGCTGCATTGTTAAGTTTGAG

Plasmid map

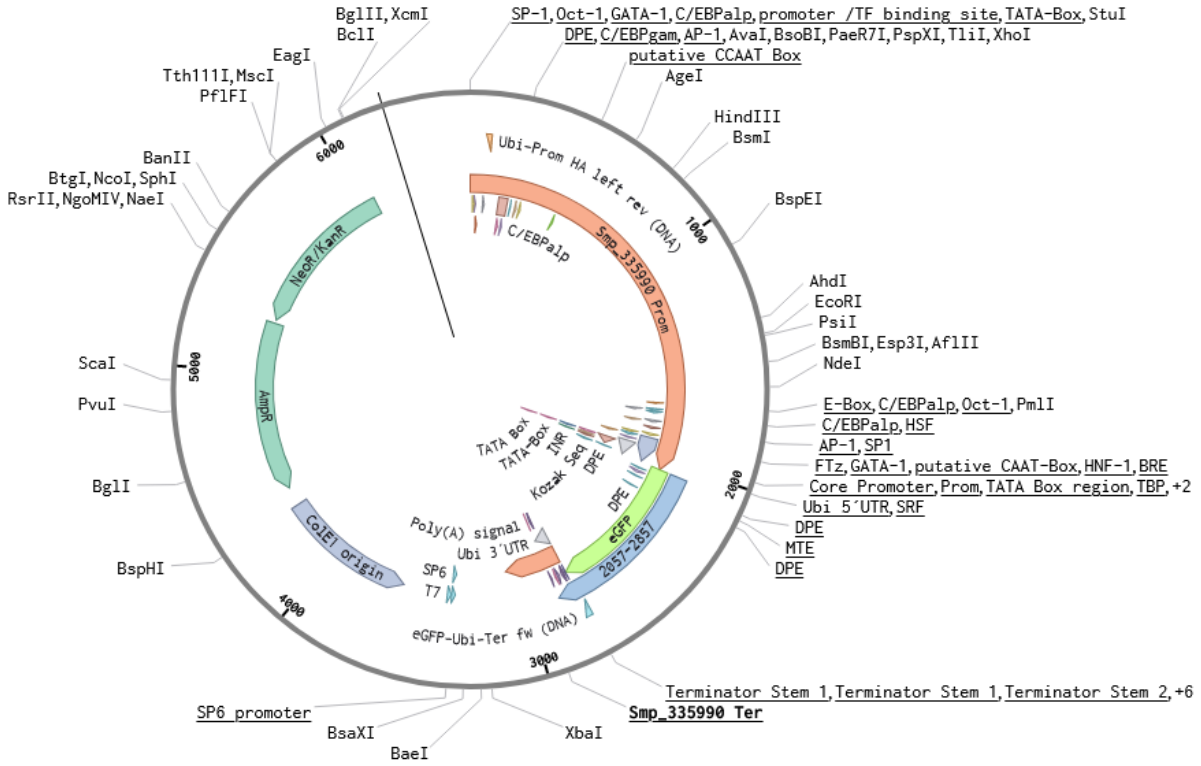

2.13 Websites and bioinformatics tools

Websites, databases and bioinformatics tools used in this work are listed in Table 21.

Table 20. List of databases and bioinformatic tools used in this study.

Description	Name	Link
Genome data base:		
helminth genome database	**WormBase ParaSite**	https://parasite.wormbase.org/index.html
Transcriptom data bases:		
Bulk RNA-Seq of whole worms and their isolated gonads	**SchistoXYZ**	https://schisto.xyz/
Bulk RNA-Seq of the parasitic lifestages	**SchistoXYZ**	https://schisto.xyz/
Single cell transcriptomics data of adult *S. mansoni*	**SchistoCyte Atlas**	https://www.collinslab.org/schistocyte/
Single cell transcriptomics data of ovaries, isolated from mature female *S. mansoni*	***S. mansoni* gonad scRNA-Seq**	https://gonadsc.schisto.xyz/
Protein structure and domain analysis:		
Protein structure and domain analysis, and ortholog finder	**Phyre2**	http://www.sbg.bio.ic.ac.uk/~phyre2/html/page.cgi?id=index
Protein structure and domain analysis	**AlphaFold Protein Structure Database**	https://alphafold.ebi.ac.uk/
Functional domain analysis	**SMART**	http://smart.embl-heidelberg.de/
Prediction of protein-protein interaction	**STRING: functional protein association networks**	https://string-db.org/
Protein sequence database	**UniProt**	https://www.uniprot.org/
Alignment tools:		
Amino aicd sequence alignment	**Clustal Omega**	https://www.ebi.ac.uk/jdispatcher/msa/clustalo
Amino acid, nucleic acid sequence alignment; genome data bank	**NCBI BLAST**	https://blast.ncbi.nlm.nih.gov/Blast.cgi

Description	Name	Link
Regulatory DNA motifs:		
Promotor motif prediction	**BDGP: Berkeley Drosophila Genome Project Neural Network Promoter Prediction Tool**	https://www.fruitfly.org/seq_tools/promoter.html
Promotor motif prediction	**AliBaba2.1 TRANSFAC 4.0**	http://gene-regulation.com/pub/programs/alibaba2/
Promotor motif prediction, core promotor prediction	**YAPP eukaryotic core promoter prediction tool**	http://www.bioinformatics.org/yapp/cgi-bin/yapp.cgi
Prediction of poly-adenylation sites	**DNAFSMiner-DNA**	https://mybiosoftware.com/dnafsminer-dna-functional-site-miner.html
RNA secondary structure:		
Prediction of RNA secondary structure	**RNAfold Webserver Vienna tool**	http://rna.tbi.univie.ac.at/cgi-bin/RNAWebSuite/RNAfold.cgi
CRISPR/Cas tools:		
Design of single guide RNAs and off-target prediction	**CHOPCHOP**	https://chopchop.cbu.uib.no/
Sanger Sequencing based estimation of CRISPR/Cas induced indel frequency and editing efficiency	**TIDE: Tracking of Indels by Decomposition**	https://tide.nki.nl/
Next generation sequencing based determination of CRISPR/Cas induced indel frequency and base specific position. Determination of editing efficiency.	**Cas-Analyzer**	http://www.rgenome.net/cas-analyzer/#!
Next generation sequencing based determination of CRISPR/Cas induced indel frequency and base specific position. Determination of editing efficiency.	**CRISPResso2**	http://crispresso2.pinellolab.org/submission
RNAi off-target analysis:		
Estimation of dsRNA dependent RNAi off-targets	**siRNA finder (si-Fi**)	https://www.scienceopen.com/document?vid=94ed2acd-34ae-438d-9c48-61171f2ad047
Primer Tm calculator:		
Determination of optimal PCR conditions	**NEB Tm calculation tool**	https://tmcalculator.neb.com

2.14 Software

Microscopic images were processed with LasX software (Leica Microsystems, Germany) or CellSens software (Olympus, Germany). ImageJ was used to perform stitching by using the Mosaic plugin (204, 205). The surface of analyzed samples was determined by the selection brush plugin (206–208). ZEN 3.4 blue software (Zeiss, Germany) was used to analyze the fluorescence spectrum of CLSM images (172). Phylogenetic analysis was performed by MEGA11 (209, 210). Benchling cloud-based software (Benchling, USA) and SnapGene (Dotmatics, USA) was used for creating plasmid cards, primer design, and to perform alignment and *in silico* restriction analysis. Statistics were carried out with the use of GraphPad Prism V.8 (GraphPad Software, USA) and Excel 2016 (Microsoft, USA). Graphics were created using GraphPad Prism V.8 and BioRender software (BioRender, USA).

3 Methods

3.1 Ethic statement

Experiments involving hamsters were performed in agreement with the European Convention for the Protection of Vertebrate Animals used for Experimental and other Scientific Purposes (ETS No 123; revised Appendix A) and were approved by the Regional Council (Regierungspraesidium) Giessen (V54-19c 20 15h 02 GI18/10).

3.2 Recovery and maintenance of biological material

3.2.1 Maintenance of the *S. mansoni* life cycle and recovery of larval stages

The complete life cycle of *Schistosoma mansoni* passes through several hosts. At the Institute of Parasitology at JLU Giessen, the freshwater snail *Biophalaria glabrata* (*B. glabrata*; SAY 1818) serves as intermediate host and the Syrian golden hamster (*Mesocricetus auratus;* Waterhouse 1839) as final host (211). The strain of schistosomes originated from Liberia (Bayer AG, Mohnheim (211)).

To infect Syrian hamsters, the animals were bathed in water (about 1.5 cm high) containing cercariae (212). To soften the hamsters' skin, they were bathed for 20 min in prewarmed snail water (water level approx. 1 cm) and transferred to water containing cercariae for infection. The hamsters remained in the water containing cercariae for 40 min. In the meantime, the cercariae penetrated the skin of the host. Within 6 weeks, the parasites developed from a juvenile stage (schistosomulum) into adult worms, which reside first in the portal vein of the hamster and later in its mesenteric veins (212).

S. mansoni couples produce eggs, which are mainly excreted in the feces of the final host. However, many eggs also accumulate in the liver. To obtain miracidia, the first larval stage developing inside the egg, for the infection of the intermediate snail host, the liver was removed from the perfused host and grounded in a blender. The homogenized liver was then washed in PBS and centrifuged at 5,000g for 10 min at 10°C. The resulting pellet was rinsed twice with 0.95% saline and transferred to a covered Erlenmeyer flask with a standpipe. A light source was attached to the end of the flask. As a result, miracidia hatching was induced by their phototactic properties, and these larvae collected by pipetting. These miracidia were further used to infect *B. glabrata* snails.

The freshwater snail *B. glabrata* is kept as an intermediate host in snail water in incubators at 26°C with a day/night cycle consisting of 16 h light and 8 h darkness. For polymiracidial infection, the snails were placed individually in wells of 12-well microtiter plates, each well

containing one snail and 10-15 miracidia in 2 mL of snail water. The snails were incubated for 12 h before they are returned. For mono-miracidial infections, snails were wiped dry by a paper towel. A single miracidium was pipetted to a drop of 10 µl snail water and transferred to a well of a 12-well microtiter plate. The shell aperture of the previously wiped snail was then placed on the miracidium-containing drop. The snail was then incubated on a light plate for 15 min. Afterwards, 100 mL of sterile tab water was added directly to the snail to prevent its drying. After one hour, 2 mL of snail water was added. Infection was performed overnight as described above.

About 21 d post infection, the infected intermediate hosts were kept in the dark to prevent uncontrolled hatching of cercariae. After 9 more days, the snails were transferred to 12-well microtiter plates containing snail water to be illuminated. This induced hatching of cercariae within 2–4 h, which were collected by pipetting for final host infection.

3.2.2 Perfusion of hamsters and recovery of adult *S. mansoni*

About 46 d after the infection of the final host, the adult worms were obtained by perfusion (213). For this, the hamsters were first anaesthetized with isoflurane and then injected subcutaneously with ketamine and xylazine. After the abdominal cavity was exposed, an anterior-posterior incision of the portal vein was done. The hamsters were then injected with perfusion medium (36°C) into the left ventricle. This caused bleeding out in a controlled manner, and the blood was then filtered with a nylon cloth to collect the worms by using a soft brush to carefully transfer the worms to prewarmed M199^{+++} medium. After perfusion, the livers of the hamsters were removed to isolate the eggs.

3.2.3 Recovery and maintenance of adult *S. mansoni*

To obtain adult *S. mansoni* worms for *in vitro* cultivation, nucleic acid isolation, egg or ovary isolation, hamsters were infected with 1,500 up to 2500 (mixed-sex or single-sex) cercariae. Adult schistosomes were harvested by hepatoportal perfusion 42 d post infection. Adult *S. mansoni* worms of the Liberian strain were obtained from hamsters (*Mesocricetus auratus*) as final hosts by perfusion (65). Adult schistosomes were harvested by hepatoportal perfusion 42 d post infection. From each hamster, 20 stably paired couples, 30 separated males, 50 separated females, or 50 pairing-inexperienced (single-sex) worms were transferred into 5 mL preheated M199^{+++} (37°C, M199 supplemented with 10 nM Hepes, 1% ABAM and 10% NCS). The worms were cultivated at 37 °C and 5% CO_2. Before starting experiments, the worms adapted to the *in vitro* culture conditions for one day. For each biological replicate, 10

S. mansoni couples (obtained from one hamster) were transferred to one well of a 6-well plate containing 3 mL of prewarmed $M199^{+++}$ medium.

For conducting (re)pairing experiments, a modified version of the recently described ABC169 medium (49) was employed, which was described by Li *et al.* (57). This modified medium, known as ABC169/LDL, is based on the Basch medium (214) and includes the addition as described in Table 3. Worms were cultured in 12-well plates containing 3 mL of prewarmed ABC169/LDL medium at 37°C and 5% CO_2. For (re)pairing experiments, 10 sFs obtained from one hamster for each biological replicate were placed in a 12-well microtiter plate and cultivated for 7 d. To facilitate re-pairing, 15 pairing-experienced males (bM) were added to the sF group, bringing the female-male ratio to 1:1.5, which has been previously shown to be optimal under these conditions (57, 215). After 72 h, any remaining supernumerary males and unpaired worms were removed, and only females from stably paired couples were used for RNA extraction.

3.2.4 Isolation of vital eggs from hamster livers

For the isolation of vital eggs from hamster livers (LE), a modified version of the isolation protocol established by Joyce *et al.* (216) was used. The objective of the protocol is the isolation of embryonated, viable eggs of developmental stage 5 to 7 in accordance with the Jurberg classification system (76).

Immediately after perfusion, the livers of infected hamsters were removed and stored on ice for further processing. Livers were transferred into 6 cm diameter Petri dishes with chilled 1xPBS (4°C). After the gall bladders were removed, the livers were cut into pieces with surgical scissors. The tissue fragments were transferred into a 50 mL reaction tube and washed twice with PBS (800 g, 10°C, 10 min). The PBS was removed, and the tissue weight was estimated. For each gram of liver tissue, 10 mL M199 medium supplemented with 1% ABAM (v/v) and 10 nM Hepes (pH=7) was used. For the dissociation of the liver tissue, 0.5 mg/mL Collagenase type II, 1 mg/mL Dispase II and 1.5 mg/mL Hyaluronidase were added to the medium. Finally, the liver fragments were homogenized in the dissociation mixture using a blender (approx. 20-30 s) and transferred to a 750 mL Erlenmeyer flask. To prevent the unintentional hatching of miracidia, the Erlenmeyer flask was covered with aluminum foil. The enzymatic digestion of the liver tissue was carried out for 16 h, shaking at 135 rpm at 37°C.

After dissociation, the suspension was filtered under the lamina flow hood. For this purpose, sieves with mesh sizes of 45, 125, 150 and 180 µm were stacked on top of each other, and the suspension was filtered. LEs remained in the 45 µm sieve. Subsequently, LEs were

washed with 200 mL PBS, taken up in 50 mL PBS and transferred to a 50 mL reaction vessel. To pellet isolated LEs, a swing-bucket centrifuge was used (10 min, 800 g, RT, deactivated brake, Eppendorf). The supernatant was discarded (by pipetting), and the pellet was resuspended in sterile 12.5 mL PBS. In order to reduce remaining tissue debris and the amount of empty eggshells, a percoll gradient was prepared by mixing 8 mL percoll solution with 32 mL 0.25 M sucrose solution. The gradient was carefully layered with the LE containing solution and centrifuged (10 min, 800 g, RT, deactivated brake). Subsequently, the supernatant was discarded, and the pellet was resuspended in 3 mL sterile PBS. Moreover, a second percoll gradient was prepared in a 15 mL reaction vessel by mixing 2.5 mL percoll solution with 7.5 mL 0.25 M sucrose solution. Again, the LE-solution were carefully layered onto the gradient. Following the protocol, the suspension was fractionated by centrifugation (5 min, 800 g, RT, deactivated brake), whereby LEs accumulated as pellet. After centrifugation, this step was repeated to remove any remaining liver cells. Subsequently, the pellet was resuspended in 10 mL $M199^{+++}$ supplemented with chloramphenicol at a final concentration of 50 µg/mL (1/1,000 stock solution). In order to prevent any bacterial contamination, the eggs were incubated in antibiotics-containing media for 1 h at 37°C. Meanwhile, LEs were allowed to settle. The supernatant was removed and replaced with 5 mL of sterile M199 supplemented with 1% ABAM, 20% NCS, 0.25% human LDL concentrate (M199egg). Total numbers of LEs were determined by counting only intact eggs. Next, the suspension was adjusted to a final concentration of 1,000 LEs/mL. Finally, LEs were cultivated in a 50 mL cell culture flask with valve at 37°C and 5% CO_2. The medium was changed every 2-3 d. Under these conditions, eggs remained viable for up to 14 d and/or were used for further experiments.

3.2.5 Isolation and enrichment of unembryonated, *in vitro* laid eggs

For the isolation of unembryonated eggs, consisting of a zygote and 30-40 accompanying vitellocytes (76), *in vitro* laid eggs (IVLEs) at 0-24 h were collected. For this, the media of couples 24 h post perfusion was collected and rinsed through a 180 µm sieve to remove remaining worms and debris. Furthermore, under sterile conditions, the IVLEs containing suspension was rinsed through a 15 µm cell strainer. IVLEs remained in the cell strainer and were washed twice with sterile PBS supplemented with 1% ABAM. Subsequently, IVLEs were resuspended in 10 mL $M199^{+++}$ supplemented with chloramphenicol (50 µg/mL) and transferred to a 50 mL reaction vessel. This step was followed by an incubation for 1 h at 37°C. Subsequently, IVLEs were centrifuged for 10 min at 600 g at RT, and the supernatant was discarded. Additionally, IVLEs were transferred into 2 mL M199egg, the cell number was determined, and 1,000 IVLEs in 2 mL medium were transferred to a 12-well microtiter plate.

They were either used immediately for further experiments or used for miracidia hatching after 6 d of development at 37°C, 5% CO_2.

3.2.6 Miracidia hatching assay

A miracidia-hatching assay was carried out to generate miracidia for either the infection of the intermediate host, or as part of experimental downstream analysis, or for *in vitro* cultivation. For this, egg containing medium from *in vitro*-cultivated couples was collected in a reaction vessel. Samples were centrifuged at 500 rpm at room temperature for 2 min. Subsequently, the supernatant was discarded, and IVLEs were transferred into a 1 mL M199egg-containing 12-well microtiter plate. The IVLEs were cultured for 6 d to ensure complete embryonic development of the miracidium (76). After 6 d, the medium was carefully discarded, and 1 mL of sterile tap water was added. Phototactic hatching (15) was performed on a light plate for 2 h.

For the hatching of LEs, the procedure was identical to that described above, except that the LE were cultured *in vitro* for 2 d under described conditions. The number of hatched miracidia was determined, and the biological material was used for further experiments or analysis.

3.2.7 Cultivation of *Biomphalaria glabrata* embryonic (Bge) cells

In order to revive *Biomphalaria glabrata* embryonic (Bge) cells (CRL-1494, American Type Culture Collection, Manassas, USA) from cryo-culture (217), cells were incubated at 37°C in a water bath until 80% of cryo-culture was thawed. The 1 mL of Bge-medium was added at RT. Subsequent, the suspension was transferred into a 15 mL reaction vessel and centrifuged at 700 g for 5 min at RT. Afterwards, the glycerin-containing supernatant was discarded, and the cells were resuspended in 7 mL Bge-medium (RT) and centrifuged as described above. Cells were then resuspended in 5 mL Bge-medium supplemented with 10% heat-inactivated NCS and 1% ABAM. Cells cultivated in a 50 mL cell culture flask at 26°C under atmospheric conditions for at least 7 d (218, 219).

After adaptation to the *in vitro* conditions, Bge cells were maintained in 10 mL supplemented Bge-medium as described above (218, 219). Cells were cultivated to 70-80% confluence (about 10 d) and then carefully collected by using a 10 mL serological pipette. Subsequently, cells were then split 1:5 and distributed in a total volume of 10 mL, replenished with fresh supplemented Bge-medium in 50 mL cell culture flasks.

Bge cells at a confluence of 70-80% were used for the preparation of cryo-cultures. The cells were carefully resuspended by using a 10 mL serological pipette and transferred to a 15 mL

reaction vessel. Cells were pelleted by centrifugation at 700 g for 5 min at RT and the supernatant was discarded. To prepare the cells for cryo-cultivation, cells were resuspended in 1 mL supplemented Bge medium. The cells were then split into two cryotubes, and 1 mL of freezing medium (85% NCS, 15% DMSO; RT) was added. Immediately, the cryotubes were transferred to a freezing container already pre-cooled to 4°C. The container was then transferred to a -80°C freezer. After 16-24 h, the cryo-cultures were transferred to liquid nitrogen for long-term storage.

3.2.8 Collection of Bge cell-conditioned medium

Bge cell-conditioned medium was used as supplement for the *in vitro* cultivation of sporocysts to simulate the intermediate snail host. For this, the medium of a Bge culture at a confluence of 70% was exchanged with prewarmed (26°C), Hepes-free, complete StemMACS iPS-Brew XF medium (MACS Media, Miltenyi Biotec) supplemented with 5% NCS. StemMACS iPS-Brew XF medium is an optimized medium for pluripotent human and/ or embryonic stem cells (220, 221), which has already been successfully used for the cultivation of Bge and isolated germ cells of *S. mansoni* (Quack and Moescheid, unpublished data). The medium was conditioned for 7 d and collected as described before (222). In brief, the supernatant was collected and stored at 4°C for immediate usage or frozen in liquid nitrogen and stored at -80°C as Bge cell-conditioned medium.

3.2.9 Miracida transformation and sporocyst *in vitro* culture

A modified protocol based on the works of Chernin (223, 224), Voge and Seidel (225), and Yoshino and Laursen (226) was developed for the transformation of miracidia and *in vitro* cultivation of sporocysts. For the *in vitro* transformation of miracidia into sporocyst, isolated LEs were hatched under sterile conditions as described in 3.2.6. Miracidia were collected and washed with 50 mL PBS using a 15 µm cell strainer. Subsequently. miracidia were transferred into a reaction vessel with CBSS buffer (223) supplemented with 1 g/l trehalose (CBSS+T) and 1% ABAM. Subsequently, miracidia were incubated for 2 h at 26°C under low oxygen conditions (5% O_2, 5% CO_2). Due to this treatment, miracidia were immobilized and finally counted. Approximately 1,000 up to 2,500 miracidia were transferred into a well of a 12-well plate, and the remaining CBSS+T was exchanged by 3 mL sporocyst-medium (48% CBSS+T, 48% M199 without supplements, 5% 7 d Bge cell-conditioned StemMACS iPS-Brew XF medium, 1% ABAM).

To warrant sporocyst viability, it is essential to ensure that the medium is free of Hepes. Miracidia were cultivated at 26°C under 5% O_2 and 5% CO_2 for at least 24 h. This leads to the

transformation of the miracidia into sporocysts, which can be recognized by an accumulation of detached ciliated plates. Optionally, the ciliated plates can be removed by washing the sporocysts using a 15 µm cell strainer. This step is crucial if sporocyst are used for nucleic acid isolation, protein analyses, or for transfection experiments. Sporocysts older than 7 d were very fragile and were not washed with a cell strainer.
Sporocysts can be cultivated for at least 6 weeks under the conditions described, changing the medium every 2-3 d.

3.2.10 Transplantation of *in vitro* generated sporocyts into the intermediate snail host

Transplantation of *in vitro* generated sporocyts was carried out according to the refined transplantation method established by Jourdane and Théron (222, 227, 228). First, recipient snails with a shell diameter of approximately 1 cm were anaesthetized with 0.08% (v/v) sodium pentobarbital (Nembutal, Sanofi Sante Nutrition Animale) for a minimum of 4 h at 26°C. For transplantation, each snail was kept expanded by a microretractor, which was made from glass according to the instructions of Mouahid *et al.* (228). The microretractor was gently fixed in the male genital orifice. An incision was made in the tegument of the *cephalopedal sinus* using a cannula. One to five *in vitro* cultured sporocysts aged 4 to 7 d after transformation were inoculated with a thin, drawn-out syringe. Elder sporocysts were very fragile and showed an elongated appearance. They were carefully aspirated with the syringe. The microretractor was carefully removed and the snails were immediately transferred to sterile snail water containing 0.02% (w/v) nitrofurantoin (Sigma-Aldrich) and kept for 16 – 20 h at 26°C to avoid microbial infection. Before being used for the first cercariae shedding, the snails were kept for at least 8 weeks as described in 3.2.1.

3.2.11 Gonad isolation from adult *S. mansoni*

The isolation of the gonads was based on the protocol described by Hahnel *et al.* (73, 229). In order to isolate testes and ovaries, adult *S. mansoni* were separated by sex immediately after perfusion by adding 0.25% (w/v) tricain as described before (230). Couples started to separate after 1 min and were finally separated using two feather-weight forceps. Subsequently, 50 worms each were transferred into 2 mL reaction tubes and washed twice with 2 mL plain M199 at RT.

In order to obtain fully developed gonads, stable schistosome couples were selected. To obtain undeveloped, immature gonads, the gonads from pairing-inexperienced worms were isolated

(55, 73). Furthermore, schistosomes were treated with 500 µl each of tegument stripping (TS) solution at 37°C and 1,200 rpm agitation in a thermal shaker (TS-100, Biosan) to dissolve the tegument. The incubation with the TS solution was repeated once for females and twice for males. To pursue organ isolation, TS solution was removed by repeated washing (3 x) with 2 mL plain M199 medium. The exposed subtegumental muscle syncytium was degraded by proteolytic digestion with elastase. For this purpose, the enzyme was freshly dissolved at a final concentration of 5 U/mL in plain M199 medium. Samples were incubated in 500 µl elastase-containing medium at 37°C for 30 to a maximum of 40 min. In the meantime, the samples were carefully mixed every 5 min by gently shaking the reaction vessels by hand. Subsequent progression of the enzymatic digestion was observed by an increasing turbidity of the medium, which was caused by the loss of the structural integrity of treated tissue. Due to the constant shaking of the samples, digested tissue formed a clearly visible conglomerate in the reaction vessel towards the end of the incubation period. To determine the appropriate time-point to stop the enzymatic reaction, 20 µl aliquots were taken at regular intervals and examined by light microscopy (DM IL LED, Leica Microsystems; Germany). Particular attention was paid to already exposed gonads and their integrity. Fully exposed organs were collected. The samples were transferred to 6 cm diameter Petri dishes, and the reaction tubes were washed 4 times in plain M199 to completely transfer the material. Exposed organs were collected with a 10 µL pipette and transferred to Petri dishes (30 mm diameter) with fresh medium. This process was repeated until tissue debris was removed. The isolated organs were transferred to 2 mL reaction vessels with a reservoir (Biozym). Testes were pelleted in a benchtop centrifuge for 5 minutes at 1,000 g and ovaries for 1 min at 8,000 g. The supernatant was removed, and 20 µl of RNAzol RT (Sigma-Aldrich) was added to prevent RNA degradation. Immediately after isolation, samples were frozen in liquid nitrogen and store at -80°C.

To verify the vitality of the isolated testicular and ovarian cells, the organs were stained immediately with Calcein-AM cell viability dye at a concentration of 1 µg/mL in prewarmed M199. For this purpose, the gonads were resuspended in 50 µl dye-solution and incubated for 10 min at RT. Calcein-AM can permeate the cell membrane. Due to structural changes catalyzed by cellular esterases (231), a Calcein-AM accumulation in intact cells can be observed at a wavelength of 517 nm using an excitation wavelength of 494 nm (232, 233). The suspension was then transferred to a microscope slide and analyzed by fluorescence microscopy (inverse laboratory microscope DM IL LED, Leica Microsystems; Germany). Organs showing an intensive green fluorescence were considered as vital.

3.3 Nucleic acids

3.3.1 DNA Isolation from adult worms

Genomic DNA (gDNA) was isolated from parasites using the DNAzol reagent (genomic DNA isolation reagent, ThermoFisher Scientific) following the manufacturer´s instructions with some amendments. Briefly, up to 50 worms were collected in a 1.5 mL reaction tube und washed twice with 1xPBS. Subsequently, remaining PBS was discarded, and 50 µl DNAzol reagent was added. Worms were either immediately proceeded for DNA isolation or frozen in liquid nitrogen and stored at -20°C. To isolate gDNA, worms were homogenized for 30 sec using a mechanical pestle. Subsequently, 450 µl DNAzol was added to the homogenate. Next, samples were centrifuged for 10 min at 10,000 g at RT to remove insoluble tissue fragments, RNAs, and polysaccharides from the homogenate (234). The supernatant was transferred to a new 1.5 mL reaction tube, and 250 µl of 100% Ethanol was added. Samples were thoroughly mixed by inverting and then incubated for 3 min at room temperature followed by DNA precipitation at 12,000 g for 10 min at 4°C. Finally, the supernatant was discarded, and the pellet was washed twice with 800 µl of 75% ethanol at 4,000 g for 2 min at 4°C. The pellet was resuspended in 1 M Tris-HCl buffer (pH=7, NEB), and the DNA concentration was determined photometrically (BioSpectrometer basic, Eppendorf) or by electropherogram analysis using the BioAnalyzer 2100 and the DNA 1000 chip according to the manufacturer's instructions (Agilent Technologies). Samples were either used immediately for further analysis or stored at -20°C until usage.

3.3.2 DNA isolation from schistosome eggs

gDNA from either IVLEs or LEs was isolated using DNAzol reagent. At least 500 up to 5,000 eggs were transferred to 1.5 mL siliconized low binding reaction tubes and washed twice with PBS. For this, the samples were centrifuged at 1,000 g for 1 min at RT. The supernatant was discarded, 50 µl DNAzol reagent was added, and eggs were frozen in liquid nitrogen. This was followed by two freeze-thaw cycles. Eggs were incubated at 65°C for 10 min in a thermoshaker (ThermoMixer, Eppendorf) and shaken at a maximum speed of 1,400 rpm. As mentioned before, eggs were homogenized for 30 s by using a mechanical pestle. Finally, 450 µl DNAzol reagent was added. gDNA was isolated and precipitated using DNAzol reagent as described in 3.3.1.

3.3.3 DNA isolation from larval stages

gDNA from the larval stages of miracidia, sporocyts or cercariae was isolated using DNAzol reagent as previously described in 3.3.1. with some modifications as described below. The number of larvae used for gDNA extraction ranged from 500 to 5,000. To isolate gDNA from small amounts of biological material, a minimum of 50 individuals of the larval stages was used, the volumes of reagents used for this approach were halved, and the DNA was precipitated at 15,000 g for 20 min at 4°C.

3.3.4 DNA isolation from bacteria cell cultures

Plasmid DNA from *E. coli* DH5α or βcomp10 strains (NEB) was isolated from overnight cultures using the monarch mini plasmid miniprep or midiprep kit (NEB) according to the manufacturer's instructions.

For the transfection of eucaryotic cells such as schistosome cells, the usage of an endotoxin-free plasmid stocks was indispensable. For this, an overnight culture of *E. coli* DH5α or βcomp10 strains harboring the plasmid of interest were prepared. Endotoxin-free plasmid in sufficient quantity for the subsequent transfection of schistosomes was purified with the PureLink Expi Endotoxin-Free Maxi Plasmid Purification Kit (ThermoFisher Scientific) according to the manufacturer's instructions. Plasmids were either used directly for further experiments or stored at -20°C for later use.

3.3.5 RNA isolation from whole worms

Total RNA was isolated from adult schistosomes using the RNAzol RT reagent (Sigma-Aldrich) according to the manufacturer´s instructions with some alterations. In brief, 5 to 10 adult worms were transferred to 1.5 mL reaction tubes and were washed twice by using DEPC treated PBS. Furthermore, remaining PBS was discarded, and 50 µl RNAzol RT reagent was added. Worms were either stored at -80°C, or RNA was isolated. For this, worms were homogenized for 30 s on ice using a mechanical pestle. Subsequently, 450 µl RNAzol RT solution was added. To precipitate DNA, proteins and polysaccharides (235), 200 µl of nuclease-free water (NEB) was added, the mixture was vigorously shaken for at least 15 s, and incubated for 10 min at RT. Next, remaining cellular content was precipitated by centrifugation at 12,000 g for 15 min, leaving the RNA in the supernatant. The RNA was then precipitated according to the manufacturer's instructions and dissolved in an adequate volume of nuclease-free water.

The BioAnalyzer 2100 and an Agilent RNA 6000 Pico or Nano Chip were used to analyze the quantity and quality of extracted RNA via electropherogram analysis. The electropherogram was obtained according to the manufacturer's instructions (Agilent Technologies). To determine RNA quality, the presence of two distinct RNA peaks, corresponding to 18S and 28S RNA, was evaluated. The isolated RNA was immediately used for reverse transcription (3.3.8 or 3.3.9). Alternatively, isolated RNA was stored at -80°C until usage.

3.3.6 RNA isolation from schistosome eggs

Total RNA was isolated from eggs using the RNAzol RT reagent as described in 3.3.5. with some alterations in the decomposition of the biological material. For this, up to 10,000 eggs were transferred into a 1.5 mL reaction tube, washed twice with DEPC-treated PBS and aspirated in 50 µl RNAzol. Samples were frozen into liquid nitrogen and either stored at -80°C for later processing or thawed slowly on ice. Furthermore, samples were manually grinded using pestles. Afterwards, 200 µl RNAzol RT was added to the homogenate. To lyse as many eggs as possible, the samples were incubated for 10 min on a thermoshaker at 65°C and 1,400 rpm with shaking and then shock-frozen in liquid nitrogen. After the samples were thawed on ice, a 10 µl aliquot was analyzed microscopically. If more than 75% of the eggs were disintegrated, 250 µl of RNAzol RT was added, RNA was isolated, and its concentration was determined as described above. Otherwise, the eggs underwent another freeze-thaw cycle.

3.3.7 RNA isolation from isolated gonads

Total RNA was isolated from isolated gonads using RNAzol RT reagent, as described in 3.3.5., with some alterations. Briefly, at least 50 isolated gonads were transferred into a 1.5 mL reaction tube and aspirated in 50 µl RNAzol RT immediately after gonad isolation. The samples were manually grinded using pestles, and 200 µl RNAzol RT was added to the homogenate. RNA precipitation was carried out as described above with divided volumes and the addition of 1 µl RNase-free glycogen (ThermoFisher Scientific) at a concentration of 20 mg/mL to increase the efficiency of precipitation (236). The BioAnalyzer 2100 and an Agilent RNA 6000 Pico Chip were used to analyze the quantity and quality of extracted RNA via electropherogram. An electropherogram was obtained according to the manufacturer's instructions, as described above.

3.3.8 cDNA synthesis for RT-qPCR

Reverse transcription of 10 - 100 ng of RNA was performed using the QuantiTect Reverse Transcription Kit (Qiagen), which includes a step for removing gDNA. In brief, 2 µl of gDNA wipeout buffer was incubated with total RNA in a total volume of 14 µl at 42°C for 2 min. Next, 6 µl containing 5x Quantiscript RT (reverse transcriptase) buffer, RT primer mix, and RT was added to the mixture. Next, it was incubated at 42°C for 60 min, followed by enzyme inactivation at 95°C for 3 min. Finally, cDNA was diluted at a ratio of 1:5 or 1:10 in RNase-free water before being used as a template for RT-qPCR.

3.3.9 cDNA synthesis of full-length transcripts

Total RNA isolated from adult *S. mansoni* was reverse-transcribed using a Superscript IV kit. For this, 1 µg of total RNA, 1 µl of oligo(dt)25 (50 µM), and 1 µl dNTP mix (10 mM) were combined to a total volume of 14 µl. The mixture was incubated at 65°C for 5 min and placed on ice. Subsequently, 4 µl of 5x first-strand buffer, 1 µl of 0.1 M DTT, and 1 µl of superscript IV reverse transcriptase were added, and the total mixture was incubated at 50°C for 2 h. The enzymatic reaction was terminated by incubation at 70°C for 15 min. Furthermore, 1 µl of RNase H was added to cleave RNA-DNA hybrid double strands. Finally, the mixture was incubated at 37°C for 20 min and diluted to 1:5 using nuclease-free water.

3.4 Transcriptional analysis by RT-PCR

3.4.1 Primer design for RT-qPCR

Primers used for RT-qPCRs were designed by using the primer design function with integrated prime18 software tool (237) of the Benchling software (Biology Software). Primers were designed to bind on neighboring exons of the same gene to impede amplification of products derived from contaminating gDNA by amplifying 180-200 bp fragments from cDNA during RT-qPCR. In addition, primers were designed to prevent the formation of homo- or heterodimers as well as hairpin structures. Moreover, the Tm calculator tools from NEB and Benchling were used to analyze the optimal melting temperature (Tm), which was 60±1°C in all cases. Primers were commercially synthesized by Integrated DNA Technologies IDT (Belgium) and/ or Microsynth Seqlab (Germany) and were used at a final concentration of 400 nM in a 20 µl total reaction volume.

Primer efficiencies were determined according to the specificity of PCR products and the absence of primer dimers. This was done under standard PCR conditions using the Q5-

polymerase PCR kit (NEB) according to the manufacturer´s instructions and the following PCR conditions: 98°C, 5 min, 35 cycles of 98°C for 20s, 60°C for 20s, and 72°C for 20s. Only primers amplifying one specific product without the formation of primer dimers were considered for RT-qPCR. Finally, the amplification efficiency (primer efficiency) of these primers was determined. For this, the PCR product was purified from 2% agarose gel by using the monarch gel extraction kit (NEB). The eluate served as template to prepare a standard curve with 1:10 dilution series to calculate primer efficiencies (201, 238). An efficiency between 1.80 to 2.00 (90-100%) was considered as suitable.

3.4.2 RT-qPCR

Transcript levels were determined by reverse transcriptase quantitative (real time) PCR (RT-qPCR) with primers specific for genes of interest. Reaction mixtures consisted of 10 µl 2x Quanta PerfeCTa SYBR Green SuperMix (Qiagen) or 2x KAPA SYBR FAST qPCR mix (KAPA Biosystems), 0.8 µl specific primer mix (forward and reverse primer, each 10 µM), 5 µl template cDNA and 4.2 µl PCR-grade water (Carl Roth). RT-qPCR was carried out using the following cycling conditions: initial denaturation 95°C for 3 min, followed by 55 cycles of DNA denaturation at 95°C for 10 s, primer annealing at 60°C for 15 s and elongation at 72°C for 20 s. The amplification process was followed by a melt curve analysis at 60 to 95°C with stepwise increase of 1°C for 20 s each cycle (Qiagen Rotor-Gene Q, Q-Rex). By taking the primer efficiency into account, the transcription levels of the genes of interest were determined using the Pfaffl method (239) (Formula 1). Sm*letm-1*, a confirmed RT-qPCR reference gene for *S. mansoni in vitro* studies, served as control (152, 201, 240). RT-qPCR was carried out as described applying selected primers (Table 11).

$$transcriptional \log(2)\ fold\ change = \log(2) \frac{Primer\ E(target\ gene)^{(CT\ control - CT\ treatment)}}{Primer\ E(reference)^{(CT\ control - CT\ treatment)}}$$

Formula 1. Determination of transcriptional changes by Pfaffl.
Pfaffl 2001 (239). Abbreviation: Primer E, primer efficiency.

3.5 *In silico* analysis

3.5.1 Bioinformatic domain analysis and phylogenetic classification

Annotations for genes analyzed in the course of this thesis were gathered by collecting data of transcriptome and genome databases schisto.xyz (55, 62, 240), WormBase ParaSite (143), and alphafold (241, 242), respectively. To predict the domain structures by SMART (243), the amino acid (aa) sequence of these genes was analyzed. Furthermore, the protein structure of selected proteins was *in silico* investigated by a comparative analysis to already known structures of other members of the same protein family using Phyre2 (Protein Homology/analogY Recognition Engine V 2.0 (244)), applying the intensive modelling mode.
For the generation of a phylogenetic tree, orthologs of selected genes were identified by NCBI protein BLAST (245) and the ortholog finder function of parasite.wormbase.org (143). Moreover, also *S. mansoni* paralogs were identified in parasite.wormbase.org (143). Orthologs from *Stylophora pistillata* and *Acropora millepora* served as outgroup controls of evolutionary basal organisms (stem: *Cnidaria*; Supplemental Table S1). Alignment was performed by MUSCLE (MUltiple Sequence Comparison by Log-Expectation(246)). Phylogenetic classification was carried out by MEGA11 (molecular evolutionary genetics analysis, (210)) applying the following parameters: Maximum likelihood setting was applied as statistical method of choice. As test of phylogeny, the Dayhoff model with 1,000 Bootstrap replicates was performed analyzing the amino acid sequences of certain proteins. As tree inference, the nearest neighbor interchange (NNI) heuristic method was used (247).

Furthermore, the aa sequences of the ligand-binding domains (LBD) and the DNA-binding domains (DBD) of investigated nuclear receptors and their orthologs from *S. rodhaini, S. haematobium*, and *S. japonicum* were determined by SMART (243) and compared by the Clustal Omega – Multiple Sequence Alignment tool (209, 248), respectively. The prediction of potential interaction partners was done utilizing the STRING Protein-Protein Interaction Network tool (249, 250) on the *S. mansoni* database by using the full STRING network as network type, a medium confidence (0.400) score, and a cut-off size of 10 interactions.

3.5.2 *In silico* analyses of regulatory promoter and terminator elements of SmUbi

The promoter and terminator sequence of Smp_335990 (Sm*ubi*) for canonical promoter/terminator elements was analyzed *in silico* using different bioinformatics tools. Both the promoter and the terminator sequence of Sm*ubi* were analyzed using a variety of tools (Table 20). Potential core-promoter sequences were investigated by the BDGP: Berkeley *Drosophila* Genome Project Neural Network Promoter Prediction Tool (251). Furthermore, the analysis of putative regulatory sequence motifs within the potential promotor was predicted by

a comparative analysis by using AliBaba 2.1. TRANSFAC 4.0 software (252) and the YAPP eukaryotic core promoter prediction tool (253, 254). Furthermore, the terminator sequence was analyzed for potential polyadenylation sites by the DNADSMiner-DNA tool (255), whereby the mRNA secondary structure was investigated for terminator hairpin structures by the RNAfold Webserver Vienna tool (255, 256). Moreover Sm*ubi* transcription during the parasitic lifecycle, as well tissue dependent transcription was analyzed using the RNA-Seq databank schisto.xyz (55, 62)and the scRNA-Seq atlas of whole worms (61). Finally, the protein structure was analyzed by Phyre2(244).

Nucleotide sequences of upstream and downstream untranslated regions (UTRs) of Smp_335990 were retrieved from WormBase ParaSite (143, 168), version V7 and V10 of the draft genome of *S. mansoni* (143, 257, 258). The annotation of SmUbi was confirmed by the usage of the protein homology/analogy recognition engine Phyre2 (259). To predict the promoter region and regulatory elements of SmUbi, adjacent sequences up to the three kb upstream of the start codon were *in silico* analyzed. Promoter elements were identified by the Berkeley *Drosophila* Genome Project Neural Network Promoter Prediction Tool, using a minimum promoter score of 0.8 for eukaryotic promoters (251). In addition, I used the AliBaba2.1 TRANSFAC 4.0 transcription factor binding site prediction tool (252) to identify potential transcription factor binding sites. Moreover, potential promoter sequences were predicted by AliBaba2.1 TRANSFAC (260), applying the following parameters: the Pairsim function was set to 50, the matrix width set to 10 bp, a minimum number of overlapping predicted transcription factor binding sites was limited to a total number of four for each site with a minimum sequence conversation of 75% coverage, and the factor class was set to 4.

In addition, the potential promotor sequence was analyzed for canonical core promotor elements by the YAPP eukaryotic core promoter prediction tool by applying a cut-off score of 0.8 (253, 254). The promoter analysis was conducted analyzing the promotor sequence including the predicted core promoter fused with the sequence of eGFP (717 bp) in order to analyze potential transcription start sites (TSS). Subsequently, TSS prediction was performed by YAPP (253, 254). A comparative analysis applying the AGAT software-package (261, 262) was performed to determine potential Kozak sequences of other genes in the *S. mansoni* genome version V9 (263). To this end, ubiquitously and abundantly transcribed genes were screened for the presence of potential Kozak sequences and patterns similar to SmUbi (61). Specifically, the sequences of Smp_009580, Smp_106930, Smp_042160, Smp_056970, Smp_054160, Smp_182890, Smp_099870, Smp_179300, Smp_111340, Smp_090120, Smp_072330, Smp_003770, Smp_017430, Smp_040130, Smp_155060, and Smp_335990 were compared (264). Based on these results, the potential Kozak sequence of SmUbi was identified.

The 3´UTR of SmUbi defined by WormBase ParaSite (143, 259) was analyzed, based on version 7 of the *S. mansoni* genome (257, 258). To identify the polyadenylation signal, 600 bp downstream from the stop codon were analyzed with the DNAFSMiner-DNA Functional Site Miner polyadenylation side prediction tool (255). Subsequently, the RNA secondary structure of the predicted 3´UTR was computed, including the stop codon and predicted polyadenylation site. The RNAfold Webserver Vienna tool (255, 256) was used to investigate potential RNA secondary structures characteristic of translation termination loops. Calculation of secondary structures was performed by applying the minimum free energy (MFE) model and an activated partition function.

As reporter-gene construct (3.6.3. and 3.6.4.), I used an enhanced green fluorescent protein (eGFP) under the control of the promotor and terminator sequences of SmUbi (143, 168) for transfection/transformation analyses.

3.6 Cloning

3.6.1 Transformation of *E.coli*

As chemically modified, competent strains, *E. coli* DH5α or βcomp10 (NEB), were used for transformation. For transformation, 50 µl of the bacteria culture at OD600 = 0.6 was mixed with 0.005 pmol of the purified plasmid from the Gibson assembly or with 50 ng of ligated plasmids and incubated for 30 min on ice. Plasmid DNA was introduced into the bacteria by heat shock at 42°C for 30 s and immediately cooled for 3 min on ice. Subsequently, 300 µl of LB medium at RT was added to the preparation and incubated at 37°C for 30 min. After transformation, the preparation was spread onto selective LB agar plates and incubated overnight at 37°C. A plasmid-encoded antibiotic resistance (kanamycin and/ or ampicillin) was used as a selection marker. Successfully transformed bacterial clones were removed from the plates and transferred to selective LB liquid medium and cultivated at 37°C shaking at 135 rpm. From these cultures, plasmids were isolated and sequenced by Mircosynth Seqlab using gene or vector-specific sequencing primers.

3.6.2 Gibson assembly

Gibson assembly was used as the method of choice for the site-specific insertions of DNA fragments into plasmid backbones by applying homology-directed DNA assembly (265). With this method, several large DNA fragments can be assembled in a certain order, which is determined by the selection of the homologous sequence segments at the 3'-ends.

Fragment(s) to insert were amplified with specific primers, featuring 3´ overhangs homologous to the insertion site of the plasmid backbone. These homologous sequences were 18–30 bp in length. For Gibson assembly, 0.15 pmol/µl of each PCR product were added to 0.01 pmol/µl of linearized target plasmid and mixed with NEB Builder HiFi DNA Assembly Master Mix (NEB). The mixture was incubated at 50°C for 30 min. Incubation was extended to 2 h if more than three fragments were simultaneously integrated into a plasmid. Subsequently, the plasmid was used for EPO into *E. coli* DH5α or βcomp10 strains (NEB).

3.6.3 Cloning strategy of the reporter-gene construct

For the construction of an eGFP reporter-gene construct, driven by a native schistosomal promoter, a plasmid was constructed based on the pJC53.2 vector backbone (Table 19). For this purpose, 1 µg of pJC53.2 plasmid DNA was processed by 1 µg restriction enzyme AhdI (NEB) in a total volume of 50 µl 1x CutSmart buffer (NEB) at 37°C for 2 h. The two resulting DNA fragments were separated due electrophoresis. The fragment at 3,240 bp was extracted using Monarch Gel Extraction Kit (NEB).

To construct the reporter-gene, three different DNA fragments, a full-length eGFP and the putative promoter and terminator sequences of Smp_335990, encoding the schistosomal ubiquitin gene (SmUbi), were amplified. Primers for amplification of the ubiquitin promoter or terminator were designed based on previous *in silico* analyses to verify promoter or terminator associated sequences.

Amplicons of the target inserts were obtained by PCR using a final reaction volume of 20 µl containing 100 ng schistosomal gDNA or 10 ng pET30a_eGFP (kindly provided by Jim Collins). Fragments containing the putative ubiquitin promoter (2,056 bp) and terminator (580 bp) sequences were generated using gRNA. In addition, fragments encoding eGFP (717 bp) were generated using pET-30a_SmDHFR-eGFP (Quack *et al*., unpublished data). For the assembly of the reporter-gene construct, 1 µM of each primer (Table 1) and the recommended concentration for the Q5 High-Fidelity Polymerase Kit (NEB) were used. Template DNA was initially denatured at 98°C for 3 minutes, followed by 35 amplification cycles consisting of denaturation at 95°C for 30 seconds, primer annealing at 55°C for 30 seconds, and extension at 72°C for 1:15 minutes (Bio-Rad, S1000 Thermal Cycler). Aliquots of the PCR products were then analyzed by agarose gel electrophoresis. The fragments were then purified using the Monarch Gel Extraction Kit. This step was followed by an additional PCR to generate homology arms for performing a Gibson assembly (265) as the ligation method of choice (3.6.2). Primers were designed with homology arms to both the promoter and a truncated terminator sequence

(302 bp) of the previously prepared pJC53.2 backbone flanking the eGFP fragment. The Q5 High-Fidelity Polymerase Kit was used to prepare PCR reaction mixtures as previously described. Primers with 20-26 bp overhangs were used to amplify the fragments (Gibson primers, Table 13). The PCR was performed according to a two-step PCR protocol. First, the template DNA was initially denatured at 98°C for 5 min, followed by 10 amplification cycles consisting of denaturation at 95°C for 30 s, primer annealing at 54°C for 30 s and extension at 72°C for 1:15 min, followed by another 25 cycles with 62°C as an annealing temperature and a final extension step at 72°C for 5 min. Generated PCR products were analyzed by agarose gel electrophoresis and fragments were purified using the Monarch Gel Extraction Kit. The final reporter-gene construct, pJC53.2_UbiProm-eGFP-UbiTer, was assembled according to the instructions of the NEBuilder Hifi DNA Assembly Cloning Kit (NEB; 3.6.2). Assembled plasmids were transformed into chemically competent *E. coli* DH5α (NEB) by heat shock and selected by kanamycin and ampicillin containing LB plates at 37°C (overnight). The plasmids of the positive clones were verified by Sanger sequencing (Microsynth SeqLab).

3.6.4 Cloning strategy to generate plasmids for dsRNA/ ribo-probe syntheses

For dsRNA or ribo-probe synthesis, T7 promoter-driven constructs were cloned into plasmid vector pJC53.2 (266), as described in Moescheid and Puckelwaldt *et al.* (152). For cloning, 1 µg of pJC53.2 plasmid DNA was digested by *Ahd*I (NEB) in a total volume of 50 µl containing 1x CutSmart buffer (NEB) at 37°C for 2 h. Resulting DNA fragments were separated by agarose gelelectrophoresis, and amplicons of appropriate length were extracted using the Monarch DNA Cleanup and Gel Extraction Kit (NEB).

Amplicons of a size of approximately 500 bp were obtained by Q5 (NEB) PCR using a final reaction volume of 20 µl, including 100 ng *S. mansoni* cDNA generated by reverse transcription of extracted total RNA of couples as described in 3.3.9. PCR was performed using 1 µM of each primer targeting the respective transcripts and the recommended concentrations of components for the Q5 High-Fidelity Polymerase Kit (NEB). For PCR, template cDNA was initial denatured at 98°C for 3 min, followed by 35 cycles consisting of denaturation at 95°C for 30 s, primer annealing at 60°C for 20 s, and elongation at 72°C for 45 s (BioRad, S1000 Thermal Cycler). Agarose gel electrophoresis was performed on each aliquot of the PCR product. Amplicons were then extracted from the gel using the Monarch DNA Cleanup and Gel Extraction Kit and eluted in a final volume of 20 µl elution buffer. This was followed by an additional PCR to generate 3' A-overhangs (AccuPrime Taq DNA Polymerase High Fidelity kit; Invitrogen). For this purpose, 20 µl of the fragment-containing eluate was used as a template, and selected primers for corresponding templates were used for amplification. The template

DNA was initially denatured at 98°C for 3 min, followed by five 3'A-overhang-generating amplification cycles consisting of denaturation at 95°C for 30 s, primer annealing at 58°C for 30 s, and extension at 67°C for 5 min (Bio-Rad, S1000 Thermal Cycler). The resulting fragments were purified as described above.

The plasmids were then ligated to pJC53.2 using T4 ligase (NEB) as described in the T4 DNA ligation protocol (NEB). The recombinant plasmids were transformed into *E. coli* DH5α (NEB) by heat shock and selected by kanamycin and ampicillin-containing LB plates at 37°C. The sequence integrity of the plasmid inserts of selected clones was verified by Sanger sequencing (Microsynth SeqLab).

3.7 RNAi - Transcript knock-down by RNAi

For RNAi experiments, parasites were cultured for either 15 d or 22 d (couples), or 20 d (re-pairing experiments) starting one day after perfusion, with dsRNA added at a concentration of 30 µg/mL per approach. Medium was changed every 2-3 d including the addition of fresh dsRNA. Worm viability was monitored regularly along with medium replacement as described previously (81). Phenotypes were observed blinded using an inverted laboratory microscope (DM IL LED, Leica Microsystems) and graded according to the following scheme: 0, complete absence of movement; 1, only intestinal movements or occasional head and tail movements; 2, reduced motility; 3, normal activity; and 4, hyperactivity (152). In addition to morphological changes, attachment of the worms to the Petri dish, pairing status (either paired or separated), and oviposition were determined.

3.8 Physiological analysis of retinoic acid signaling

3.8.1 Effects of retinoic acids on *S. mansoni* reproduction

To determine the effects of 9cis-retinoic acid (RA) on *S. mansoni* reproduction, couples were cultured with added RA. For this purpose, 10 couples each were cultured in M199^{+++} supplemented with 5 µM RA. In order to assess the effects on the maturation of female schistosomes, pairing experiments were performed in RA-supplemented BaschABC/LDL medium at a concentration of 5 µM. Repairing experiments were conducted as described in 3.7.1. The RA stock solution was prepared at a concentration of 10 mM in DMSO. Couples in the control group received DMSO equivalent to RA-treated worms. RA was renewed daily by changing the medium. Viability parameters such as pairing rate, motility, attachment rate, and egg production were recorded daily.

3.8.2 RAR inhibition assay

Inhibitor experiments were performed with the cis-retinoid receptor (RAR) antagonist CH 55 (4-[(1E)-3-[3,5-bis(1,1-dimethyletyl)phenyl]-3-oxo-1propen-1-yl]-benzoic acid; Cayman Chemical Company (267)) at total concentrations of 10, 25, and 50 µM on 10 couples each. The stock solution was prepared at a concentration of 10 mM in DMSO (Sigma-Aldrich). DMSO (0.005% v/v); correspondingly, the highest concentration of DMSO in the course of CH 55 treatment was used as control. Schistosomes were cultured for 48 h, and the medium, which was supplemented with the respective inhibitor concentrations, was changed every 24 h. During the treatment period, viability, attachment, pairing rate, morphology, and oviposition were monitored every 24 h as previously described. To determine the effect of inhibitor treatment on cell proliferation, worms were treated with 10 µM EdU 24 h before the experiment was terminated. Finally, worms were fixed with either 4% PFA in PBS or AFA-fixative. Then, worms were prepared for further staining by the EdU staining protocol (3.9.1.) or carmine red (3.9.2.), respectively.

3.9 Staining methods

3.9.1 EdU staining

For the determination of cell proliferation (268), EdU (5-Ethinyl-2'-desoxyuridin) was added in a final concentration of 10 µM, 24 h before the end of the *in vitro*-culture period. Subsequently, couples were selected for EdU staining as follows: couples were first separated by adding 0.25% (w/v) tricain as described before (230). Female and male worms were separately collected in 1.5 mL reaction tubes and washed with PBS. The supernatant was discarded, and the worms were fixed with 4% paraformaldehyde in PBSTx at 4°C overnight. Worms were washed with PBSTx for 3 min and dehydrated in 50% methanol in PBSTx for 10 min, followed by incubation in 100% methanol for 10 min. Fresh 100% methanol was added for storage, and samples were stored at -20°C until further use.

Specimens were rehydrated by incubation in 50% methanol in PBSTx for 10 min, followed by a further incubation step in PBSTx for 10 min. Furthermore, worms were bleached for 1 h, under bright light in a 1 mL solution of 1.2% H_2O_2 (v/v), 5% deionized formamide (v/v) in 0.5 x SSC, before staining was performed using the Click-iT Plus EdU Alexa Fluor 488 imaging kit (Thermo Fisher Scientific), and with Hoechst 33342, as previously described (269). In order to permeabilize the worms for staining, they were incubated with proteinase K for 30 minutes. Worms were then fixed with 4% PFA in PBSTx for 10 min.

The Click-iT kit (ThermoFisher Scientific) was used to stain EDU-labeled DNA with Alexa Fluor 488. Subsequent steps were performed without light in volumes of 500 µL at RT and agitation at 130 rpm. For each sample, a Click-iT reaction was freshly prepared according to the manufacturer's protocol. Samples were incubated for 30 min in 500 µl reaction buffer. Afterwards, samples were washed twice in PBS. Additionally, cellular DNA was stained by Hoechst 33342 (diluted 1:1,000 in PBSTx) overnight at 4°C and 80 rpm. The following day, the solution was removed, and the samples were rinsed twice in PBS, before they were mounted on slides with FluorCare. The cover glass was fixed with clear nail polish, and the slide was stored at 4°C and protected from light until it was examined by confocal laser scanning microscopy (CLSM).

3.9.2 Carmine-red staining to prepare worms for CLSM

The morphological fine structure of either female or male worms were assessed by CLSM of carmine red stained worms (38, 270, 271). To this end, couples or separated worms were fixed in freshly prepared AFA for at least 24 h at RT. Staining was performed with CertistainH carmine red (Merck) for at least 30 min (38, 271). For destaining, the worms were incubated three times in acidic ethanol (70% (v/v), ethanol, 2.5% (v/v), hydrochloric acid (Roth) for 5-10 min. The intensity of the staining of the worms was carefully monitored by bright-field microscopy. Initially the worms appeared red. However, optimal destaining/staining was characterised by a pink color of the worms. The worms were dehydrated in 80%, 90% and, 100% ethanol for 5 min each before mounting on a slide in Euparal (Roth). For imaging by CLSM, carmine red was excited using an argon-ion laser at 488 nm, whereby a 470 nm long pass filter was used for detection. Background signals and optical section thickness were defined by setting the pinhole size to airy unit 1 (272).

3.9.3 Determining the volume of the ovary

To determine the volume of the ovary, female worms were stained with either carmine red or Hoechst 33342 for CLSM analysis. Z-stacks were generated, and images were analyzed using LasAF software. To define the lower and upper end of the ovary as the z-stack boundary, the maximum extension of the ovary on the z-axis (3D image) was determined microscopically. Fifteen individual images were taken along the z-axis, keeping the distances between the individual planes constant for each sample. The surface area of the area containing mature oocysts was determined using the ImageJ measurement function by applying the selection brush tool (206, 208). Subsequently, the resulting surface area (μm^2) of each image was then multiplied by the defined Z-stack travel distance (µm) of each individual image. An

approximation of the total volume (µm^3) of each ovary was obtained by summing the volumes obtained for each individual slice.

3.9.4 Lipid staining

Oil-Red O (Sigma-Aldrich)) was used to stain the lipid-rich vitelline droplets in the vitellarium of mature *S. mansoni* females. For this, a modified Oil-Red O staining protocol (49, 273) was used. Couples were separated using 0.25% tricain in PBS and washed twice in PBS. Fixation with 2% paraformaldehyde in PBSTx was performed overnight at 4°C on a shaker at 135 rpm. Afterwards, the worms were washed twice in PBSTx and incubated in 99% propane 1,2-diol for 5 min at RT (10 worms/mL). The worms were allowed to settle, and the supernatant was replaced by an equal volume of 0.5% (w/v) Oil-Red O (powder; Sigma-Aldrich) dissolved in propane 1,2-diol. Staining was performed on a shaker at 135 rpm for 45 min at RT. The Oil-Red O solution was then replaced with an equal volume of 85% propane 1,2-diol, and the solution agitated for 5 min. This step was repeated twice. Finally, the worms were washed with PBS and embedded in ROTI Mount FluorCare (Carl Roth, Germany) for immediate microscopic analysis. Phase contrast microscopy was performed with an inverted laboratory microscope (DM IL LED; Leica Microsystems, Germany).

3.9.5 Live dead staining

Viability of parasite life stages was screened by applying a Hoechst 33342, SYTOX Orange and Calcein-AM (HCS) co-staining to determine cellular integrity. For this the parasites were incubated in an appropriate volume of plain M199 medium containing 2 µM Hoechst 33342, 5 µM SYTOX Orange and 2 µM Calcein-AM (each from ThermoFisher Scientific). Parasites were incubated for 30 min and washed twice with M199 and then mounted on a slide in ROTI MOUNT FluorCare (Roth). The samples were analyzed by fluorescence microscopy according to the manufacturer´s instructions. SYTOX orange was used to stain DNA from cells with permeabilized cell membranes (274) and Calcein-AM to stain cells with intact cell membranes due to cellular esterase activity (231, 275). Hoechst 33342 served as DNA counterstaining of both vital and dead cells (276).

3.9.6 Whole mount *in situ* hybridization – WISH

Whole mount colometric *in situ* hybridization (WISH) is a method for localizing specific transcripts using RNA probes. The protocol described is a modified protocol according to Collins *et al.* (67, 277). The procedure and the necessary steps are described in the following subchapters.

3.9.6.1 WISH probe synthesis

Two master mixes were prepared, which differed in their composition only in the RNA polymerase. Template DNA, T3 or SP6 RNA polymerase, 10x transcription buffer, a DIG-NTP mix from our own production, murine RNase inhibitor (NEB) and DEPC water were used. The preparations were incubated overnight at 28°C. After addition of DNase at 36°C for 20 min, LiCl-mediated precipitation of the RNA was performed. For RNA precipitation, 1/10 LiCl solution (7.5 M) of the volume of in vitro transcription and a 3x volume excess of 100% ethanol (-20°C) were added and the mixture incubated at -20°C for 30 min. After centrifugation (16,000 g for 30 min at 4°C), the supernatant was removed, and 500 µl 70% Ethanol was added to the pellet. Another centrifugation step followed (16,000 g at 4°C for 4 min), and the supernatant again carefully discarded. The remaining pellet was air-dried for a maximum of 10 min under the fume hood. After addition of 30 µl DEPC water, 1 µl murine RNase inhibitor, and careful resuspension, an aliquot of 1 µl of the quality of riboprobes was analyzed using a 1.5% TAE agarose gel.

3.9.6.2 Sample preparation and hybridization

Localization of specific transcripts by WISH was performed based on the method established for plathelminth by King and Newmark (278), and as previously described (57, 230, 278, 279). The protocol used in this thesis was modified as described below. First, couples were separated by adding 0.25% (w/v) tricain, as described before (230). Separated males and females were killed by incubation in 0.6 M MgCl2 for 1 min while shaking, and then immediately fixed for 4 h in 10 mL 4% formaldehyde dissolved in PBSTx at RT. Fixed worms were washed twice in PBSTx, then dehydrated in 100% methanol, and afterwards stored at -20°C for at least 16 h. Schistosome couples were separated, and male and female worms separately transferred into 15 mL reaction vessels. For the following procedure, volumes of 10 mL were used for each solution. Pursuing the WISH protocol, worms were rehydration by incubation in 75% methanol for 2 min followed by 10 min incubation in 50% methanol dissolved in PBSTx. Subsequently, worms were washed twice in PBStx to remove remaining methanol, and

bleaching solution was added (9 mL DEPC treated H_2O, 500 µL deionized formamide, 250 µL 20x SSC pH=7, 400 µL 30% H_2O_2), samples were bleached for 1 h shaking under bright light. After bleaching, the samples were rinsed with PBSTx twice and permeabilized by proteinase K (Ambion; bM: 25 µg/mL; pairing experienced females, bF: 15 µg/mL) dissolved in PBSTx for 45 min, respectively. After permeabilization, worms were rinsed twice in PBSTx. To inactivate remaining proteinase K and to post fixate treated samples, the worms were incubated in 4% formaldehyde in PBStx for 15 min, and washed in a mixture of prehybridization solution and PBSTx (1:1) for 10 min.

The parasites were placed in small 40 µm mesh baskets in a 48 well-plate in 300 µL prehybridization solution for 2 h at 55°C while shaking. The following buffers in volumes of 300 µl were used for sample processing in a 48-well plate. For hybridization, DIG-labelled single stranded ribo-probes, synthesized as described above were used for colorimetric WISH. The probes were diluted in hybridization buffer at a concentration of 200 ng probe/ 1 mL and incubated at 78°C for 5 min to dissolve the secondary structures. The probes were allowed to cool to 55°C, ensuring that the temperature of the probes did not fall below 55°C. The probe-containing solution was transferred in one well of the 48-well plate, which has previously been preheated to 55°C on a heating plate. Subsequently, hybridization was performed at 55°C overnight (at least 16 h) while shaking at 135 rpm. The incubation was followed by a series of washing steps for 30 min each with pre-warmed wash buffers (2x SSC + 0.1% TritonX-100, 0.2x SSC + 0.1% TritonX-100, 0.1xSSC + 0.1% TritonX-100, pH=7) at 55°C. The samples were washed twice with 2x SCC and once each with buffer containing 0.2x SCC and 0.1x SCC in order to reduce non-specific mRNA binding of the riboprobe.

For the procedure, it was made sure that the pH of the buffers used for hybridization was always correct, while otherwise probe may bind ectopically (Figure 11)

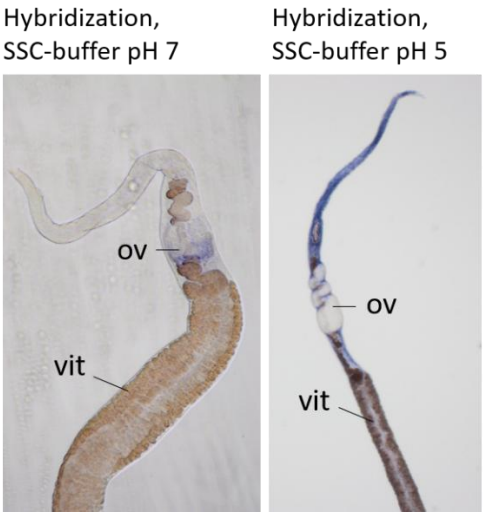

Figure 11. Example of the pH-dependent influence on probe specificity during WISH.
For hybridization, specific probes for Smp_174260 transcripts were applied to mature females obtained from a couple.Smp_174260 is an ovarian-preferentially and pairing-specifically expressed gene (55, 62). Hybridization was performed under different pH values of the SSC-buffer. Whereas at pH=7, the result was correct (left side), if remarkably differed at pH=5. Abbreviations: ov, ovary; vit, vitellarium.

3.9.6.3 Antibody incubation and colorimetric reaction

DIG-UTP labelled ribo-probes were used to hybridize target transcripts. To detect the location of target transcripts within the worm tissue, an anti-DIG-AP antibody for colorimetric detection was used.

Baskets containing worms were incubated in 300 µl of TNT buffer at RT for 5 min after the hybridization procedure had been completed. This was followed by two TNT incubations at RT for 10 min each, with shaking at 100 rpm. Baskets were transferred in 300 µl colorimetric block solution (7.5% heat-inactivated horse serum in TNT) and were incubated for at least 2 h at RT, with shaking at 100 rpm. In the meantime, the anti-DIG-AP antibody was diluted at a 1:2,000 ratio in pre-chilled colorimetric block solution at 4°C. Samples were incubated in 300 µl antibody-containing solution overnight at 4°C, with shaking at 100 rpm. The next day, samples were incubated in TNT buffer at RT (5 min, 10 min, followed by 6x 20 min each), shaking at 100 rpm, to remove unbound antibodies. Afterwards, worms were transferred to a well of a 24 well plate and developed in 500 µl AP-buffer supplemented with 450 µg/mL nitro-blue tetrazolium (NBT) and 175 µg/mL 5-bromo-4-chloro-3'-indolyphosphate (BCIP). Thereby, the development time differed target gene-dependently between 2 to 24 h. Development was stopped by incubating the worms twice in 1 mL of PBSTx for 5 min, followed by a final

destaining step with 1 mL 100% ethanol for 10 to 20 min. The duration of destaining depended on the staining intensity of individual samples. Worms were incubated in 80% glycerol in PBS for at least 30 min before mounting on a slide. Pictures were taken using a Leica microscope (M125 C) and a Leica camera (DMC2900; Leica).

3.10 Transformation methods

3.10.1 Worm transfection by particle bombardment

Particle bombardment (PB) was used as transfection method of choice to verify gene expression of the SmUbi-eGFP-SmUbi reporter gene construct. For this, the stationary PDS 1000/He system was used (Bio-Rad, Hercules, CA) according to our previous protocol (94, 95). Plasmid DNA was isolated using the PureLink Expi Endotoxin-Free Maxi Plasmid Purification Kit (Thermo Fisher Scientific) and precipitated onto gold particles (0.6 µm) using $CaCl_2$, spermidine, and ethanol (94, 95) at a final concentration of 5 µg DNA/600 ng gold. For this, male schistososomes were transfected, given their absence of autofluorescence in the eGFP channel. The culture medium was removed, and male worms were positioned centrally in a Petri dish; 10 male schistosomes were included in each biological replicate. The ballistic parameters applied were helium gas pressure at 1,550 psi, 3 cm target distance, 15 inHg (381 mmHg) atmosphere, and 23°C. After PB, pre-warmed $M199^{+++}$ at 37°C was added to the worms. Worms were maintained in culture for 48 h before further analysis. For microscopic analyses, the nuclei of the worms were stained with Hoechst 33342 (Invitrogen) for 120 min. Afterward, worms were examined using fluorescence microscopy (IX71 Inverted Fluorescence Microscope Pred IX73, Olympus) and CLSM (TCS SP5 vis confocal laser scanning microscope, Leica). The acquired images were analyzed using CellSens software (Olympus) and LAS X software (Leica). Worms showing eGFP-induced fluorescence were washed with PBS, transferred to 50 µl RNAzol RT reagent, and subsequently frozen in liquid nitrogen. Next, total RNA was isolated from these worms, and its concentration and integrity were evaluated as described in 3.3.5. Furthermore, cDNA of each sample was synthesized by reverse transcription of 100 ng total RNA as described in 3.3.8. PCRs using these cDNAs were performed in 25 µl reaction volumes with 200 µM dNTPs, 0.5 µM each primer, 1 µl cDNA, and FIREPol DNA Polymerase (Solis BioDyne). Finally, the eGFP transcript of 717 nt was amplified by PCR using the primers eGFP_fw and eGFP_rev (Table 13): 98°C, 30s, 35 cycles of 98°C for 30s, 55°C for 30s, and 72°C for 60s; 10 ng pJC53.2_ SmUbi-eGFP-SmUbi plasmid-DNA served as a positive PCR control.

3.10.2 Transformation of parasites by electroporation

Electroporation (EPO) was used to transfect parasitic life stages with nucleic acids or proteins. For this, a 4 mm electroporation cuvette containing plain phenol red-free OptiMEM (Gibco) was used to transfer up to 10,000 eggs, 2,000 4-7 d old sporocysts, or 10 paired adult worms to a final volume of 200 µl. Additionally, 100 µl OptiMEM-containing nucleic acids and/or protein were added to the cuvette, and the sample was gently mixed. The sample was incubated at RT for 5 min before EPO was applied by a single pulse at 125 V for 20 ms using the square wave function (Gene Pulser Xcell Electroporation Systems, BioRad). Parasites were regenerated for 10 min before being transferred to an appropriate volume of stage-specific medium and cultured for at least 48 h.

3.11 Editing of the *S. mansoni* genome

The genome of *S. mansoni* was edited by a CRISPR/Cas9 and/or Cas12a based method. For this schistosome material at different life stages, such as eggs (Figure 12) were edited. The CRISPR/Cas based editing approach of the *S. mansoni* genomic safe harbor site 1 was carried out according to Ittiprasert and Moescheid *et al* (169, 172, 189, 280). as described in the following chapters.

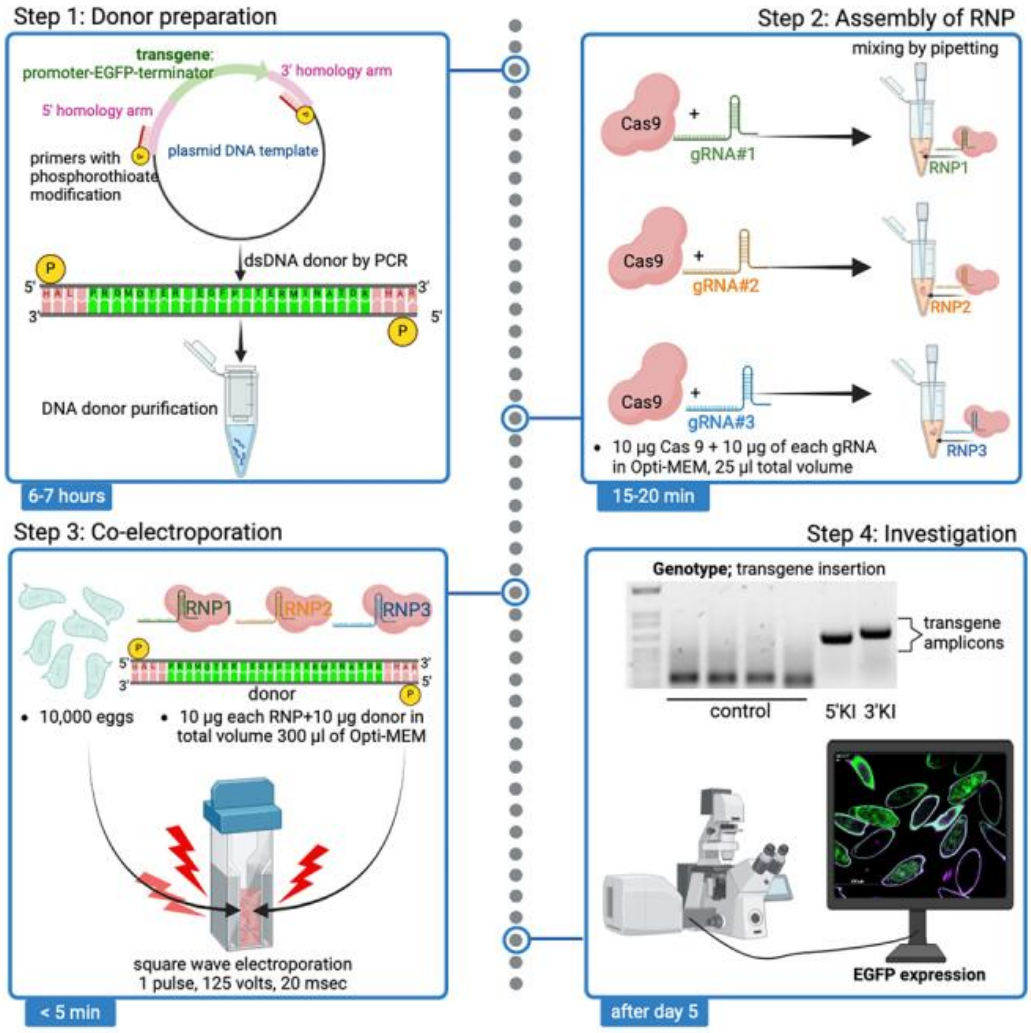

Figure 12. Transformation of *S. mansoni* eggs with CRISPR/Cas RNPs and editing of target-specific genomic loci.

Step 1, Illustration of donor preparation. **Step 2**, Assembly of CRISPR/Cas-enzymes and corresponding guide RNAs into riboprotein complexes (RNPs). **Step 3**, Introduction of CRISPR/Cas material and donor DNA into *S. mansoni* eggs via EPO. **Step 4**, Analysis using PCR, RT-qPCR, and fluorescence microscopy. Illustration from Ittiprasert *et al*. (280).

3.11.1 CRISPR/Cas

A first protocol was established targeting the *S. mansoni* genomic safe harbor site 1 (GSH1) located on chromosome 3; 13380432-13381848 (172). To this end, single guide RNAs (sgRNAs) specific targeting GSH1 were designed using the CHOPCHOP tool (261, 281), by using the version 7 annotation of the *S. mansoni* genome (258). Experiments were performed using Alt-R A.s. Cas12a (Cpf1) V3 (A.s. Cas12a, IDT), Alt-R L.b. Cas12a (Cpf1) Ultra (L.b. Cas12a, IDT) and Alt-R S.p. Cas9 Nuclease V3 (Cas9, IDT). CRISPR/Cas material was introduced as riboprotein complexes (RNPs) by EPO. RNPs were formed by using sgRNAs (Table 16) specific for the *S. mansoni* GSH1, chairing a similar cleavage site (A.s./L.b. Cas12a sgRNA, 5'-GAG AUC AAU UAU CUG ACA AUG GAA-3'; S.p. Cas9 sgRNA 5'-GAG AUC AAU UAU CUG ACA AU-3'). A gRNA with a scrambled, non-schistosomal sequence (5'-GCA CUA CCA GAG CUA ACU CA-3', IDT) was used to generate RNPs not targeting the *S. mansoni* genome.

3.11.2 Cas9 and Cas12a *in vitro* activity assay

The capacities of the two RNPs to cleave GSH1 at the predicted cleavage site were tested. RNPs were formed from specific guide RNAs with either Cas9, A.s. Cas12a, or L.b. Cas12a nucleases. For this purpose, an *in vitro* cleavage assay was performed (282). From *S. mansoni* gDNA, a 750 bp long fragment harboring the predicted cleavage site in the middle was amplified. The amplicon was obtained by PCR using the recommended concentrations and volumes for the GoTaq reagent (Promega). Amplification was performed using GSH1 targeting primers (TIDE primer pairs, Table 12), and the PCR was performed as follows: gDNA was initially denatured at 98°C for 3 min, followed by 35 amplification cycles consisting of denaturation at 95°C for 20 s, primer annealing at 60°C for 30 s and elongation at 72°C for 1 min.

To perform the *in vitro* Cas activity assay RNPs were formed by mixing the respective gRNA with the respective Cas enzyme at an equimolar concentration of 30 nM in a total volume of 20 µl in 1x Cas reaction buffer. The mixture was incubated for 15 min at 37°C to form RNPs. Cas enzymes without the addition of gRNA served as controls. In addition, 50 ng of the resulting GSH1 fragment dissolved in 10 µl Cas reaction buffer was added to the reaction. The reaction was incubated for 1 h and terminated by incubation at 90°C for 10 min. The mixture was applied to a 2% agarose gel. Successful cleavage of the substrate DNA resulted in 350 bp fragments.

3.11.3 Editing of the GSH1 of adult schistosomes

To determine the success of GSH1 targeting by using RNPs, KO were performed. RNPs were applied, formed by either Cas9 or Cas12a, and the corresponding sgRNAs. To determine the potential off-target effects on GSH1 of respective enzymes, sgRNA with a scrambled sequence was utilized for RNP formation. Plain Opti-MEM (Gibco) without RNPs served as control. For each biological replicate, RNPs were introduced into 10 adult unpaired schistosomes (5 worms of each sex) 45-49 d after mice infection. All experiments were performed in ten biological replicates.

To generate RNPs, 10 µg of the respective Cas-enzyme and 10 µg of corresponding sgRNA were carefully mixed in a final volume of 100 µl of Opti-MEM and incubated for 15 min at RT. In between, an appropriate number of schistosomes were washed in pre-warmed 37°C Opti-MEM and distributed into 4 mm electroporation cuvettes prepared with 100 µl Opti-MEM at RT. Finally, 100 µl of RNP solution was added to prepared worms. Subsequently, the solutions were gently mixed, incubated for 5 min, and electroporated at 125 V, 20 ms, square wave (BTX, ECM 830 Electro Square Porator). For recovery the cuvette was immediately placed in a bio-safety cabinet for 10 min at RT. The worms were then transferred to a new well of a 6-well plate with a finale volume of 3 mL of prewarmed $M199^{+++}$. Furthermore, the schistosomes were incubated for up to 10 d (37 C, 5% CO_2), with 50% of the medium replaced every second day.

3.11.4 Trypsinization and editing of the GSH1 in eggs

Transmission electron microscopy (TEM) studies on developed *S. mansoni* eggs have described the presence of proteins in pores and on the surface of the eggshell (83, 283). I hypothesized that the presence of proteins, particularly in these pores, could drastically reduce transfection efficiency. To reduce the effect of this natural barrier, the eggs were digested with trypsin-EDTA immediately before transformation.

For each replicate 10,000 LEs were collected in a 1.5 mL microtube. The LEs were pelleted by gravitation under exclusion of light for 5 min. Subsequently, the medium was carefully discarded and replaced by 1 mL Opti-MEM. LEs were washed twice. Next, the supernatant was discarded and replaced with 500 µl prewarmed (37°C) 0.25 Trypsin-EDTA (Corning). After gently mixing, the tube was incubated for 5 min at 37°C. Trypsin was inactivated by the admission of 1 mL M199egg (37°C). Additionally, LEs were washed twice with 1 mL Opti-MEM as described before and the supernatant was replaced by 100 µl Opti-MEM.

After trypsin treatment, LEs were immediately used for transfection with RNPs, as described above. The procedure was performed using 10,000 LEs per biological replicate. After incubation for at least 48 h (37°C, 5% CO_2), eggs were examined.

3.11.5 Tracking of rhodamine-labeled RNPs

Tracking of fluorescently-labelled RNPs after transfection was used as a viable tool to monitor the successful penetration of desired tissue and cells (170, 256). For this approach, a sgRNA was tagged with a rhodamine-containing RNA labelling reagent according to the manufacture's manual (*Label* IT® Nucleic Acid Labelling Reagents Rhodamine Kit; Mirus). Labelled RNPs were formed by using either Alt-R S.p. Cas9 or Alt-R L.b. / A.s. Cas12a (Cpf1) V3 and regarding purified and labelled sgRNA as described by Nasri *et al.* (256). In short, 10 µg of Cas-enzyme and 10 µg of previous labelled sgRNA were carefully mixed in a final volume of 100 µl of Opti-MEM (Gibco) and incubated for 15 min at RT. The incubation was performed in the absence of light. The supernatant was replaced with 100 µl of Opti-MEM, and 1,000 IVLEs were trypsinized as described above. A total volume of 100 µl of labelled RNP solution was added. Transfection was performed by EPO at 125 V, 20 ms, square wave (BioRad) using a 4 mm electroporation cuvette. Subsequently, the cuvette was placed in a biosafety cabinet for 10 min at RT, and 1 mL of M199egg at 37°C was added. Next, IVLEs were incubated at 37°C for 1 h. Finally, labelled RNPs were localized by CLSM (TCS SP5 vis confocal laser scanning microscope, Leica). The fluorescence was observed with excitation and emission wavelengths 576 nm and 597 nm, respectively (256). Image processing was performed using LasX software (Leica).

3.11.6 Determination and comparison of KO efficiency by TIDE analysis

DNA libraries were prepared for Sanger direct sequencing to obtain an overview of the success of genome editing by RNPs. Worms or eggs from editing experiments were transferred to 1.5 mL microtubes, the medium containing the supernatant was discarded and replaced with 50 µl of DNAzol. DNA was isolated as described in 3.3.1.

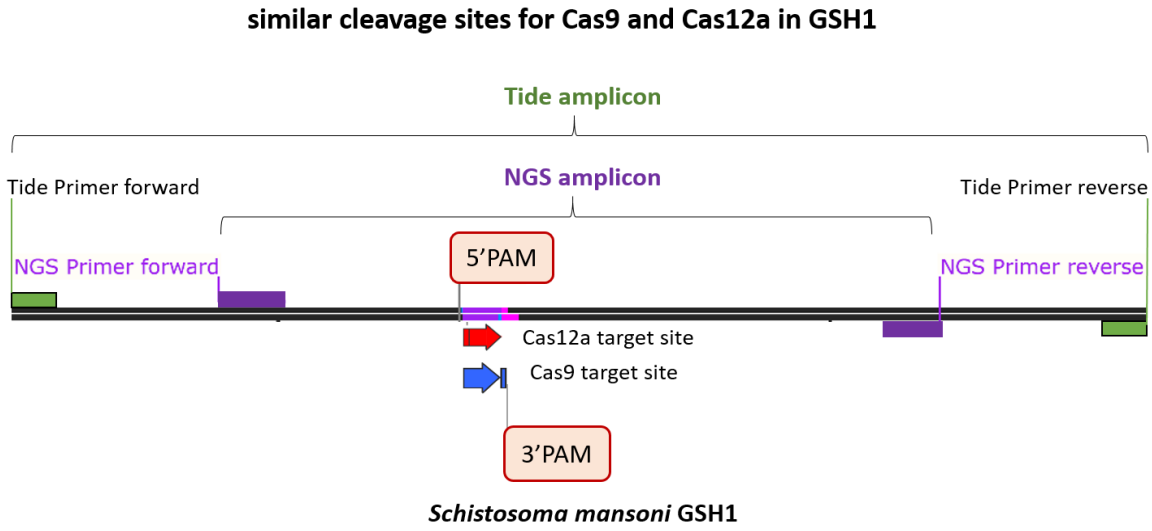

Figure 13. CRISPR/Cas-mediated cleavage of *S. mansoni* GSH1 and amplification of the target locus for sequencing-based downstream analysis.
PAM sites for both Cas9 and Cas12a enzymes were chosen to elicit similar Cas-mediated cleavage of GSH1. Primer binding sites based on Sanger sequencing (Tide) and next generation sequencing (NGS) are shown. Abbreviations: NGS, next generation sequencing; PAM, protospacer adjacent motif.

The library was generated by amplification of a 720 bp fragment containing the expected Cas9/12a editing site (Figure 13). The amplicon was obtained by PCR using the recommended concentrations and volumes for the GoTaq reagent (Promega). Amplification was performed using specific TIDE primers targeting the GSH1 (Table 12). In addition, the following PCR program was used (BioRad, S1000 Thermal Cycler), gDNA was initially annealed at 98°C for 3 minutes, followed by 35 amplification cycles consisting of denaturation at 95°C for 20 seconds, primer annealing at 60°C for 30 seconds, and extension at 72°C for 1 minute. The size of the relevant PCR products was verified by gel electrophoresis and purified using the NucleoSpin Gel and PCR Clean-up Kit (Macherey-Nagel). The concentration of the purified amplicons was determined spectrometrically. In addition, the concentration was adjusted to 15 g/µl according to the sequencing service provider (Genewiz / Microsynth Seqlab), and the appropriate forward or reverse primer was added to the mixture at a final concentration of 4 µM. Primers for performing PCR as described above were used as sequencing primers.

Sanger sequencing was performed to analyze CRISPR/Cas-mediated indels (deletions and insertions) at the GSH1 locus. For this, the program TIDE: Tracking of Indels by Decomposition tool (202) was used. By comparing the sequencing data of the treated group to an untreated control or controls containing a gRNA with a scrambled sequence, the editing efficiency by Cas9 or Cas12a was determined.

3.11.7 Next generation sequencing and KO efficiency analysis by CRISPRESSO and CasAnalyzer

DNA libraries were generated for next-generation sequencing (NGS) to verify successful editing by RNPs. Worms or eggs from editing experiments were transferred to 1.5 mL microtubes, the medium containing the supernatant was discarded and replaced with 50 µl of DNAzol. DNA was isolated as described in 3.3.1.

The library was generated by amplification of a 378 bp fragment including Illumina adapter sequences containing the expected Cas9/12a editing site (Figure 13). The amplicon was obtained by PCR using the NGS GSH3757 primer pair with Illumina adapters (Table 12) and the recommended concentrations of the GoTaq PCR Kit. In addition, the following PCR program was used (BioRad, S1000 Thermal Cycler). gDNA was initially denatured at 98°C for 3 min, followed by 10 pre-amplification cycles consisting of denaturation at 95°C for 20 seconds, primer annealing at 55°C for 30 seconds, and extension at 72°C for 35 seconds. This step was followed by 25 final amplification cycles similar to the pre-amplification cycles described above but using an annealing temperature of 62°C for 30 seconds.

PCR products were sized by gel electrophoresis and purified using a NucleoSpin Gel and PCR Purification Kit (Macherey-Nagel). Finally, a DNA 1000 chip (Agilent Technologies) was used with the Agilent 2100 Bioanlyzer system to determine the DNA concentration of the distinct band at 378 bp. NGS libraries were prepared and sequenced according to the Amplicon-EZ protocol (Genewiz). Data gathered from NGS of GSH1 knock out experiments were analyzed for editing efficiency as well as indel frequency by using the bioinformatics tools CRISPResso2 (284) and CRISPR RGEN Tools Cas-Analyzer (285). The analysis using CRISPResso was evaluated using NGS data as paired end reads, using the optimal parameters as follows: Minimum homology for alignment on amplicon, 60%, base editing target base C and result base T, pegRNA extension quantification window size to 5, quantification window was set by -3 and plot window size to 30, and the TruSeq2PE adapter trimming setting was used. For the use of the CRISPR RGEN tool Cas-Analyzer, sense and antisense reads of NGS sequencing were both used. Furthermore, the following setup was used: Nuclease type was set to single

nuclease as detection mode, all NGS datasets were tested against the specified reference, the comparison range was set to 70, wild type marker was set to 5, and minimum frequency was set to 1.

3.11.8 Generation of donor DNA via PCR for 5’ C6-PEG-10 50 bp HA donor

The donor DNA template consisting of 3,351 bp of SmUbi promoter (2,056 bp), eGFP (717 bp), and SmUbi terminator (578 bp) flanked by HAs of 50 bp each was amplified by PCR using 5' C6-PEG10- modified primers with 50 bp homology arms (HA), which were homologous to GSH1 (Table 14). The donor was 5´ modified by an amine group, a C6 linker (AmC6), and polyethylene glycol (PEG10) treatment (286, 287). Briefly, 10 µM 5'-amine C6 modified primers (IDT) were incubated with 1 mM Bis-PEG10-NHS ester (BroadPharm) in 1x borate buffer (Thermo Fisher) for 18 h at RT. Primers were desalted and dissolved in Tris-buffer using a Bio-Spin 30 column (Bio-Rad). These PEG10-5'AmC6- modified primers were used to amplify the donor template using GoTaq Green Master Mix DNA Polymerase (Promega). The SmUbi-eGFP-SmUbi construct with the 600 bp HA sequence (172) targeting GSH1 was used as template DNA with the following PCR conditions: 98°C, 5 min, 6 cycles of 95°C, 20 s, 56°C 30 s, and 72°C 3:35 min, followed by 25 cycles of 95°C, 20 s, 68°C 3:35 min, and 72°C 3:35 min. The presence of an amplicon of the expected size, 3,451 bp, was confirmed by agarose gel electrophoresis. The amplicon was isolated as described above.

3.11.9 Knock-in of the SmUbi-eGFP-SmUbi transgene in eggs of *S. mansoni* using Cas9/12a RNPs.

Genome editing of *S. mansoni* eggs either with CRISPR/Cas9 or Cas12a was performed according to the protocol of Ittiprasert and Moescheid *et al.* (172, 189, 280) with some modifications.

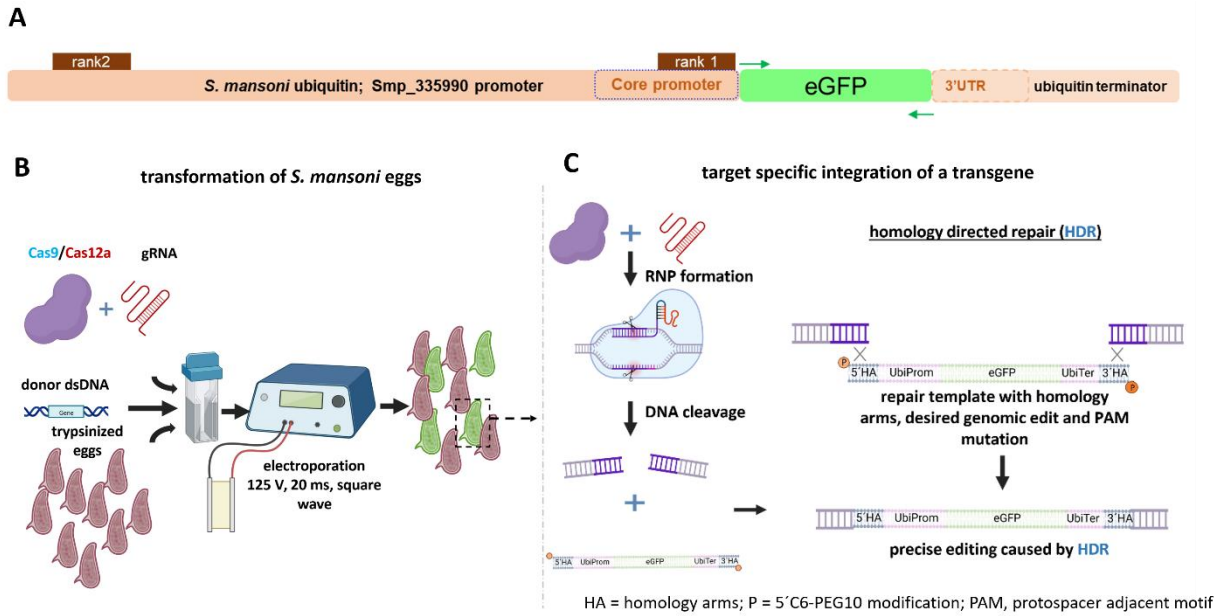

Figure 14. Workflow of CRISPR/mediated target-specific integration of a reporter-gene.
A, Illustration of the SmUbi-eGFP-SmUbi reporter-gene construct. The core promoter and the predicted rank1 and rank2 promoters are highlighted. **B**, Transformation of trypsinized eggs with Cas9/Cas12a ribonuclear complexes and the dsDNA donor template by EPO. **C**, CRISPR/Cas-mediated integration of the 5' C6-PEG10 modified donor with 50 bp homology arms, homologous to target locus, by homology directed repair.

For each experimental replicate, 5,000 to 10,000 LEs were collected. Consequently, LEs were trypsinized as described in 3.11.4. and transferred into a 4 mm electroporation cuvette. RNPs were formed as described in 3.11.3. Meanwhile, 10 µg of each 50 bp HA 5'C6-PEG10 3.11.8 modified UbiProm-eGFP-UbiTer donor dsDNA dissolved in Opti-MEM (Gibco) was added to LEs in a total volume of 200 µl. LEs were incubated with donor dsDNA for 5 min at RT, before 100 µl of RNP solution containing 10 µg Cas-enzyme and 10 µg gRNA was added (Figure 14 A, B). Experimental groups in which only donor DNA was added, and a non-treated group, served as controls. EPO was performed as described in 2.1 Subsequently, LEs were transferred to a well of a 12-well plate in a total volume of 2 mL M199egg and incubated (37 C, 5% CO_2). Aliquots of treated LEs were collected after 5- and 10-d post treatment for downstream analysis. Edited eggs were exposed to light 48 h after transformation to generate miracidia for infection of the intermediate snail host.

To increase the chances of editing cells of the germline, further knock-in (KI) experiments using Cas12a RNPs with up to 24 h old IVLEs were conducted. Up to 2,000 IVLEs were collected in a 1.5 mL reaction tube und processed as described above. IVLEs were examined microscopically after 7 d, and attempts were made to introduce the resulting potentially transgenic miracidia into the parasitic cycle via infection of the intermediate host.

3.11.10 Analysis for verification of successful knock-in by PCR

To demonstrate the successful KI of SmUbi-eGFP-SmUbi in GSH1 by homologous directed repair (HDR, Figure 14 C), primers were designed specific to the modified GSH1 locus (Figure 15).

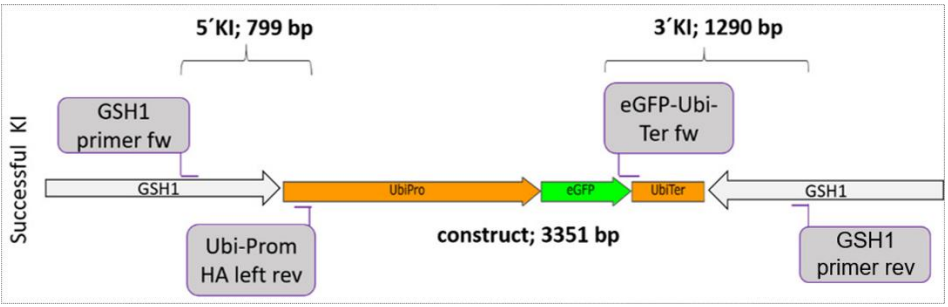

Figure 15. Proof of successful transgene integration into the *S. mansoni* GSH1 by PCR.
The primer binding sites and the resulting amplicon sizes after successful SmUbi-eGFP-SmUbi transgene integration into *S. mansoni* GSH1 are shown.

At 5- and 10-d post-transfection, LEs were harvested from experimental or control groups. The 5' and 3' transgene integration into GSH1 was analyzed by PCR on gDNA from each sample. A primer pair spanning 799 nt of the upstream region of GSH1 and part of the ubiquitin promoter (Table 15) was used to verify the 5' terminus. For analyzing the 3' end, a primer pair covering 1,290 nt of the modified GSH1 locus, specifically a chimeric primer covering the eGFP was used coding-sequence and the terminator combined with a primer for GSH1 (Table 15). Specific primers amplifying the GSH1 located at a significant distance from the HAs of the donor DNA template were designed for the KI analysis. These primers were each combined with primers specific for the donor DNA to investigate the success of transgene integration (Table 15). Both PCRs were performed using GoTaq Master Mix DNA polymerase (Promega), 10 ng gDNA and 10 µl reaction volume as follows. PCR conditions were 98°C for 5 minutes, 38 cycles of 95°C for 30 seconds, 60°C for 30 seconds, and 72°C for 80 seconds. As *S. mansoni* internal control, a PCR was performed amplifying a 1,466 bp fragment by using GSH1-specific primers (Table 15). The amplification of the 4,732 bp fragment representing the

complete reporter-gene integrated into GSH1 was not possible due its length and the PCR conditions.

In order to determine successful integration at the sequence level, amplicons of the modified GSH1 were analyzed using Sanger sequencing. The amplicon size was verified by gel electrophoresis. DNA fragments of correct sizes were isolated using the NucleoSpin Gel and PCR Clean-up kit (Macherey-Nagel). DNA samples were prepared for Sanger sequencing according to Genewiz descriptions and submitted with PCR primers specific to each respective amplicon. Subsequently, the resulting sequences were compared with the predicted reference sequence by Benchling software.

3.11.11 Verification of eGFP transcription

Reverse transcriptase PCR (RT-PCR) was performed to verify the successful transcription of the integrated UbiProm-eGFP-UbiTer construct. For this 3,000 LEs of each biological replicate were collected 10 d after editing attempts, and RNA was isolated as described in 3.3.6. Furthermore, cDNA was synthesized as described in 3.3.8. Subsequently, the cDNA was used for PCRs to carry out the transcription of the transgene UbiProm-eGFP-UbiTer while using eGFP-specific primers (Table 11). Primers amplifying the transcripts of the housekeeping gene Sm*gapdh* (Table 11) served as normalization control. Ten ng of the donor dsDNA containing the eGFP sequence were used as positive control. Amplicons were obtained due PCR using a final reaction volume of 25 µl including 3 µl cDNA, 1 µM of each primer and recommended volumes for the GoTaq reagent (Promega). PCR was carried out by using the following program: initial denaturation at 98°C for 3 min followed by 40 amplification cycles, consisting of denaturation at 95°C for 30 s, primer annealing at 55°C for 30 s and elongation at 72°C for 1 min. Amplicons were analyzed by agarose gel electrophoresis.

3.11.12 Verification of eGFP expression by CLSM

To determine the presence of eGFP in LEs or IVLEs after treatment with RNPs in combination with donor dsDNA and the larval development, CLSM was done (confocal laser scanning microscope, Zeiss Examiner.Z1 AX10; Camera, Carl Zeiss AxioCam MRc) using an inverse objective with 20-fold magnification (Zeiss W Plan-Apochromat 20x/1.0 DIC (UV) VIS-IR 421402-9800) (172). Images of live LEs respectively IVLEs in M199egg in tissue culture dishes were obtained at an excitation wavelength of 488 nm. Images were captured and analyzed using ZEN 2011 software (Zeiss) to distinguish eGFP fluorescence signals from eggshell autofluorescence, an approach developed by Ittiprasert *et al.* (172).

3.11.13 Editing of Sm*thr-β* by Cas12a

In order to apply the genome editing method to a gene of interest, knockout of Sm*tr-β* (Smp_174260) has been tested. Our recent study (172) demonstrated the increase of KO efficiency by the use of three overlapping sgRNAs. For this purpose, three overlapping L.b. Cas12a sgRNAs (Table 17) targeting the translational start site were designed using the CHOPCHOP tool (261): sgRNAthr-β1, 5´-GUA CUA GCA UUA UCU CAA UAU AUU-3´; sgRNAthr-β2, 5´-UUU CGU ACU AGC AUU AUC UCA AUA-3´; sgRNAthr-β3, 5´-UGU AAA UAA UUU UGU UUC GUA CU-3´. Proof-of-principle experiments were performed by introducing RNPs into *S. mansoni* couples by EPO as described in 3.10.2. An amount of 3.5 µg RNPs of each L.b. Cas12a/sgRNA combination were simultaneously introduced. Subsequently, couples were cultured in Basch ABC/LDL at 37°C and 5% CO_2 (57). After 2 d, the medium was replaced with freshly prepared BaschABC/LDL. After 3 d, IVLE's were collected for downstream analyses. gDNA was isolated from worms (3.3.1.) and IVLE's using DNAzol (3.3.2.). A 750 bp fragment with the predicted cleavage site in the middle was amplified by PCR as described in 3.11.6. The amplicons were isolated form the agarose gel and sequenced by Sanger direct sequencing. KO efficiency was determined by TIDE analysis (202).

3.12 Statistics

Data received from RT-qPCR analysis were statistically analyzed by comparative testing of the normalized transcription-levels as previously described in Moescheid and Puckelwaldt *et al.* (152). Statistical analyses were carried out using the GraphPad Prism V.8 software (GraphPad Software, San Diego; USA). Data were tested for Gaussian normal distribution by applying the Komogorov-Smirnov test. For statistical analysis, the two-tailed t test was applied for parametric distributed data and the two-tailed Mann-Whitney test was applied for non-parametrically distributed data. P-values < 0.05 were considered as statistically significant.

4 Results

4.1 Characterization of ovary-preferentially and pairing-dependently expressed nuclear receptors of *S. mansoni*

Previous comparative transcriptome studies of adult schistosomes and their (isolated) gonads revealed that, among others, genes encoding nuclear receptors (NRs) are regulated in a pairing-dependent manner (Figure 16) (55). Additionally, some of these NRs seemed to be expressed tissue-specifically with, for instance, a preference in female ovaries (55). Members of the NR superfamily are ligand-activated transcription factors that play diverse roles in differentiation, development, proliferation, and metabolism of cells, emphasizing their biological importance (85). To this end, I focused on identified but yet uncharacterized NRs of *S. mansoni*. This preselection comprised among others potential retinoic acid (Smp_144170 SmRAR, and Smp_097700 SmRXR1) and thyroid hormone receptors (Smp_133490 SmTHRα, and Smp_174260 SmTHRβ).

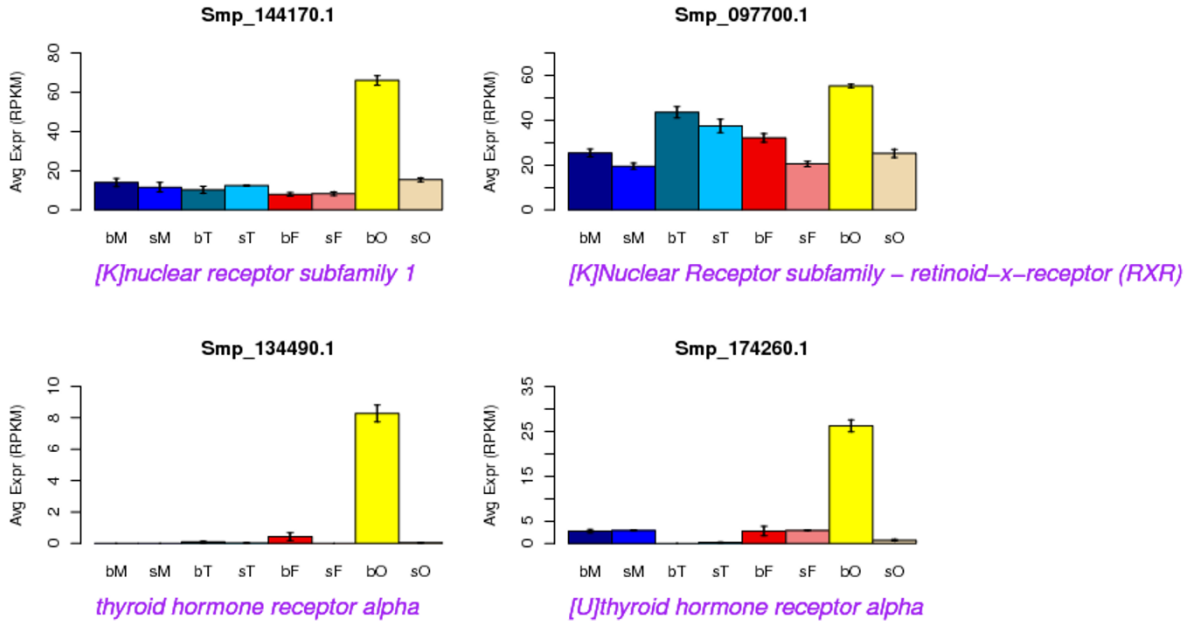

Figure 16. Pairing-dependently and ovary-preferentially transcribed nuclear receptors of *S. mansoni.*

Previous transcriptome analyses of pairing-experienced and -inexperienced male and female schistosomes and their isolated gonads by Lu *et al.* (55) revealed the pairing-dependent and ovary-preferential transcription of the four putative nuclear receptors shown here. Abbreviations: bM, bisex male (pairing-experienced male); sM, single-sex males (pairing-inexperienced male), bT, testes of bM; sT, testes of sM; bF, bisex female (pairing-experienced female); sF, single-sex (pairing-inexperienced female); bO, ovary of bF; sO, ovary of sF.

4.1.1 Phylogenetic classification of *S. mansoni* NRs

Based on their annotation in the *S. mansoni* draft genome V10 (143, 288), NRs, which were found to be transcribed in an ovary-preferential and pairing-dependent manner (55) were assigned to the sub-family of type II NRs. These receptors included members of the NR classes RAR, RXR and THR (Figure 16) (55, 62, 143). Until today, the knowledge about the function of these *S. mansoni* NRs is rather limited. In order to validate the given annotations, a phylogenetic analysis was carried out by comparative analysis of the paralogs and orthologs of these receptors (Figure 17).

The evolutionary distance of these receptors to other known type II NRs was revealed by phylogenetic analyses using MEGA11 (210), by analyzing the amino acid sequences of SmRAR, SmRXR-1, SmTHRα and SmTHRβ paralogs and orthologs from other organisms at different evolutionary distances (Figure 17). The phylogenetic classification showed that RAR-like as well as THR-like NRs of trematodes clustered separately from other invertebrates as well as vertebrates, suggesting the existence of trematode-specific subgroups within the class of type II NRs. Furthermore, SmRAR displayed distinct evolutionary classification compared to other RARs of *S. mansoni*, such as Smp_097700 (SmRXR-1) and Smp_073470 (SmRXR-2). These receptors were identified as potential dimerization partners of SmRAR in previous studies (104, 140, 148). Additionally, SMART domain analysis of both paralogs confirmed their identity as NRs and classified them as members of the retinoid-x-nuclear receptor (RXR) family (168, 243). As a trematode ortholog of SmRAR, a RXR from *Fasciola hepatica* was found. Phylogenetic analysis of this RXR revealed a close evolutionary distance to the *S. mansoni* SmRXR-1, and it was shown to be more distantly related to SmRXR-2. In contrast, SmRAR appeared more closely related to RAR-like orthologs from other trematodes, such as *Opisthorchis viverrini* and *Dicrocoelium dendriticum*, than to orthologs from the nematode *C. elegans* (RAR-like NHR-23) or *D. melanogaster*, mice, and human.

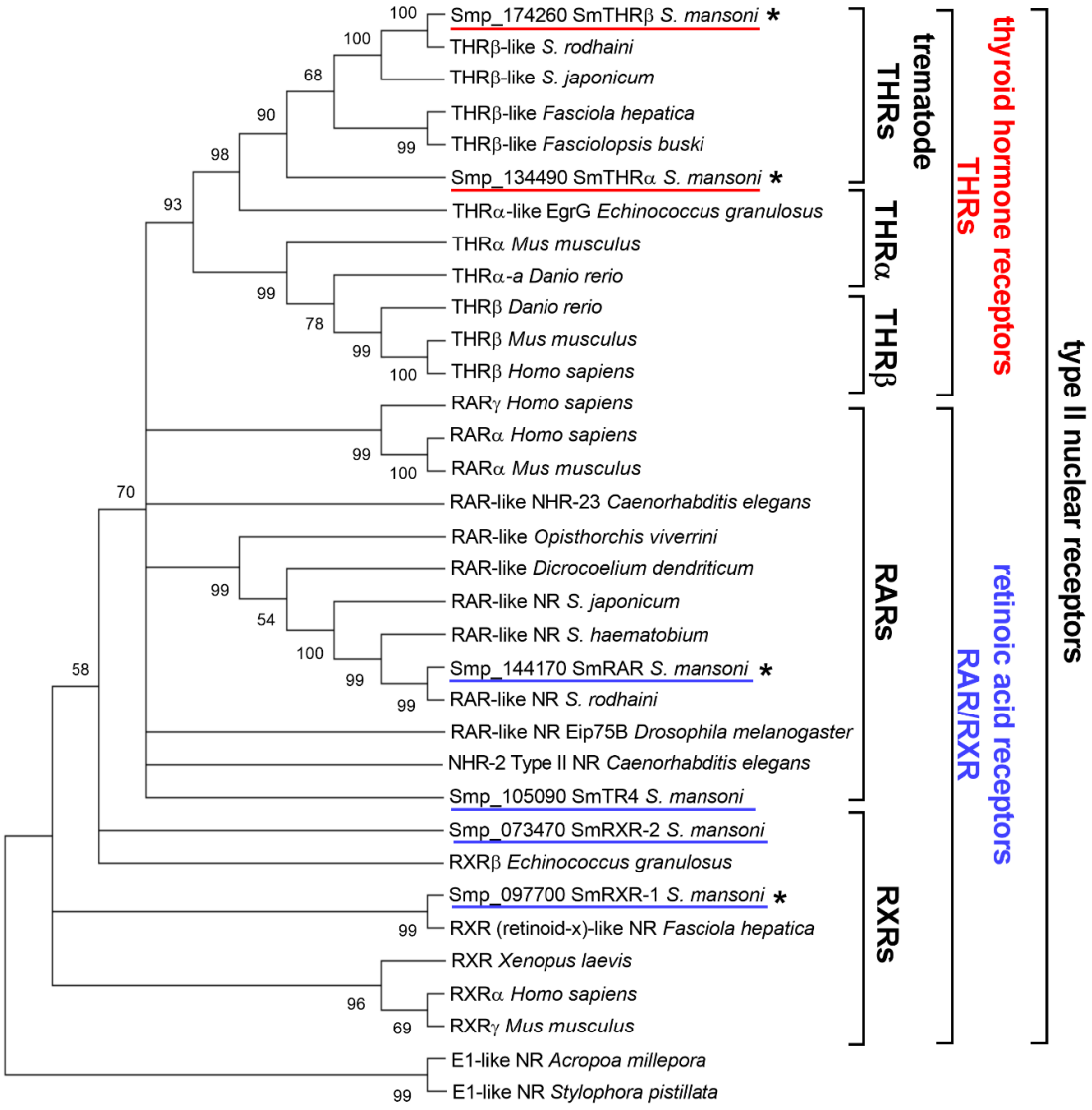

Figure 17. Phylogenetic analysis of *S. mansoni* retinoic acid and thyroid hormone receptors.
Using MEGA11 (210), phylogenetic analysis of putative *S. mansoni* members of type II nuclear receptors (NRs) was performed comparing orthologs from other invertebrate and vertebrate species. This analysis positioned SmRAR within the RAR-like, SmRXR-1 within the RXR, and SmTHRα/β in a trematode-specific THR-like clade of NRs. NR orthologs of *Acropora millepora* and *Stylophora pistillata*, members of the evolutionary basal stem of Cnidaria, served as outgroup references. The nucleotide sequences used for the phylogenetic analysis and the most important genes for my study are marked with asterisks. Type II NR *S. mansoni* paralogs are underlined.

Next, the phylogenetic analysis of SmTHRα and SmTHRβ classified both NRs as thyroid hormone receptors. To verify the subgroup affiliation assigned by transcriptome studies (61, 62, 289), the aa-sequences of these NRs were compared to other representatives of these subgroups from model organisms (Figure 17). The analysis revealed a relatively close evolutionary proximity of SmTHRα to other THRαs from vertebrate model organisms. Furthermore, SmTHRα showed an intermediate evolutionary distance to two different subgroups of THRs, THRα and a trematode-specific clade of THRs. Thus, SmTHRα is evolutionarily close to the *Echinococcus granulosus* (EgrG) THRα ortholog and other trematode THRβ orthologs, including *Fasciola hepatica* and *Fasciolopsis buski*. SmTHRβ, on the other hand, was shown to be more distant from SmTHRα, but especially from THRβs of vertebrate model organisms. SmTHRβ was assigned to a trematode-specific subgroup of THRs, which could not be assigned to either THRα or THRβ.

4.1.2 The RAR-like NR of *S. mansoni* shows a typical structure and is pairing-dependently expressed in intermediate-stage oocytes

In order to determine the identity of SmRAR, a reanalysis of its predicted annotation as a member of the NR subfamily 1 (55, 62) or RAR (retinoic acid receptor)-like NRs (168, 241, 242) was conducted. SMART domain analysis (243) of the amino acid sequence of SmRAR indicated a typical domain structure for a NR, consisting of variable N- and C-terminal regions and a zinc-finger domain connected to a ligand-binding domain by a hinge region (Figure 18 A) (91). Additionally, the comparative structural analysis of the predicted protein structure by Phyre2 (244) revealed highest similarities to the RAR beta subfamily (RARb, Figure 18 B).

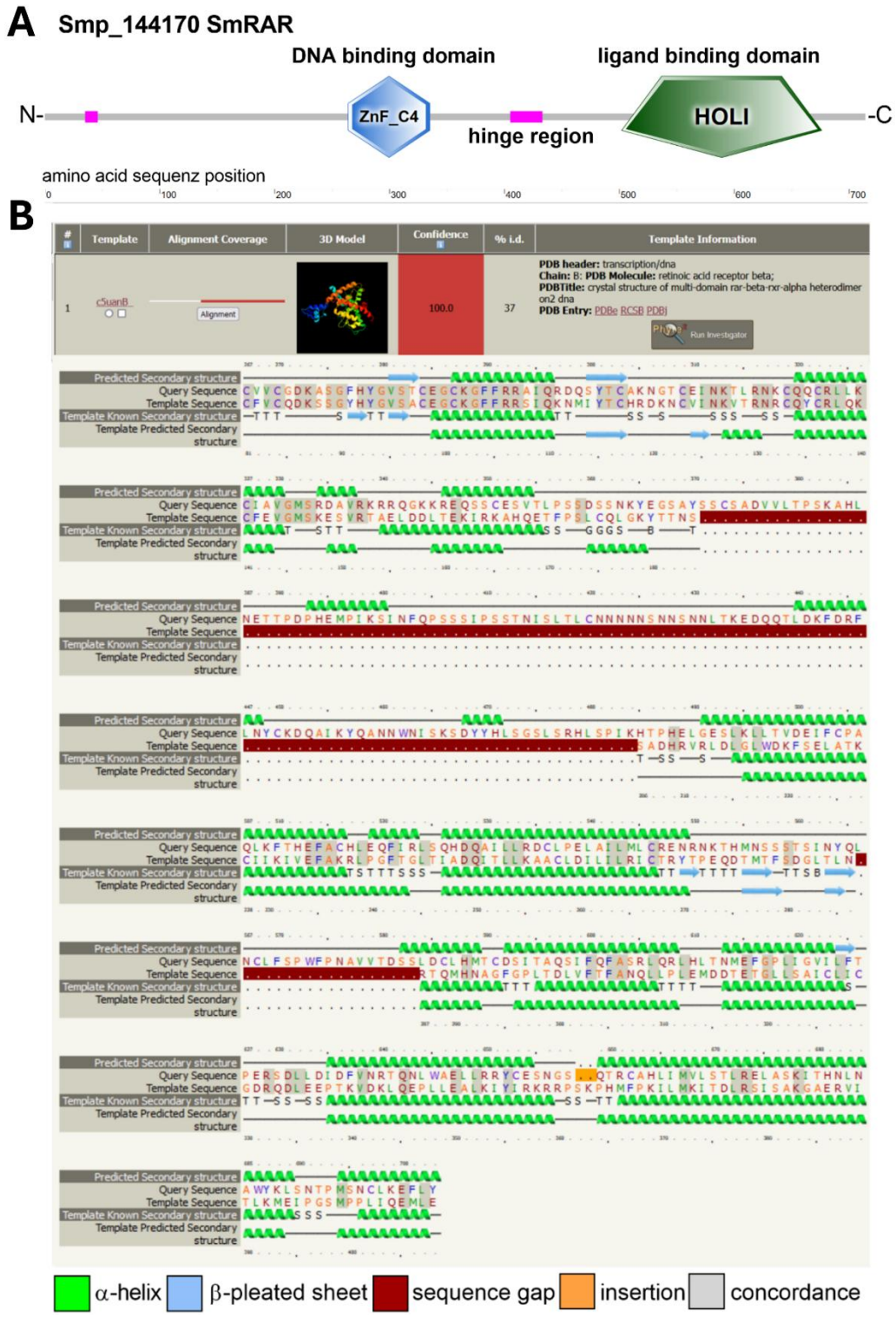

Figure 18. Bioinformatic domain analysis revealed SmRAR as an ortholog of the human RAR.
A, The domain structure of Smp_144170 (SmRAR). SMART domain analysis (243) of SmRAR revealed the characteristic NR structure consisting of unstructured N- and C-terminal domains as well as a DNA-binding domain (ZnF_C4), which is linked by a hinge region to the ligand-binding domain (HOLI). **B**, The amino acid sequence and the predicted protein structure of SmRAR were compared to already characterized nuclear receptors from model organisms using Phyre2 (244). By analyzing the alignment coverage, SmRAR was verified as nuclear receptor and was assigned with highest similarity to the human retinoic acid receptor beta family.

Previous bulk RNA-Seq studies indicated that SmRAR is an ovary-preferentially and pairing-dependently transcribed NR (55, 62). Moreover, the first scRNA-Seq atlas of isolated mature ovaries generated by Zhigang Lu, a former member of the Grevelding lab (Figure 19; Moescheid and Lu *et al*., submitted; gonadsc.schisto.xyz) revealed that SmRAR is expressed in oocytes at an intermediate developmental stage and in mature oocytes (Figure 20 A). Furthermore, cluster analysis of this scRNA-Seq study assigned SmRAR as one of the marker genes of the intermediate germ-cell cluster. To confirm these findings, RT-qPCRs were conducted by analyzing cDNA from pairing-experienced (bM, bF) and pairing-inexperienced (sM, sF) males and females, respectively, as well as their isolated gonads (bT, bO, sT, sO). The results confirmed the ovary-preferential and pairing-dependent expression of SmRAR, which is consistent with the available transcriptional profile data (Figure 20 B) (55, 62).

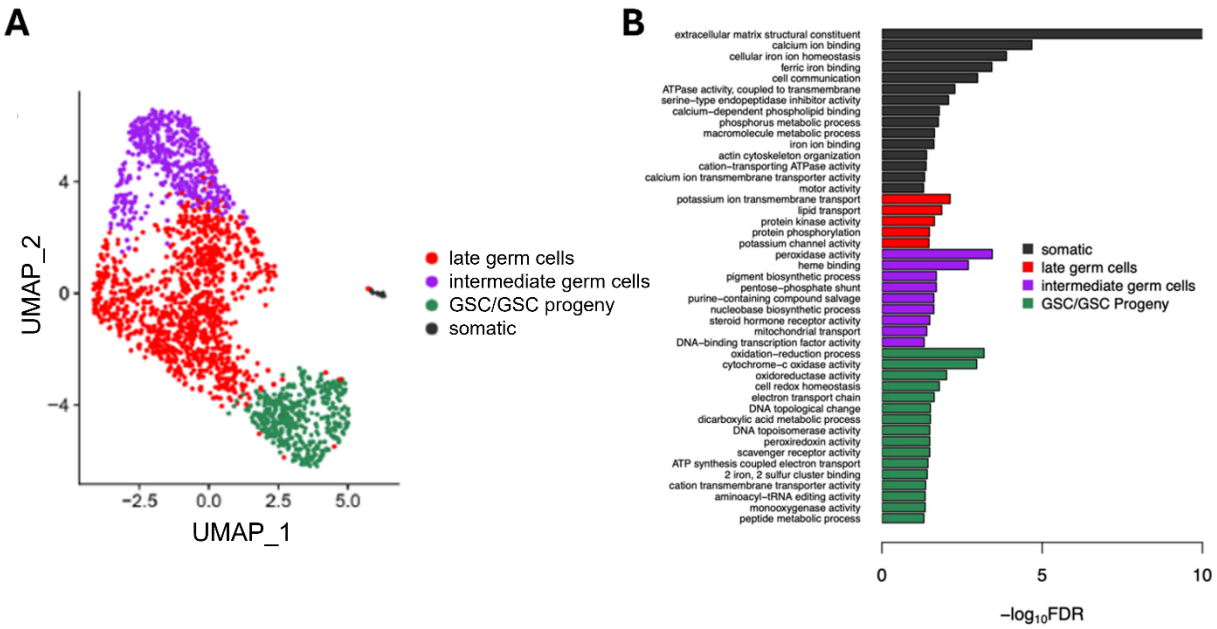

Figure 19. Single cell atlas of the mature ovary.

A, The UMAP (Uniform Manifold Approximation and Projection) representation of 1,967 cells in four clusters. Cells of the ovary of sexually differentiated *S. mansoni* females can be grouped into four distinct clusters: a germinal stem cell/germinal stem cell progeny (GSC/GSC progeny) cluster, an intermediate germ cell cluster, a late germ cell cluster (primary oocytes), and a somatic cluster with characteristics of muscle and neuronal cells. **B**, GO terms associated with marker genes of each indicated cluster. Significant terms are grouped and color-coded according to the cluster to which they have been assigned (Moescheid and Lu *et al.,* submitted; gonadsc.schisto.xyz).

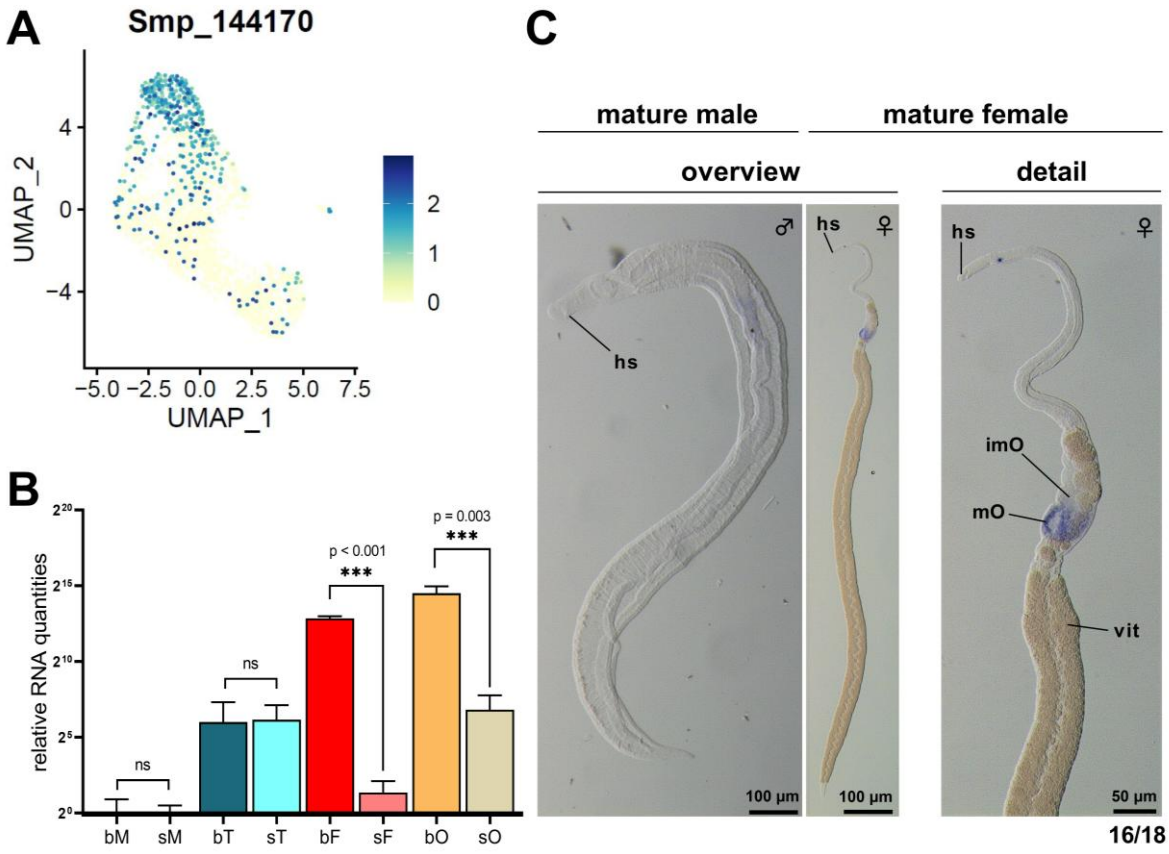

Figure 20. Sm*rar* is pairing-dependently and ovary-preferentially transcribed, and transcripts localized in the posterior part of the ovary.

A, UMAP visualization of the scRNA-Seq data of mature ovaries, showed Sm*rar* (Smp_144170) transcription primarily in oocytes of an intermediate developmental stage. In addition, transcription at a lower level was shown in mature oocytes. (Moescheid and Lu *et al*., submitted). **B**, RT-qPCR analyses of Sm*rar* transcripts in adult schistosomes and their gonads revealed an ovary-preferential and pairing-dependent transcription pattern, with significant differences between pairing-experienced and -inexperienced males and females. *P<0.05, **P<0.01, ***P<0.001 by t-test. **C**, Whole-mount *in situ* hybridization showed specific localization of Sm*rar* transcripts in the posterior part of the ovary of paired female *S. mansoni*, with 16 out of 18 worms examined worms displaying this pattern. No specific signals were detected in male schistosomes. Abbreviations: hs (head sucker), imO (part of the ovary containing immature oocytes), mO (part of the ovary containing mature oocytes), and vit (vitellarium).

To validate the ovary-specificity of Sm*rar* transcription, Sm*rar* transcripts were localized by whole mount *in situ* hybridization (WISH) within the tissue of mature male (bM) and female (bF) worms. Subsequently, specific signals in the posterior part of the ovary were observed, which contains differentiated oocytes (Figure 20 C) (38). In contrast, no signals were detected in the anterior part of the ovary, where oogonia, immature, stem cell-like oocytes are located (Figure 20 C) (38, 40). Correspondingly, no signals were detected in male worms. These

findings align with the expectations of a gene primarily expressed in the ovary. Additionally, a higher signal intensity at the edges of the posterior part of the ovary correlates with the clustering results from the scRNA-Seq data, indicating a preferential expression in intermediate-stage oocytes. Fully matured oocytes occupy the center of the posterior part of the ovary of paired females (38, 40), where a lower signal intensity was detected.

4.1.3 Functional characterization indicates an important role for SmRAR in maintaining mature oocytes

To gain initial insights into the biological functions of SmRAR, gene-specific knock-down (KD) experiments were conducted using RNAi. To prevent RNAi-dependent off-target effects on other NRs, the double-stranded RNA was designed to be Sm*rar*-specific without covering the highly conserved DNA-binding domain (DBD) and ligand-binding domain (LBD) (85). To minimize dsRNA-dependent off-target effects on the transcription of genes analyzed by RT-qPCR, the whole-length dsRNA sequence was compared to the mRNA sequences of selected genes using BLASTn (290). For the genes, which were selected for further downstream analysis to assess regulatory effects of Sm*rar*, no significant sequence similarities of sufficient length were found, which could induce RNAi off-target effects (152). Furthermore, primers for downstream analysis by RT-qPCR were designed exon-spanning and avoiding any overlap with the dsRNA sequence.

RNAi was conducted using 10 couples, and 6-9 biological replicates were prepared in total. The couples were treated identically, except that one group received dsRNA while the other served as untreated control. Previous studies using non-schistosomal control dsRNA at concentrations of 30-60 µg/ml showed no noticeable phenotypes upon RNAi (57, 152). After 15 d, Sm*rar* KD efficiency was assessed through RT-qPCR. The couples were first separated, and RNA was extracted from female worms. Thus, a significant reduction in Sm*rar* mRNA levels (94.2±8.2% compared to the control) was detected (Figure 21 A).

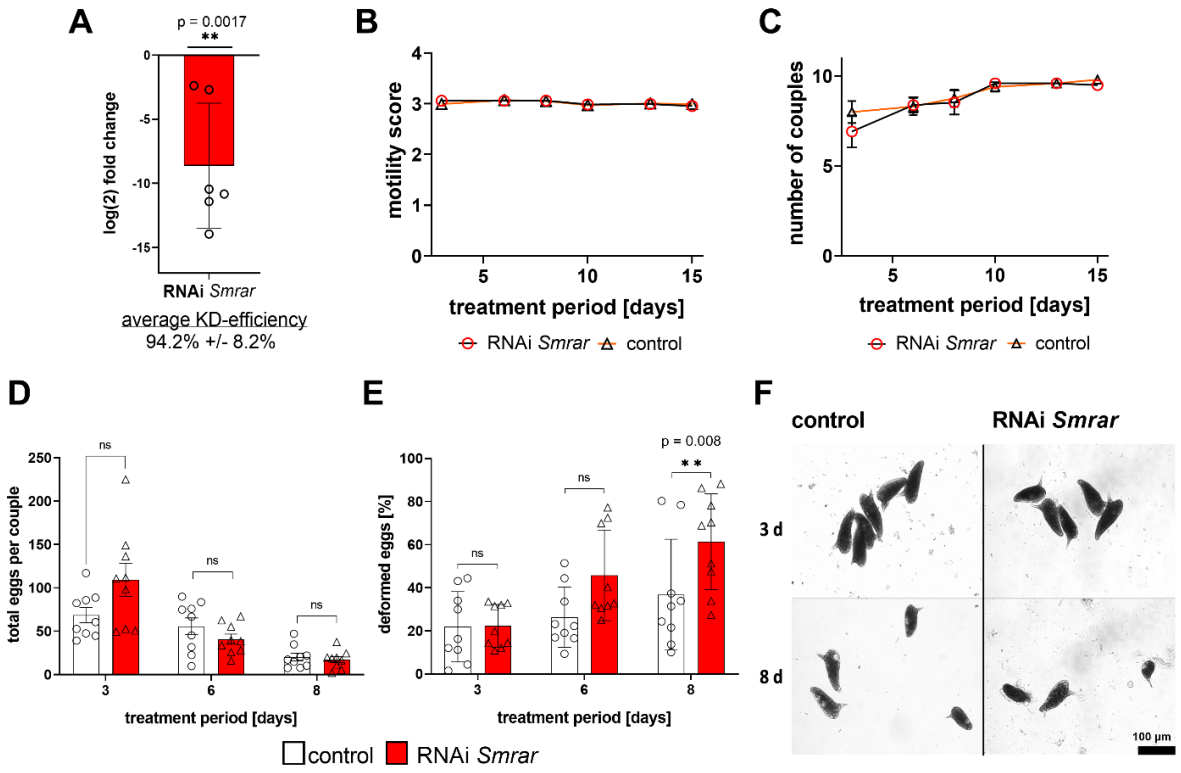

Figure 21. Sm*rar* RNAi affected egg morphology and embryo development at an early stage. Schistosome couples were treated with 30 µg/ml Sm*rar* dsRNA every 2–3 d for 15 d (red bars). Worms treated under the same conditions with DEPC-water without dsRNA served as control (white bars). **A**, By RT-qPCR, a high KD-efficiency (94,2±8,2%) was found for Sm*rar* transcripts in females, which had been separated from males before analysis. **B-C**, Phenotype analyses covering worm motility (A), scored from 0 (no motility) to 4 (hyperactive motility), and pairing stability (**C**) showed no RNAi-dependent effect (triangles and circles represent the biological replicates, n=9). **D**, The number of eggs produced *in vitro*, monitored over an 8-d period, showed no significant differences after RNAi treatment. **E**, A significant increase in malformed eggs (smaller, non-embryonated eggs, without spines or with deformed spines) were observed 8 d upon RNAi**. F**, By bright-field microscopy, the morphology of eggs was analyzed after 3 and 8 d. After 8 d, egg morphology altered, and significantly more eggs were reduced in size. Abbreviation: KD, knock-down. **P<0.01, determined by t-test. A, n=6; B-F, n=9.

Furthermore, all experimental groups were monitored daily to assess physiological and morphological effects, by using a standardized scoring system (152). Throughout the experimental period, worms in all groups remained viable, and no reduction in motility or pairing stability was observed (Figure 21 B, C). As a physiological readout, the percentage of normal and malformed eggs per couple was determined during the first 8 d of treatment. Here, no significant difference in the total number of *in vitro*-laid eggs between the RNAi and control groups was found (Figure 21 D). However, after 8 d, a significant increase in malformed eggs was observed in the Sm*rar* RNAi group (Figure 21 E). In contrast to the untreated control, eggs

laid by dsRNA-treated couples were smaller, spines were occasionally missing or deformed, and embryos were absent in these eggs (Figure 21 F). Additionally, by analyzing the egg content, the number of zygote-containing eggs was significantly reduced in the RNAi group after 8 d of treatment (68.4±19.5%; P<0.001) compared to the control (Figure 22 A, B).

Previous findings suggested a potential influence of the Sm*rar* RNAi on the female gonad, specifically the ovary. To evaluate the effect of Sm*rar* RNAi on the ovary, the intricate structures of the ovaries in both RNAi and control females at 15 d was examined by CLSM analysis (Figure 22 C, D). In addition, EdU staining was performed to investigate the potential effects on stem-cell proliferation (Figure 22 F). CLSM analysis revealed a significant reduction in the number of mature oocytes, exclusively in the RNAi group, as well as a significant decrease in ovary volume. The volume of the posterior part of the ovary, containing mature oocytes was determined by Z-stack analyses (Figure 22 C, D). The reduced ovary volume corresponded to the smaller size of the posterior part of the ovary that was consistently observed in female schistosomes of the RNAi group (Figure 22 C, D). Moreover, by analyzing the ovaries of females from couples treated with a non-schistosomal control dsRNA, coding for a 500 bp fragment of the *E. coli ampR* gene (152), I observed no RNAi-dependent effects, which corresponded with the appearance of the untreated control (Supplemental Figure S1). Recently, *ampR* dsRNA has been described as a suitable RNAi control for long-term dsRNA treatment (22 d, 30 µg/mL dsRNA) (152). Furthermore, cell proliferation of oogonia was determined by an EdU proliferation assay. Here, no differences in the number of EdU-positive, proliferating oogonia were observed between the control and RNAi groups (Figure 22 E). Additionally, no effects of RNAi on the vitellarium were detected (Figure 22 C). Testes of male schistosomes from dsRNA-treated couples were also examined. I found no alterations in their morphology, the sizes of the testicular lobes, or the seminal vesicles (Figure 23 A). Likewise, the number of EdU-positive spermatogonia was similar between the two experimental groups (Figure 23 B).

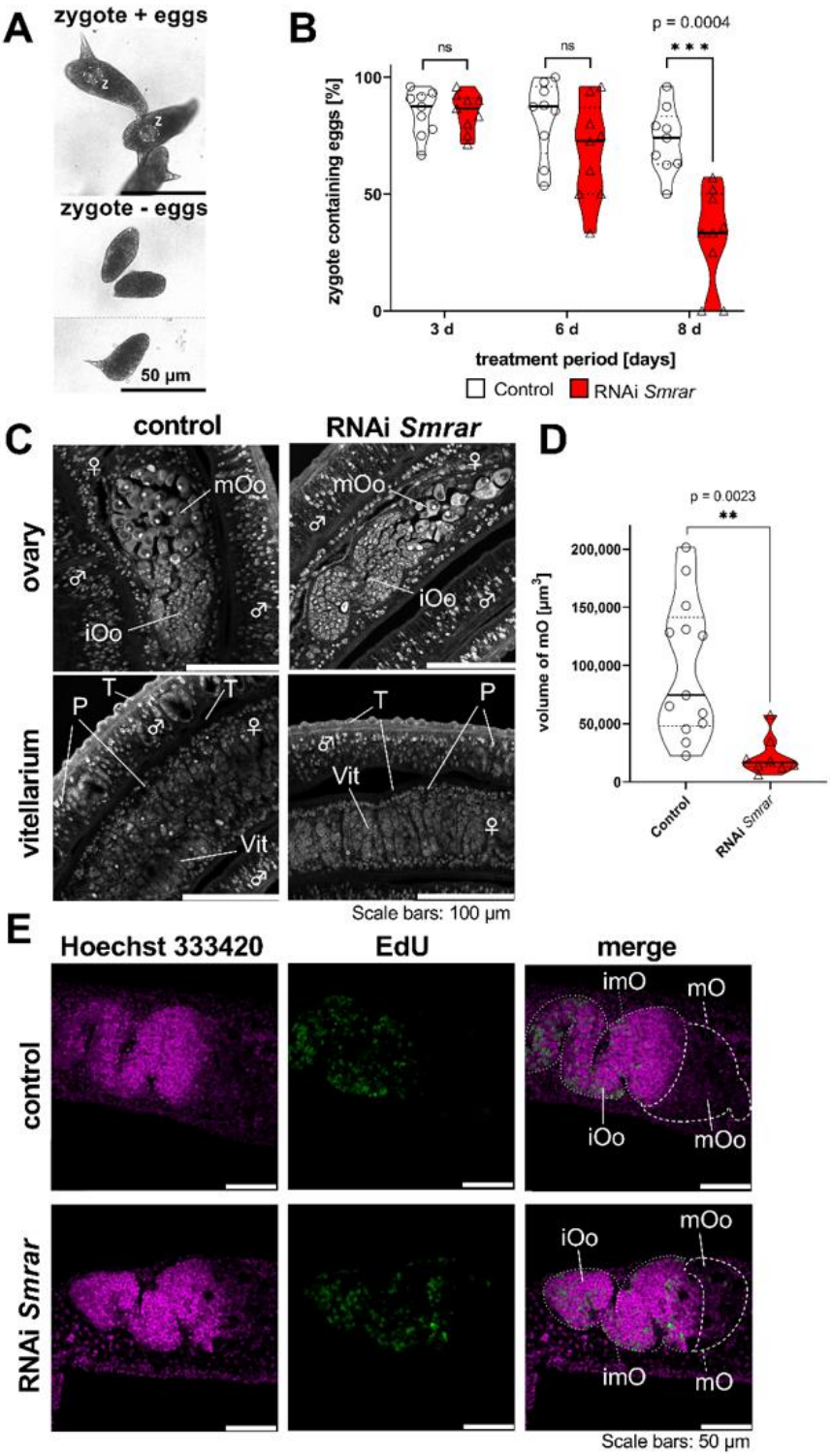

Figure 22. Knock-down of Sm*rar* resulted in a drastic reduction in the number of zygote-containing eggs and a deficiency of primary oocytes.

Schistosome couples were treated with 30 µg/ml Sm*rar* dsRNA for 15 d. **A**, After treatment, the morphology of the eggs produced *in vitro* was investigated by bright-field microscopy. **B**, The weighted distribution (violin plot) of zygote-containing eggs showed a significant reduction in dsRNA-treated couples (red) compared to the control group (white) after 8 d. **C**, The size of the mature ovary in the dsRNA-treated pairs was reduced, as observed by CLSM analysis. The vitellarium of the treated females

and the parenchyma and tegument of both sexes showed no morphological changes. **D**, The violin plot of the volume distribution of the posterior part of the ovaries based on comparative Z-stack analysis during CLSM showed a significant reduction of the ovary volume in the RNAi group only. **E**, CLSM analysis of EdU-treated females showed a similar abundance of stained cells in the control and RNAi groups, and signals (green) were mainly observed in the anterior part of the ovary containing immature oocytes (oogonia). The dimensions of the ovary sections were similar in both groups, whereas the dimension of the posterior part of the ovary containing mature oogonia was significantly reduced in the RNAi group. The nuclei were counterstained with Hoechst 33342 (purple). Abbreviations: iOo, oogonia; imO, immature part of the ovary; mOo, mature oocyte; mO, mature part of the ovary; P, parenchyma; T, tegument; Vit, vitellarium; z, zygote. *P<0.05, **P<0.01, ***P<0.001 by t-test. A, n=9; B-D, n=6.

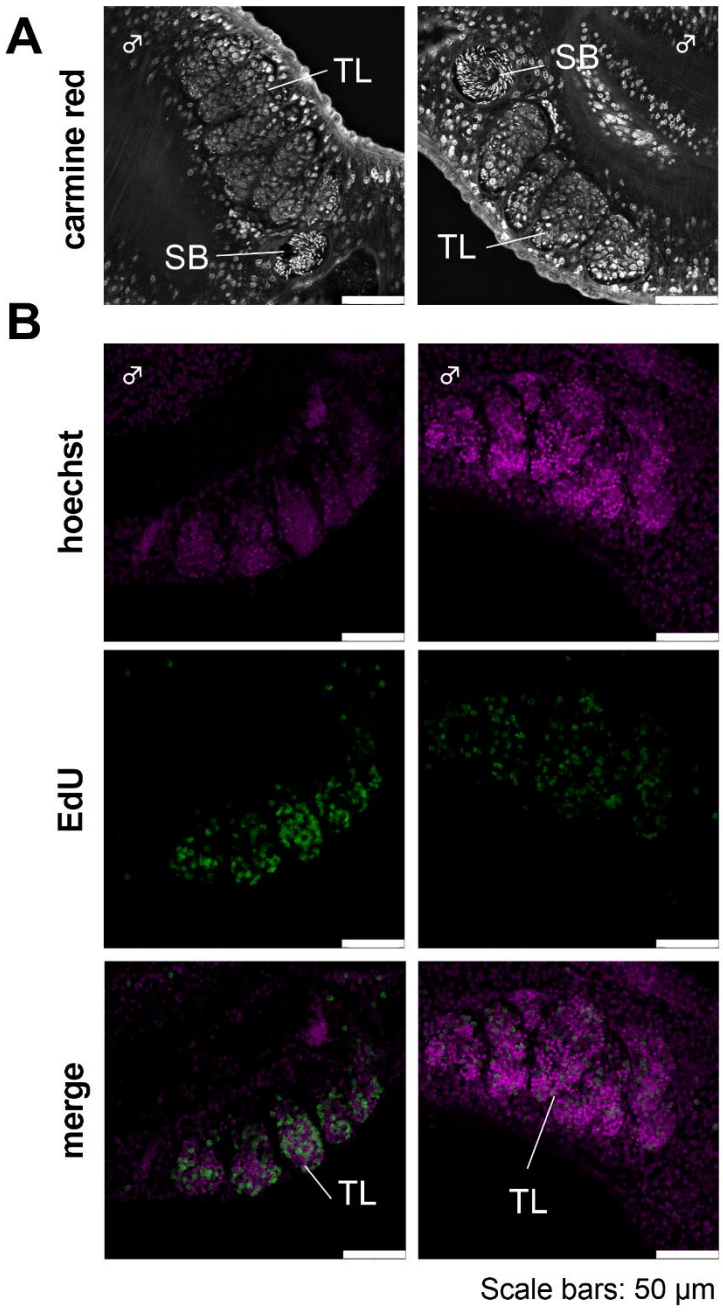

Figure 23. No Sm*rar* knock-down effect in testes.

Couples were treated with 30 µg/mL Sm*rar* dsRNA every 2 to 3 d for a period of 15 d. After treatment, the couples were analyzed using CLSM. **A**, No differences in the testicular fine structure were observed between the two experimental groups. **B**, No discrepancies in the number of EdU-positive cells in the male reproductive organs was observed. Abbreviations: SB, Seminal bladder; TL, testicular lobes.

4.1.4 Downregulation of meiosis-associated genes associates with Sm*rar* RNAi

To investigate the effects of Sm*rar* RNAi-dependent effects on gene expression, the transcript profiles of various genes were analyzed. To this end, I made use of the newly established scRNA-Seq atlas of mature ovaries. Here, candidate genes for Sm*rar* regulation were selected according to the following parameters: (i) SmRAR interaction partners predicted from literature, (ii) genes preferentially transcribed in the ovary, and (iii) genes already known to play roles in schistosome reproduction. The potential interaction partners of SmRAR were predicted by STRING analysis (Figure 24), such as Smp_163290 (SmNCor) and Smp_266960 (SmGli1) (73, 74). Furthermore, orthologs of *meiob* and *bmpg*, which are preferentially transcribed in the ovary of paired females and known ovarian marker genes of *S. mediterranea* and *S. mansoni*, were selected for downstream analyses (Figure 24) (22, 95). Subsequently, transcriptional changes of the selected genes were determined by RT-qPCRs (Figure 25 A). Transcripts of selected genes were displayed according to the oocyte developmental trajectory consistent with the scRNA-Seq atlas of mature ovaries (Figure 25 B).

Protein interactions predicted by STRING interaction network for SmRAR

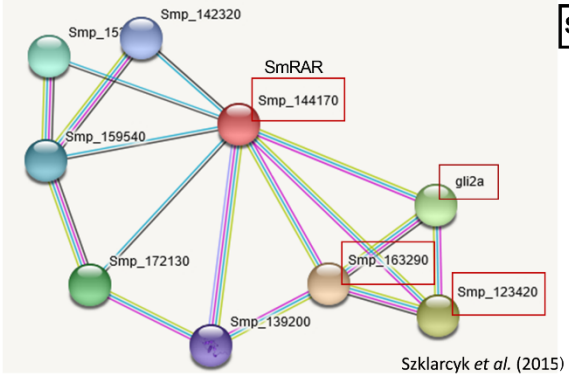

Smp_number / name:	Annotation:
Smp_144170 / SmRAR	RA-related orphan receptor alpha; RAR-like nuclear receptor (Szklarcyk *et al.* 2015, Lu *et al.* 2016)
Smp_123420 / SmDarnt Smp_341950 (genome V.10)	Arylhydrocarbon receptor nuclear translocator homolog (Darnt) (Szklarcyk *et al.* 2015)
Smp_163290 / SmNcor	Nuclear receptor co-repressor related protein (Ncor) (Szklarcyk *et al.* 2015)
Smp_266960 / SmGli1	Transcriptional activator *cubitus interrups*, Gli2a; SmGli1 (Lu *et al.* 2016; Chen *et al.* 2022)

Genes sharing a similar transcription pattern as *Smrar* (Lu *et al.* 2016; Lu *et al.* 2018)

Smp_number / name:	Annotation:
Smp_333540 / SmMeiob	Meiosis-specific with OB domain-containing protein (Lu *et al.* 2018, Wendt *et al.* 2020)
Smp_078720 / SmBmpg	Bone marrow proteoglycan (Lu *et al.* 2018, Wendt *et al.* 2020)

Figure 24. String protein-interaction network analysis revealed potential SmRAR binding partners and genes that may be controlled by SmRAR.

Genes coding for potential interaction partners of SmRAR, which were predicted by STRING analysis (249) and which are ovarian marker (55, 61, 62) genes in *S. mediterranea* and *S. mansoni* .

Among the investigated genes were Smp_123420 (putative aryl hydrocarbon receptor nuclear translocator homolog, SmDarnt) (249, 250), SmFGFR-A (Smp_175590), and SmFGFR-B (Smp_157300) (200). For these three genes, no significant changes were observed in the transcription levels of females of the Sm*rar* RNAi group versus the the control. In contrast, Smp_333540 (meiosis-specific OB domain-containing protein, SmMEIOB (62)), a known GSC progeny marker, which was identified in EdU-negative germ cells in a previous study (61), showed a significant reduction in the transcript level upon RNAi (Figure 25 A). Moreover, a significant reduction in the transcript level of Smp_078720 (bone marrow proteoglycan homolog, SmBmpg (61, 62)) was observed. Sm*bmpg* was identified as a *S. mansoni* marker gene for mature, EdU-negative oocytes by Wendt *et al.* (61). Another potential SmRAR interaction partner predicted by STRING was SmGli1 (Smp_266960, transcriptional activator glioma-associated oncogene (51)). This gene was shown before to play a key role in males for the induction of pairing-dependent female maturation (51). The scRNA-Seq atlas data showed Sm*gl1* transcripts in the somatic cell cluster of the ovary. Sm*rar* RNAi caused a significant reduction in Sm*gli1* transcript levels. The most significant decrease in transcript level was observed for Sm*ncor* (Smp_163290), a nuclear receptor co-repressor-related protein known as SmNCoR (243) or thyroid-hormone- and retinoic acid receptor-associated co-repressor (TRAC). This protein is involved in complex formation with histone deacetylases (HATs) and chromatin remodeling. Studies have shown that this protein plays a crucial role in regulating gene expression (291, 292).

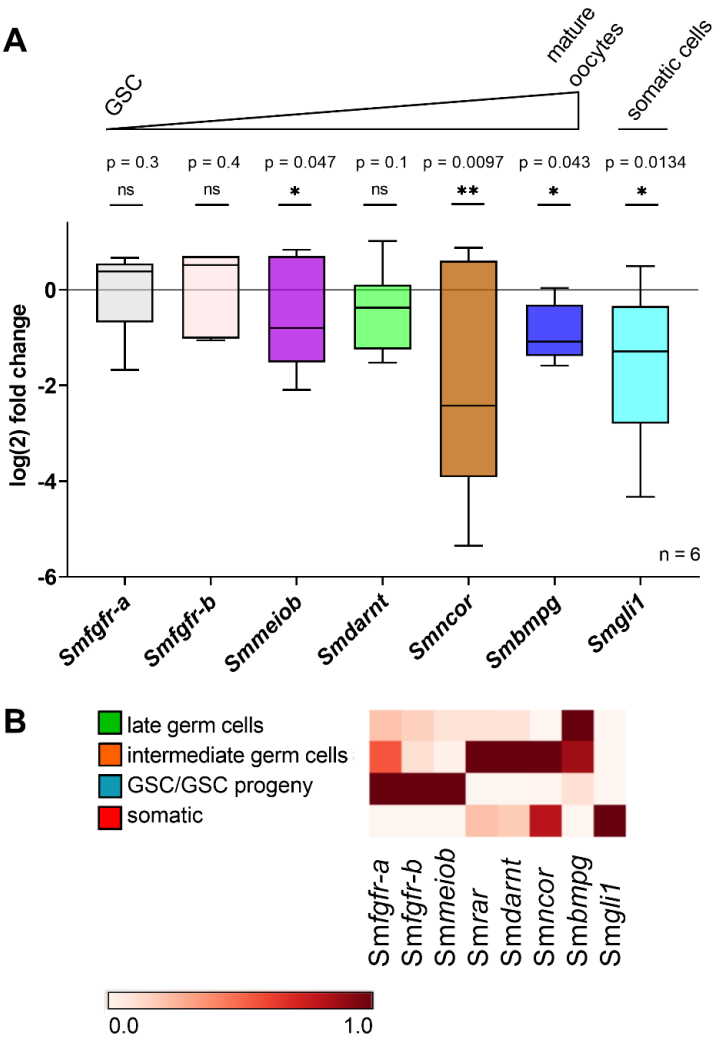

Figure 25. Meiosis-associated genes Sm*ncor*, Sm*meiob* and Sm*gli1* were significantly downregulated upon Sm*rar* RNAi.

A, Following treatment of *S. mansoni* couples with 30 µg/mL Sm*rar* dsRNA for 15 d, and RNA extraction of females (after separation form their male partners) transcript levels of selected genes (see text) were quantified by RT-qPCR (n=6). These genes represented potential interacting partners of Sm*rar* predicted by the STRING network analysis (249, 250), or they are already known to be associated with ovary development (61, 200, 293). Significant reductions in the transcript levels of Smp_163290 (Sm*ncor*, brown), Smp_333540 (Sm*meiob*, purple), Smp_ 078720 (Sm*bmpg*, blue), and Smp_266960 (Smgli1, cyan) were found. Furthermore, the investigated genes were plotted following the oocyte developmental trajectory, from immature, undifferentiated GSCs to mature oocytes. They were arranged according to the transcriptional peaks of the corresponding clusters of the scRNA-Seq atlas of the mature ovary (gonadsc.schisto,xyz). The boxplot indicates the range between the minimum and maximum values, with the 10th and 90th percentiles and median shown in the box. *P<0.05, **P<0.01, ***P<0.001 by t-test. **B**, Heatmap of the ovary scRNA-Seq cluster-associated transcript levels of Sm*rar* and representative genes for each cluster, which were analyzed by RT-qPCR (gonadsc.schisto,xyz). The heatmap illustrates the feature-standardized transcript levels for each cluster of selected genes.

4.1.5 Sm*rar* knock-down impaired oocyte maturation

To evaluate the regulatory function of SmRAR, RNAi combined with pairing experiments were performed with sexually undifferentiated, sFs to investigate the role of SmRAR in ovary development and oocyte maturation upon first-time pairing. In three biological replicates, 15 sFs were treated each with Sm*rar* dsRNA for a 7-d period. Subsequently, sFs were (first-time) paired in a culture dish with 10 bMs, in a 1.5 to 1.0 female/male ratio described previously as optimal for pairing experiments with *S. mansoni in vitro* (57). Pairing occurred within a period of 48-72 h. Unpaired schistosomes were removed after 72 h. Couples were then cultivated and monitored for an additional 13 d (in total 20 d *in vitro* cultivation). During this period, the medium was replaced every 2–3 d, along with the addition of fresh dsRNA. At the end of the experiment, couples were separated, and RNAi efficiency was determined for females using RT-qPCR. KD significantly silenced the Sm*rar* transcript level, with a reduction of 97.2±2.48%, as shown in Figure 26 A. Furthermore, physiological parameters, including pairing stability and motility, remained unaffected in both the RNAi and control groups (Figure 26 B, C).

The effects of Sm*rar* RNAi in first-time paired females were investigated morphologically. CLSM revealed differences between RNAi and control groups (Figure 26 D, Supplemental Figure S2). The ovaries of control worms (sF, first-time paired, without dsRNA addition) are characterized by stem cell-like oogonia in the anterior region and mature oocytes in the posterior region of the ovary (40, 48, 57). This was expected as a result of pairing-induced sexual maturation, as previously described (40, 57). However, first-time paired females of the RNAi group exhibited significant deficits in ovarian maturation. Although the ovaries had developed, mature oocytes were completely absent, whereas oogonia were present. This phenotype coincided with a significantly reduced ovary volume, an expected consequence of the absence of mature oocytes (Figure 26 E). Moreover, Sm*rar* RNAi intervention also affected egg morphology and zygote formation as determined by bright-field microscopy.

Next, I investigated the impact of Sm*rar* RNAi on the transcript level of genes, previously demonstrated to be significantly downregulated upon Sm*rar* RNAi (Figure 25 A), and for which critical roles in oocyte development were assumed (Figure 26 F). RT-qPCR analyses demonstrated a clear reduction in the transcript levels of Sm*meiob* (65.96±12.6%) and Sm*gli1* (45.6±10.6%). However, only a trend of transcript level reduction for Sm*ncor* was observed (Figure 26 F).

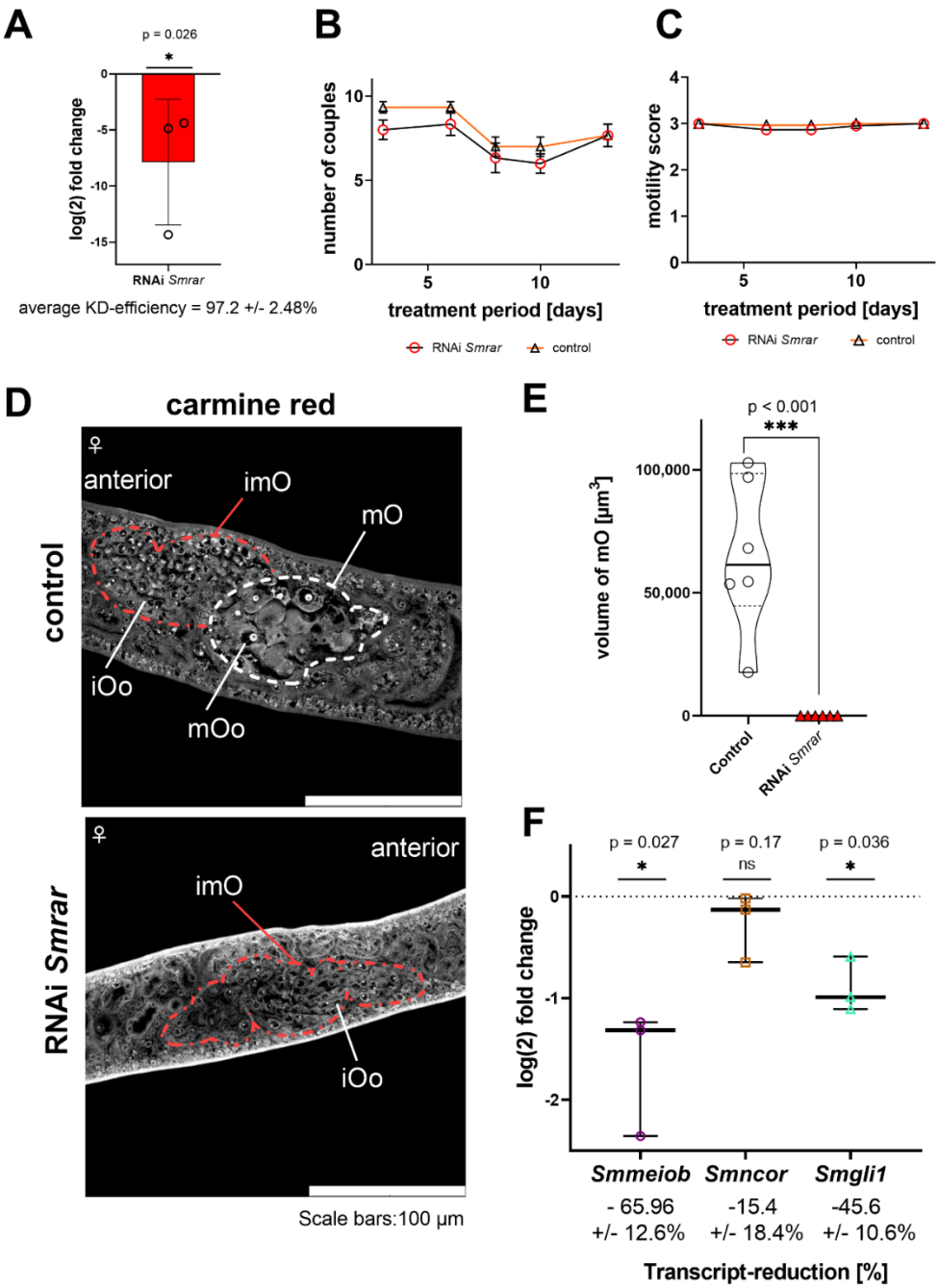

Figure 26. Sm*rar* RNAi prevented oocyte maturation during female maturation.

Sm*rar* RNAi experiments were conducted with pairing-inexperienced female schistosomes (sF) treated with 30 µg/mL dsRNA for 20 d in total. The treatment period was split into a pre-pairing (7 d) and a post-pairing (13 d) treatment period (n=3). Untreated worms served as control. After 7 d in culture with dsRNA, sFs were paired (first-time pairing) with bMs according to a previously published *in vitro*-pairing protocol (57). Couples formed between 48 and 72 h and were subsequently maintained *in vitro* for an additional 13 d, with dsRNA being added every second day during this period. **A**, log(2)fold change in Sm*rar* transcript levels, determined by RT-qPCR, showed a significant transcript reduction upon Sm*rar* RNAi. Individual biological replicates, mean, and standard deviation are shown. As physiological parameters, pairing stability (**B**) and motility (**C**; motility scores: 0 (no motility) to 4 (hyperactive motility))

were monitored. No significant differences were observed between the experimental groups. **D**, CLSM revealed the presence of immature oocytes, referred to as oogonia (iOo, red-framed region), as well as mature oocytes (mOo, white-framed region). However, the ovaries of females of the RNAi group contained no mature oocytes. **E**, Corresponding to the oocyte phenotype presented in **D**, comparative Z-stack CLSM analyses revealed a significant reduction of the volume of the posterior part of ovaries in the RNAi group. The violin plot indicates the range between the minimum and maximum values and the median visualized by the solid line. The ovaries of females of three biological replicates were examined, whereby each point represents the volume of a single ovary. **F**, RT-qPCR analysis indicated a significant reduction in the levels of Sm*meiob* (purple) and Sm*gli1* (cyan) transcripts in the RNAi group. Moreover, a trend of a reduced transcript level was observed for Sm*ncor*. The plot indicates the range between the maximum and minimum as well as the median. Each individual dot represents the log(2)fold change in transcript-level compared to the control for each biological replicate. Abbreviations: iOo, oogonia; imO, immature part of the ovary; mOo, mature oocyte; mO, mature part of the ovary. *P<0.05, **P<0.01, ***P<0.001 by Mann-Whitney test.

4.1.6 Functional characterization of Sm*meiob* by RNAi revealed a phenocopy of Sm*rar* RNAi.

Sm*rar* RNAi resulted in transcriptional downregulation of Sm*meiob*, Sm*ncor*, and Sm*gli1*. To examine the transcriptional patterns of these three genes in the ovary, the scRNA-Seq atlas of bO and whole worms (61) was employed to investigate their transcriptional distributions across oocyte populations. Furthermore, these data were analyzed in conjunction with sex- and pairing-specific transcription profiles of whole worms and their gonads (55, 62), as well as scRNA-Seq data of adult *S. mansoni* (61). Moreover, WISH was used to validate the transcriptional patterns of Sm*ncor*, Sm*meiob* (Figure 27 A, B), and Sm*gli1* (Figure 30 C). For Sm*ncor*, the ovary-preferential transcription, which was predicted by previous RNA-Seq studies (55, 62), was confirmed by WISH (Figure 27 A). According to the scRNA-Seq data of whole worms (61) and of bOs, Sm*meiob* is dominantly transcribed in late oogonia (GSC/GSC progeny), and with low abundance in intermediate-stage oocytes (Figure 27 B). WISH confirmed the proposed ovary-specific transcript profile of Sm*meiob* (Figure 27 B) in paired females (55, 62). Furthermore, Phyre2 domain analysis annotated SmMEIOB as an ortholog of the human OB-domain containing replication protein (MEIOB; Supplemental Figure S3), which is a key factor in human germ-cell development (244, 294–296).

In order to obtain additional evidence for the function of Sm*rar* in oocyte maturation and meiosis, RNAi experiments were conducted with a focus on Sm*meiob* (Figure 27 C-J) and Sm*gli1* (Figure 31), as hypothesized partners for functional association. Upon Sm*rar* RNAi, transcript levels of these genes were significantly downregulated in both sexually mature and immature females (pairing experiments). As a result of the potential functional overlap of Sm*rar* and Sm*meiob*, double KD experiments were conducted to investigate synergistic effects (Figure 27 C-J). To this end, RNAi was performed by treating 10 couples with 30 µg/mL dsRNA of each dsRNA per experiment. Worms were incubated for 15 d *in vitro*, while medium and dsRNA was exchanged, every 2-3 d. RT-qPCR results showed a significant decrease in the expression of both genes in both single and double KD experiments (Figure 27 C). In the single KD-group, the transcript level of Sm*meiob* was significantly reduced by 92.3±12.4%, whereas the Sm*meiob* and Sm*rar* transcript level were reduced by 61.7±14.9% and 77.2±17.3%, respectively. During the experimental period, only a weak influence on motility, and a slightly stronger influence on pairing stability in all treatment groups was observed. This effect only occurred at the beginning of the experiment (Figure 27 D, E). Pairing stability stabilized over time, resulting in an equal number of couples across all experimental groups after 15 d.

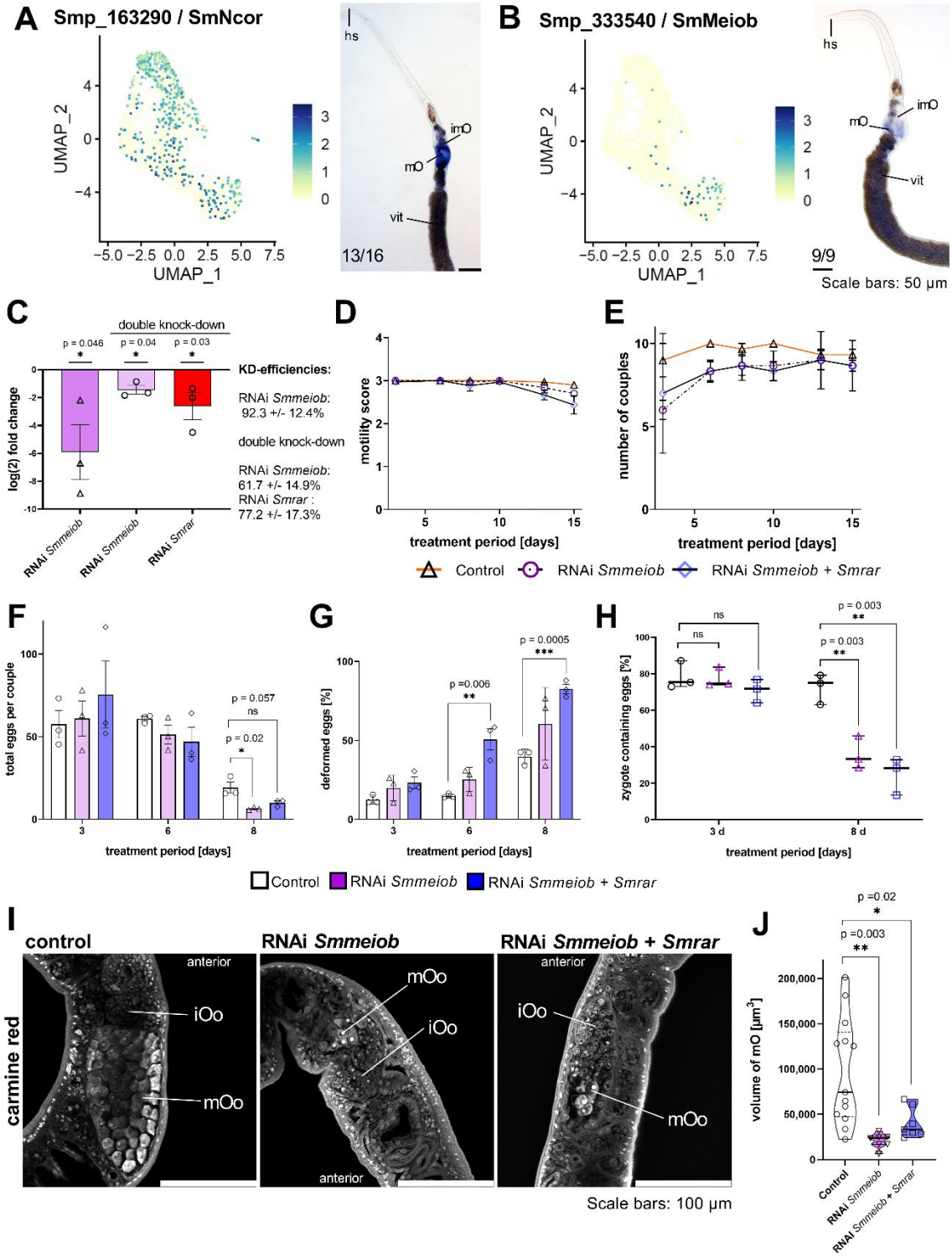

Figure 27. Sm*meiob* RNAi caused a reduction in mature oocytes in paired females.

Sm*meiob* RNAi resulted in a decrease in mature oocytes in paired female. **A-B**, The scRNA-Seq atlas of bO (gonadsc.schosto.xyz) for Sm*ncor* (**A**, left part) and Sm*meiob* (**B**, left part) revealed that Sm*ncor* is transcribed among all clusters, with a preference for late mature oocytes, whereas Sm*meiob* is preferentially transcribed in the GSC/GSC progeny cluster. WISH confirmed the preferential transcription of both genes in the ovaries (right parts of A and B). **C-E**, For RNAi, couples were treated with Sm*meiob* (purple, circles) or Sm*meiob*/Sm*rar* (blue, diamonds) dsRNAs at a concentration of

30 µg/mL each for 15 d (n=3). Control couples (orange, triangles) were treated with DEPC-water. RNAi efficiencies (**C**), motility (**D**), and pairing stability (**E**) were assessed as previously described. **C**, The transcript levels of genes following RNAi were determined using RT-qPCR, revealing a significant reduction in Sm*meiob* transcripts (92.3±12.4%). In the Sm*meiob*/Sm*rar* double KD experiment, Sm*meiob* and Sm*rar* transcripts were reduced by 61.7±14.9% and 77.2±17.3%, respectively. The graphs show average log(2) fold changes in transcript levels compared to the control and the standard deviation. Data from each biological replicate are indicated. **F-H**, The average number of eggs produced *in vitro* and the average percentage of deformed eggs were determined during an 8 d RNAi period. I observed a reduction in the number of produced eggs (**F**) and an increase in the number of deformed eggs (**G**). Both RNAi approaches were associated with a significant increase in the number of eggs without zygotes (**H**). The range between maximum and minimum values and the median are represented. **I**, CLSM analysis of the ovaries revealed a reduction in the size of the mature ovary of worms from both RNAi groups and a lower number of mature oocytes. **J**, Comparative Z-stack analysis of the posterior part of the ovaries, containing mature oocytes, revealed a significant reduction in volume resulting from Sm*meiob* and Sm*meiob*/Sm*rar* RNAi. The ovaries from females of each biological replicate (n=3) were examined, whereby each point represents the volume of a single ovary. The violin plot indicates the range between the minimum and maximum values, with the dashed lines representing the quartiles and the solid line representing the median. Abbreviations: hs, head sucker; iOo, oogonia; imO, immature part of the ovary; KD, knock-down; mOo, mature oocyte; mO, mature part of the ovary; vit, vitellarium. *P<0.05, **P<0.01, ***P<0.001 by t-test. Unless otherwise stated, there was no statistically significant difference between the control and the treated group.

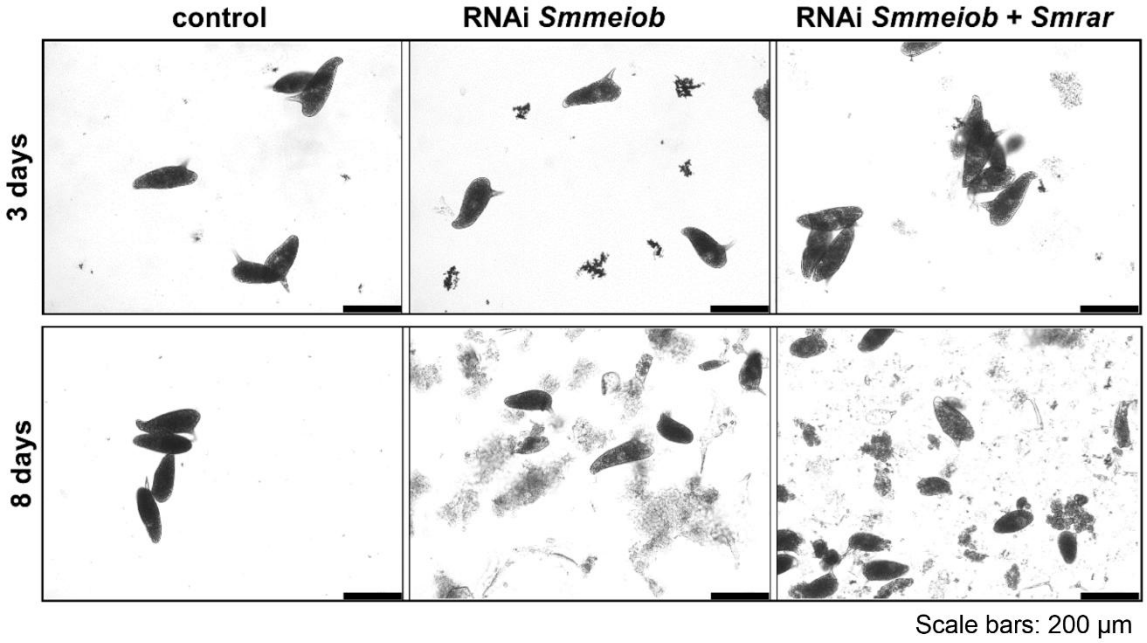

Figure 28. Sm*meiob* and Sm*meiob*/Sm*rar* RNAi caused changes in egg morphology.
Representative images of eggs produced *in vitro* from couples treated with Sm*meiob* dsRNA or a combination of Sm*meiob*/Sm*rar* dsRNA after 3 and 8 d (n=3). The eggs produced by the untreated control group showed no morphological changes. However, RNAi of Sm*meiob* and Sm*meiob*/Sm*rar* caused severe morphological changes that were characterized by a high number of reduced-sized eggs containing no zygote and lacking the typical spine. Additionally, RNAi caused an accumulation of cellular debris in the medium.

Egg production and morphology were determined by bright-field microscopy. Egg production notably diminished in the Sm*meiob* RNAi group after 8 d (Figure 27 F). A similar pattern was observed for the Sm*meiob*/Sm*rar* double KD couples. In both RNAi groups, the number of deformed eggs increased after 6 d, with a considerable increase in deformed eggs following double KD (Figure 27 G, Figure 28). In addition, in both RNAi groups, a significant reduction in the number of eggs containing a zygote was detected, with a significant bias towards the double KD-group after 8 d (Figure 27 H). Next, CLSM analysis demonstrated a significant decrease in the volume of the posterior part of the ovary, which contains mature oocytes, in both the single and the double KD. This coincided with a substantial reduction in the overall volume of the ovaries in both RNAi groups compared to the control (Figure 27 I, J). Because Sm*rar* and Sm*meiob* are not expressed in the vitellarium (Figure 20 C, 27 B) (61), no RNAi depended effect was anticipated for this organ. As expected, no obvious differences were observed between the vitellaria of females of control and the RNAi groups, neither by CLSM (Figure 27 I) nor by Oil-Red lipid staining of whole worms (Figure 29). These results provided additional support for the proposed ovary-preferential functions of both Sm*meiob* and Sm*rar*.

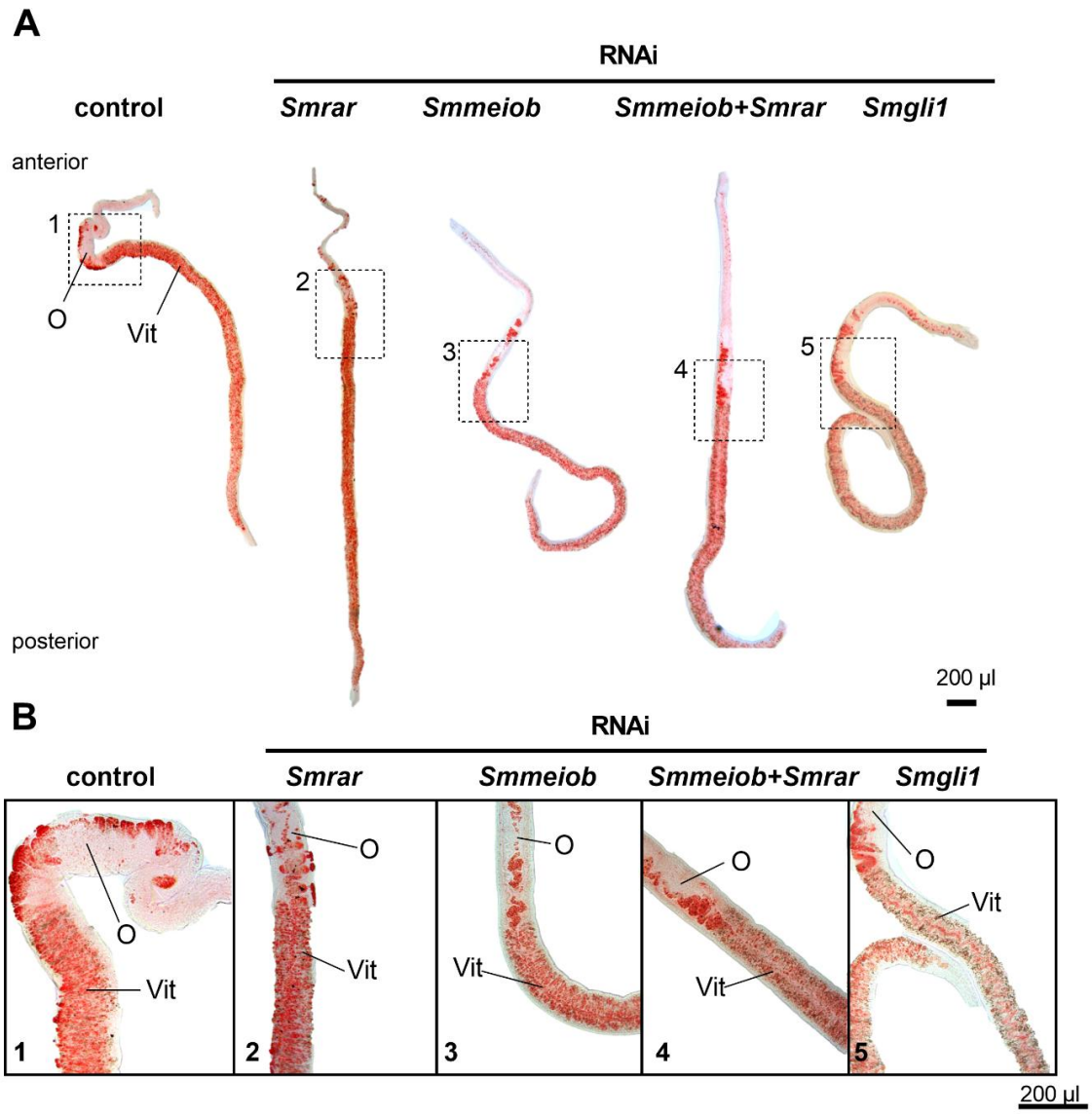

Figure 29. The lipid content of the vitellaria of paired *S. mansoni* females was not affected by Sm*rar* and Sm*meiob* RNAi.

Lipid staining was performed to investigate Sm*rar*, Sm*meiob* and Sm*gli1* RNAi-dependent effects on the vitellarium of sexually mature females. Five pairs of biological replicates (n=3) from each experimental group were treated with dsRNA. Following a 15-d treatment period, the couples were separated, and the females were stained with Oil-Red O. **A**, Representative image of a control female (no dsRNA treatment) stained with Oil-Red O. The boxes indicate areas shown in more detail below. **B**, Close-ups of parts of the female shown in A, focusing on the gonads of control and treated worms. No Sm*rar* or Sm*meiob* RNAi-dependent effects on the size of the vitellarium or its lipid content. In contrast, a much weaker intensity in lipid staining was detected in worms treated with Sm*gli1* dsRNA, which was expected due to previous findings (51). Abbreviations: O, ovary; Vit, vitellarium.

4.1.7 Functional characterization of Sm*gli1* reveals an involvement in egg formation rather than in ovary maintenance

Since Sm*gli1* was among the transcripts that had been downregulated upon Sm*rar* RNAi, subsequent RNAi experiments were performed to find evidence for a potential function of this gene in oocyte maintenance.

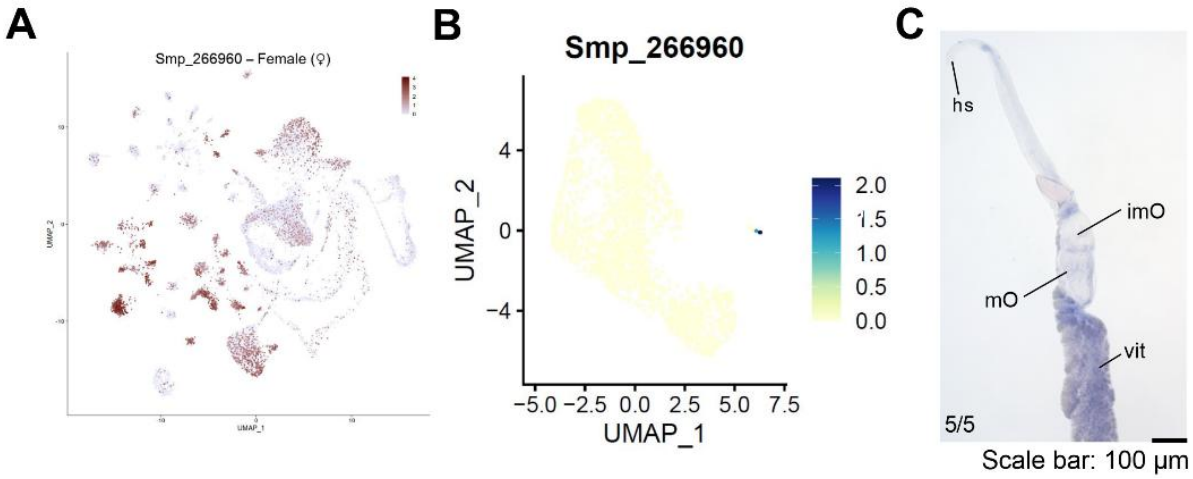

Figure 30. scRNA-Seq data and WISH localized transcripts of Sm*gli* in the vitellarium and neuronal cells of mature females.

A, The scRNA-Seq atlas of whole *S. mansoni* worms (61) showed Sm*gli1* transcripts in neuronal and parenchymal cells, muscles, neoblasts, and cells of the gonads. **B**, The scRNA-Seq atlas of mature ovaries revealed an enrichment of Sm*gli1* transcripts in the somatic cluster, which comprised genes related to neuronal and muscle cells (gonadsc.schisto.xyz). **C**, As expected, WISH of paired female schistosomes localized Sm*gli1* transcripts in different tissues, mainly in the vitellarium, as shown before (51). In the ovary, weak Sm*gli1* signals were found in the posterior part of the ovary containing intermediate stage and mature oocytes.

As shown in an independent study, Sm*gli1* transcripts were found pairing-independently in the ventral part of male worms, and in females in a pairing-preferentially manner (51, 61). Moreover, scRNA-Seq data of adult schistosomes showed the presence of Sm*gli1* transcripts in various tissues such as the ovary (Figure 30 A, B), albeit at a low level (61). WISH analysis confirmed expression along the vitellarium of bF. In addition, weak signals were found in the posterior part of the ovary, containing intermediate and mature oocytes (Figure 30 C). In the scRNA-Seq dataset of mature ovaries, Sm*gli1* transcripts were exclusively detected in the somatic cluster (Figure 30 B), which is marked by a high abundance of transcripts associated with neuronal, muscle, and ligament cells (283, 297).

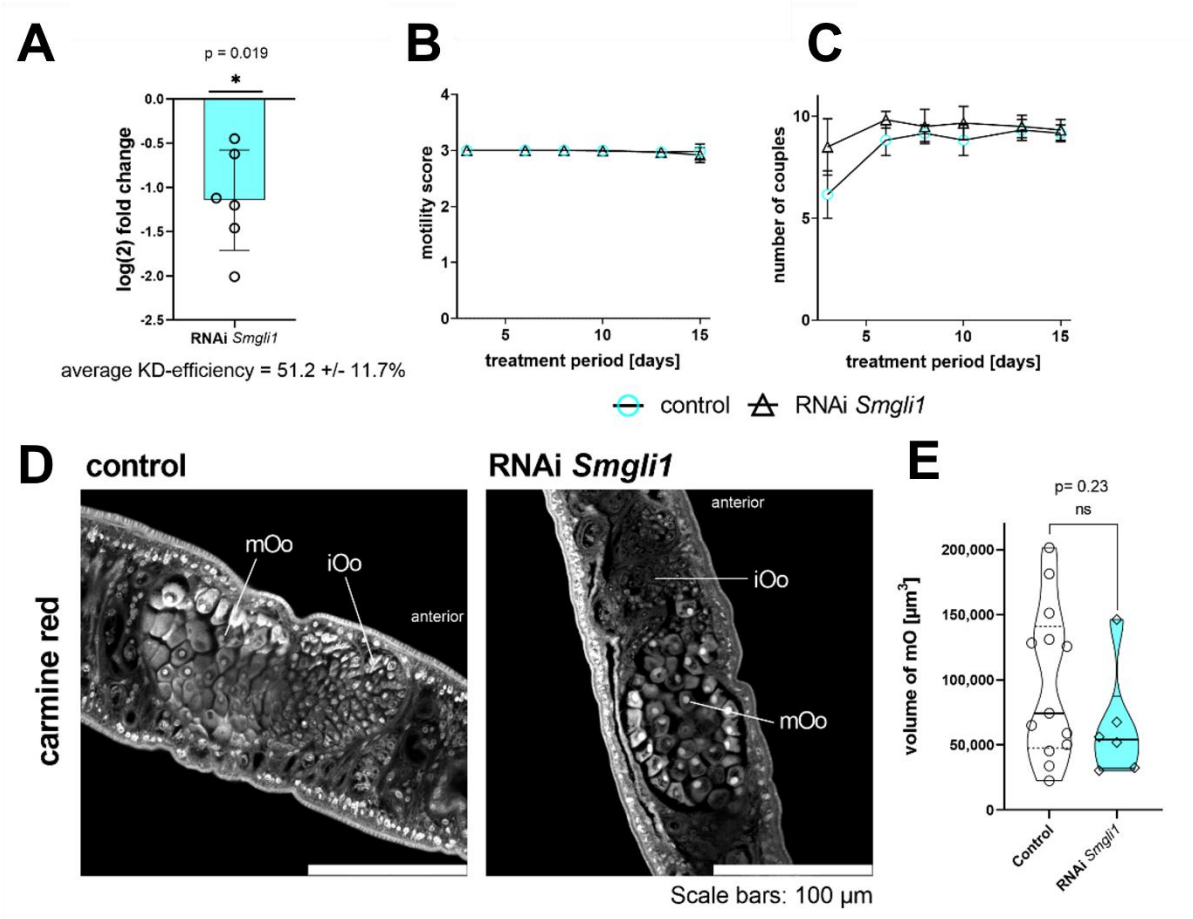

Figure 31. Sm*gli1* RNAi caused no alterations in the structure of the ovary.

A, The reduction of Sm*gli1* transcripts following RNAi was determined by RT-qPCR (51.2±11.7%). The average log(2) fold change in transcript levels, compared to the control, and the standard deviation are depicted. Each biological replicate is represented by a single point. **B-C**, Motility (**B**; motility scores: 0 (no motility) to 4 (hyperactive motility)) and pairing stability (**C**) were monitored during the RNAi experiment. No significant differences between the experimental groups were observed. **D**, CLSM showed no RNAi-dependent changes in ovary morphology. **E**, The volume of the posterior part of the ovary was determined through comparative Z-stack analyses. No significant reduction in volume associated with the Sm*gli1* RNAi was found. The violin plot shows the range between the minimum and maximum values, with the dashed lines representing the interquartile range and the solid line representing the median. Each point represents the volume of a single ovary (n=6). Abbreviations: hs, head sucker; iOo, oogonia; imO, immature part of the ovary; mOo, mature oocyte; mO, mature part of the ovary; vit, vitellarium. *P<0.05, **P<0.01, ***P<0.001 by t-test. n=6.

In order to obtain additional evidence for the function of Sm*rar* in oocyte maturation and meiosis, RNAi experiments were conducted targeting the transcripts of Sm*gli1* (Figure 31). RNAi succeeded, by reducing the transcript level of Sm*gli1* by 51.2±11.7% (Figure 31 A). As expected, neither motility nor pairing stability were affected (Figure 31 B, C). Moreover, no effects on ovary structure or volume were detected (Figure 31 D, E), including general,

morphological and sequence-independent dsRNA effects, as recently described for a non-schistosomal *ampR* dsRNA control (Supplemental Figure S1, S2) (152). After 8 d of RNAi treatment, a tendency, but not significant reduction in egg production was observed *in vitro* (Figure 32 A). However, a significant increase in the production of deformed eggs by Sm*gli1* RNAi after 8 d was observed (Figure 32 B). Nevertheless, Sm*gli1* RNAi did not affect the numbers of zygote-containing eggs (Figure 32 C). Furthermore, as expected (51), the lipid staining of Sm*gli1* RNAi-treated schistosomes demonstrated a noticeably diminished staining intensity in the vitellarium when compared to females in the control and other RNAi groups (Figure 29).

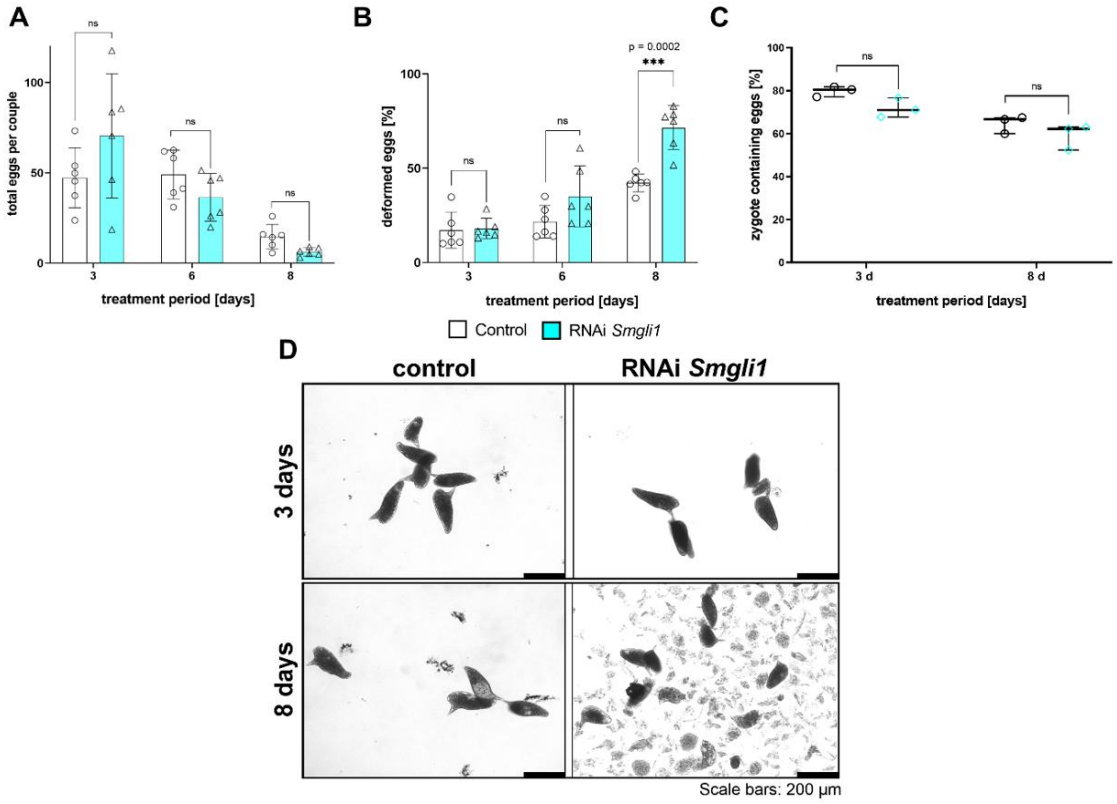

Figure 32. Sm*gli1* RNAi provoked changes in egg morphology.

The number of eggs (**A**) and their morphology (**B-D**) were examined in physiological assays and through bright-field microscopy after Sm*gli1* RNAi treatment (cyan). **A**, Compared to the control (white columns), no noticeable Sm*gli1* RNAi-dependent effects (blue columns) were observed on the quantity of eggs produced *in vitro*. **B**, After 8 d of treatment, a significant increase in the percentage of deformed eggs was observed due to Sm*gli1* RNAi. **C**, No significant differences in the number of zygote-containing eggs between the experimental groups were detected. **D**, Representative images of eggs produced *in vitro* after 3 and 8 d show that Sm*gli1* RNAi caused severe morphological changes, such as reduced size, smaller or missing spines. Furthermore, cell debris accumulated in the medium after 8 d of treatment. *P<0.05, **P<0.01, ***P<0.001 by t-test (A, B; n=6) and Mann-Whitney test (C; n=3).

4.1.8 SmTHRβ, an ovary-specifically expressed NR, plays roles in the formation of vital eggs and tissue homeostasis

Two potential thyroid hormone receptors, Smp_134490 and Smp_174260, were among the receptors, for which pairing-dependent and ovarian-preferential expression patterns were reported in recent RNA-Seq studies (Figure 16) (55, 62). Through phylogenetic analysis of thyroid hormone and retinoic acid receptors (Figure 17), and the comparison of their given annotations in additional databases (55, 61, 62, 143), Smp_134490 was annotated as thyroid hormone receptor alpha (SmTHRα), and Smp_174260 as thyroid hormone receptor beta-like (SmTHRβ) protein. Although analyses with Phyre2 (244) and annotations from other databases (55, 61, 62, 143) assigned SmTHRβ to the THRβ subgroup, my phylogenetic analyses clustered SmTHRβ to a trematode-specific THR subgroup.

Research on the function of the class of THRs in vertebrate organisms has demonstrated their essential roles in embryonic development, tissue homeostasis (108, 110). In addition, dimerization of RARs and THRs was demonstrated (103). This suggested potential overlapping functions in the maintenance of the female reproduction organs. Therefore, one aim of this study was to functionally characterize these *S. mansoni* THR orthologs.

In order to validate the annotation of SmTHRβ as a potential NR, SMART domain analysis was performed (243). This approach revealed the characteristic domain structure of nuclear receptors, which was consistent with the phylogenetic analysis (Figure 33 A, Figure 17). Furthermore, the scRNA-Seq atlas of mature oocytes (Moescheid and Lu *et al.,* submitted) indicated Sm*thrβ* transcript occurrence in intermediate-stage oocytes. Likewise, analysis of RNA-Seq data from immature and mature males and females and their isolated gonads (55) revealed a pairing-dependent and ovary-preferential transcription profile of Sm*thrβ*. WISH was performed to localize Sm*thrβ* transcripts revealing specific signals especially in the posterior part of the ovary of mature females (Figure 33 D). No specific signals were detected in male schistosomes. This result was reproducible for three independent replicates with four individuals per sex. Furthermore, the transcription patterns of bFs and inexperienced males and sFs (55) were verified by RT-qPCR (Supplemental Figure S4 A).

Descriptive analyses of SmTHRα, which were performed in the course of the Bachelor thesis of Pauline Holzäpfel (Institute of Parasitology, Justus Liebig university Giessen), localized Sm*thrα* transcripts specifically in the posterior part of the ovary, which contains intermediate and mature oocytes (38). Furthermore, THRα-characteristic NR domains were identified by SMART domain analysis (243) (data not shown). Additionally, the analysis of the transcription pattern using the scRNA-Seq atlas of mature ovaries identified Sm*thrα* transcripts specifically in intermediate oocytes (Moescheid and Lu *et al.*, submitted; data not shown).

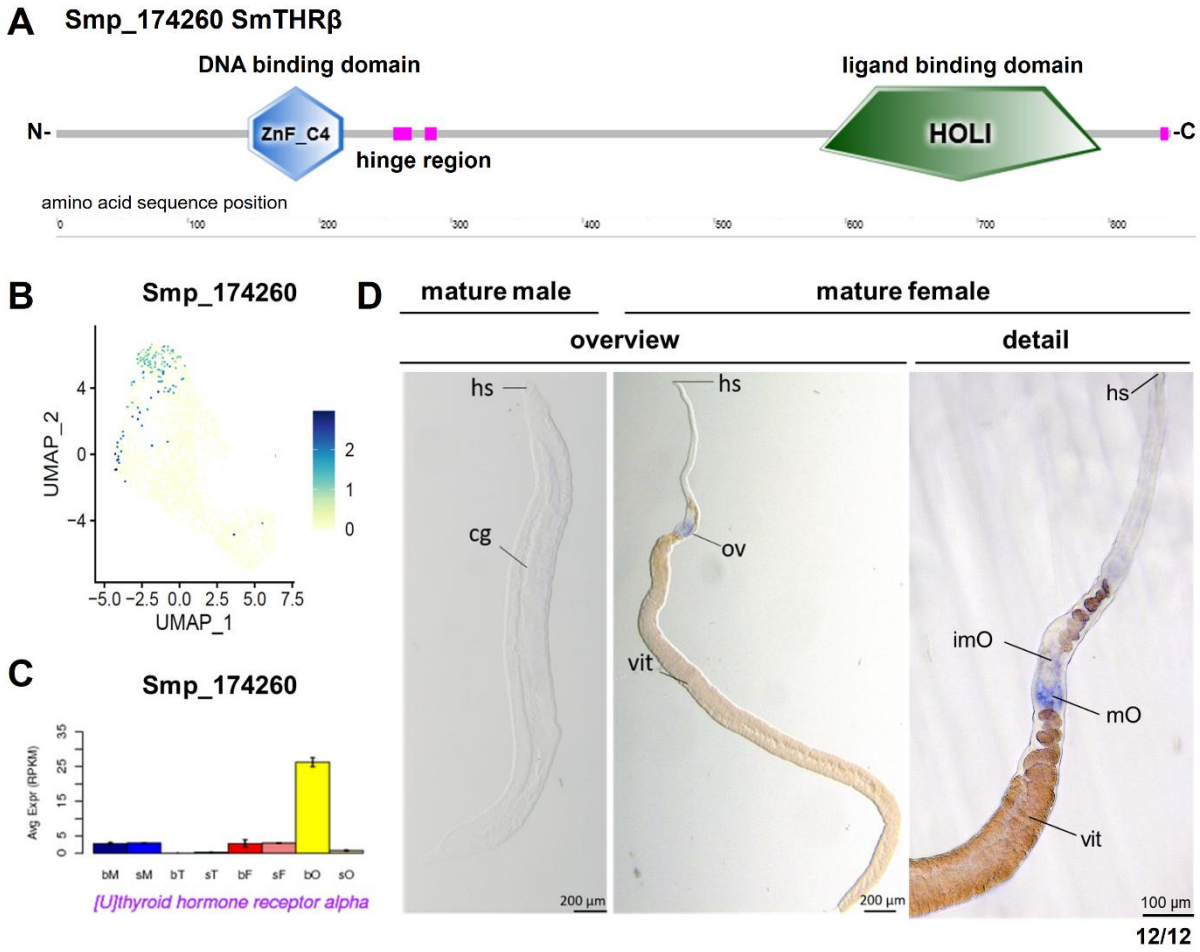

Figure 33. SmTHRβ is an ovary-specifically transcribed nuclear receptor.

A, Shown is the domain structure of Smp_174260 (SmTHRβ). SMART domain analysis (243) of SmTHRβ revealed the characteristic NR structure consisting of unstructured N- and C-terminal domains, as well as a DNA binding domain (ZnF_C4), which is linked by a hinge region to the ligand binding domain (HOLI). **B**, UMAP visualization of the scRNA-Seq data of mature ovaries, showed Sm*thrβ* (Smp_174360) transcripts primarily in oocytes of the intermediate stage. (Moescheid and Lu *et al*., submitted). **C,** Gene expression profile of potential thyroid hormone receptor beta (THRβ) Smp_174260 in adult schistosomes and their gonads (55) displayed a specific expression pattern in the ovary of mature female schistosomes (bO, yellow). **D,** Whole mount *in situ* hybridization localized Sm*thrβ* transcripts in the posterior part of the ovary of mature female schistosomes. No specific signals occurred in the tissue of male schistosomes. Abbreviations: **C**, bM, bisex male (pairing-experienced male); sM, single-sex males (pairing-inexperienced male), bT, testes of bM; sT, testes of sM; bF, bisex female (pairing-experienced female); sF, single-sex (pairing-inexperienced female); bO, ovary of bF; sO, ovary of sF. **D**, cg, *canalis gynecophoris*; hs, head sucker; imO, immature ovary; mO, mature ovary; ov, ovary; vit, vitellarium.

To functional characterize SmTHRα and SmTHRβ, RNAi experiments were performed by treating 10 couples with 30 µg/mL of target-specific dsRNA for a 14 d period, as described before. The medium was exchanged by fresh dsRNA-containing medium every second day, and six biological replicates were prepared per experiment. Couples treated in the same way but without dsRNA served as controls.

KD experiments reduced the Sm*thrα* transcript level ≥99%. However, no phenotypes related to worm vitality, reproductive biology or tissue homeostasis of *S. mansoni* were observed (Bachelor Thesis Pauline Holzäpfel, 2022).

RNAi experiments targeting Sm*thrβ* were equally successful, a significant reduction of Sm*thrβ* transcripts by 99.98±0.4% was achieved after 14 d of RNAi (Figure 34 A). Physiological parameters such as pairing attachment, motility and egg production were monitored following RNAi. Couples were stable and vital in the control as well in the treated group. Remarkably, however, after 14 d sudden detachment (Figure 34 B) and separation (data not shown) events were observed exclusively for the RNAi group and with high significance. At the same time point, the motility of treated worms significantly decreased (Figure 34 C). In addition, the percentage of malformed eggs per couple during the first 10 d of treatment were determined *in vitro* (Figure 34 D). RNAi did not significantly affect egg production capacity as such, but it provoked a drastic increase of abnormally formed eggs. Eggs from the RNAi group appeared darker, rod-like shaped without the typical spine, and they lacked a visible embryo (Figure 34 E). In addition, the morphology, especially the fine structure of the ovary, was examined after 14 d (Figure 34 F). First, the phenotypical appearance between control and treated group was investigated by bright-field microscopy (Figure 34 F, bright-field). Treated worms showed tegument damage, and tissue fragments were found in the medium (Figure 34 F, arrows). Furthermore, differences in the structure and size of the ovary were observed, which was confirmed by CLSM (Figure 34 F carmine red).

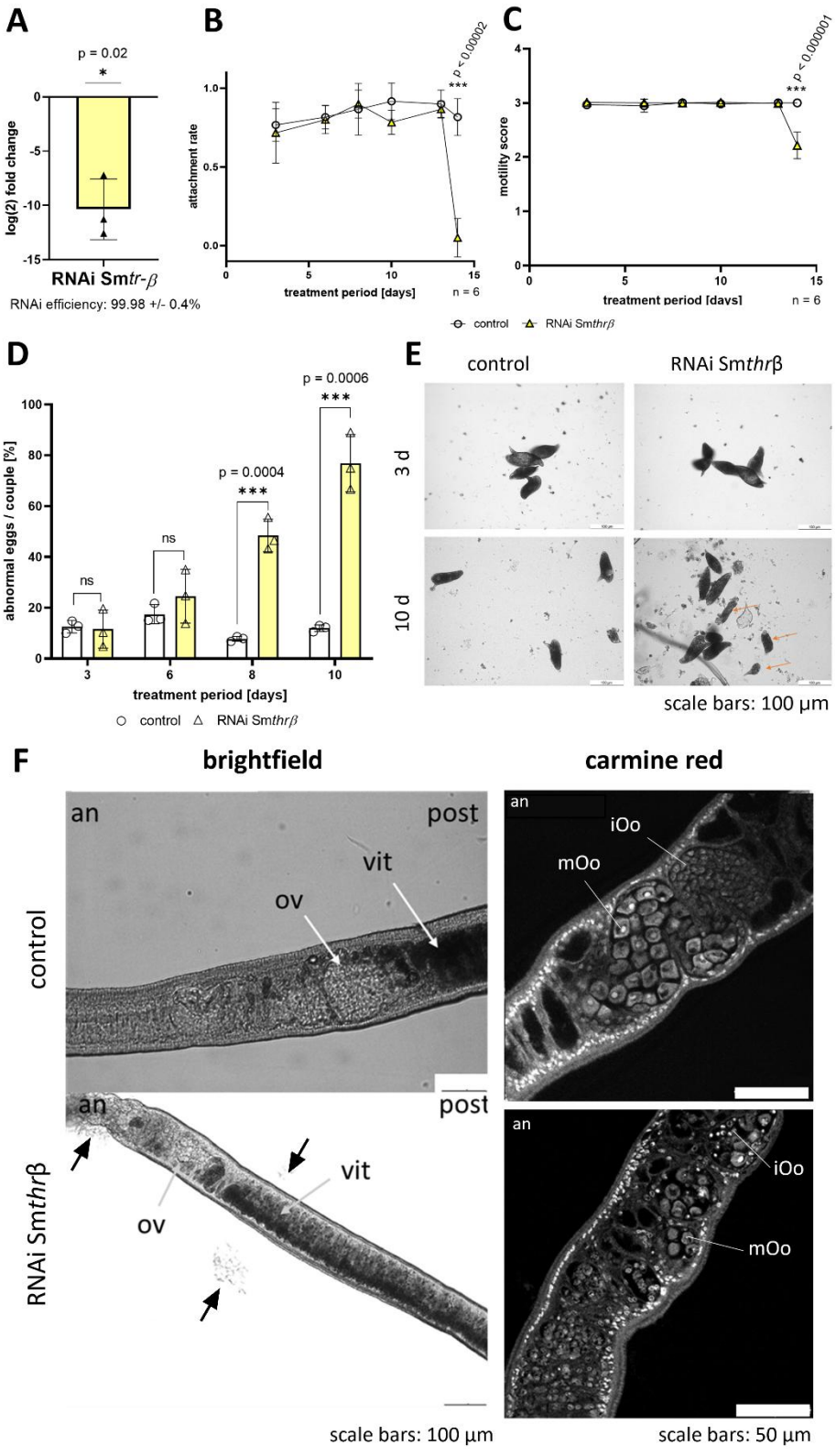

Figure 34. Sm*thrβ* RNAi drastically influenced *S. mansoni* physiology impacted egg morphology and ovary maintenance.

A, RT-qPCR revealed a significant decrease of the transcript level of Sm*thrβ* following RNAi. *P<0.05, **P<0.01, ***P<0.001 by t-test. Worm vitality (**B-C**) was monitored during the experimental period of 14 d. **B,** Over the whole observation period, worm attachment remained constant in the control group

(white). Precisely at d 14, dsRNA-treated schistosomes (yellow) detached and separated. **C,** Results of the monitoring of worm motility in a range from 0 (dead) to 3 (normal movement) during the 14-d observation period. Exactly at d 14, the motility of dsRNA-treated *S. mansoni* diminished significantly. *P<0.05, **P<0.01, ***P<0.001 by t-test. **D,** RNAi induced an up to eightfold increase of malformed eggs compared to the control after 10 d. *P<0.05, **P<0.01, ***P<0.001 by Mann-Whitney test. **E,** RNAi over a 14-d period led to the deposition of dark appearing, unembryonated eggs with elongated shape (orange arrows) and egg debris. **F,** Brightfield microscopy (left) and CLSM analysis (right) revealed differences in the structures of the ovaries of dsRNA-treated females. Treated worms showed tegument damage, and tissue fragments were found in the medium (left, arrows). Abbreviations: an, anterior; iOo, immature oocytes; mOo, mature oocytes; ov, ovary; post, posterior; vit, vitellarium; CLSM, confocal laser scanning microscopy. A, D-F, n=3; B, C, n=6.

4.1.9 SmRXR-1 is a pairing-dependently and ovary-preferentially transcribed nuclear receptor

Previous studies demonstrated that NRs of the RXR sub-family are common heterodimerization partners of THRs and RARs (85, 98). Indeed, a recent study confirmed SmRXR-1 (Smp_097700) as to be the interaction partner of SmRAR by co-immunoprecipitation (104). For SmRXR-1/SmRAR heterodimers, a regulatory role in oocyte maturation, but also in the regulation of eggshell precursor genes was demonstrated (104). Building up on the results of this thesis, I aimed to validate the regulative role of Sm*rxr-1* for ovary maturation and potential overlapping functions with other NRs. A critical role for both, SmRAR and SmTHRβ, in schistosomal reproduction was demonstrated, whereby only the RNAi of Sm*thrβ* affected worm vitality.

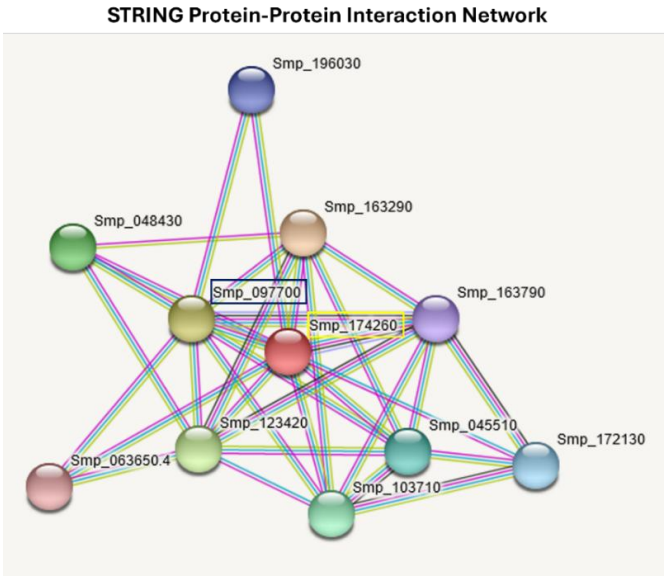

Figure 35. Identification of SmRXR-1 as potential SmTHRβ interaction partner by STRING.
Among other proteins, SmRXR-1 (Smp_097700, black frame) was identified as a possible dimerization partner of SmTHRβ (Smp_174260, yellow frame) by STRING analysis (249).

Applying STRING protein-protein interaction network analysis (249), potential interaction partners of SmTHRβ were determined (Figure 35). Among the potential binding partners SmRXR-1 was identified, a receptor for which a role in oocyte maintenance was assumed (104). By applying SMART domain analysis (243), SmRXR-1 was confirmed as NR (Figure 36 A). Its annotation as RXR was confirmed by phylogenetic analysis (Figure 17). Moreover, for SmRXR-1 a paring-dependent transcript pattern was found in females including the ovary (Figure 36 B, C), but also in other tissues such as neurons, as shown in an independent study (61), and male schistosomes (Figure 36 C). WISH analysis localized transcripts in both genders with a dominant signal appearance in the posterior part of the female ovary (Figure

36 D), which confirmed the RNA-Seq data (Figure 36 C) (55). The different transcription patterns of bMs, bFs, sMs and sFs (55) were verified by RT-qPCR (Supplemental Figure S4 B).Furthermore, the scRNA-Seq atlas of mature ovaries revealed Sm*rxr*-1 transcription in all clusters, with a clear preference for intermediate-stage oocytes (Figure 36 B, Moescheid and Lu *et al*., submitted).

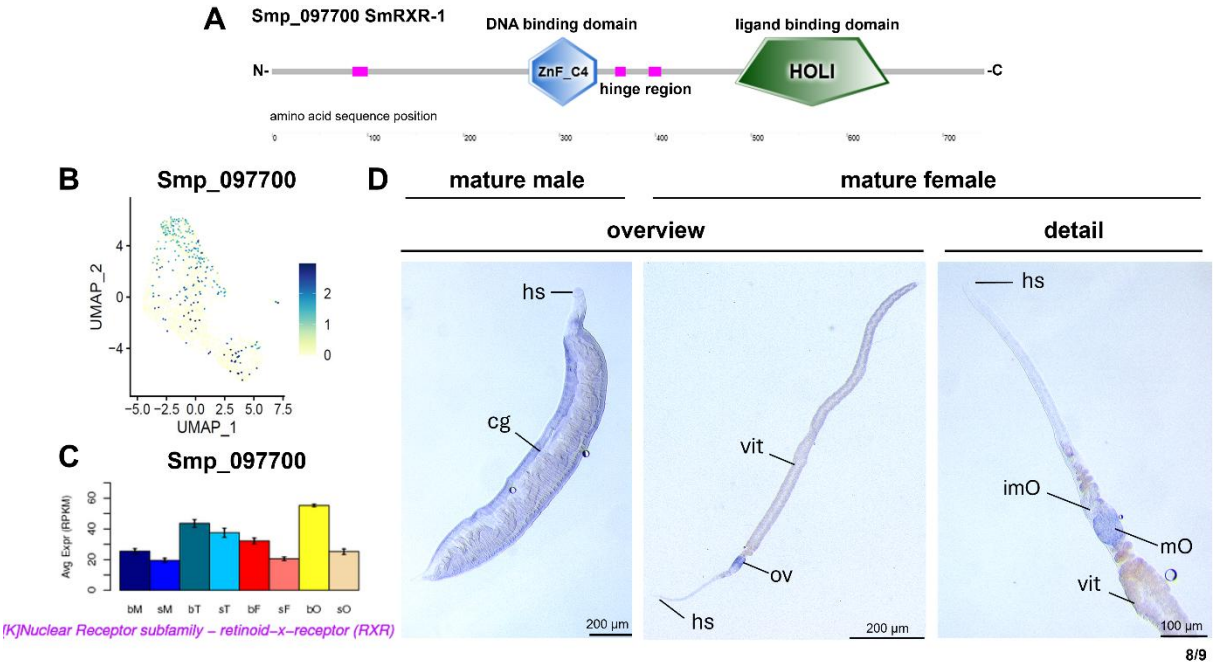

Figure 36. SmRXR-1 exhibited a pairing-preferential transcription pattern with a preference for the ovary and in intermediate-stage oocytes.

A, SMART domain analysis (243) of SmRXR-1 (Smp_097700) revealed the characteristic NR structure consisting of unstructured N- and C-terminal domains as well as a DNA binding domain (ZnF_C4), which is linked by a hinge region to the ligand binding domain (HOLI). **B**, UMAP visualization of the scRNA-Seq data of mature ovaries showed Sm*rxr-1* transcripts in all cell clusters, with a preference for oocytes of the intermediate developmental stage. (Moescheid and Lu *et al*., submitted). **C,** Gene expression profile of Sm*rxr-1* in adult schistosomes and their gonads (55) displayed its pairing-preferential expression in the ovaries of mature female schistosomes (bO; yellow). Furthermore, transcription in both sexes and their gonads was shown. **D,** Whole mount *in situ* hybridization revealed the localization of *Smrxr-1* transcripts in the posterior part of the ovary of mature female schistosomes. Furthermore, homogenous signals in all tissues of male schistosomes were found. Abbreviations: **C**, bM, bisex male (pairing-experienced male); sM, single-sex males (pairing-inexperienced male), bT, testes of bM; sT, testes of sM; bF, bisex female (pairing-experienced female); sF, single-sex (pairing-inexperienced female); bO, ovary of bF; sO, ovary of sF. **D**, cg, *canalis gynecophoris*; hs, head sucker; imO, immature ovary; mO, mature ovary; ov, ovary; vit, vitellarium.

4.1.10 Functional characterization of SmTHRβ and SmRXR reveals a key role of these receptor in the maintenance of the ovary

In order to functionally characterize possible synergistic functions of SmRXR-1 and SmTHRβ on female reproduction, single and double KD experiments were performed. Double KD experiments were carried out by treating couples with an equal amount of both dsRNAs. To this end, 10 couples were treated with 30 µg/mL dsRNA (n=3) for a period of 22 d. Medium and dsRNA were exchanged every 2-3 d. Couples treated in the same way but without dsRNA served as controls.

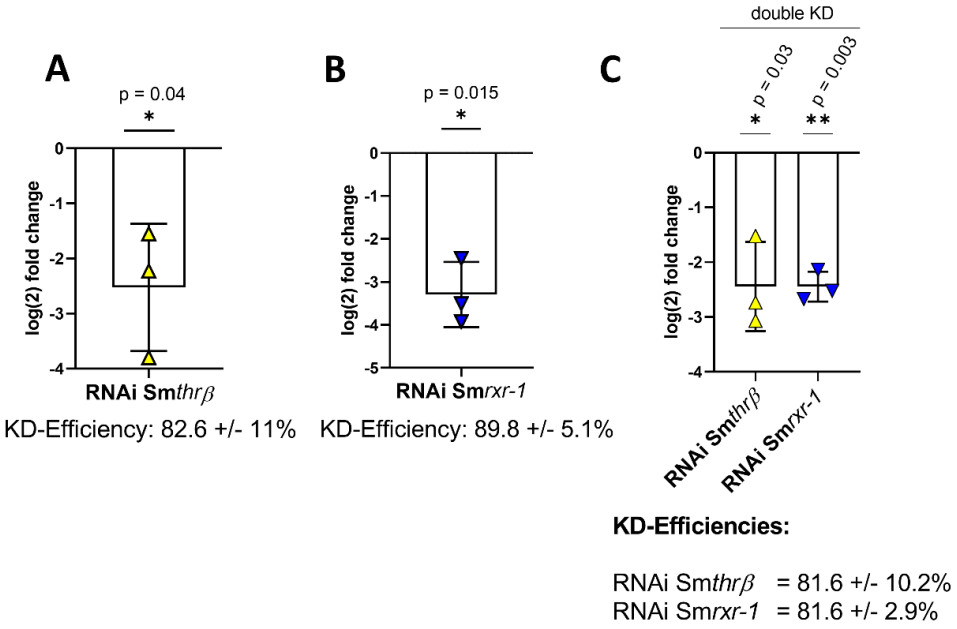

Figure 37. Successful transcript reduction by Sm*thrβ*, Sm*rxr-1*, and Sm*thrβ*/Sm*rxr-1* RNAi. Schistosome couples were treated with 30 µg/mL gene-specific dsRNA every 2–3 d for 22 d (yellow and blue triangles, n=3). Worms treated with DEPC-water without dsRNA under the same conditions served as control. The KD efficiencies were determined by RT-qPCR by analyzing transcript levels of Sm*thrβ* and Sm*rxr-1* in female worms separated from couples at d 22. Sm*thrβ* (**A**), Sm*rxr-1* (**B**) and Sm*thrβ*/Sm*rxr-1* (**C**) RNAi successfully reduced the respective transcript levels of both genes upon double KD. *P<0.05, **P<0.01, ***P<0.001 by t- test.

First the KD efficiencies of Sm*thrβ*, Sm*rxr-1* and the Sm*thrβ*/Sm*rxr-1* (double KD) RNAi were determined by RT-qPCR. The transcript level of Sm*thrβ* was significantly reduced by 82.6±11% (Figure 37 A), which corresponds to a sufficient but less efficient KD as it was shown in the previous Sm*thrβ* RNAi experiments (Figure 34 A).

By analyzing the KD-efficiencies of both the Sm*rxr-1* single KD and the Sm*thrβ*/Sm*rxr-1* double KD, transcript levels were significantly reduced with respect to the control by 89.8±5.1% and 81.6±10.2% / 81.6±2.9%, respectively (Figure 37 B, C). Next, worm vitality, pairing stability,

motility (Figure 38 A-F) and attachment were monitored. Couples were stable and vital in the control as well in all dsRNA-treatment groups; however, a significant separation rate was found in the Sm*thrβ* RNAi group after 19 d (Figure 38 A), with a significantly enhanced separation rate in the double KD-group (Figure 38 C). Likewise, the motility of all RNAi groups significantly decreased between days 16 and 22 of treatment (Figure 38 D-F). Similar to these observations, Sm*thrβ* RNAi caused a detachment rate of 70±8.2%, and especially worms from the Sm*thrβ*/Sm*rxr-1* double KD-group were 100% detached after 19 d. No significant effect on worm attachment was observed for couples treated by Sm*rxr-1* dsRNA only. Finally, the macroscopic morphology of the worms was evaluated by bright field microscopy after 22 d (Figure 38 G). No prominent changes were observed in the morphology of the control group, the Sm*thrβ*, and Sm*rxr-1* single KD-groups. However, for worms of the double KD-group a swollen, darkish appearance, particularly for female schistosomes, was found. Moreover, accumulations of cell and tissue debris were visible in the culture medium of the double KD worms.

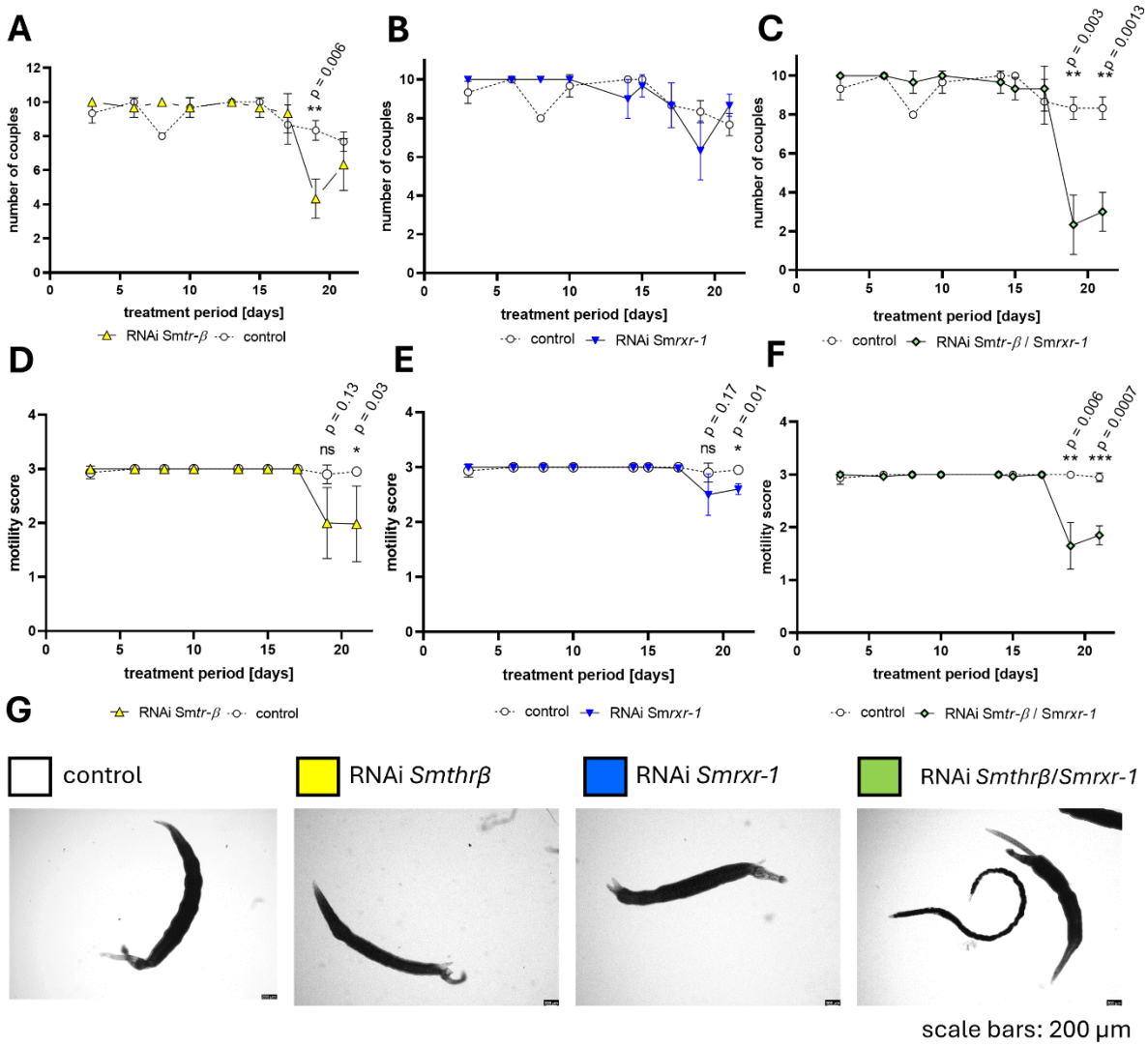

Figure 38. RNAi of Sm*thrβ* andSm*rxr-1*, alone and in combination, caused phenotypic effects. Schistosome couples (n=3) were treated with 30 µg/mL gene-specific dsRNA against the transcripts of Sm*thrβ* (yellow triangles), Sm*rxr-1* (blue triangles) and Sm*thrß*/Sm*rxr-1* (double KD, green diamonds) for 22 d. Medium and dsRNA were refreshed every 2–3 d. Worms treated with DEPC-water without the addition of dsRNA under the same conditions served as control (white circles). Phenotypic analyses focused on pairing stability (**A-C**) and motility (**D-F**). **A-C**, Control schistosomes (white circles) remained stably paired over the observation period. Exactly at d 19, couples of the Sm*thrβ* (**A**) and Sm*thrβ*/Sm*rxr-1* (**C**) RNAi groups separated. **D-F,** Motility monitoring covered the range from 0 (dead) to 4 (hyperactive movement) during the observation period. Starting from d 16, less movement of dsRNA-treated schistosomes was observed, which led to a significant reduction of motility from days 18-19 on. **G**, Bright-field microscopy showed a swollen, darkish appearance of females of the Sm*thrβ*/Sm*rxr-1* RNAi group at d 22. *P<0.05, **P<0.01, ***P<0.001 by Mann-Whtiney-test.

Next, the total number of eggs per couple (Figure 39 A-C), and the percentage of abnormally formed eggs per couple (Figure 39 D-F) were determined. The total number of eggs was not different between the control and the RNAi groups. However, the percentage of abnormal formed eggs was significantly increased upon Sm*rxr-1* (Figure 39 E) and Sm*thrβ*/Sm*rxr-1* RNAi (Figure 39 F). In both RNAi groups, the number of abnormal eggs doubled after 10 d. Furthermore, at this time point nearly 100% of the eggs produced by females of both RNAi groups were deformed. This strongly indicates a critical role(s) of SmRXR-1 in schistosome reproduction. For couples of the Sm*thrβ* RNAi group, a non-significant trend was observed in the increase of abnormal eggs. Following previous RNAi-Sm*thrβ* experiments, the number of deformed eggs was expected to increase. Given the relatively low KD-efficiency (82.6±11%, Figure 37 A), compared to Sm*thrβ* RNAi experiments conducted before (99.98±0.4%, Figure 34 A), this trend makes sense. After 10 d, some eggs of all RNAi groups exhibited a rod-like shaped appearance, without the typical spines, and many lacked visible embryos (Figure 39 G). Moreover, eggs showed the same morphological characteristics as those shown by previous Sm*thrβ* RNAi experiments (Figure 34 E).

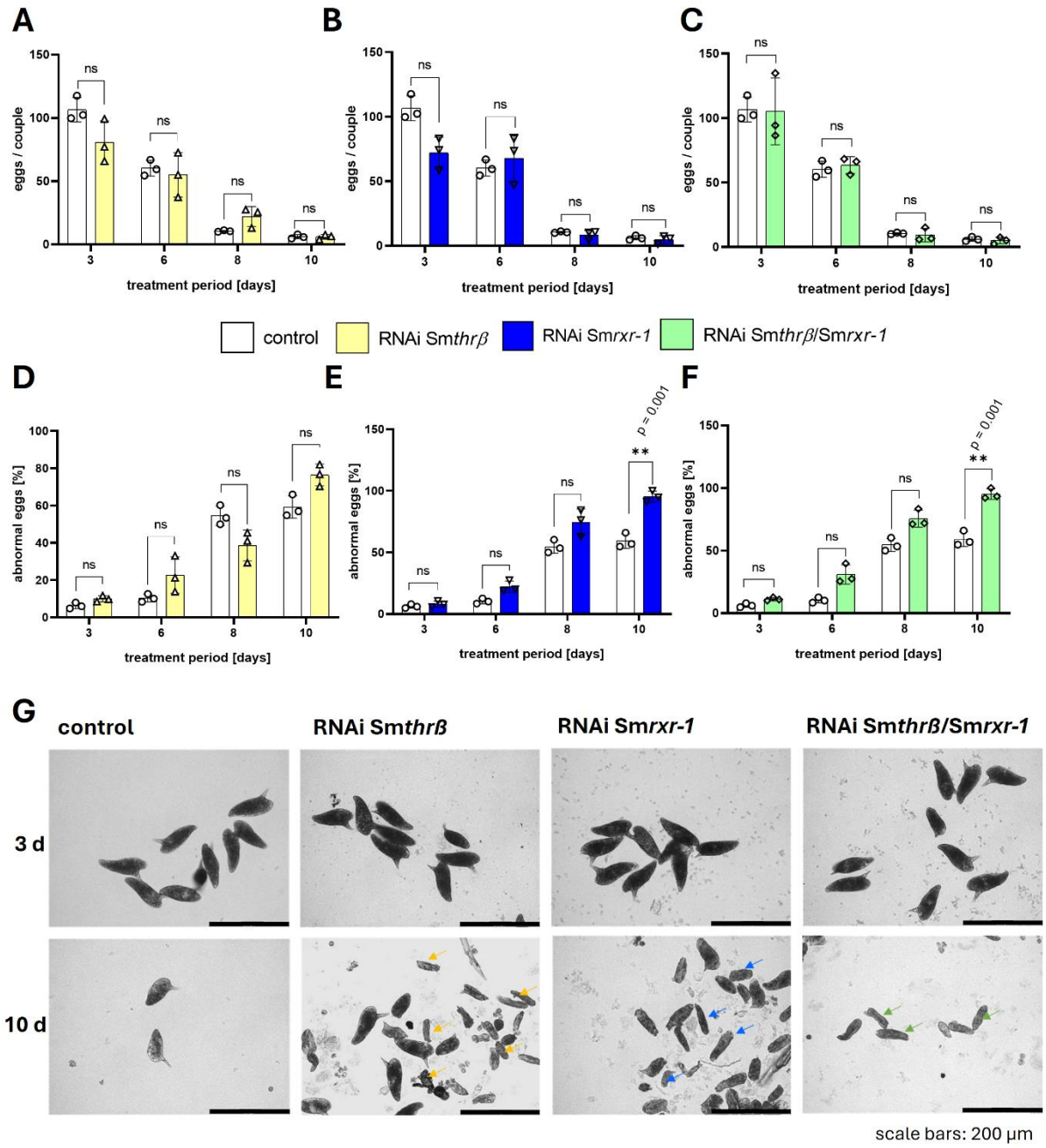

Figure 39. Sm*rxr-1 and* Sm*thrβ*/Sm*rxr-1* RNAi caused drastical changes in egg morphology. Schistosome couples were treated with 30 µg/mL Sm*thrβ* (yellow triangles), Sm*rxr-1* (blue triangles) and Sm*thrß*/Sm*rxr-1* (double KD, green diamonds) dsRNA every 2–3 d for 22 d (red bars). Worms treated with DEPC-water without the addition of dsRNA (white circles) under the same conditions served as control. **A-C**, The number of eggs produced *in vitro*, monitored over a 10 d period, showed no significant differences after RNAi for all experimental groups compared to the control. **D-F**, A significant increase in deformed, smaller, and non-embryonated eggs, some without spines or with deformed spines were observed after 10 d of Sm*rxr-1* and Sm*thrß*/Sm*rxr-1* RNAi**. F**, The morphology of eggs after 3 and 10 d was examined by bright-field microscopy. After 10 d, egg morphology altered, and significantly most eggs were deformed and/or reduced in size (arrows). *P<0.05, ** P<0.01, ***P<0.001, determined by Mann-Whitney-test. n=3.

The results strongly suggest an important role of Sm*thrβ* and Sm*rxr-1* in the reproductive biology of the female, and here specifically in the ovary, as previously shown for Sm*rar* in RNAi experiments (Figure 22, 26). To investigate the effects of Sm*thrβ* and Sm*rxr-1* single and double RNAi on ovary maintenance at the cellular level, EdU assay were performed followed by CLSM analysis in both RNAi and control females at 22 d (Figure 40 A). In addition, the structures of the ovaries (Figure 40 A) were analyzed by comparative Z-stack analysis of Hoechst-stained females (Figure 40 B).

EdU staining revealed a drastic reduction of proliferating oogonia, which are located in the anterior part of the ovary (Figure 40 A) (38). In particular, single KDs of either Sm*thrβ* or Sm*rxr-1* resulted in an almost complete reduction of the number of EdU-positive oogonia. Furthermore, in the Sm*thrβ*/Sm*rxr-1* double KD-group However, besides a reduced number of EdU-positive oogonia, the size of the ovary was reduced (Figure 40 A). In addition, CLSM analysis revealed a significant reduction in the number of mature oocytes exclusively in the RNAi groups, as well as a significant reduction in ovary volume as determined by comparative Z-stack analysis of the posterior part of the ovary (mO, Figure 41 B). The reduced ovary volume corresponded to the smaller size of the posterior part of the ovary, which was consistently observed in female schistosomes of the RNAi groups of the investigated NRs (Figure 22 D, 26 E, 40 B), but not in the Sm*gli1* RNAi (Figure 31 D) or in couples treated with a non-schistosomal dsRNA, as it was demonstrated by previous studies (152, 298).

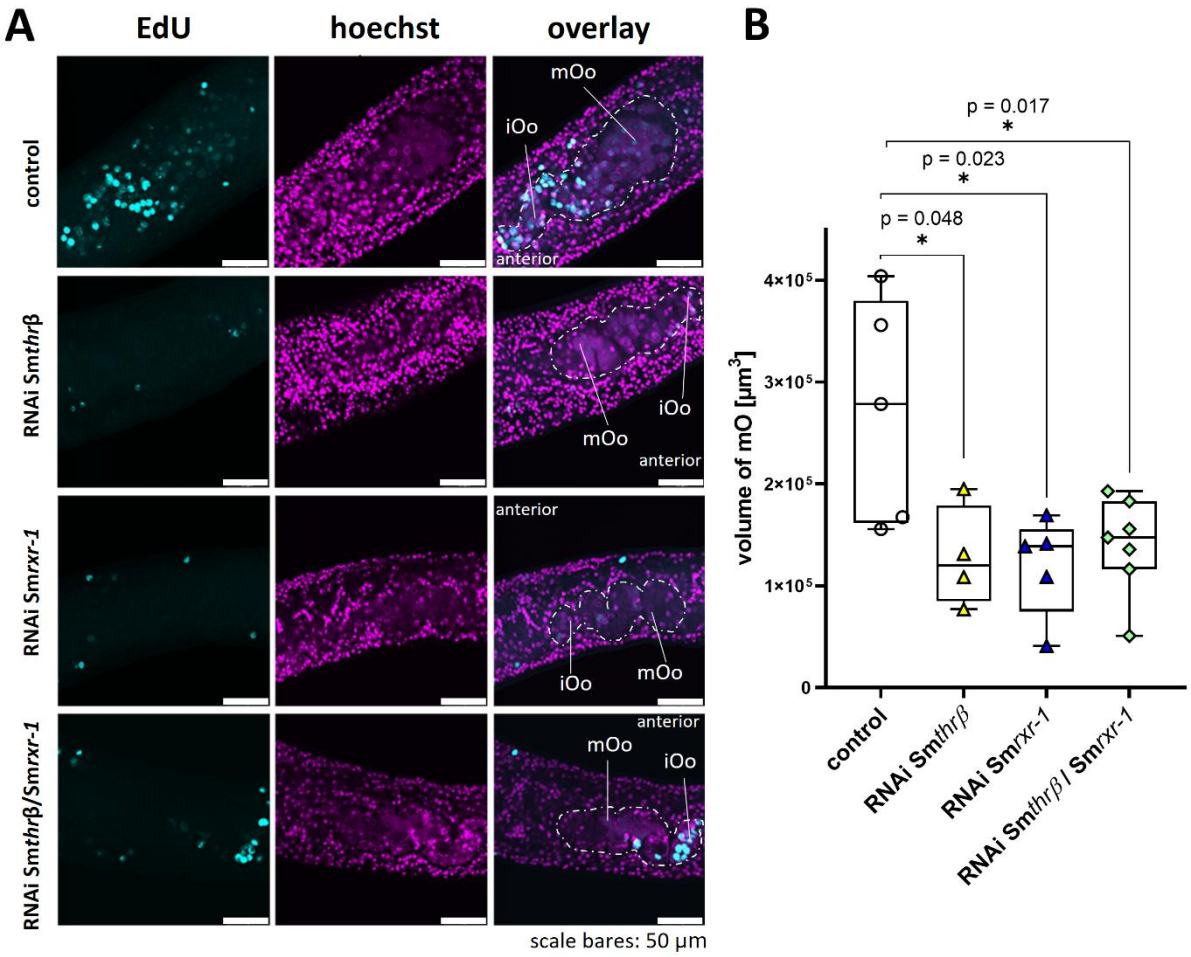

Figure 40. Sm*thrβ* and Sm*rxr-1* RNAi resulted in a drastic reduction of EdU-positive cells, less mature oocytes, and reduced ovary volumes.

For RNAi, 10 couples (n=3) were treated with 30 µg/mL gene-specific dsRNA against the transcripts of Sm*thrβ* (yellow triangles), Sm*rxr-1* (blue triangles) and Sm*thrß*/Sm*rxr-1* (double KD, green diamonds) every 2–3 d for 22 d. Worms treated with DEPC-water without the addition of dsRNA under the same conditions served as control (white circles). RNAi- dependent effects on cell proliferation in the ovary (dashed outline) were analyzed by EdU-assays (**A**), and ovary volumes determined by CLSM and Z-stack analysis (**B**). **A**, CLSM analysis of EdU-treated females showed a decrease of EdU-positive cells in all RNAi groups compared to the control. A strong reduction in the abundance of EdU-positive oogonia (cyan, iOo) was observed. **B**, Comparative Z-stack analysis of Hoechst-stained (purple) ovaries revealed a significant reduction of the volume of the posterior part of the ovary in all RNAi groups. The boxplot indicates the range between the minimum and maximum values, and the median is visualized by the solid line. Each point represents the volume of a single ovary. Abbreviations: iOo, oogonia; mOo, mature oocyte; mO, mature part of the ovary. *P<0.05, **P<0.01, ***P<0.001 by t-test. n=3.

The successful KD of Sm*thrβ* and Sm*rxr-1* in single and double KD experiments resulted in increased numbers of malformed eggs, as well as a critical effect on the number of proliferating oocytes and the number of mature oocytes.

To assess the effects of target-specific gene KD on transcription, quantitative reverse transcription of selected genes known to be associated with ovary development, pRT-qPCRs were performed (Figure 41 A-C). Sm*fgfr-a* (Smp_175590) was chosen as it was shown to play an important role in early oocyte development and ovary maintenance (200). According to the scRNA-Seq atlas for mature oocytes, Sm*fgfr-a* (Figure 25 B) is transcribed in early, Sm*nanos2*-transcribing oogonia (61) (gonadsc.schisto.xyz). Recent studies found a strong association between Sm*nanos2* and proliferating, EdU-positive stem cells, such as oogonia (61, 299). Sm*ncor* (Smp_163290) was selected, because of its regulation by Sm*rar* (Figure 25 A). For vertebrate SmNCoR orthologues, an interaction with type II nuclear receptors (NRs) has been described (98, 99). Furthermore, Sm*ncor* serves among others as a marker gene for oocyte at intermediate development (gonadsc.schisto.xyz). RT-qPCR revealed that the transcripts of these ovarian marker genes were significantly downregulated after 22 d of Sm*rxr-1* and the double KD (Figure 41 B, C). Sm*rxr-1* KD caused a significant reduction in the transcript level of Sm*fgfr-a* (Figure 41 B), which is in line with the findings of the EdU assay of dsRNA-treated couples (Figure 40 A). Moreover, a non-significant trend in the RNAi-dependent downregulation of Sm*fgfr-a* was observed in Sm*thrβ* and Sm*thrβ*/Sm*rxr-1* RNAi treated worms (Figure 41 A, C). Furthermore, Sm*thrβ* RNAi caused a reduction in Sm*ncor* transcript levels, while KD of both Sm*rxr-1* and Sm*thrβ*/Sm*rxr-1* provoked a significant decrease in Sm*ncor* transcripts. Additionally, the possible NR-internal regulation of Sm*thrβ* and Sm*rxr-1* was investigated. Conclusively, Sm*thrβ* RNAi significantly reduced the transcript levels of Sm*rxr-1*, and Sm*rxr-1* RNAi significantly reduced the transcription of Sm*thrβ* (Figure 41 A, B). This underpins the hypothesized regulatory influence of these NRs on the ovary, particularly the intermediate-stage oocytes.

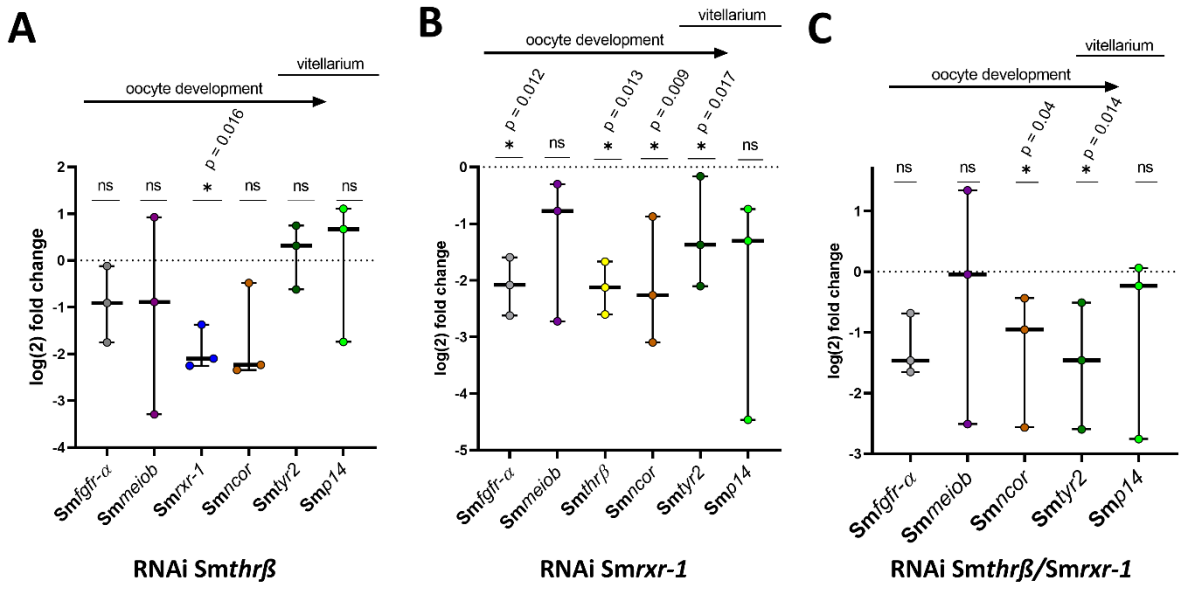

Figure 41. Sm*thrβ* and Sm*rxr-1* RNAi led the downregulation of genes involved in oocyte development and eggshell synthesis.

Schistosome couples were treated with 30 µg/mL Sm*thrβ* (**A**), Sm*rxr-1* (**B**) and Sm*thrß*/Sm*rxr-1* (**C**) every 2–3 d for 22 d. Subsequently, the couples were separated, and RNA was isolated from separated females. Next, transcript levels of candidate genes were quantified by RT-qPCR (n=3). These genes were selected on the basis of their known association with ovary development (61, 200, 293) and eggshell formation (49, 79, 300), and they were plotted following the oocyte developmental trajectory, from immature, undifferentiated GSCs to mature oocytes and transcription in the vitellarium according to the scRNA-Seq data as shown in Figure 25 (gonadsc.schisto.xyz; (61)). The tyrosinase Sm*tyr2* (Smp_013540) was found to be expressed in mature oocytes and in the vitellarium (61). Moreover for Sm*p14* (Smp_131110) transcription exclusively in S4 vitellocytes is described (64, 301).These genes were arranged according to the transcriptional peaks of the corresponding cluster of the scRNA-Seq atlas of the mature ovary (gonadsc.schisto,xyz) and scRNA-Seq atlas of whole worms (61), respectively. The boxplots indicate the range between the minimum and maximum values, with the 10th and 90th percentiles and median shown in the box. *P<0.05, **P<0.01, ***P<0.001 by t-test.

Also, the double KD of Sm*rxr-1* and Sm*thrβ*/Sm*rxr-1* led to a significant increase in the number of malformed eggs (Figure 39 E, F). As Sm*rxr-1* is not only transcribed in the ovary of schistosome females but also in their vitellarium (61), the transcripts of the S4 vitellocyte-associated genes Sm*tyr2* (Smp_013540) and the egg-shell precursor protein gene Sm*p14* (Smp_131110) were analyzed (42, 64, 79, 300) to find out whether potentially affected genes in the vitellarium play additive roles for the observed egg phenotypes. SmTYR2 has a special transcription pattern, as it is transcribed in S4 vitellocytes as well as in mature oocytes (61) (gonadsc.schisto.xyz). The vitellarium-specific transcription pattern of Sm*tyr2* was confirmed by WISH in the course of the master thesis of Theresa Huber (302). Additionally, the

SmRXR-1-dependent regulation of Sm*p14* was demonstrated in CoIP experiments (104). Among other eggshell precursor proteins, Smp14 and the tyrosinase SmTYR2 play essential roles in the formation of the eggshell (42, 64, 79, 300). No effects of Sm*thrβ* RNAi on transcript levels of Sm*p14* or Sm*tyr2* were observed (Figure 41 A). However, a significant reduction in Sm*tyr2* transcript levels was identified in the Sm*rxr-1* and Sm*thrβ*/Sm*rxr-1* KD (Figure 41 B, C). In addition, Sm*p14* was not significantly but tendentially downregulated in both RNAi experiments. This was expected since binding of the Sm*p14* promoter by Sm*rxr-1* was demonstrated in another independent study (104). Finally, the downregulation of these important genes associated with eggshell synthesis was consistent with the observed egg phenotype.

4.1.11 *In vitro* treatment with retinoid-acid and its antagonist provided further evidence for functional roles RA and RARs in *S. mansoni* reproduction

RNAi against the retinoic acid receptors Sm*rar* and Sm*rxr-1* had considerable effects on the reproductive biology of *S. mansoni*. This was particularly evident in genes associated with meiosis, such as Sm*meiob* and Sm*ncor*, and eggshell-associated genes, such as Sm*tyr2*, which were downregulated in Sm*rar* and Sm*rxr-1* RNAi experiments. This indicated a role of retinoic acid (RA) on egg production. To get further support for this assumption, *S. mansoni* couples, as well as sFs used for first-time pairing experiments, were treated with 5 µM 9cis-RA, the biological active isoform of vitamin-A (98). This corresponds to the concentration of 9cis-RA in human blood plasma (303, 304). Furthermore, 9cis-RA may represent a potential ligand for NRs of the RAR and RXR families, which was demonstrated by previous studies in vertebrates (111–114).

In total, 10 *S. mansoni* couples were treated with 5 µM 9cis-RAi for three days *in vitro* (n=9). Daily medium ($M199^{+++}$) exchange and renewal of 9cis-RA were performed. DMSO (0.005% v/v) at the same concentration used in the 9cis-RA-treated groups was added to the control couples. The treatment resulted in a significant increase in egg production after 3 d (Figure 42 A). Furthermore, the influence of 9cis-RA on initial egg-production was investigated in pairing experiments with first-time paired females. For this, 15 sF were paired with 10 bM, as described above (57). Pairing occurred within a period of 48–72 h. Unpaired schistosomes were removed after 72 h. The medium was renewed daily alongside with 9cis-RA, and egg production was monitored every 2-3 d. The start of egg production was observed in both groups after 12 d of *in vitro* culture (Figure 42 B). 9cis-RA treatment failed to induce an earlier start point for egg production, but the treatment resulted in a generally higher and significantly increased egg production after 19 d compared to the DMSO-treated control group.

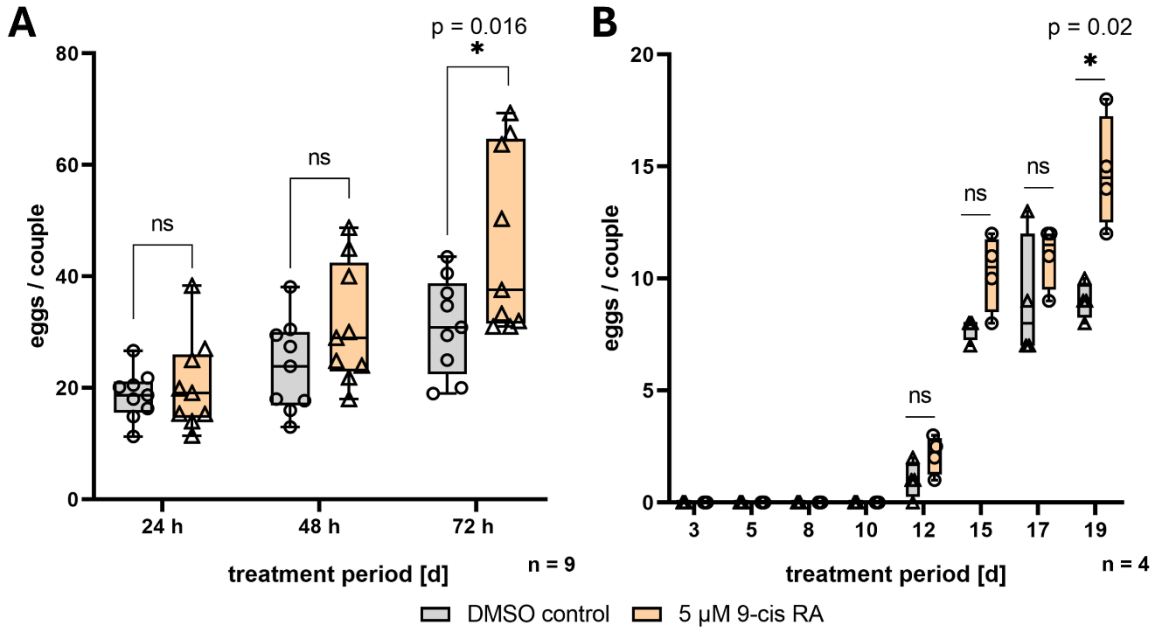

Figure 42. 9cis-RA promoted egg production of *S. mansoni* couples *in vitro*.

S. mansoni couples were treated by 5 µM 9cis-RA (yellow). DMSO at the same concentration as in the treatment groups served as control (grey). **A**, 10 couples were treated with 9cis-RA (n=9), with daily medium exchange and 9cis-RA renewal. Upon 3 d of treatment, egg production was significantly increased. **B**, By performing pairing experiments of experienced males with first-time paired females (n=4), a significant increase in egg production was observed after 19 d. Pairing occurred within 48–72 h, while unpaired schistosomes were removed after 72 h. The medium and 9cis-RA were renewed every 2-3 d. The boxplot indicates the range between the minimum and maximum values, with the 10th and 90th percentiles and median shown in the box. *P<0.05, **P<0.01, ***P<0.001, by t-test.

As first inverse experimental approach was performed to further unravel the role of RARs for female reproductive biology, especially for oocyte maturation and embryogenesis. For this, I made use of the RAR inhibitor CH-55(4-[(1E)-3-[3,5-*bis*(1,1-dimethylethyl)phenyl]-3-oxo-1-propen-1-yl]-benzoic acid). This RA antagonist is able to bind both RAR-α and RAR-β receptors with high affinities (267, 305). Experiments were conducted with 10, 25, and 50 µM CH-55 dissolved in DMSO and *S. mansoni* couples *in vitro*. DMSO (0.005% v/v), in the same concentration as in the CH-55-treated groups, was added to control couples. In this experimental series, couples were treated for 48 h, and I monitored pairing stability, motility, and egg production - as before. Scoring was done every 24 h, and after 48 h the worms were fixed for CLSM analysis.

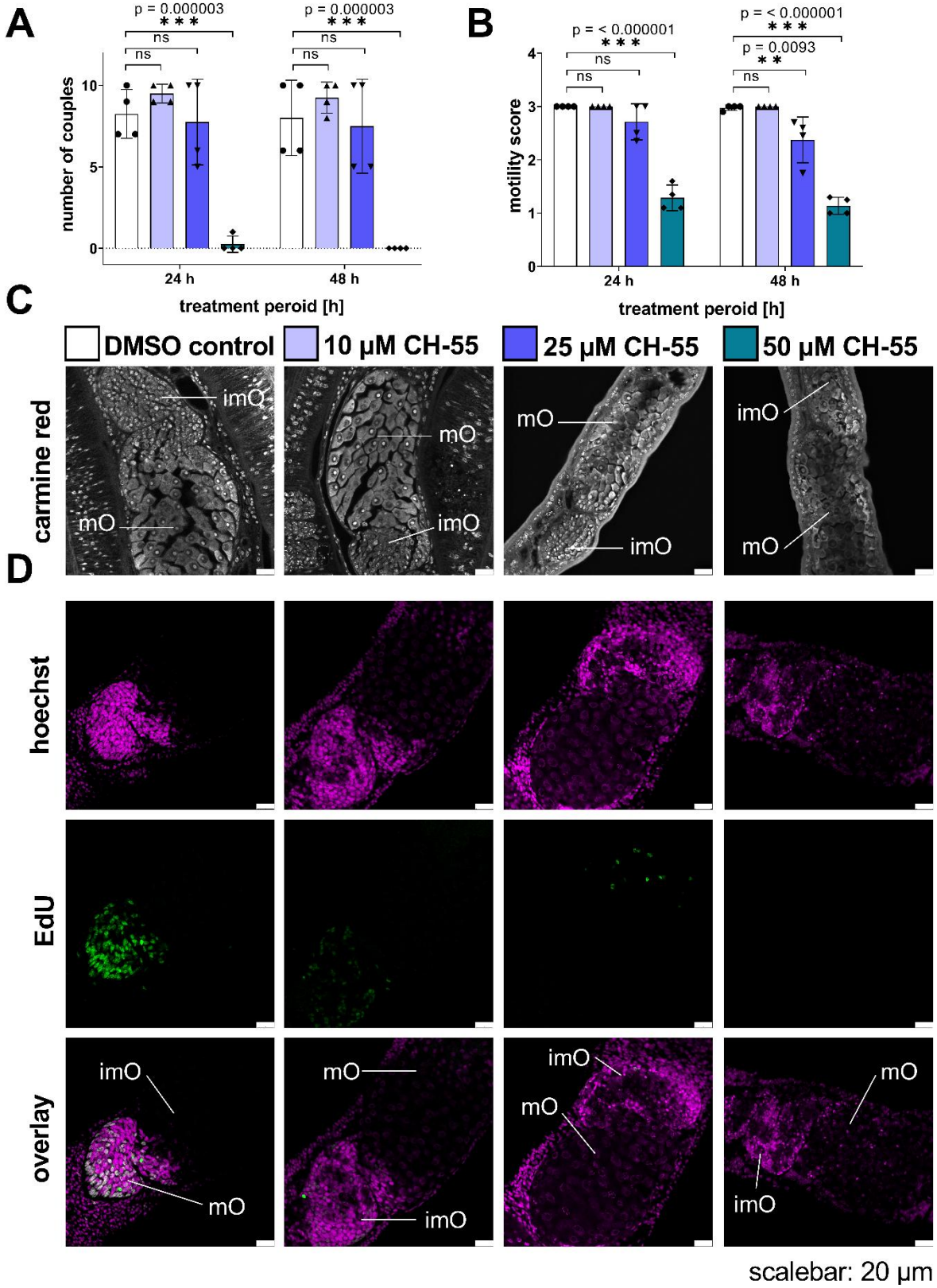

Figure 43. CH-55 treatment affected pairing stability, worm motility, oocyte maturation, and oogonia proliferation.

S. mansoni couples were treated with 10, 25, and 50 µM of CH-55, RAR receptor antagonist, dissolved in DMSO, *in vitro*. DMSO (0.005% v/v) only was added to control couples. The inhibitor treatment was

conducted for 48 h. **A**, Number of paired couples during 48 h of treatment. Control schistosomes (white) as well as schistosomes treated with 10 µM (light blue) and 25 µM (blue) CH-55 remained paired at a constant, comparative number. With 50 µM CH-55 (turquoise), a significant decrease of pairing stability was observed after 24 h, and all couples separated after 48 h. **B**, In worms treated with 25 µM and 50 µM CH-55, a significant concentration-dependent reduction in motility was observed at both time points. CLSM analysis with a focus on the ovary showed less mO in females treated with 25 µM and 50 µM CH-55 after 48 h, along with a reduced size of the anterior part of the ovary, which contains mO. **D**, CH-55 caused a concentration-dependent decrease of EdU-positive oocytes in the ovary. The strongest effect occurred at a concentration of 50 µM, here, no EdU-positive cells were noted. Abbreviations: imO, immature ovary; mO, mature ovary. *P<0.05, **P<0.01, ***P<0.001 by Mann-Whitney test. Scale bars: 20 µM.

In concentrations of 10 and 25 µM CH-55, treatment had no effect on pairing stability (Figure 43 A) and the motility (Figure 43°B), which was similar to the control. Worms treated with 50 µM CH-55, however, exhibited a remarkable pairing-instability after 24 h. Nearly all couples separated in this treatment group (Figure 43 A). Also, the motility of treated worms significantly decreased at this time point (Figure 43 B). CLSM analyses with worms treated for 48 h showed that 25 and 50 µM CH-55 reduced the numbers of mO, and in the highest concentration ovary size was also reduced (Figure 43 C). Already with 10 µM CH-55, the number of EdU-positive cells declined compared to the control. In worms treated with 50 µM CH-55, no EdU positive cells were found (Figure 43 D).

With respect to egg production, CH-55 treatment led to a concentration- and time-dependent decrease of the total number of eggs, while the number of deformed eggs increased over time (Figure 44 A, B). The deformations observed comprised abnormal eggshells, reduced sizes of eggs, abnormally formed or missing spines. In addition, cell debris accumulated in the medium (Figure 44 C). The latter points to “free” vitellocytes and oocytes released in the medium without being encapsulated by an eggshell. Using 50 µM CH-55, treatment completely inhibited egg production already after 24 h. Therefore, 25 µM CH-55 was the highest possible concentration to evaluate egg quality after 48 h, which showed a significant high number of deformed eggs (59.4±26.3%) compared to the control (23.7±8.7%) at this time point (Figure 44 B). The observed effects are precisely the opposite of the findings after treatment of *S. mansoni* couples with 9cis-RA (Figure 42 A). In conclusion, the pilot approaches with 9cis-RA and the RAR inhibitor CH-55 substantiated the assumptions about important role(s) of RA and RARs for the reproductive biology of female *S. mansoni*.

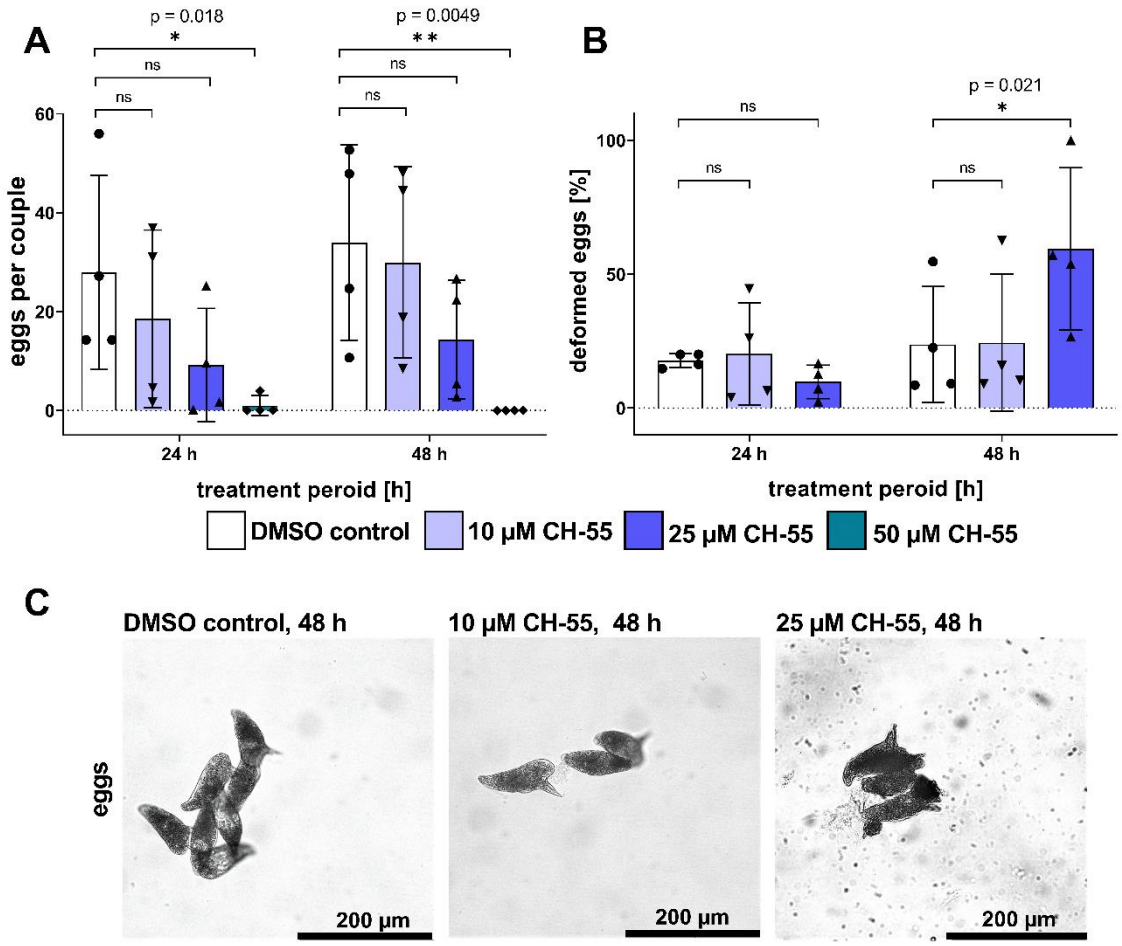

Figure 44. CH-55 treatment affected egg production and quality.

Eggs produced *in vitro* by CH-55-treated *S. mansoni* couples were monitored during the incubation period of 48 h. Couples were treated with DMSO (0.005% v/v, control, white), or 10 µM (light blue), 25 µM (blue), and 50 µM (turquoise) CH-55, which was added every 24 h for a total period of 48 h. **A**, With increasing CH-55 concentration, a constant decrease in the total number of eggs per couple was observed already within 24 h. Worms treated with 50 µM CH-55 stopped egg production after 48 h. **B**, Compared to the control, the proportion of deformed eggs increased with a peak after 48 h with 25 µM CH-55. **C**, Bright-field microscopy showed egg deformations such as reduced sizes, abnormal spines, and the accumulation of cell debris after 48 h with 50 µM CH-55. *P<0.05, **P<0.01, ***P<0.001 by Mann-Whitney test.

4.2 Establishment of transgenic schistosomes

Until now, functional gene analysis in schistosome research has relied on gene KD approaches using RNAi. However, RNAi can lead to ectopic effects, such as deregulation of off-target genes or RISC-dependent post transcriptionally regulated genes (151–154). Recently, the feasibility of CRISPR/Cas9 and Cas12a-mediated gene KO in *S. mansoni* was demonstrated by transfecting *S. mansoni* adult worms, eggs and sporocysts (33, 169–172). For the transfection of eggs a lentiviral as well as a RNP based approach was used, targeting the *S. mansoni omega-1* locus (33, 169). Adult worms and sporocysts were recently successfully transfected with Cas9 RNPs by EPO targeting the oxamniquine resistance *slut-or* locus (170). However, successful gene KO was not found in all cells, nor was it possible to select for edited schistosomes. To overcome these hurdles, a further aim of this thesis was the establishment of a CRISPR/Cas protocol in combination with multiple transformation methods to achieve the stable integration of an eGFP reporter-gene construct into a genomic safe harbor site (GSH).

4.2.1 Establishment of an eGFP reporter-gene construct

For the expression of a reporter-gene, such as the well-established eGFP (159, 306, 307), the selection of a suitable promoter is essential. In the context of this work, I searched for regulatory elements allowing reporter-gene expression in all tissues as well as in all life stages to ensure selection during the entire parasitic life cycle. To this end, the promoter and terminator regions of Smp_335990 were chosen, which encodes the *S. mansoni* ubiquitin gene (SmUbi, Figure 45). This gene met all criteria when analyzing its transcription patterns based on previous RNA-Seq studies (55, 61, 62).

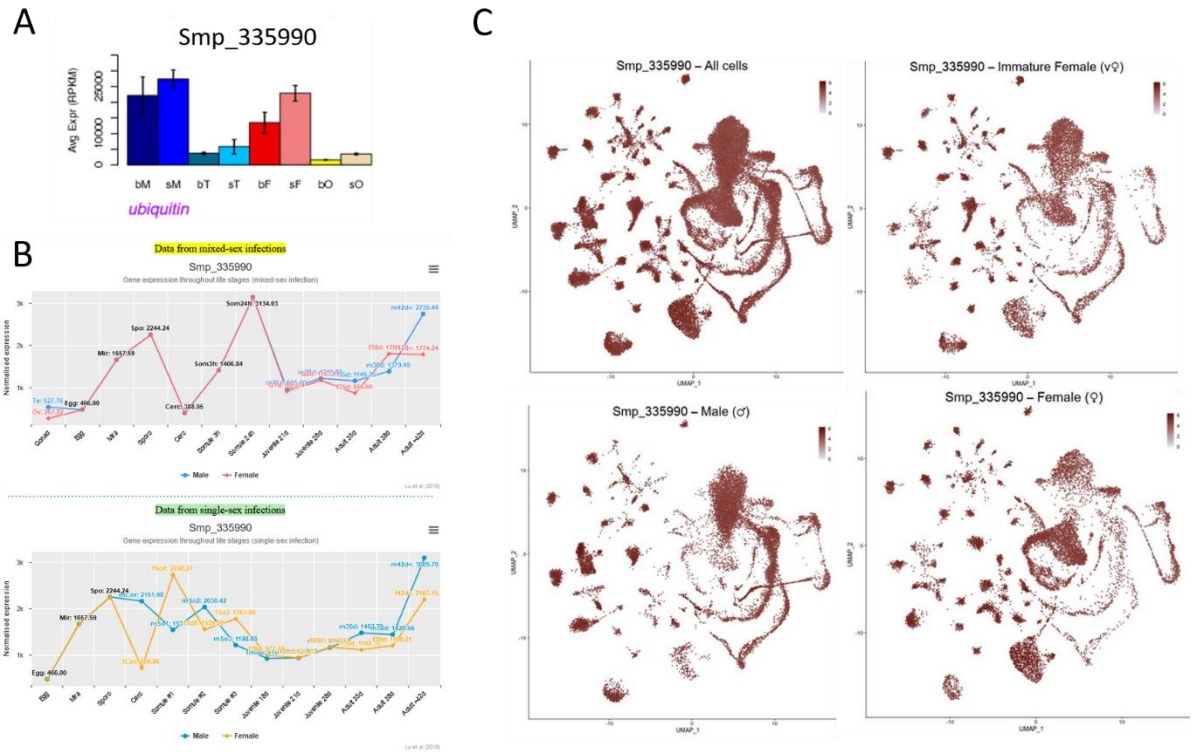

Figure 45. RNA-Seq data of Sm*ubi* revealed its ubiquitous transcript pattern in both sexes and all cell types of adults, and in the different life stages of *S. mansoni.*

Compilation of Smp_335990 (SmUbi) transcript patterns based on various RNA-Seq datasets. **A**, The levels of SmUbi transcripts in adult schistosomes and their isolated gonads are presented (55). **B**, The transcript levels of Sm*ubi* across all life stages of *S. mansoni* (paired, top; unpaired, bottom) are displayed (62). **C**, The cell type-independent transcript profile of Sm*ubi* is shown as determined by single-cell atlas data of *S. mansoni* (61), which showed transcript occurrence of Sm*ubi* in all tissues. Abbreviations: bM, bisex male (pairing-experienced male); sM, single-sex males (pairing-inexperienced male), bT, testes of bM; sT, testes of sM; bF, bisex female (pairing-experienced female); sF, single-sex (pairing-inexperienced female); bO, ovary of bF; sO, ovary of sF.

Based on the results of previous transcriptomics approaches, Smp_335990 appeared to be strongly, ubiquitously, and stage-independently expressed was selected (55, 61, 62) (Figure 45 A-C).The annotation of Smp_335990 was validated by comparing several databases. WormBase ParaSite (143, 168) annotation indicated that Smp_335990 represents an ubiquitin-like domain-containing protein (A0A5K4F9I1; UniProt). Protein structure prediction using Phyre2 (244) confirmed this identity and identified Smp_335990 as an ortholog of the human ubiquitin gene (UBB) (308, 309).

To further analyze the major promoter elements of the 2,056 bp region upstream of the coding sequence of SmUbi, the Neural Network Promoter Prediction tool (251) was used to predict two core promoters at positions 1,981 to 2,030 bp (promoter rank 1, Figure 31 A, Table 21) and 156 to 205 bp. These predictions were further analyzed using TRANSFAC 4.0 (251, 259), YAPP eukaryotic core promoter predictor (253), and compared to known consensus promoter elements (254, 310, 311). In the core promoter rank 1 (Table 21), typical sequence elements for transcription initiation were present, including TATA- and CAAT-boxes, the B recognition element (BRE, the transcription initiator element (INR), and the downstream promoter element (DPE). Consensus sequences of enhancer elements including Fushi tarazu (FTz and CAAT/enhancer-binding sites (C/EBPalp,) were present as were binding sites for the serum response factor (SRF), hepatocyte nuclear factor 1 binding element (HNF-1), heat shock transcription factor 1 (HSF), and octamer-binding transcription factor 1 (Oct-1). The Kozak sequence, which is necessary for ribosome binding and translation initiation (312), was identified *in silico* by comparing the potential Kozak sequences of *S. mansoni* genes that are abundantly transcribed showing similar transcription strengths (61, 62) and expression patterns (61, 289) as SmUbi. To determine the consensus sequence, I analyzed the sequence 6 bp downstream and 5 bp upstream of the translation start. To this end 5´-NNT/CA/GNA/G/TATGNC/AN-3´was found to be the consensus sequence of the *S. mansoni* Kozak sequence. Furthermore, the potential terminator sequence, including the 3´UTR (143, 257) of SmUbi, was also analyzed (Figure 46 A; Table 21). DNAFSMiner, a tool for analyzing functional sites in DNA sequences (255), revealed a polyadenylation signal within the SmUbi 3´UTR. Additionally, RNAfold (313) predicted several potential stemloop structures, which are typica indicators of transcription termination sites (314).

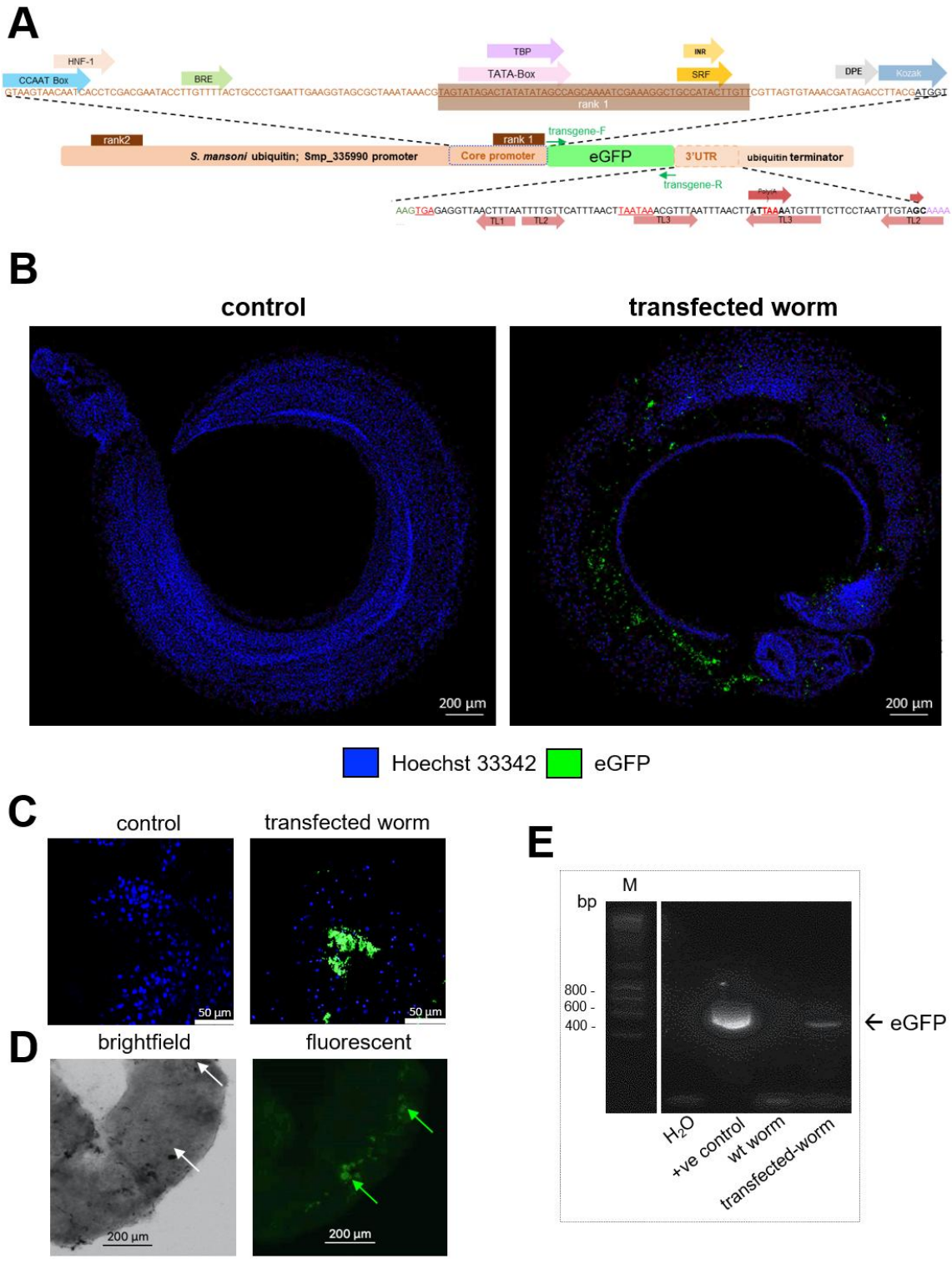

Figure 46. Bioinformatic prediction and experimental verification of the regulatory activity of the *S. mansoni* ubiquitin (SmUbi) gene promoter and terminator.

A, Overview of SmUbi (Smp_335990) promotor and terminator elements. Bioinformatic tools were utilized to identify major promoter and terminator elements: The Berkeley *Drosophila* Genome Project Neural Network Promoter Prediction Tool, AliBaba2.1 TRANSFAC 4.0 (251), and YAPP eukaryotic core promoter predictor (253, 254), respectively. These tools predicted two core promoters, each containing a CCAAT enhancer-binding site (light blue arrow), hepatocyte nuclear factor 1 binding element (NHF-1), B recognition element (BRE), TATA-Box-containing region (TBP), transcription initiator element (INR),

serum response factor (SRF), and a downstream promoter element (DPE). The predicted terminator region contained three terminator stem-loop structures and the polyadenylation signal, which were determined by the RNAfold Webserver Vienna tools (313) and the DNAFSMiner-DNA Functional Site Miner polyadenylation side prediction tool (255), respectively. To monitor SmUbi promoter-induced eGFP reporter-gene expression, male *S. mansoni* worms were transfected with the pJC53.2_SmUbi-eGFP-SmUbi plasmid using PB (159, 160). After 48 h, transfected and untreated control worms were counterstained with Hoechst33342 (blue) and analyzed by CLSM (**B** and **C**). Green fluorescence was observed in the transfected worms, while no eGFP signal was found in control worms. **D**, Brightfield microscopy also confirmed the presence of clusters of gold particles in the tissue (white arrows), which matched the presence of eGFP signals (green arrows). **E**, RT-PCR confirmed the presence of eGFP transcripts only in the transfected worms, with no eGFP transcripts found in control worms. +ve, positive RT-PCR control; H2O, control RT-PCR without template. Abbreviations: CLSM, confocal laser scanning microscopy; eGFP, enhanced green fluorescent protein; WT, wild-type.

To construct eGFP reporter gene-containing plasmids, based on the pJC53.2 backbone, the promoter and terminator sequences of Sm*ubi* were cloned flanking the eGFP reporter-gene (Table 19). To study the functionality of SmUbi-eGFP-SmUbi reporter-gene construct, adult male schistosomes were transfected by PB (Figure 46 B, C and D). (159, 160). Transfection conditions were most effective at a helium pressure of 1,550 psi, a 1.5-inch Hg vacuum, a particle size of 0.6 µm, and 5 µg plasmid DNA to penetrate as deeply as possible into the tissue. About 48 h after PB, green fluorescing tissue regions were detected in males by fluorescence microscopy (Figure 46 B, C, D). Furthermore, eGFP transcripts were confirmed by RT-PCR (DNase I-treated RNA) in SmUbi-eGFP-SmUbi-transfected males (Figure 46 E).

Table 21. Predicted SmUbi core promoter, terminator, and regulative motifs

Promoter element	Abbreviation	*S. mansoni* Sequence 5´- 3´	Position in construct	Source
Promoter Rank 1	**Prom rank 1**	TAG TAT AGA CTA TAT ATA GCC AGC AAA ATC GAA AGG CTG CCA TAC TTG TT	1981 - 2030 bp	(251)
Core Promoter	**Core Prom**	GTA AGT AAC AAT CAC CTC GAC GAA TAC CTT GTT TTA CTG CCC TGA ATT GAA GGT AGC GCT AAA TAA ACG TAG TAT AGA CTA TAT ATA GCC AGC AAA ATC GAA AGG CTG CCA TAC TTG TTC GTT AGT GTA AA CGA TAG ACC	1912 – 2051 bp	(310)
Enhancer Box	**E-Box**	CAC GTG	1712 – 1717 bp	(315)
CCAAT/ enhancer-binding protein binding site	**C/EBPalp**	ACT TTA TTT T	1747 – 1756 bp	(251, 254)
Octamer-Binding Transcription Factor 1	**Oct-1**	TAT TTT ACA T	1751 – 1760 bp	(251, 259)
CCAAT/ enhancer-binding binding site	**C/EBPalp**	TAT TAC CTA AA	1761 – 1771 bp	(251, 254)
Heat Shock Transcription Factor 1	**HSF**	GAG AAG TTG CTG	1812 – 1823 bp	(251)
Activator protein 1	**AP-1**	TGC TGAC TAA	1819 – 1828 bp	(251, 316)
Transcription Factor SP-1	**SP1**	TAG GAG GTT CA	1850 -1860 bp	(251)
Fushi Tarazu element	**FTz**	AAA TGT GAC TA	1888 – 1898 bp	(251, 317)
GATA-binding factor 1	**GATA-1**	ACT AGA ATG T	1895 – 1904 bp	(251)
CAAT-Box like sequence	**CAAT-Box**	GTA AGT AAC AAT C	1912 – 1924 bp	(311, 318, 319)
Hepatocyte nuclear factor 1 binding element	**HNF-1**	AAC AAT CAC CT	1918 – 1928 bp	(251, 320)

Promoter element	Abbreviation	*S. mansoni* Sequence 5´- 3´	Position in construct	Source
B recognition element	**BRE**	TTG TTT T	1940 – 1946 bp	(252, 311, 319, 321)
TATA-Box containing region	**TATA-Box**	TAT AGA CTA TAT ATA GCC A	1984 – 2002 bp	(252, 311)
TATA-Box binding protein	**TBP**	GAC TAT ATA TAG	1988 – 1999 bp	(251)
CCAAT/ enhancer-binding protein binding site	**C/EBPalp**	CAA AAT CGA A	2004 – 2003 bp	(251)
Serum response factor	**SRF**	GCC ATA CTT G	2019 – 2028 bp	(251)
Transcription Initiator Element	**INR**	CCA TAC T	2020 – 2026 bp	(252, 311)
downstream promoter element	**DPE**	AGA CC	2047 – 2051 bp	(252)
Kozak-Sequence	**Kozak**	CTT ACG ATG GT Consensus : [CN(T/C) (A/T)NN ATG A(A/T)]	2051 – 2061 bp	(264, 312)
Core Terminator:	**Abbreviation**	***S. mansoni* Sequence 5´- 3**	**Position in construct**	**Source**
mRNA 3´Untranslated Region	**3´UTR**	GAG GTT AAC TTT AAT TTT GTT CAT TTA ACT TAA TAA ACG TTT AAT TTA ACT TAT TAA AAT GTT TTC TTC CTA ATT TGT AGC	2777 – 2857 bp	(143, 257)
Polyadenylation signal	**Poly(A)**	TGA (52 bp) ATT AAA (21 bp) GC	2774 – 2857 bp	(255)

4.2.2 Cas-mediated editing of *S. mansoni* GSH1

Recent studies have demonstrated initial success in CRISPR/Cas-mediated genome editing in trematode parasites like *S. mansoni* (33, 169, 172, 280, 322). The feasibility of CRISPR/Cas-mediated gene KO in *S. mansoni* was demonstrated in independent studies by transfecting adult worms, eggs and sporocysts (33, 169–172). A lentiviral and RNP-based approach targeting the *S. mansoni omega-1* locus was used for transfection of eggs (33, 169), while adult worms and sporocysts were transfected with Cas9 RNPs by EPO targeting the oxamniquine resistance *slut-or* locus (170). However, the editing efficiencies remained comparatively low and failed in introducing edited life stages in the lifecycle. In my work, the editing efficiencies of *Streptococcus pyogenes* Cas9 (S.p. Cas9, Cas9) and *Acidaminococcus spec*.Cas12a (A.s. Cas12a, Cas12a) were compared (189) with the aim to enhance the editing efficiency. Furthermore, I intended to establish a protocol for germline transgenesis.

In order to establish chromosomal integrations (KI) or deletions for KO and subsequent phenotype analyzes, one prerequisite is the successful and efficient transformation of schistosomes and/or their larval stages. Therefore, transformation experiments were performed using ribonucleoproteins (RNPs) assembled from Cas9 or Cas12a and corresponding single guide RNAs (169, 172, 280, 287) (gRNAs) as the method of choice. The gRNAs, for Cas9 and Cas12a respectively, were selected to edit the same position of the *S. mansoni* genomic safe harbor site 1 (GSH1; Figure 47 A) (323). GSHs are characterized as continuously euchromatized, non-coding regions without confirmed regulatory genetic elements, which suggests a suitable site for integration of genetic sequences (197, 280). A recent study identified three suitable GSHs by analyzing the chromatin structure, histone modifications, and chromosomal HIV integration sites across the parasitic life cycle (172). Indeed, GSH1(1,416 bp; location, chromosome 3:13380432–13381848) was proven to be editable by the CRISPR/Cas9-system using three overlapping gRNAs (172). For this triple gRNA approach, DNA cleavage provoking staggered ends was assumed (173, 174), which finally led to a significant increase in HDR mediated transgene integration by transforming LEs (172). Given its PAM motif 5´-NGG-3´, Cas9 is more suitable for editing GC-rich loci (191). Conversely, Cas12a showed the PAM motif 5'-TTTN-3' (190). Theoretically, this feature suggests that Cas12a may be more suitable for AT-rich genomes (191), such as that of *S. mansoni* (258). Therefore, it was hypothesized that DNA cleavage by Cas12a in combination with a single crRNA (Cas12a gRNA) could lead to staggered DNA ends, increasing the efficiency of gene editing compared to Cas9 in combination with a single gRNA.

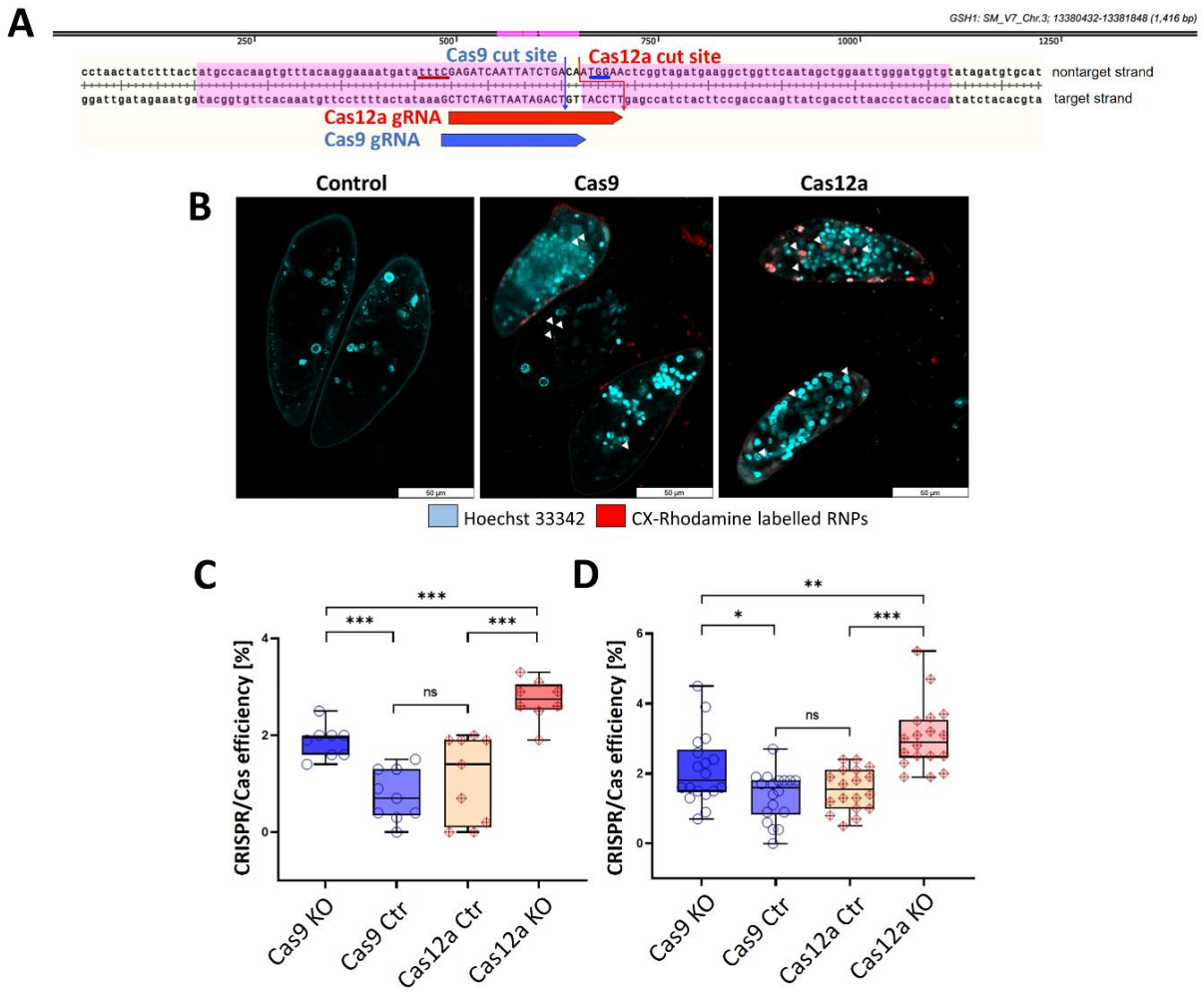

Figure 47. RNA-guided AsCas12a- and SpCas9-catalysed editing of GSH1 in adult schistosomes and their eggs.

Synoptic overview of the comparative approach using Cas9 and Cas12a for programmed gene editing using *S. mansoni* eggs and adults as biological targets for EPO-based transformation. **A**, schematic overview of the *S. mansoni* GSH1 target sites for Cas9 (blue arrow) and Cas12a (red arrow). DNA cleavage by Cas9 was expected to result in blunt-ended DNA strands, whereas Cas12a was expected to cause the staggered cleavage of the DNA strand. **B**, LEs were subjected to EPO in the presence of CX Rhodamine-labeled RNPs (red). LEs were counterstained with Hoechst33342 (blue) and examined by CLSM 24 h later. The introduction of RNPs was demonstrated (arrows) with both nucleases. The majority of Cas9 RNPs accumulated around the eggshell, a dissimilar pattern to that observed in the Cas12a RNP-treated LEs, where signals were also found inside the eggs. TIDE analysis (**C**, **D**) confirmed the successful deletion of target sequence in the schistosomal GSH1 locus applying RNPs derived from Cas9 (blue) and Cas12a (red). Low background activity (low mutation rate) was found with RNPs containing a scrambled gRNA sequence (faint blue, orange). In both, LEs (**C**) and adult schistosomes (**D**), editing by Cas12a RNPs (red) was significantly more effective compared to editing by Cas9 RNPs. Abbreviations: Ctr, control; KO, knock-out; ns, not significant. *P<0.05, **P<0.01, ***P<0.001 by t-test. **C**, n=18; **D**, n=9.

To compare the suitability of the Cas9 or Cas12a for GSH1 editing using single gRNAs, respectively, the two selected Cas-enzymes were examined for editing efficiency by applying RNPs to LEs and adult schistosomes for KO experiments (Figure 47 B-D). Further, gDNA was isolated, and the obtained samples sequenced by next generation sequencing (NGS; Figure 48).

To establish genome editing in schistosomes a (i) suitable life stage or stages of the parasite, (ii) compatible method for gRNA delivery, (iii) replacement construct in case of KI experiments, and (iv) optimal enzyme to efficiently edit the target region of choice must be found. To this end (i), the egg stage was used as a biological target because of its suitability for EPO-mediated transformation, and because the probability is high to introduce CRISPR-material into the zygote (present in the early egg-stage). First, the accessibility of LEs to RNPs of both enzymes was determined using an RNP-tracking approach, where fluorescence-labelled RNPs were introduced into LEs by EPO. Each guide RNA was labelled with a CX-rhodamine fluorescent tag prior to assembly of RNP complexes with either Cas9 or Cas12a nucleases (26,65,66). After isolation form livers, LEs were immediately exposed to these RNPs by square wave EPO. CLSM was used to confirm the entry of the RNPs into the LEs. Within 24 h of EPO, RNPs were delivered into the eggs, some including larval tissue/developing miracidium, and colocalized with Hoechst33342-stained nuclei for both Cas enzymes (Figure 47 B). This demonstrates the successful delivery of Cas12a RNPs into LEs by EPO. Here, the labelled RNPs were able to penetrate the eggshell and were finally detected inside the egg. For Cas9 RNPs, the majority of Cas9 RNPs passed through the eggshell and comparatively lower amounts of labelled RNPs were found inside. In summary, both RNPs were successfully delivered to the eggs. Of note, most Cas9 RNPs appeared to accumulate in the eggshell, whereas a wider distribution of signals was observed in Cas12a RNP-treated LEs.

After exhibiting the accessibility of LEs to RNPs of both enzymes, the LEs were transfected with freshly prepared, unlabeled RNPs of either Cas9 or Cas12a to showcase the cleavage capability of RNPs to target GSH1. To demonstrate the accessibility of GSH1 in adult worms, 10 couples for each biological replicate (n=9) were transfected with RNPs from both enzymes targeting GSH1.The KO efficiencies of Cas9 and Cas12a targeting the GSH1 locus as well as the background activity and/or mutation rates were determined. To this end, RNPs were formed using gRNA targeting the GSH1, while gRNA consisting of a not schistosomal, scrambled sequence served as control. After 7 d, PCR fragments containing the Cas target sites in the middle of the sequence were amplified and sequenced by Sanger direct sequencing of the corresponding amplicons. This was accomplished for 18 (LEs) and 9 (adult schistosomes) biological replicates. Editing efficiencies were determined by TIDE (Tracking of Indels by DEcomposition) (202) analysis (Figure 47 C, D). Both Cas enzymes showed

significant genome editing compared to the background activity/mutation rate. There was no difference between the scrambled gRNA control for Cas9 and Cas12a. Compared to Cas9, editing GSH1 was significantly more efficient when Cas12a was used, in both LEs (Figure 47 C) and adult worms (Figure 47 D).

To investigate the editing efficiency of GSH1, the editing position as well as the sizes of the generated deletions, amplicons of target locus were sequenced by NGS, and the results analyzed in high resolution by CRISPResso (284) and CRISPR RGEN Tool Cas-Analyzer (285) (Figure 48 A, B). Cas12a showed an up to 100x higher editing efficiency compared to SpCas9 RNPs in adult schistosomes (Figure 48 B). In addition, KO experiments applying Cas12a RNPs resulted in deletions of approximately 20 bp, while Cas9 RNPs resulted in the deletion of just one bp. These results highlight the capability of both Cas enzymes to edit the *S. mansoni* genome. However, Cas12a displayed an increased efficiency for the KO experiments. Next, the suitability of these enzymes for introducing a transgene into GSH1 was tested.

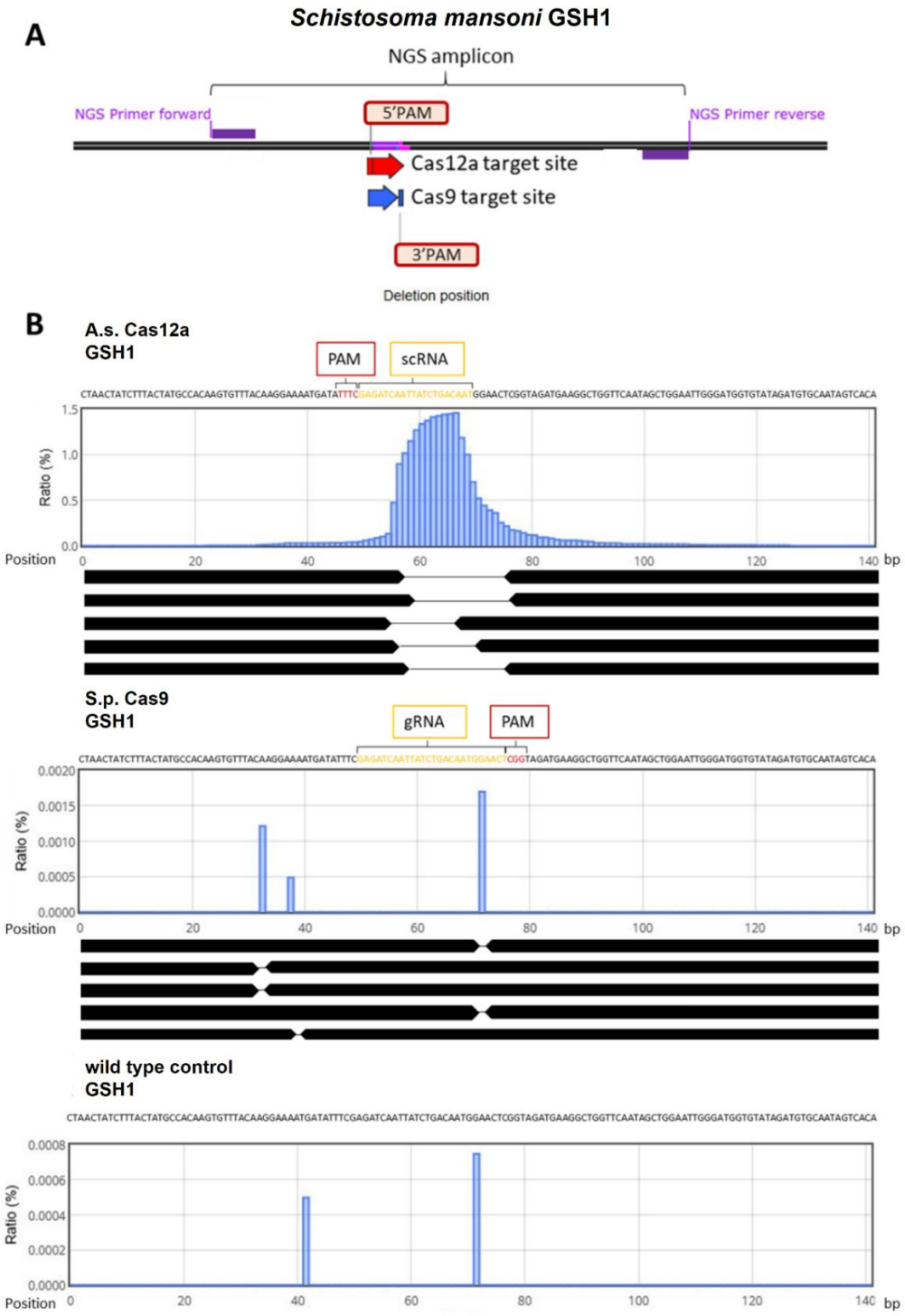

Figure 48. Highest editing efficiency and deletion of long DNA fragments was achieved by A.s. Cas12a.

A, Schematic illustration of the GSH1 locus including the predicted Cas12a (red) and Cas9 (blue) target sites, and amplicon analyses by NGS (purple). **B,** Single gRNA binding site (yellow) and PAM (red) at the GSH1 locus for the corresponding Cas12a or Cas9 enzymes. The individual graphs (blue) show the deletion events at the respective position in percent. The editing efficiency per position by Cas12a was 100x higher compared to Cas9-based editing. Representative edited single reads of the sequencing are shown in black, whereby the gaps illustrate deletion events. Abbreviations: gRNA, guide RNA; NGS, next generation sequencing; PAM, protospacer adjacent motif.

4.2.3 Integration of a donor with microhomology arms into the GSH1 of *S. mansoni*

To generate stably transformed schistosomes, it would be advantageous to target germ-cells of an early developmental stage. Therefore, it was important to find the most appropriate life stage for transformation, which is the early egg stage. After the suitability of the SmUbi-eGFP-SmUbi had been proven, a HDR knock-in (KI) approach was performed. For this, the eGFP reporter-gene construct was flanked by 50 bp short homology arms matching the GSH1 at target cleavage site (189, 280, 287) by PCR using 5´ overhang primers. Afterwards, the amplicon was 5´-C6-PEG10 modified, to enhance HDR (homologous directed DNA repair) efficiency (287) (Figure 49 A). An independent study using donors modified with 5' C6amine-PEG10 with ~50 nt HA (homology arms) showed the highest HDR efficiencies when editing a target gene in HEK293 cells with Cas9 combined with a single gRNA (287). Based on this principle and considering the size of the transgene to be introduced (3,351 bp), the donor template was created and 5' modified based on this study. This donor DNA construct was finally used for KI experiments with LEs.

Following this approach, the GSH1 of LEs was targeted for a KI approach. In order to impede donor degradation by Cas12a, a base was exchanged by target point mutagenesis. The 5' HA of the donor template contained the Cas12a PAM recognition site (5'-TTTC-3') and part of the Cas12a target sequence. One base of Cas12a PAM 5'-TTTC-3' was modified to 5'-TCTC-3' to remove the donor intrinsic Cas12a PAM motif (Figure 49 A).

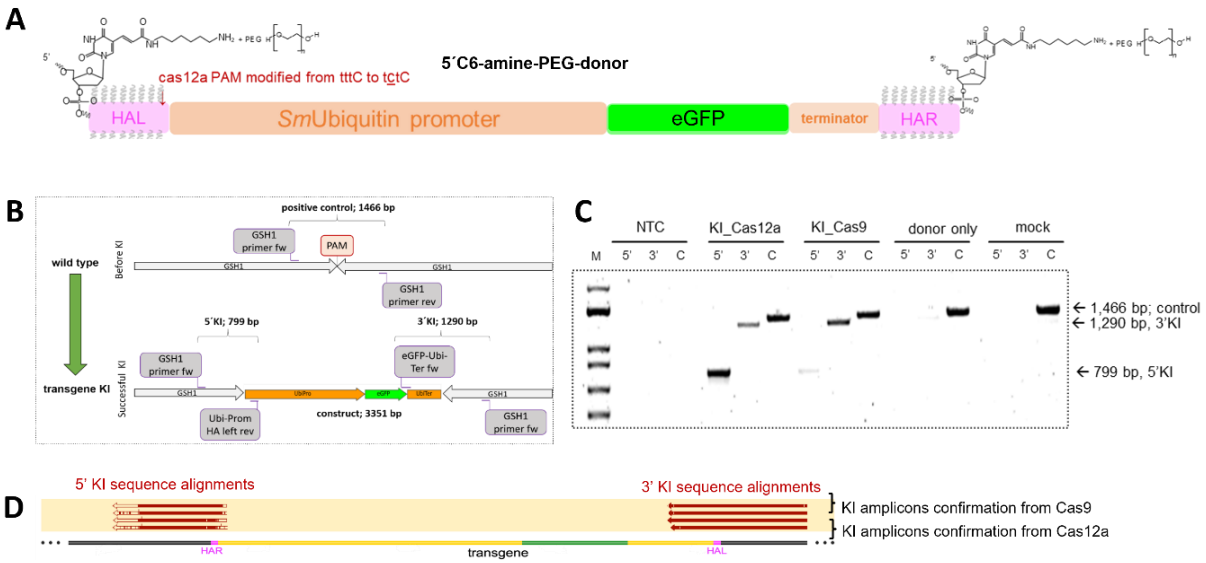

Figure 49. Successful integration of SmUbi-eGFP-SmUbi into GSH1 by RNP-mediated chromosomal integration.

A, Graphical illustration of the HDR donor template with 50 bp microhomology arms, which includes the ubiquitin promoter and terminator (SmUbi, orange) flanking the eGFP (green) reporter-gene. The potential Cas12a PAM site inside the microhomology arms (pink) was altered by primer-mediated site-directed mutagenesis, to avoid Cas12a-mediated cleavage of the donor template. The 5' end of the donor template was amine- and C6-PEG10-modified. **B**, A schematic overview of the GSH1 locus is given after the successful KI of the SmUbi-eGFP-SmUbi reporter-gene, which includes the primer binding sites for KI analysis by PCR. **C**, PCR analyses demonstrated the successful chromosomal integration of the SmUbi-eGFP-SmUbi donor template, with DNA fragments specific for the integration sites being obtained by PCR and sequenced by Sanger direct sequencing. **D**, For both Cas enzymes, alignment analyses of these fragments confirmed the successful integration of the donor template (yellow and green) into GSH1 (grey), as indicated by red bars. Abbreviations: HA, homology arms; KI, knock-in; primer fw, forward primer; primer rev, reverse primer.

In addition, the design of gRNAs and selection of the corresponding PAM recognition sites of both nucleases enabled transgene integration using the same HA sequences of the donor template targeting GSH1. For both nucleases, transgene integration was achieved at a ratio of 1:1:1 (w:w:w) of the Cas-enzymes (Cas9/Cas12a), the respective gRNAs, and the 5´-modified donor template. This succeeded by selecting predicted and almost identical cleavage sites for both Cas enzymes at GSH1 (Figure 48 A). To transfect LEs with SmUbi-eGFP-SmUbi, LEs were co-electroporated with RNPs and a donor template. As transfection control, electroporated wild-type LEs (mock) were transfected with the donor template in the absence of RNPs. At 10 d after EPO, eggs were collected, and gDNA was isolated and analyzed for transgene integration (Figure 49 B, C). Two primer pairs were designed to amplify: (i) the 5'-integration site, including sequences within GSH1, as well as in the SmUbi promoter region of the transgene (5'-KI, 799 bp, Figure 49 B), and (ii) the 3' integration site, including the 3'

sequence of eGFP and GSH1 (3'-KI, 1,290 bp, Figure 49 B). Both primer pairs amplified specific 5'-KI and 3'-KI integration fragments, demonstrating GSH1 editing and KI by both nucleases (Figure 49 C). Compared to the amplicons obtained by Cas12a-treated LEs, 5'-KI amplicons in the Cas9 group showed lower band intensity (Figure 49 C). Nonetheless, Sanger sequencing confirmed the integration of the transgene at the programmed cleavage site. Furthermore, the precise integration of SmUbi-eGFP-SmUbi into GSH1 resulting from HDR was confirmed by SnapGene alignment, obtained from purified 5'-KI and 3'-KI amplicons (Figure 49 D). This analysis finally confirmed transgene integration. In addition, no 5'-KI or 3'-KI fragments were amplified from gDNA of the control groups. A 1,466 bp fragment of the unedited GSH1, which was amplified in all experimental groups, served as a PCR control. Consistent with this findings, eGFP transcripts were not detected by RT-PCR of RNA/cDNA from control groups and only found in DNase I-treated RNA samples from KI groups (Figure 50 A).

After the successful integration of the eGFP reporter-gene into GSH1 by both Cas-enzymes and verification of eGFP transcription by RT-PCR (Figure 49 C, D; Figure 50 A), transfected LEs were examined to analyze eGFP expression. To this end LEs were examined by CLSM 5 and 10 d after transfection (Figure 50 B-D). Fluorescence intensity at an emission wavelength of 509 nm was recorded and analyzed in eggs from the Cas9 and Cas12a editing experiments. In terms of eGFP-positive LEs, eggs from the Cas12a group significantly outnumbered eGFP-positive eggs from the Cas9 group at both time points post- EPO (Figure 50 B, C). For this analysis, only eggs containing a miracidium with >50% eGFP expression in the examined section plane (two dimensions) were counted as eGFP-positive. No differences in growth and survival were observed between transfected LEs and LEs from the control groups. From six biological replicates, the average percentage of eGFP-positive eggs was 43.6□19.9% and 26.3□7.2% in the Cas12a group after 5 and 10 d, respectively. In total, 20.2□10.1% and 21□16.2% of the LEs in the Cas9 group were eGFP-positive at the same time points (Figure 50 B). Moreover, a weak eGFP signal at 509 nm was detected in LEs transfected with donor only (no RNP) (Figure 50 B, C). Differences in the total emission spectra were detected and analyzed as described in a recent study (172) to verify the emission spectra specific for eGFP (Figure 50 D). This approach allowed eGFP-specific signals to be clearly distinguished from eggshell autofluorescence. This analysis revealed eGFP expression in numerous cells of the transfected eggs, including miracidia that developed in some of these eggs.

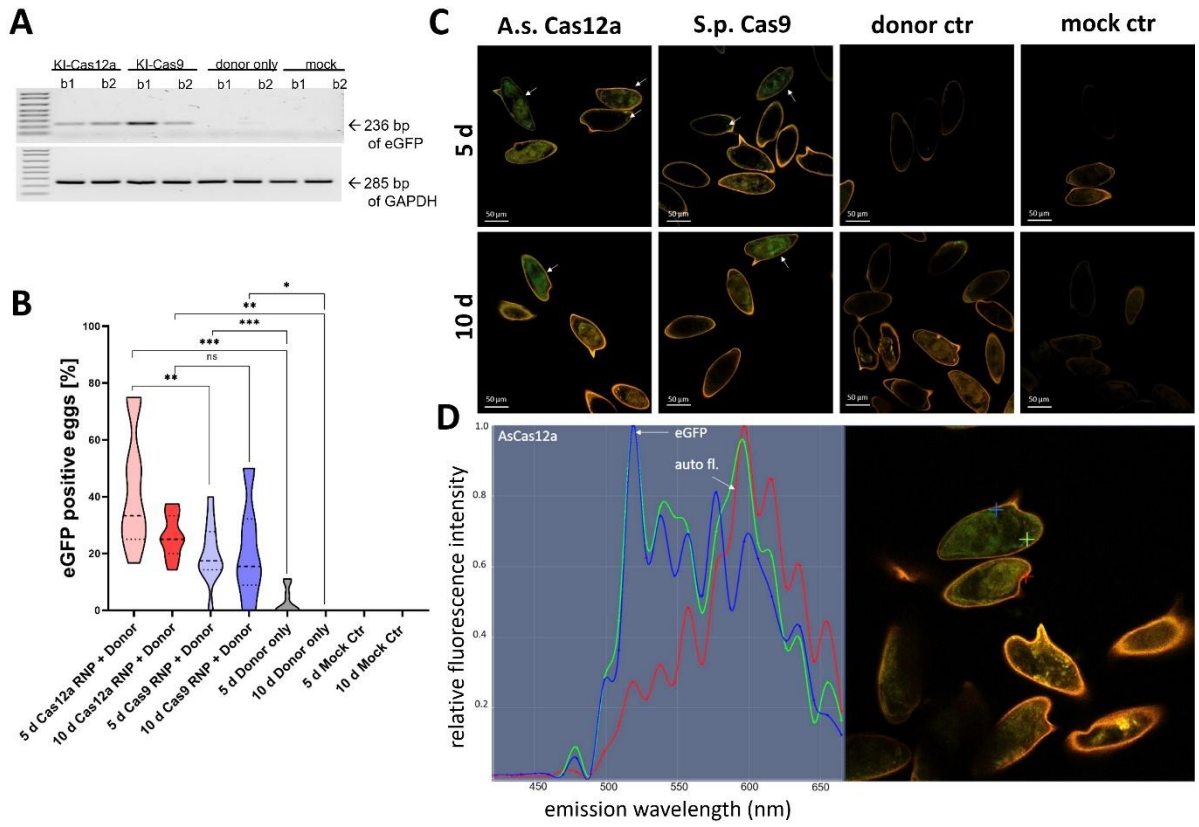

Figure 50. Detection of eGFP-positive miracidia in eggs after RNP-mediated integration of the reporter-gene.

A, The RNA/cDNA of eggs from all experimental groups was analyzed by RT-PCR to monitor eGFP expression at the transcript level. This approach showed EGFP transcripts (236 bp) in LEs of the KI group only, using Cas12a and Cas9. DNase I-treated RNA was used for RT-PCR to remove contaminating DNA and/or residual donor DNA. Lanes b1 and b2 show the result of two independent biological replicates. No EGFP transcripts were detected in the control groups (top panel). The housekeeping gene GAPDH (Smp_0569701, 285 bp, bottom panel) was used as a control for successful cDNA synthesis and RT-PCR. **B,** Shown is the proportion of eggs with eGFP- positive larvae 5 d and 10 d after treatment with RNPs plus donor DNA (> 10.000 eggs per replicate; n=6). AsCas12a (green) displayed the highest editing rate, even after 10 d. AsCas12a- and SpCas9 (red)-treated eggs contained significantly more fluorescence-positive larvae compared to the donor only control (gray). No fluorescence signals were found in untreated eggs. *P<0.05, **P<0.01, ***P<0.001 by t-test. **C**, Green-fluorescing miracidia and cell cluster (arrows) were detected after 5 d and 10 d in eggs that had been treated with Cas12a or Cas9 RNPs targeting GSH1. The reporter-gene SmUbi-eGFP-SmUbi served as donor DNA. Autofluorescence is shown in orange. Scale bars: 50 µm. **D,** Verification of eGFP signal in transformed LE after 5 d following editing. Using the Zeiss Zen blue 3.4 software, different positions of the fluorescence spectrum were sampled to distinguish them from the background fluorescence (orange). The typical eGFP spectrum (blue and green arrow) was detected in the larvae and found to be distinct from the auto fluorescence spectrum of the egg (red arrow). Abbreviations: auto fl., autofluorescence; ctr, control, KI, knock-in.

To summarize, most effective transformation and editing conditions for LEs were empirically determined employing 10 µg 5´-C6-PEG10 modified linearized donor DNA with 50 bp homology arms, and 10 µg RNPs derived from Cas12a in OptiMEM (Figure 50 B). Furthermore, SmUbi-eGFP-SmUbi reporter gene activity was demonstrated by green fluorescing embryos/miracidia using CLSM after 5 d and 10 d post EPO (Figure 50 C). In parallel, integration of the transgene was confirmed by PCR and eGFP transcript occurrence by RT-PCR. The eGFP typical fluorescence spectrum was detected in edited LEs and could be distinguished from background fluorescence (Figure 50 D). Finally, even the successful hatching of potentially transgenic (green fluorescing) miracidia was possible. Based on these results, the next aim was to (re-)introduce these transgenic miracidia into the life cycle.

4.2.4 Generation of transgenic schistosomes using CRISPR/Cas12a

Based on the results obtained so far, it was shown that GSH1 can be edited by Cas9/12 enzymes with Cas12a being superior to Cas9 in terms of editing efficiency. Furthermore, GSH1 integration and expression of the SmUbi-eGFP-SmUbi transgene were demonstrated. Based on these results, an attempt was made to (re-)introduce transgenic miracidia into the cycle. The aim was to deliver generate a transgenic *S. mansoni* line, a goal that has not yet been achieved in the schistosome research field.

Preliminary data indicated the possibility that miracidia hatch from potentially transgenic LEs. In these pilot experiments, however, the successful infection of the intermediate snail host failed. To rule out any negative effects of EPO on the hatching and infection capacities of miracidia, different EPO-voltages were tested. Other EPO conditions (20 ms pulse, square wave) were maintained. The initial voltage used was 125 V, which has also been used in various transformation protocols for mammalian cells (324, 325), and which has been successfully used for LEs (172, 280). For EPO experiments, 300 LEs per cuvette were electroporated in 200 µl OptiMEM (n=3) at voltages ranging from 125 V - 250 V. Eggs were then cultured in M199egg, and a miracidia hatching assay was performed after 5 d (Figure 51). Survival and/or larval growth inside the egg was not significantly affected in the 125 V group compared to the control group: 26.6±3.2%, 125 V group, and 31.9±2.6%, control, non-electroporated group. In contrast, hatching decreased progressively and significantly with increasing voltage.

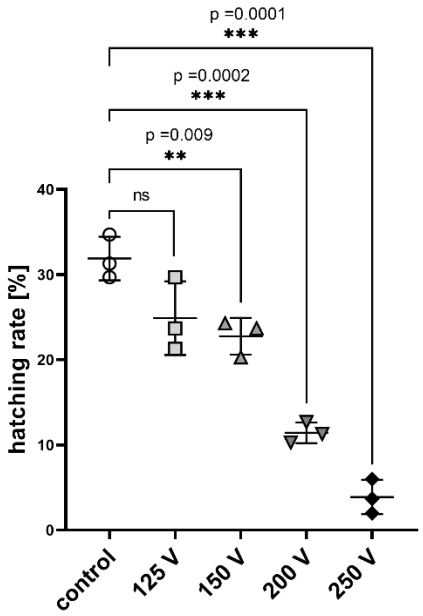

Figure 51. Voltage-dependent miracidia hatching after electroporation.

To evaluate the effects of EPO on the hatching capacity of miracidia from eggs, 300 LEs per replicate (n=3) were treated with different voltages. Miracidia hatched after EPO at 125, 150, 200 and 250 V. Only in the 125 V group, miracidia hatching was not significantly affected in comparison to the control group. *P<0.05, **P<0.01, ***P<0.001 by t-test.

As the EPO conditions did not significantly affect miracidia development and hatching, the alternative infection method of sporocyst transplantation (222, 227, 228) was tested to ensure successful infection of the intermediate snail host (Figure 52 A). To this end, 5,000 LEs were electroporated (n=3) with 10 µg each of Cas12a RNPs and the SmUbi-eGFP-SmUbi donor DNA at a 1:1:1 ratio at 125 V, as previously described. LEs only electroporated by the donor DNA and eggs electroporated without RNPs and/or the donor DNA served as control. Potentially transgenic eggs were cultured in M199egg medium for 5 d at 37°C and 5% CO_2. Subsequently, miracidia were allowed to hatch(by illumination) from these eggs and *in vitro*-transformed into sporocysts by incubating in CBSS (223, 224). A culture period followed for 4 – 7 d (Figure 52 B). To this end, optimal culture conditions for sporocysts were established, without co-cultivation with Bge-cells (326): 5% O_2, 5% CO_2, 26°C in M199sporo medium (3.2.9). Sporocysts remained viable and showed longitudinal growth even after 28 d of *in vitro* culture (Supplemental Figure S5).

Next, sporocyst were examined for eGFP expression. For this approximately 500 sporocyts were stained by Hoechst 33342 and used for CLSM (Figure 52 B, C). The results demonstrated that eGFP-positive signals were only detected in sporocysts resulting from Cas12a-mediated KI experiments (Figure 52 B, C, D). The majority of sporocysts displayed mosaic patterns (Figure 52 C), with about 15% of all sporocysts exhibiting eGFP-positive signals. Furthermore, transgene integration in these sporocysts was confirmed by Sanger direct sequencing of the 3´- integration site (Supplemental Table S2). With the help of an inverse fluorescence microscope, the manual enrichment of eGFP-positive sporocysts was achieved. These preselected sporocysts were used for manual transplantation into snails of the genus *Biomphalaria* according to the protocol of Jourdane and Theron (222, 227, 228). This way, 40 snails were manually (surgically) infected with 1 to 5 sporocysts, each. In addition, 20 snails each were infected the same way with sporocysts from the control groups. Afterwards, the snails were cultured for eight weeks. About 5% of the snails infected this way produced and released cercariae, whereas no cercariae were obtained from the snails of the control groups. This is partly due to an insufficient number of snails used or to increased lethality of the snails due to the surgical transplantation procedure. To confirm transgene presence in the obtained cercariae, 50 individuals were collected from each snail, and gDNA was isolated for the amplification of an eGFP-specific fragment of 236 bp length by PCR. This PCR fragment was found in cercariae released by one snail (Snail A, Figure 52 E). Cercariae siblings from the same snail were employed for infecting the final host.

Since sporocyst transplantation is laborious, I also tested the classical way of snail infection. For this, miracidia were hatched 48 h after transformation by EPO and directly used for mono-miracidial infections. To this end, a single miracidium was placed in a 10 µl drop on a microtiter plate and incubated with the snail for 15 min, followed by an additional 2 h incubation period in 100 µl, followed by overnight incubation in a total volume of 2 mL. A total of 185 snails were infected in this way, with 3.2 % of the snails shedding cercariae after 8 weeks, and 6.7% after 10 weeks of incubation. According to PCR analysis, one third of cercariae obtained from these snails were eGFP-positive. Siblings of (positive) cercariae from different snails were pooled and used for hamster infection to ensure. This way I wanted to increase the probability of mixed-sex infections, which finally should lead to the establish of a transgenic line. Other attempts, such as poly-miracidial infection of snails (10-15 miracidia/snail), as well as infection with miracidia from 6- to 10 d-old, *in vitro* cultivated LEs or IVLEs failed, only eGFP PCR-negative cercariae were obtained. For LEs, 48 h cultivation after transformation was determined to lead to the highest hatching rate of miracidia. The optimal time point for miracidia hatching of IVLEs was 5 to 7 d after egg recovery. However, most miracidia obtained from IVLEs either lost their viability after a short time-period or showed a damaged habitus. As this reproducibly occurred in all test groups, *in vitro*-culture conditions must be optimized for IVLEs.

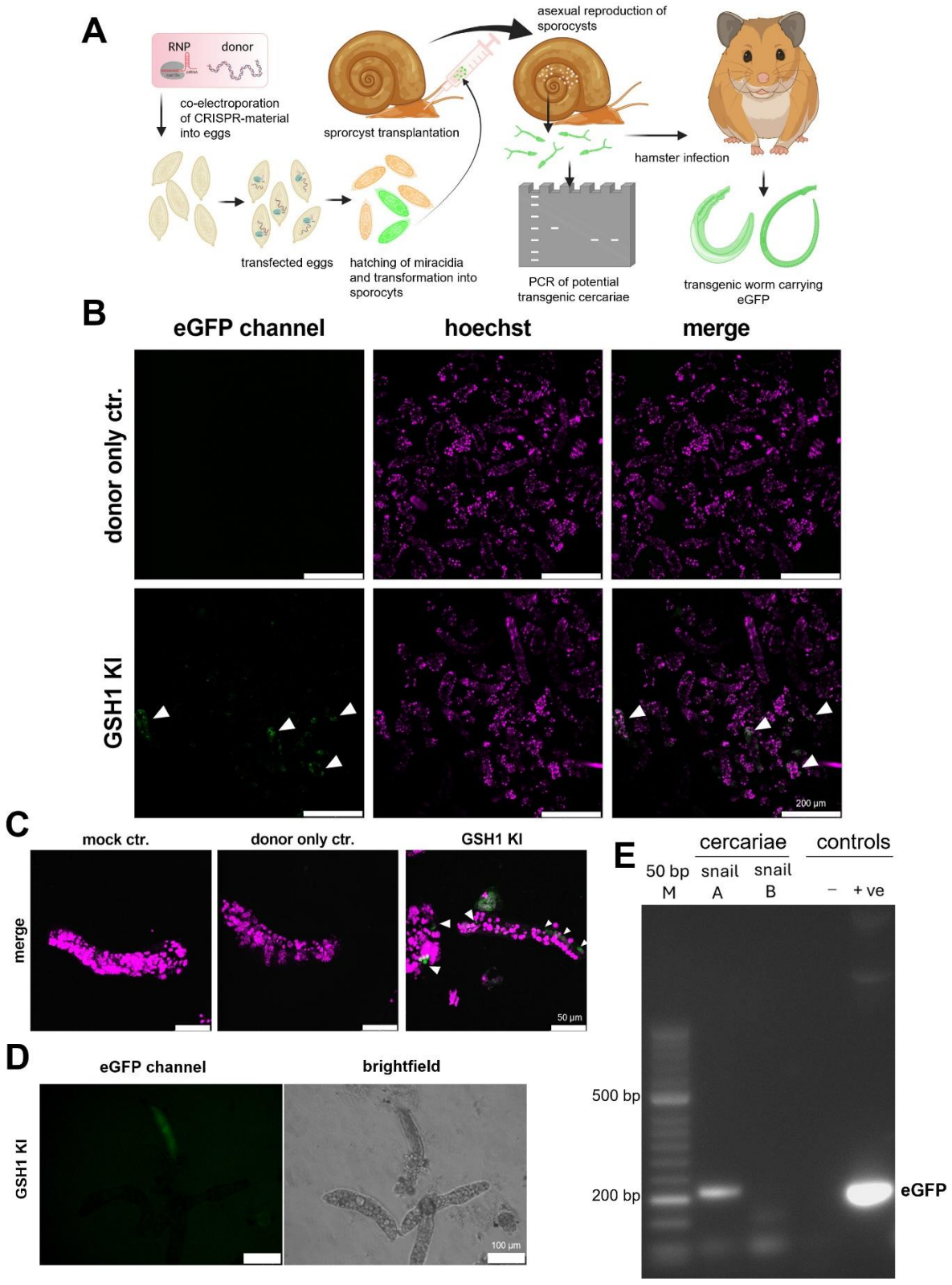

Figure 52. Transplantation approach of transgenic sporocysts into the intermediate snail host. **A,** Workflow of the generation and transplantation of potentially transgenic sporocysts (**B-D**) into snails of the genus *Biomphalaria*. Transplantation was done according to an established sporocyst transfer protocol(222, 227, 228). **E**, PCR confirmed transgene presence in tested cercariae. Siblings of PCR-positive ceracriae were used for infecting hamsters as definite host. **B**, Overview of 4 d old sporocysts

derived from miracidia of KI experiments using the SmUbi-eGFP-SmUbi transgene with 5'-C6-PEG10-modified microhomology arms and A.s. Cas12a RNPs. Sporocysts were counterstained with Hoechst33342 (purple) and analyzed using CLSM. In control sporocysts, which were derived from LEs only transfected with donor DNA, no eGFP signals were detected; eGFP-positive signals were only identified in sporocysts of the KI group (arrows). **C**, Maximum projection of 20 overlaid Z-stacks of sporocysts from editing experiments. Also here, eGFP-positive cells/tissue were identified in sporocysts of the KI group (arrows). **D**, Snap-shot image of living sporocysts derived from fluorescence microscopy, which was applied to enrich eGFP-positive sporocysts for transplantation experiments. **E**, An eGFP-specific fragment was PCR-amplified from cercariae of snail A. Siblings of these cercariae were employed for final-host infection. Plasmid DNA harboring the pJC53.2_SmUbi-eGFP-SmUbi construct served as positive control. Abbreviations: ctr, control; KI, knock-in; -, eGFP-negative control; +ve, eGFP-positive control.

Infection of hamsters with (eGFP PCR-positive) cercariae from both the mono-miracidial infections (Figure 53 A-D) and the transplantation experiments (Figure 53 E, F) led to the recovery of adult schistosomes. Both female and male worms were recovered from hamsters infected by the pooled cercariae of the mono-miracidial infections. Couples and separated worms were cultured *in vitro* for further analyses. In order to assess eGFP fluorescence, couples were separated and each sex individually analyzed. By fluorescence microscopy of living, not imbedded, adult schistosome males (Figure 53 A) and females (Figure 53 B), green fluorescing signals were detected throughout whole worms and exclusively in worms from KI experiments, not in control worms. In contrast to infection with pooled cercariae from mono-miracidial infections, only females (sF) were recovered from hamsters infected with cercariae originating from the transplantation experiment (Figure 53 E). It can be assumed that in this case only a single female sporocyst survived, which reproduced asexually to generate clonal cercariae (4, 327). Indeed, all sFs obtained from this infection were eGFP-positive. Next, CLSM was used to analyze the distribution of eGFP signals in more detail (Figure 53 C - F). For this, worms preselected by fluorescence microscopy were counterstained with Hoechst33342, imbedded in ROTI FluorCare, and immediately used for CLSM. Although with weak intensity, eGFP-positive signals occurred in tissues of both sexes. In contrast to the control, these eGFP signals were detected in both bFs (Figure 53 D) and sFs (Figure 53 E, F) of the KI group only, including their ovaries. However, no eGFP-positive signal was found in the testes of the bM, which had been obtained from KI experiments. This suggests that transgene integration occurred in parenchymal precursor stem cells during larval development. As additional evidence for transgene presence in adult worms, transgene-specific PCR amplicons were amplified by PCR (Figure 53 G). Sanger direct sequencing of these amplicons confirmed transgene integration into GSH1 (Figure 53 H, Supplemental Table S3). Here, variations in the precision of the transgene integration site within GSH1 at the 5´-integration site were found.

Altogether, eGFP-signal occurrence in adults and their gonads provide strong and first evidence for successful germline transgenesis in *S. mansoni*. Furthermore, these results also reinforce the suitability of the GSH1 locus for transgene integration approaches and for maintaining insertion-locus integrity throughout the life cycle of *S. mansoni* (172, 280).

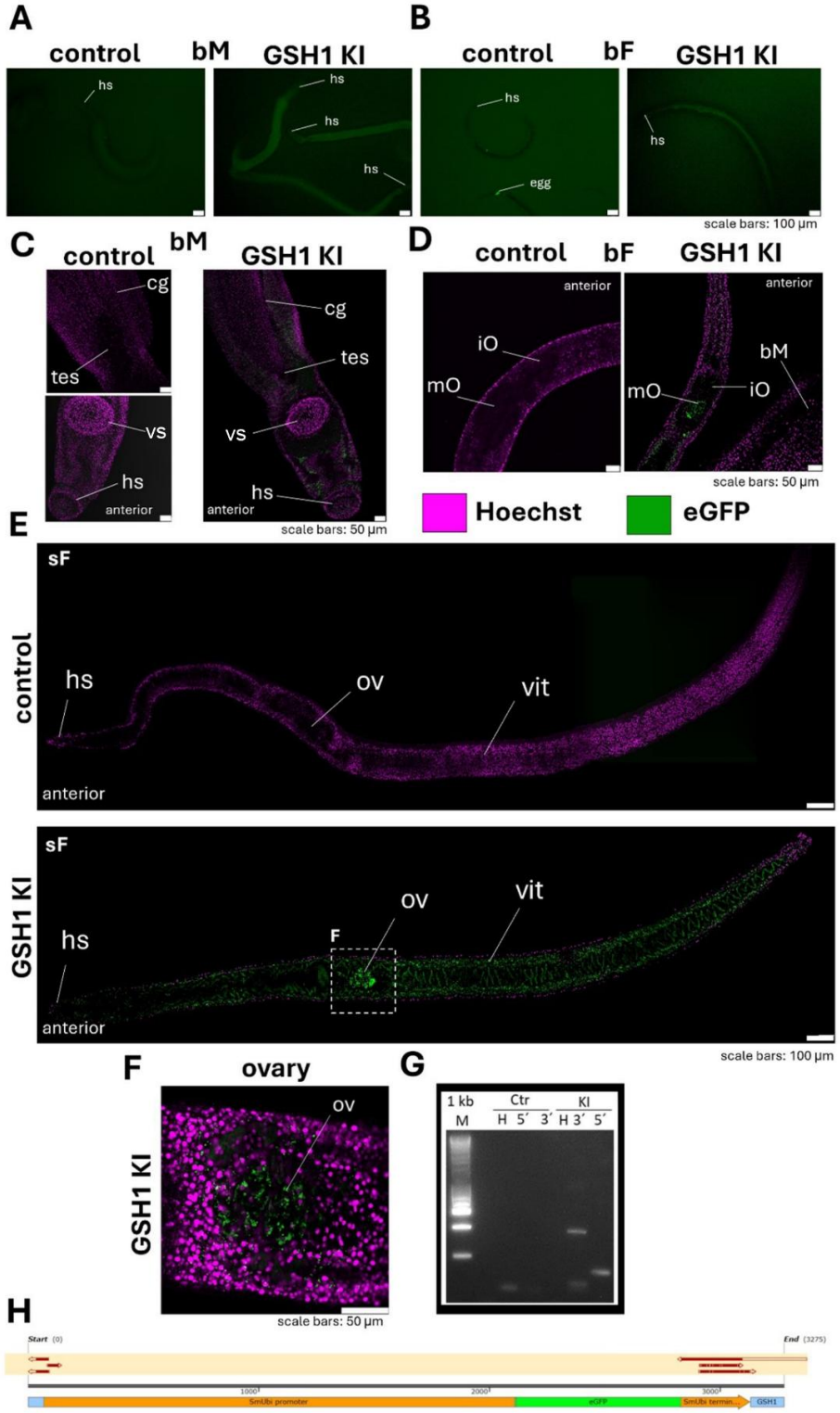

Figure 53. CRSIPR/Cas12a-mediated germline integration of an eGFP reporter-gene into the GSH1 of *S. mansoni.*

Adult *S. mansoni* were obtained from hamsters infected with cercariae from either mono-miracidial snail infection (**A-D**) or sporocyst transplantation (**E**) generated from potentially transgenic miracidia. For this, LEs were used as starting material and electroporated with A.s. Cas12a RNPs and donor DNA to target GSH1. Transgene integration of the 5´C6-PEG10 modified SmUbi-eGFP-SmUbi donor by HDR

was mediated by 50 bp microhomology arms. Worms finally obtained from CRISPR/Cas-untreated LEs as starting material served as controls. Fluorescence microscopy of living males (**A**) and females (**B**) exhibited green fluorescing signals in worms from KI experiments only, not in control worms (originating from miracidial infections). The distribution eGFP signals within the worms was analyzed using CLSM (**C-D**). For this, worms were counterstained with Hoechst33342 (purple). **C**, eGFP-positive signals were found in the parenchyma of males from KI experiments. **D**, CLSM analysis revealed eGFP-positive signals in the parenchyma and ovaries of paired experienced females (bFs) obtained from KI experiments. No eGFP-specific signals were found in the ovaries of control bFs. **E**, Transplantation experiments of sporocysts, which were previously selected based on eGFP-positive signals, led to the recovery of females only, which showed a single-sex habitus inexperienced(sF). Also, by CLSM, no eGFP-positive cells were found tissues of control sFs. In contrast, eGFP signals were detected in all tissues of sFs originating from transplantation experiments with eGFP-positive sporocysts. Of note, , the ovaries of these females showed intense eGFP-specific fluorescence, as illustrated by a representative specimen in detail in **F**. **G**, Transgene integration was confirmed by amplifying the 3´- and 5´-integration sites using specific primer pairs capable of amplifying the transgene integrated into GSH1. **H**, Sanger direct sequencing confirmed transgene integration. To confirm transgene integration from both sides, primers were used that allowed sequencing of either site of the transgene or GSH1. Abbreviations: bF, pairing-experienced females; bM, pairing-experienced males; cg, *canalis gynecophoris*; Ctr, control; hs, head sucker, imO, immature ovary; KI, knock-in; mO, mature ovary; ov, ovary; sF, pairing-inexperienced females; tes, testes; vit, vitellarium; vs, ventral sucker.

CLSM analysis showed eGFP signals in female ovaries (Figure 53 D, F, and Figure 54 A). To match these results with the regulatory elements driving transgene expression, I analyzed the Sm*ubi* transcript profile in the RNA-Seq cell atlas of mature ovaries (gonadsc.schisto.xyz). The results showed that Sm*ubi* is transcribed in all four oocyte clusters, with a particular preference for somatic oocytes, but also for the GSC/GSC progeny cluster (Figure 54 B, C). CLSM analysis of sF from transplantation experiments indicated eGFP signals in the sO (Figure 53 F), which mainly contains immature, stem cell-like oogonia (19). These *in silico* data are consistent with the observations in the bO in females obtained from KI experiments, which showed eGFP-positive signals in the whole ovary compared to the control (Figure 54 A). The results also underline the suitability of the SmUbi promoter/terminator for transgene expression, including germ cells. However, not all cells showed eGFP expression (Figure 54 A), which might point to heterozygosity for the transgene. Furthermore, to test the possibility of transgene inheritance, eGFP PCR-positive cercariae obtained from snails infected with transgenic miracidia were used for coinfection-experiments with WT carcariae to obtain worms of both sexes. eGFP-positive F0 worms were obtained and the life cycle continued for two further generations. CLSM analysis of F1 and F2 worms showed eGFP signals at comparable levels, with an average of 16.6±10.7% in male and 13.7±8.6% in female worms being eGFP-positive

(Supplemental Figure S6). Signals were also found in the ovaries of F1 and F2 females, which confirmed germline transmission of the transgene. The amount of eGFP positive signals in worms diminished between F3 and F4.

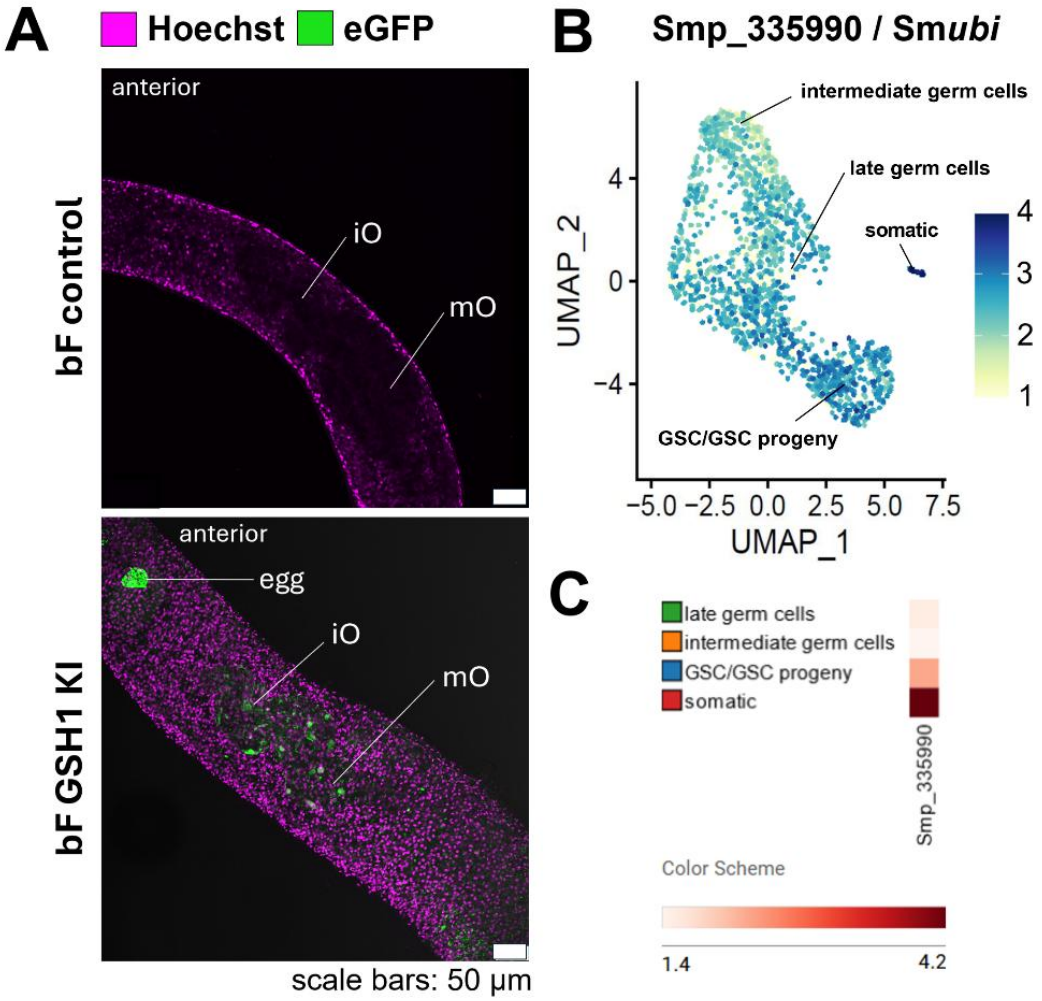

Figure 54. SmUbi promoter activity during oocyte maturation.

A, CLSM analysis showed eGFP signals (green) in the ovary of Hoechst33342-counterstained (purple) paired females obtained from KI experiments of eggs and subsequent mono-miracidial snail infections. The scRNA-Seq atlas of female ovaries (gonadsc.schisto.xyz, **B**, **C**) showed Sm*ubi* transcript occurrence in all four ovary clusters with highest Sm*ubi* transcript levels in the somatic cell cluster followed by the GSC/GSC progeny cluster (immature oocytes). **B**, UMAP plot of Sm*ubi* transcript levels at single cell resolution. **C**, Heatmap of Sm*ubi* transcript levels in the different ovarian clusters. Abbreviations: bF, pairing-experienced female; iO, immature ovary; mO, mature ovary.

4.3 CRISPR/Cas12a application in *S. mansoni* – editing of Sm*thrβ*

After demonstrating the stable integration of a transgene into *S. mansoni* GSH1 and constitutive transgene expression, an attempt was made to adapt the method for functional gene characterization. The potential power of the CRISPR/Cas system for gene characterization in trematodes was previously investigated in few studies that concentrated on KO experiments (33, 170, 322). As a proof of concept for gene KO in *S. mansoni* based on the new editing approach, I tried modifying the locus of the Sm*thrβ* gene. In this thesis, RNAi experiments targeting the transcripts of Sm*thrβ* revealed a critical role of this NR in embryonic development, ovarian maintenance and tissue homeostasis (4.1.8). Given the suggested importance of this receptor in reproduction, the Sm*thrβ* locus was selected as a target for initial editing experiments to prove the accessibility of this locus to CRISPR/Cas-mediated editing – and as an example for editing-based KO approaches of candidate genes of interest. Based on the recently described increase in editing efficiency at GSH1 using three overlapping gRNAs (172, 280), this approach was adapted for Sm*thrβ* using L.b. Cas12a RNPs. In this experiment, L.b. Cas12a was chosen instead of A.s. Cas12a due to its described tolerance to temperature fluctuations and comparatively higher editing efficiency (328) (Supplemental Figure S7). For this, three different PAM sites, suitable for the design of overlapping Cas12a gRNAs (scRNAs), were found in the 5´-UTR of Sm*thrβ* (Figure 55 A).

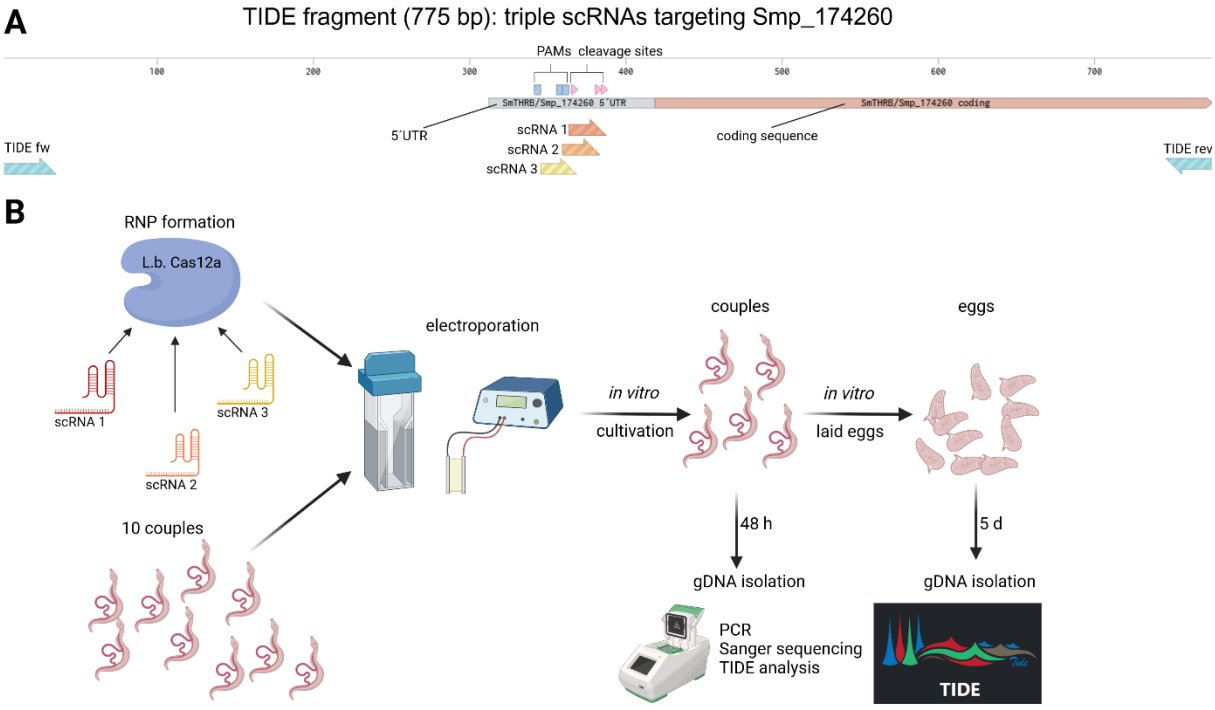

Figure 55. Editing of the Sm*thrβ* locus by three overlapping gRNAs.

A, Schematic overview of the Sm*thrβ* gene fragment which was selected for an editing approach and the determination of editing efficiency by TIDE (202). The three overlapping Cas12a gRNA (scRNA) sequences are indicated as well as predicted PAM (dark blue) and cleavage sites (pink). Shown is this part of the Sm*thrβ* locus containing the predicted 5´-UTR region (grey) and the first exon (orange), based on the *S. mansoni* genome version V10 (143, 168). Primers for the amplification of target fragment are shown in light blue. **B**, Schematic illustration of the workflow for the gRNA-promoted editing of Sm*thrβ* using L.b. Cas12a RNPs formed with three overlapping gRNAs. Couples were transfected with CRISPR/Cas-material, and the gDNA of couples and *in vitro*-laid eggs was analyzed by PCR and TIDE. Abbreviations: PAM, protospacer adjutancy motif; RNP, ribonucleotide complex; scRNA, Cas12a guide RNA; UTR, untranslated region.

For initial editing experiments, RNPs at ratio of 1/1/1 using 3.5 µg L.b. Cas12a enzyme for each respective gRNA were electroporated in 10 couples (n=3; Figure 55 B, 56 A). Couples electroporated without CRISPR/Cas-material served as controls. Subsequently, worms were cultivated for 48 h. Furthermore, the IVLEs produced by couples after EPO were collected and cultivated for additional 5 d. My assumption was that part of the eggs could have been transfected before they were released form the female to the *in vitro*-culture environment. Eggs were maintained in M199egg to ensure embryonic development *in vitro* and to reduce numbers of remaining vitellocytes, knowing that progression of embryonic development causes vitellocyte degradation (76). This way, I expected a reduction of “co-edited” vitellocytes and at the same time to increase the probability to “enrich” for edited zygotes inside the eggs.

Subsequently, gDNA was extracted from couples as well as IVLEs from both the Cas12a-treated and the control groups. Editing efficiency was determined by Sanger direct sequencing-based TIDE analysis (Figure 56 A, B) (202). Tide analysis detected an editing efficiency of 5.7±2.3% in couples (Figure 56 A) and of 2.8±0.2% in 5 d old IVLEs (Figure 56 B). Editing efficiencies of both couples and IVLEs were significant higher as the background mutation rates of the CRISPR/Cas-untreated controls, which were 0.76±0.3% and 0.78±0.44%, respectively. These results demonstrated the accessibility of the Sm*thrβ* locus for Cas12a-mediated editing. In addition, there was first evidence of incorporation of edited cells in eggs produced by couples following transfection. However, this experiment could not finally demonstrate whether editing also succeeded for oocytes or zygotes or only for somatic cells like e.g. vitellocytes.

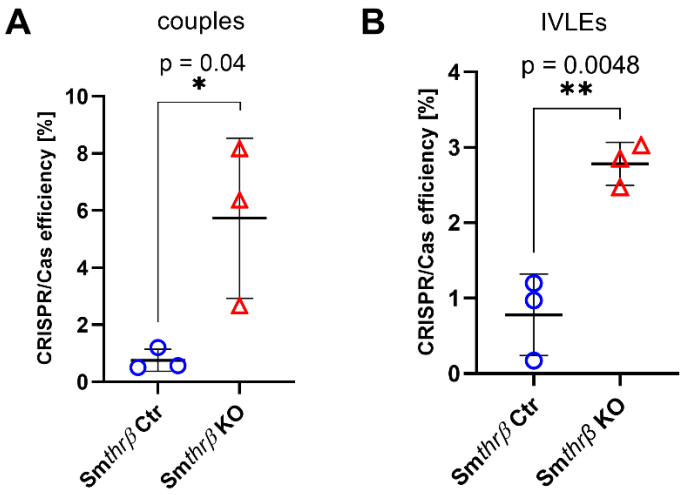

Figure 56. Successful editing of the Sm*thrβ* locus in *S. mansoni* couples and their *in vitro*-laid eggs.

TIDE analysis confirmed the successful editing of target sequence in the Sm*thrβ* locus applying RNPs derived from L.b. Cas12a (red) in combination with three overlapping gRNAs. The background mutation rate (blue) of target locus was found to be at a low level in electroporated couples (**A**) or eggs of these couples laid *in vitro* (**B**). In both, couples (**A**) and in 5 d-old *in vitro*-laid eggs (**B**) indel rates were significantly increased compared to the controls. Abbreviations: Ctr, control; indel, insertions/deletions at target locus; KO, knock-out. *P<0.05, **P<0.01 by t-test. n=3.

5 Discussion

In the context of the increasing prevalence of parasitic diseases and the increase in resistance against antiparasitic drugs (10, 35, 36, 329), such as described for schistosomiasis, it is of utmost importance to understand the reproductive biology of these parasites in order to find ways to interrupt the life cycle and thus prevent the spread of disease. The current strategy for controlling schistosomiasis is the use of praziquantel (PZQ). PZQ is currently the only effective anti-schistosomal drug, able to kill adult worms in the definitive host. Recent studies identified a first target of PZQ, $SmTRPM_{PZQ}$, which was categorized as a transient receptor potential channel of the melastatin subfamily (TRPM) (330–332). PZQ binding-dependent activation of $SmTRPM_{PZQ}$ caused a strong Ca^{2+} influx, which resulted in fatal spastic paralysis of schistosomes (330–332). However, PZQ treatment does not affect juvenile worms, or larva development inside the eggs, which are excreted in the faeces (*S. mansoni, S. japonicum*) or urine (*S. haematobium*) (333, 334). In the past decades, also with respect to potential resistance against PZQ (36), great efforts have been made to find suitable, novel treatment strategies that can eliminate both adult parasites and larval stages (335–340). To prevent reinfection with *Schistosoma spp*. (341, 342), it is crucial to find new targets such as factors essentially involved in germ-cell maturation and/or embryogenesis in order to develop new treatment strategies to interrupt the life cycle.

Given the essential role of male-induced maturation of female germ cells and their role in embryonic development (18, 38, 55, 65), understanding the mechanisms that control their differentiation is of enormous importance. Oocytes are of specific interest due to their capacity for totipotency and their irreplaceable role in propagating throughout generations and generating genetic diversity via meiotic recombination (343, 344). Previous bulk RNA-seq approaches of paired and unpaired schistosomes and their isolated gonads revealed potential NRs, which were ovary-preferential and pairing-dependently transcribed (Figure 16) (55, 62). As expected for TFs, transcript levels, of SmRAR and SmTHRα/β were low (55), and as such not been detected in whole-worm scRNA-Seq atlas of adult schistosomes (61), although WISH analysis (Figure 20 C, 33 D, 36 D) (87), showed ovary-specific transcription of analyzed NRs.

Bioinformatic analysis of new scRNA-seq data of fully differentiated ovaries from paired *S. mansoni* females resulted in the first organ-specific single-cell atlas of ovary cells of a parasitic platyhelminth. In total, we found four ovarian cell clusters: somatic cells, germ-cells and progeny, intermediate-stage cells, and late germ cells (Figure 19; Moescheid and Lu *et al*., submitted; gonadsc.schisto.xyz). Within the data sets of this atlas, transcripts of these NRs were found mainly in oocytes of an intermediate stage of development (Figure 20 A, 33 B, 36 B).

5.1 SmRAR and SmRXR-1 are key factors in oocyte differentiation in *S. mansoni*

Smp_144170, previously annotated as RAR-like retinoic acid nuclear receptor, was one of the potential NRs, found to be transcribed in a pairing-dependent manner in intermediate-stage oocytes. KEGG pathway analyses predicted a crucial role for Smp_144170 in oocyte maturation (345, 346). After validating its pairing-dependent and ovary-localized expression in bF by RT-qPCR and WISH its predicted annotation was confirmed by analyzing its domain structure and phylogeny. Typically, NRs share characteristic domain structures with a variable amino-terminal domain and several distinct transactivation regions. These regions are a conserved DNA-binding domain (DBD), a nuclear localization motif, and a highly conserved carboxy-terminal ligand-binding domain (LBD) (85, 88, 91). Since Smp_144170 has all the typical characteristics of the NR class, it was finally confirmed to be a member of RAR-like receptor family (Figure 17). Furthermore, it was possible to assign Smp_097700 to the clade of RXR receptors. Previous studies annotated Smp_097700 as RXR (SmRXR-1) as well (104, 141). These results are in agreement with previous studies on schistosome NRs, where a putative accelerated evolutionary rate based on the accumulation of more substitutions than their orthologs has been reported (139, 146).

In vertebrates, RA-family NRs, which include RARs and RXRs, have been functionally associated with fertility (347), cell differentiation, embryogenesis, and post-embryonic development (107, 122, 305, 348). Additionally, RARs have been postulated to play critical roles in the initiation of oocyte meiosis, structural gonadal organization, and spermatogenesis (119, 122, 347, 349–351). This may also apply to schistosomes, given the gonad-specific/preferential expression of different retinoid acid NRs (61, 87, 289). Moreover, there is increasing evidence for RARs in mollusks, hemichordates, sea urchins, and other invertebrates. However, little is known about their function (352–354), except for planarians in which a negative effect of RA on head regeneration was described (87, 355). With regard to putative RAR-ligands, RAs play essential roles in the development of the central nervous system in vertebrates (86, 107, 109, 356), the regulation of hormone metabolism (357), tissue homeostasis (358) and cell fate determination (117, 358). The different forms of RA include 9cis-RA (98, 122, 357), 13-cis-RA (98, 350, 359) and all-trans-RA (98, 122, 147, 360). In *S. japonicum*, 9cis-RA has been identified as a potential ligand of an SjRXR ortholog (140). However, the ligand of SmRAR remains unknown and warrants further study in the future.

Functional characterization of SmRAR by RNAi in both bF and sF (first-time paired females) revealed in both cases reproducible developmental phenotypes, including reduced ovary volume, failure of oocyte differentiation, disruption of egg formation and reduced number of zygotes in eggs. These results are in line with previous work describing *S. mansoni* SmRXR-1 as a constitutively expressed member of the RXRα subfamily (55, 61, 62, 104, 141, 142, 146,

148, 361). Additionally, sex- and tissue-independent transcription with a preference for the ovary was demonstrated for Sm*rxr-1* by RT-qPCR and WISH in this thesis.

In independent studies, co-immunoprecipitation experiments confirmed the heterodimerization of SmRAR with SmRXR-1. The resulting heterodimer was found to bind to the promoter region of the eggshell precursor protein Smp14 *in vitro* (Figure 57 A) (104, 361), which is tissue-specifically expressed in the vitellarium (80, 104, 148). Moreover, Sm*rxr-1* KD experiments showed a tendency in RNAi-dependent reduction of transcripts of Smp*14* (Figure 41 B). These previous studies and the ovary scRNAseq data obtained also emphasized regulatory roles of HATs in ovarian maturation. In particular, the HATs SmCBP1 (Smp_105910) and SmGCN5 (Smp_070190), for which the scRNA-Seq data indicated co-transcription with SmRAR and SmRXR-1 in intermediate oocytes (Figure 57 B, Moescheid and Lu *et al*., submitted), were shown to interact with the SmRXR-1/SmRAR heterodimer (104). RXR/RAR heterodimers were described to re-model the chromatin structure by binding the specific RAR response element (RARE) of a particular promoter (147). For SmRXR-1 binding, the RARE consensus sequence 5´-PuGGTCA-3´ was proven, whereby SmRAR was not able to bind this sequence *in vitro* (361). Besides this, chromatin structure is a target of histone modifications such as histone acetyltransferase (HAT)-mediated acetylation (362). By targeting RAR/RXR-associated HATs in *S. mansoni* with a chemical inhibitor, effects on female reproductive organs were observed (104). Inhibitor treatment resulted in malformed, smaller eggs, a less proliferative vitellarium, and in a reduced number of mature oocytes. These phenotypes were similar to those observed in Sm*rar*, but also in Sm*rxr-1* and Sm*rxr-1*/Sm*thrβ* RNAi experiments. The vitellarium phenotype was not observed in Sm*rar* RNAi-treated worms. This may be explained by the fact that SmRAR is mainly expressed in the ovary of paired females (55), whereas SmRXR-1 shows pairing-independent expression (55) in all tissues (61) with a preference to the bO. Therefore, it is likely that SmRXR also forms heterodimers with other NR partners (130), also in the vitellarium, which could lead to complex mosaic phenotypes after inhibitor treatment.

RNAi experiment knocking down Sm*rxr-1* transcripts in both single and double KD experiments with Sm*rar* dsRNA caused the reduction of the Sm*tyr2* (tyrosinase 2) transcripts. Sm*tyr2* is pairing-dependently transcribed in the vitellarium and ovary and plays a fundamental role in eggshell formation (42, 55, 61, 79). The successful KD of Smp_165360 during Theresa Huber's master thesis (302) resulted in an egg phenotype similar to these observed during Sm*rxr-1* or Sm*rxr-1*/Sm*thrβ* RNAis, which is characterized by smaller and dark eggs, a change in egg morphology, and the absence of the typical spine. Analyses of the domain structure and annotations in databases identified Smp_165360 as a potential Myst4 HAT (SmMyst4; Supplemental Figure S8 A) (143, 168, 242, 243, 363). In addition, analysis of the RNA-seq studies revealed female- and pairing-specific transcription in S3-S4 vitellocytes (Supplemental

Figure S8 B, C) (55, 61). This was confirmed by WISH (Supplemental Figure S8, D). Analyses of the gene expression of Sm*myst4* RNAi-treated couples indicated the downregulation of Sm*tyr2* (302). Since a vitellarium-dependent phenotype, a downregulation of Sm*tyr2*, and comparable phenotypic changes in egg morphology were identified after the inhibition of SmRXR-1/SmRAR-associated HATs and upon RNAi of Sm*rxr-1*, SmMyst4 could also be a potential co-activator recruited by SmRXR-1 (85, 98). During mammalian embryogenesis, an NR-dependent recruitment of Myst4 HATs was demonstrated in bovine oocytes (364, 365) and was shown to be a potent histone H3 and H4 acetylase (366). For members of the MYST-family, regulative roles in apoptosis, cell cycle and stem cell homeostasis have been found (367), which could also apply to vitellocyte development in schistosomes. The potential interaction between SmRXR-1 and SmMyst4 could be determined in future studies by co-immunoprecipitation experiments as described by Carneiro *et al.* (104).

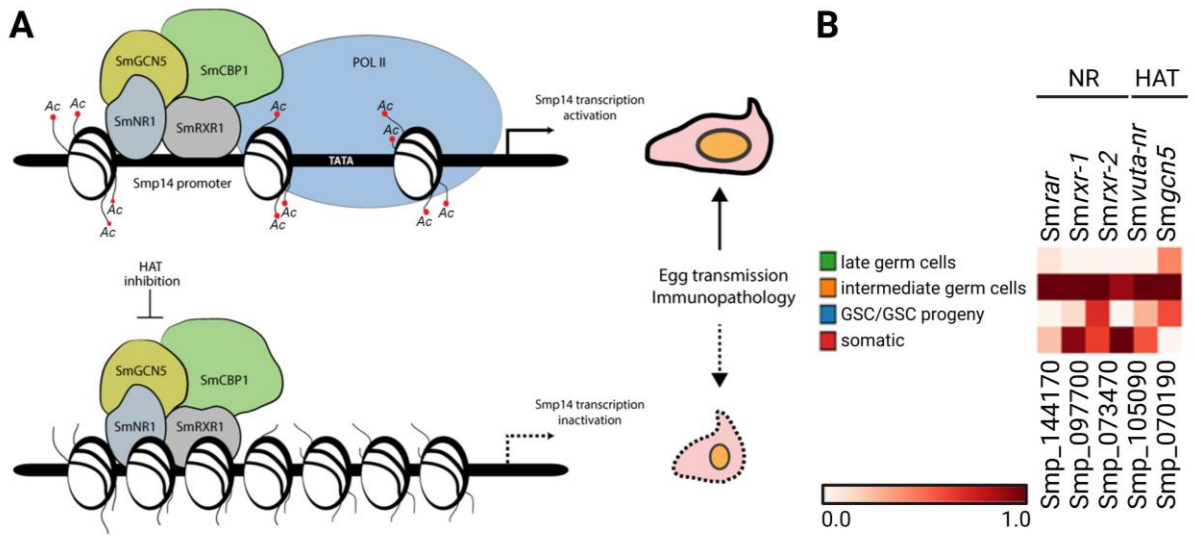

Figure 57. Model of the SmRXR-1/SmRAR dependent recruiting of specific HATs.

A, The SmRXR-1/SmRAR (SmNR1) heterodimer forms a complex with two histone acetyltransferases, SmGCN5 and SmCBP1, and binds to a specific DNA response element in the Smp14 promoter (104, 361). This complex leads to chromatin remodeling, the recruitment of RNA Pol II to the promoter, and subsequent transcription of the Smp14 gene. The resulting of Smp*14* expression is necessary for eggshell formation, which is crucial for both; egg dissemination and granuloma formation (80). Disrupting the histone acetyltransferase activities of either SmCBP1 or SmGCN5 by e.g. inhibitors hinders chromatin decondensation, preventing RNA Pol II from accessing the promoter, and ultimately stop Sm*p14* transcription (104). This interference compromises eggshell integrity and can reduce the transmission and immunopathology of schistosomiasis. Illustration by Carneiro *et al.* 2014 (104). **B**, Heatmap of the oocyte scRNA-Seq cluster-associated transcript amounts of the nuclear receptors (NRs) Sm*rar*, potential retinoid-x nuclear receptors (RXR-1/-2), an annotated vitamin-A-activated nuclear receptor (Sm*vita-nr*), and the SmRAR-associated histone acetyl transferases (HATs) Sm*cbp1* and Sm*gcn5* (104). All selected genes were found to be co-transcribed in oocytes of the intermediate-stage

cluster. The heatmap illustrates the feature-standardized transcript-levels for each cluster of selected genes (Moescheid and Lu *et al*., submitted).

In vertebrates, RAR/RXR heterodimers play a critical role in the differentiation of gonadal cells by regulating mitotic and meiotic processes during spermatogenesis (119, 122, 123, 349–351) and oogenesis (120, 368, 369). These findings are consistent with the obtained results in the course of this thesis and suggest a conserved function for SmRAR and SmRXR-1 also in schistosomes. However, there is one notable exception: Sm*rar* transcription is pairing-dependent, and this has fundamental biological consequences for females. The absence of pairing-regulated key factors such as SmRAR, SMRXR-1, and SmMEIOB caused a failure of oocyte differentiation (Figure 22, 26, 27 C-J, 40). Furthermore, the analysis of the *S. mansoni* genome (143) revealed two additional RARs that belong to the class of retinoid-X/opsin nuclear receptors (Smp_073470, SmRXR-2; and Smp_105090, SmVitA-NR; Figure 17, D1 B). These paralogs were found to be co-transcribed with Sm*rar* and Sm*rxr-1* (Figure 57 B), with highest transcript levels in intermediate-stage oocytes and lowest levels in mature oocytes. This supports the hypothesis that SmRAR as well as its paralogs are involved in oocyte differentiation and post-oogonia cell division. Furthermore, the existence of RA isoforms raises the possibility of differential dimerization of SmRAR with different RXRs and possibly other type II NRs, such as THRs (111, 120, 122). In vertebrates, RA and RARs play essential roles in meiosis initiation (111, 112, 120, 123, 347, 369), which suggests a similar role for SmRAR and its potential dimerization partner(s) in schistosomes (104). Additionally, treatment of *S. mansoni* with 9cis-RA induced a significant increase in egg production, whereby agonizing *S. mansoni* RAR by CH-55 (267) caused a significant decrease in oocyte proliferation and egg production. This phenotype did not completely overlap with the phenotype observed in worms obtained from Sm*rar* RNAi experiments. However, a strong decrease in EdU-positive, proliferating oogonia was also observed upon Sm*rxr-1* RNAi. Therefore, it might be possible that CH-55 act as inhibitor of SmRXR-1. In addition, the observed effects could be caused by a combination of several factors, as it cannot be ruled out that the other two identified RARs (Figure 57 B) were also inhibited by CH-55. The specificity of vertebrate RARs was described for CH-55 (267). Although the RARs/RXRs of *S. mansoni* showed evolutionary distance to vertebrate RARs in phylogenetic analyses (139, 370) and clustered in a trematode-specific clade of retinoic acid receptors (Figure 17), binding of other *S. mansoni* RARs/RXRs by CH-55 cannot be excluded. These results and the identification of orthologs of all proteins required for RA signaling (122, 371, 372) in the scRNA-Seq data set of mature ovaries (Supplemental Figure S9, Moescheid and Lu *et al*., submitted) highlighted the importance of RA-dependent reproduction in schistosomes.

The proposed function of SmRAR in oocyte differentiation and meiosis was corroborated by the examination of ovarian marker gene expression following Sm*rar* RNAi. This included the receptor tyrosine kinase genes Sm*fgfr-a* and Sm*fgfr-b*, which were found to play crucial roles in gonad differentiation, stem cell biology, morphology, and embryogenesis in other studies (171, 200, 373). Previous analyzes of the transcriptome of adult schistosomes and their gonads revealed transcript patterns of both genes in the ovaries, with a clear bias towards immature female ovaries (55). Further, Sm*fgfr-a* and *-b* transcripts were identified in the GSC cluster in the oocyte scRNA-Seq dataset (Figure 25 B). Given that transcripts were mainly found in intermediate-stage oocytes, no Sm*rar*-induced regulation of Sm*fgfr-a*/*-b* was expected, as confirmed by RT-qPCR. In contrast to Sm*rar*, Sm*rxr-1* transcripts were found in immature oogonia. Here, Sm*fgfr-a* and-*b* were found to be co-transcribed with Sm*nanos-2* (Supplemental Figure S10), for which an association with EdU-positive oogonia was recently described (61). Nonetheless, Sm*rxr-1* RNAi caused transcript depletion of Sm*fgfr-a*, which was consistent with the results of the Sm*rxr-1* RNAi-dependent reduction of EdU-positive oogonia. This result is the first indication that Sm*rxr-1* is also involved in the regulation of early oogenesis*,* probably hierarchically upstream of SmRAR. Furthermore, it supports the previous conclusion that Sm*fgfr-a* and *-b* play roles in controlling stem-cell (oogonia-associated) progression (171, 200, 373).

Sm*darnt* was among the genes predicted by STRING as a SmRAR interaction partner, but not for SmRXR-1. However, according to RT-qPCR analysis, it was not regulated following Sm*rar* RNAi. Previous RNA-seq studies revealed a pairing-dependent transcript profile for Sm*darnt* in the ovary (55, 61), and scRNAseq showed transcripts mainly in intermediate-stage oocytes (Moescheid and Lu *et al*., submitted). ARNTSs and aryl hydrocarbon receptors (AHRs) regulate genes involved in cell differentiation and proliferation (374, 375). For instance, in mammalian ovaries, they control fertility and embryogenesis (375, 376). Thus, it can be hypothesized that although Sm*darnt* may be involved in oocyte maturation in *S. mansoni*, it may be controlled by a Sm*rar*-independent process. In addition, the prediction of a protein interaction using STRING analysis is not necessarily an evidence for a gene regulatory connection.

In contrast, Sm*gli1* was one of the genes significantly downregulated by Sm*rar* RNAi. Sm*gli1* was previously shown to control the sexual maturation of female gonads, but not the maintenance of their differentiation status (51). In vertebrates, Gli orthologs are regulated by the Wnt signaling pathway (377–379), which plays an essential role in the regulation of meiosis-associated genes (380). In *C. elegans*, Gli has been shown to play an essential role in ovarian development (59). Above these findings, Sm*gli1* has been identified as an ortholog of *C. elegans* SEX-1 (Supplemental Figure S9). In *C. elegans*, SEX-1 is a key factor in the RA-

regulated organization of the gonads during larval development (59, 371). RA isoforms also were found to affect the regulation of Wnt signaling in mammalian cells (120, 380, 381). Additionally, Sm*gli1* has been found to be expressed in neurons (51, 61), but also in and around the ovaries of *S. mansoni* females (55, 61). Furthermore, the scRNA-Seq data and WISH analyses provided first evidence that in the paired female Sm*gli1* transcripts are not localized in oocyte clusters but in the somatic cluster, which are characterized by the expression of genes associated with neuronal and muscular functions (51, 61). These cells may belong to the thin layer of ligamentous, muscular and neuronal cells surrounding the ovary (283, 297). Sm*gli1* RNAi in paired females caused no morphological changes in the ovaries and no effect on the number of mOo. In an independent study, a key role for SmGli1 for vitellarium differentiation was found (51, 60). This could explain the observed changes in egg morphology, as S4 vitellocytes synthesized in the vitellarium provide precursor proteins required for eggshell formation (19, 49, 60, 64). It can be concluded that the observed phenotype is mainly a result of processes in the vitellarium that affect eggshell synthesis and egg formation. However, additional effects of ovarian processes affecting egg formation cannot be completely excluded. These processes are likely to be independent of zygote formation, which was unaffected by Sm*gli1* RNAi. Moreover, in vertebrates, RA affects Gli expression in neurons (150-152). In *S. mansoni*, Sm*gli1*, Sm*rar*, and Sm*rxr-1* are co-transcribed in neuronal cells of adult worms, particularly in neuronal cluster 6 (61). Pairing-dependent differences in gene regulation have been confirmed for these and other genes expressed in this specific cluster (55, 61). This paves the way for future studies of the neuron 6 cluster in adult worms and their expression repertoires to investigate their contribution to male-induced maturation of *S. mansoni* females (56). As the RT-qPCR approach in this work cannot distinguish between ovary-associated and ovary-intrinsic effects, it remains an open question whether the external or internal role(s) of SmGli1 may influence oogonia division and/or oocyte differentiation in mated females.

Sm*ncor* was also found to be significantly downregulated in paired females following Sm*rar*, Sm*rxr-1*, and Sm*rxr-1*/Sm*thrβ* RNAi. Furthermore, STRING analysis (249) (Figure 24, 35) predicted the interaction of SmRAR and SmRXR-1 with the *S. mansoni* NCoR orthologs, as expected (85, 98). Thus, the downregulation of Sm*ncor* is a likely consequence Sm*rar* and/or Sm*rxr-1* RNAi. In vertebrates, NCoR, also known as TRAC, is a component of chromatin-remodeling complexes that regulate various processes, including the repression of RAR/RXR heterodimers (85, 98, 292). This affects cell fate determination, cell differentiation, lineage progression, and the regulation of epigenetic modifications. Additionally, GEI-8, a NCoR/SMRT ortholog in *C. elegans*, is involved in muscle physiology and arrests gonadogenesis upon site-specific mutation (382, 383). In *S. mansoni*, Sm*ncor* is expressed in a pairing-independent manner in both male and female worms, with the highest levels in oocytes. Trancripts occured

in all four ovarian cell clusters, with a preference for intermediate-stage and mature oocytes (55, 61). This is consistent with obtained WISH results and the previous RNA-Seq data of adult worms (61). However, in contrast to paired, adult females, Sm*ncor* was not significantly downregulated in first-time paired females after Sm*rar* RNAi but showed a trend for downregulation upon Sm*rar* RNAi.

Sm*bmpg*, which encodes a putative bone marrow proteoglycan homolog, was also downregulated following Sm*rar* RNAi. Sm*bmpg* and its planarian ortholog (SMED30019646) have previously been described as marker genes for mature oocytes in data analysis of the *S. mansoni* adult cell atlas (61) and *S. mediterranea* female germ-cell analysis (384), respectively. These results are consistent with the obtained Sm*rar* RNAi results, as a reduction in the number of mature oocytes would lead to an overall reduction in Sm*bmpg* transcripts.

Finally, Sm*meiob* transcript levels were significantly reduced by Sm*rar* RNAi. In addition, Sm*rxr-1* RNAi also resulted in a trend towards Sm*meiob* transcript reduction. The non-significant downregulation might be a consequence of the comparatively low Sm*rxr-1* KD efficiency (~80%) compared to Sm*rar* KD (>90%). Sm*rxr-1* transcripts occurred in nearly all cell-clusters, and there is strong evidence for its involvement in pathways not associated to the ovary (55, 61, 104, 141). Further experiments, such as double KD experiments with SmRAR, would be needed to assess the regulatory role of SmRAR/SmRXR-1 heterodimers in oogenesis. In contrast to Sm*ncor* and Sm*bmpg*, Sm*meiob* was found to be exclusively transcribed in the male testis and female ovary (55, 56, 61), and it is regulated in a pairing-dependent manner with a bias towards immature oocytes (55, 61). From its predicted structure, SmMEIOB showed the highest similarity to the human OB-containing meiosis-specific homolog RPA1 (MEIOB; Supplemental Figure S3) (296, 385). RARs play a key role in the regulation of meiosis-associated genes, such as *meiosin*, *stra8*, and *meiob*, all of which have been reported to be involved in mammalian germ-cell differentiation (118, 131, 294, 386, 387). Cluster analysis and transcript localization by fluorescent *in situ* hybridization (FISH) revealed Sm*meiob* transcription in cells representing the GSC progeny cluster and differentiating oocytes (intermediate-stage oocytes, gonadsc.schisto.xyz) (61, 293). Vertebrate orthologs of SmMEIOB play essential roles in meiotic recombination during oogenesis and spermatogenesis in humans and other organisms (295, 387–390). As an ssDNA-binding protein, MEIOB is an essential regulator of recombination between paired chromosomes during meiosis I (294, 387, 388). In this context, a correlation between MEIOB loss-of-function and premature ovarian insufficiency (POI) has been demonstrated (390). In my study, RNAi experiments revealed a comparable role of Sm*meiob* in oocyte maturation for *S. mansoni*, representing the first functional characterization of a trematode ortholog of MEIOB. The similarities in the RNAi phenotypes of Sm*rar*, Sm*rxr-1*, and Sm*meiob*, and the additive effects

of the Sm*rar*/Sm*meiob* double KD, which affected the number of mature oocytes and zygote-containing eggs, support the conclusion that these genes contribute to the regulation of meiosis in *S. mansoni* oocytes (Figure 58).

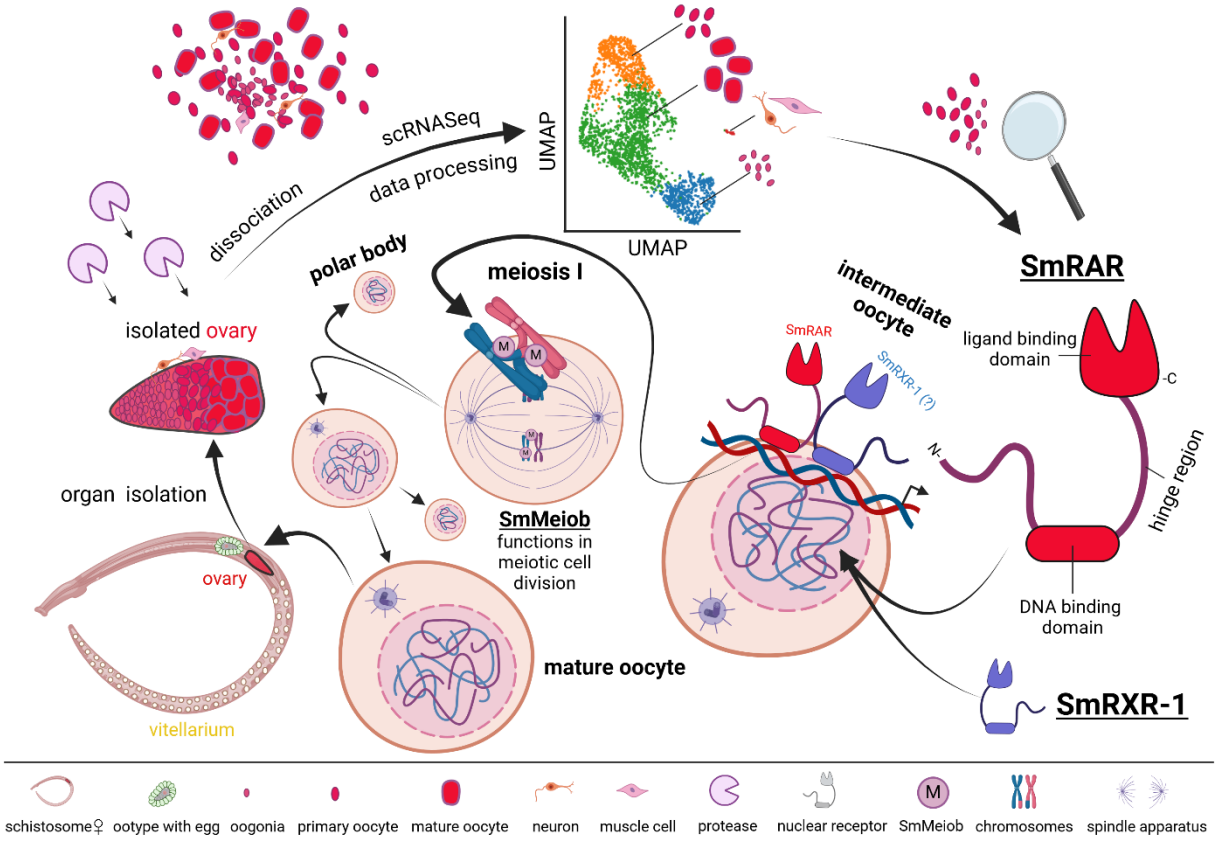

Figure 58. Identification of SmRAR and SmRXR-1 mediated regulation of oocyte maturation by scRNA-Seq analysis of mature ovaries.

Ovaries (bO) from sexually mature female *S. mansoni* were isolated using the previously established organ isolation protocol (73). Isolated ovaries were then enzymatically dissociated into single cells. Single-cell RNA-Seq analysis of these cells revealed four distinct cell clusters within the ovary of mature, paired females: GSC/GSC progeny, intermediate stage oocytes, mature oocytes (representing primary oocytes), and somatic cells that exhibited features of both muscle cells and neurons (Moescheid and Lu *et al*., submitted). Analysis of the transcriptional patterns among the ovarian clusters of the pairing and ovary-preferentially transcribed nuclear receptors SmRAR and SmRXR-1 (55) revealed transcriptional peaks of these receptors in intermediate stage oocytes. Functional analysis of these receptors by RNAi and previous studies (104, 141, 142) characterizing SmRXR-1 suggested heterodimerization of both receptors and highlighted a crucial role in the regulation of meiosis I.

In conclusion, by using the first organ-specific scRNA-Seq atlas combined with functional analyses of selected genes, SmRAR, SmRXR-1, and SmMEIOB were shown to play key roles in oocyte maturation and meiosis regulation in female *S. mansoni* (Figure 58). The function of SmRAR and SmRXR-1 as NRs of the RAR family and their role in oocyte maturation, as well

as ovarian maintenance were demonstrated. In particular, the role of SmRAR in regulating Sm*meiob* and Sm*ncor* implies an additive influence of RA, and thus of the host environment, on one of the most crucial steps of female schistosome sexual reproduction - the oocyte differentiation. The characterization of these receptors has highlighted the crucial role of NRs in transcriptional regulation and added new perspectives to the fascinating sexual biology of schistosomes.

5.2 SmTHRβ plays multiple roles in tissue homeostasis and schistosome reproduction

In the *S. mansoni* genome version V10 (143), two genes coding for putative thyroid hormone receptors (THRs), Smp_134490 and Smp_174260, were identified (145). According to the bulk RNA-Seq analysis of pairing-experienced and inexperienced female and male *S. mansoni* and their isolated gonads (55), both genes were found to be pairing-dependently and ovary-preferentially transcribed (Figure 16) (55, 62). Phylogenetic analysis of THRs and RARs (Figure 17), as well as the comparison of their annotations in additional databases (55, 61, 62, 143) confirmed their identities as THRα (Smp_134490) and SmTHRβ (Smp_174260). SmTHRß was interestingly grouped within a trematode specific subgroup within the THR family. This was expected, given that SmRAR also clustered into a trematode-specific subgroup, which reflects the evolutionary distance between trematode NRs and their vertebrate orthologs (139, 145, 391). In the course of this thesis and the bachelor thesis of Pauline Holzäpfel the transcription patterns predicted by RNAseq were confirmed by RT-qPCR and WISH. For both; SmTHRα and SmTHRβ, WISH showed specific transcription patterns in the posterior part of the ovary. Moreover, the scRNA-Seq atlas of bO showed transcripts of both genes preferentially in intermediate-stage oocytes (gonadsc.schisto.xyz). Since the posterior part of the ovary hosts differentiated, maturating oocytes (38), it seems likely that both receptors may contribute to processes guiding the embryonic development of schistosomes (108, 392), as it was shown for SmRAR and SmRXR-1 (4.1 and 5.1.1.).

Like other type II NRs, THRs are able to form dimers with RXRs and RARs (103, 393). Together with the RNA-Seq data, this suggests potential overlapping functions in the maintenance of female reproductive organs, as it has been shown for SmRAR. Therefore, a further aim of this work was to functionally characterize both *S. mansoni* THR orthologs. Although an exceptional high KD efficiency of $\geq$99% was obtained, no RNAi-dependent phenotype of Sm*thrα* was observed by RNAi (Bachelor's thesis Pauline Holzäpfel, 2022). In general, this gene seemed to be low-abundantly transcribed, and according to the meta-analysis of gene expression over the life cycle, it showed the highest transcript levels in eggs

(62), whereas its transcript level was extremely low in the adult stage, which is in agreement with scRNA-Seq data from the cell atlas of adult worms (61). This low level of expression suggests no important function at the adult stage or a function that should be compensated by other NRs. This and the egg-dominating expression profile of Sm*thrα*, probably explains the lack of phenotype in adults following RNAi.

In contrast, RNAi experiments knocking-down Sm*thrβ*, were less efficient (about 83% reduction in the transcript amount). Nonetheless, a remarkable effect on egg quality was observed (Figure 34 E, D). As for Sm*rar* KD, the number of abnormal eggs significantly increased from day 8 of *in vitro* culture on in Sm*thrβ* dsRNA-treated couples. At the same time, the number of mature oocytes decreased upon RNAi. Both observations corresponded to the Sm*rar* and Sm*rxr-1* KD phenotypes, which supports the assumption that SmTHRβ is an important player in the pairing-dependent differentiation program of oocytes in females and as such being involved in regulating meiosis. The involvement of THRs in the meiosis was described by several studies before, which investigated the orchestration of vertebrate spermatogenesis (394–397). The findings may also apply to oogenesis in female *S. mansoni*. Additionally, it seems likely that *S. mansoni* THRs may also play post-meiotic roles e.g. being involved in the early embryonic development of the first schistosome larva - the miracidium (107, 108, 145, 354, 394). This assumption is supported by the phenotypes of the ovaries and of the deposited eggs after Sm*thrβ*, Sm*rar* and Sm*rxr-1* RNAi, respectively. In particular, eggs from Sm*thrβ* and Sm*rxr-1* RNAi experiments showed deformation and no signs of embryonic development. (Figure 34 E, 39).

Although not (yet) biochemically confirmed, the data clearly indicate that SmTHRβ could be a dimerization partner for SmRAR and/or other type II NRs, as outlined above such as SmRXRs (103, 393). Notably, STRING analysis predicted SmTHRβ as potential interaction partner of SmRXR-1 (Figure 35) (249, 250, 398). Based on these predictions, single and double KD experiments targeting Sm*thrβ* and Sm*rxr-1* were performed. Successful silencing of Sm*thrβ* in single and double KD experiments caused drastic separation-rates and worm detachment as well as reduction of motility. The latter effects were not observed in Sm*rxr-1* single or Sm*rar* KD experiments. The time point of phenotypic changes upon Sm*thrβ* RNAi differed among the experiments, which can be associated with different KD efficiencies. Sm*thrβ* transcript reduction of more than 95% caused fatal separation-rates, a reduced motility and vitality after exactly 14 d, whereas >80% reduction caused the same phenotype after 19 d upon single and double KD. This underlines a possible role(s) of SmTHRβ in various tissues (399, 400), especially since an increase of tissue fragments was observed in the medium as well as a notable reduction of proliferating oogonia. In vertebrate model organisms, studies reported that THs and THRs play crucial roles in the regulation of neuronal development and neuronal

maintenance (110, 401, 401–403). While in *S. mansoni*, Sm*thrβ* transcripts have been identified in certain neuronal clusters (61), an involvement of SmTHRβ in neuronal processes can be postulated, but remains to be proven. The substantial and significant decrease in SmTHRβ transcript abundance may have caused neuronal dysfunction or even depletion, and consequently led to decreased muscle activity. Of note, this effect was discovered specifically upon Sm*thrβ* RNAi, as it was observed only in Sm*thrβ* single and Sm*thrβ*/Sm*rxr-1* double KD experiments, but not in Sm*rxr-1* single or other KD experiments, which were conducted in the scope of this thesis. A similar phenotype, related to viability parameters, and tissue homeostasis has been recently described for the *S. mansoni* NR FTZ-F1 (Smp_328000) (87), which was shown to form heterodimers with SmRXR-1 by yeast-one hybrid experiments (404). This could indicate that SmTHRβ, as a member of the type II NR superfamily, could also be an inter-actor or regulator of FTZ-F1.

RNAi-dependent variations in the transcription of selected genes, which are expressed in the ovary and vitellarium, as well as genes encoding proteins predicted to interact with Sm*thrβ* and/or Sm*rxr-1*, were assessed by RT-qPCR. RT-qPCR revealed notable differences between the Sm*thrβ* and Sm*rxr-1* experiments. No significant downregulation of Sm*tyr2* and Sm*p14* transcripts was detected in the Sm*thrβ* KD. This is one hint indicating that SmTHRβ has no regulative function in the vitellarium (61, 64, 79), and it adds to similar indications by previous RNA-Seq studies (55, 61). Notably, Sm*thrβ* RNAi resulted in a significant decrease in Sm*rxr-1* transcripts, and vice versa. This suggests the possibility of reciprocal regulation (405) of these two NRs by the presence of their respective ligands. Furthermore, interaction between these two NRs was predicted by STRING analysis (249, 250, 398), supporting this hypothesis. Indeed, the regulation of NRs by a negative feedback loop has been described previously (406). The reduction in transcripts of the respective NRs coincided with the reduction of the size of the ovary and the following reduction in intermediate-stage oocytes. To confirm this, further interaction assays such as co-immunoprecipitation experiments (104) or *in vitro* NR binding assays (407–409) with the promoter sequences of the respective receptors would be required.

SmNCoR was predicted as one of the potential interaction partners of Sm*thrβ* (Figure 35). Sm*thrβ* RNAi led to a non-significant but notable reduction in Sm*ncor* transcript levels. Considering the relatively low KD efficiency of Sm*thrβ* (>80%) compared to e.g. Sm*rar* (>95% KD efficiency), a non-significant reduction in SmTHRβ downstream regulated genes may have occurred, as the remaining amount of Sm*thr*β transcripts may lead to sufficient protein for downstream processes.

In addition, Sm*thrβ* RNAi led to a trend of reduced Sm*fgfr-a* transcripts. Since Sm*fgfr-a* is associated with ovary development and germ-cell proliferation (61, 200), the result of Sm*thrβ*

RNAi is consistent with the EdU-phenotypes observed for Sm*thrβ*, Sm*rxr-1*, and the Sm*thrβ*/Sm*rxr-1* double KD.

In contrast to the KD experiments of Sm*rxr-1* and Sm*rar*, the KD of Sm*thrβ* caused no significant downregulation of Sm*meiob*, but to led an exceptionally strong dysregulation (inconsistent strong up- and down-regulation between the biological replicates) of Sm*meiob* transcription. Although SmTHRβ is involved in oocyte proliferation and meiosis (394, 396), it may not directly be involved in the regulation of Sm*meiob*. In model organisms, *stra8*, *meiosin*, and *meiob* regulation was shown to be controlled by RA signaling (121, 122, 131, 132, 368), which fits to the scenario found here. In addition, Sm*thrβ*/Sm*rxr-1* double KD led to a strong dysregulation of Sm*meiob*, which was not observed in the Sm*rxr-1* single KD. This suggests that either SmTHRβ acts independent from SmRXR-1, recruits SmRXR-1 (410), or it is hierarchically superior to Sm*rxr-1* transcription.

Finally, the data indicate that besides RA, host TH may represent another factor to realize the male-dependent sexual maturation of the female. The major TH in human blood is thyroxine (T_4), the second, activated form is triiodothyronine (T_3) (411). Previous studies with *S. mansoni* infected mice, which were injected with T_4 , showed significant effects on worm survival and morphology(Figure 59) (412, 413). Worms from treated mice were significantly larger than worms from control mice. Moreover, a significant higher egg burden was found in mice treated with T_4, which highlights the importance of both THs and THRs in schistosomes.

In summary, the results obtained in this thesis along with recent studies characterizing schistosomal NRs (49, 87, 104, 140, 142, 145, 171, 200), demonstrated key roles of NRs in the development and homeostasis of specific tissues, including the ovary of *S. mansoni*. In addition, strong evidence was obtained that SmRAR, SmRXR-1, and SmTHRβ as well as RA are key factors in the male-governed sexual maturation of the *S. mansoni* female.

5.3 Expanding the molecular toolbox for *S. mansoni*: CRISPR/Cas as a suitable tool for genome editing

Functional gene analysis in trematodes is challenging, as many larval stages are not accessible to RNAi approaches, given their multiple hosts during the parasitic life cycle. Furthermore, many larval stages must be cultured under non-standard physicochemical culture conditions (4, 19, 329). Facing these problems and the limitations of RNAi (151, 152, 154), functional genomics of helminths are still a big challenge (33, 323, 414). In the last decade, CRISPR/Cas gene editing has emerged as a state-of-the-art technique for genome manipulation (181, 183, 415) with recent reports involving CRISPR/Cas-mediated gene editing in trematodes (33, 170, 171, 174, 322, 416), such as *S. mansoni* (33, 170, 171, 416). However, no successful gene KOs were observed in all cells of treated parasites, nor was it possible to select edited schistosomes. To overcome these hurdles, another aim of this study was to test CRISPR/Cas-based editing methods for the stable integration of an eGFP reporter-gene construct into the *S. mansoni* GSH1 (172). Besides comparing the editing efficiencies of two different Cas enzymes, a new method was established to efficiently integrate a reporter-gene into GSH1 using 5'-C6-PEG10 modified 50 bp microhomology arms through programmed CRISPR-Cas9/Cas12a induced HDR.

The genome coordinates for GSH1 were bioinformatically predicted based on genome annotation and chromosome structure, followed by experimental validation (172). The first successful editing of GSH1 was achieved by using a Cas9-based editing approach with three overlapping gRNAs (172). However, this protocol was prone to errors such as ensuring the successful penetration of the three RNPs into target cells. The use of three overlapping gRNAs leads to staggered-end DNA cleavage, enhancing the editing efficiency at the target locus (172). To reduce the probability of errors while maintaining editing efficiency, experiments were carried out with Cas12a-enzymes, as these enzymes are known to process DNA to staggered ends (189, 190, 262), which, in contrast, enhanced programmed transgene insertion compared to Cas9 (Figure 47).

For a proof-of-concept, both LEs and adult schistosomes were transfected using EPO with Cas-containing RNPs. However, treatment of adult schistosomes with RNPs delivered via EPO failed to achieve penetration and distribution of RNPs in all tissues, which is consistent with another, independent study (170). This outcome is not surprising, as exposure of adult-stage schistosomes to CRISPR/Cas through EPO is likely to result in genetic mosaicism (170). Furthermore, the obtained results were consistent with earlier reports about deletion mutations at CRISPR/Cas targets in LEs, schistosomula, and adult schistosomes (33, 169–171, 416). Therefore, editing of adult schistosomes is only suitable for proof-of-principle experiments, or for the KO of (sub)tegumentally transcribed genes (170), where the method could be an

alternative to RNAi experiments. Beyond that, in order to establish a genetically modified organism it is necessary to target stages with a limited number of stem cells, like the egg at its early phase of development (76, 417).

In order to address these issues and to establish genetically, homogeneously modified schistosomes, RNPs were introduced into LEs, which were isolated from the livers of infected final hosts and comprised egg populations representing various developmental stages. These included non-embryonated (stage 0) eggs, which are containing a zygote and a few vitellocytes (76). CLSM analysis of LEs transfected with RNPs, including rhodamine-labelled Cas9-gRNAs (170) or Cas12a-gRNAs, demonstrated the feasibility of the transfection by EPO in penetrating the eggshell (Figure 47 B). Cas12a RNPs showed greater efficiency in accessing embryonic cells compared to Cas12a RNPs. Moreover, RNP-tracking experiments on early-stage eggs revealed successful transfection (Supplemental Figure S11). The higher efficiency of Cas12a RNPs could be attributed to their smaller size, as the Cas12a-RNP complex (Cas12a: 150.9 kDa) was smaller than the Cas9-RNP complex (Cas9: 161.3 kDa) (190, 191). This likely facilitated the uptake of the Cas12a-RNP complex through the egg's pores, for which an average diameter of 0.33-0.64 µm was found by transmission electron microscopy (418, 419). In addition, the efficiency of the transfection process was further enhanced by the comparatively smaller Cas12a gRNA (41-44 nt) compared to Cas9 gRNA (100 nt) (190, 191). After delivery, RNPs of both Cas-enzymes were observed in numerous cells within the egg. However, not every cell in the egg appeared positive for the RNPs. To improve this, alternative transfection methods, such as lipid nanoparticles (420), PB (159, 421–423), and/or other techniques (322, 424–428) could be tested. Alternatively, larval stages like sporocysts should be considered as targets for Cas-mediated editing to enhance cell transfection efficiency (170), which was already shown in preliminary experiments in the course of this work by editing 4 d old sporocysts (data not shown).

In addition to the differences in eggshell penetration-efficiency between the two Cas enzymes, analysis of GSH1 indel-frequencies revealed a significantly higher editing efficiency of Cas12a compared to Cas9 in both eggs and adult schistosomes. The editing efficiency of Cas12a using a single gRNA was comparable to that of Cas9 using two to three gRNAs (172). These differences could be due to several factors, such as i) the efficiency bias of Cas12a in penetrating the eggshell, ii) differences in the cleavage profiles of the nucleases (Cas9, blunt-ended; Cas12a, staggered ends) (190), iii) differences in the efficiency of NHEJ, which depends on the gRNA sequence and the current cell-cycle state of the cells during treatment (429–431), and/or iv) any combination of these factors.

The utility for CRISPR-Cas-induced HDR repair (286) was demonstrated by the integration and constitutive expression of a reporter-gene in embryonating miracidia, sporocysts, and

adult worms. Previous work had demonstrated the ability to integrate a transgene into GSH1 using 300 bp homology arms, but failed to introduce edited miracidia into the parasite life cycle (172, 280). To establish this method, Cas9 and Cas12a were each introduced alongside a 5'C6-PEG10 modified donor template encoding an eGFP reporter-gene under the control of the strong native *S. mansoni* ubiquitin promoter (SmUbi) (172). The promoter and terminator sequences were analyzed in more detail and several core elements were identified (310, 311, 318, 319, 321). These included a Kozak sequence (312), several potential transcription factor binding sites, such as FTz, HNF1, HSF, and a *S. mansoni* poly(A) signal (251, 310, 317, 320) (Figure 46 A, Table 21). The identified promoter elements may contribute to the constitutive transcriptional activity of the associated ubiquitin gene throughout the schistosome life cycle (62).

Recent studies have shown that transgene integration by HDR is limited to 4 kb (172, 432, 433), whereas the use of microhomology arms, were shown to facilitate the integration of transgenes up to 9 kb in length (286, 434–436). For reporter-gene integration, as previously shown in human cell lines (HCT116, HEK293T, H1 and WTC G3), a 5'-C6-PEG10 modified donor DNA template with 50 bp microhomology arms was used to prevent DNA degradation by endonucleases and enhance HDR-efficiency (286). This approach represented a significant improvement compared to the Cas9 approach (172, 280). Similarly, using Cas12a RNPs and a single crRNA, comparable and even higher integration rates were achieved with the modified donor template compared to Cas9 and up to three gRNAs (172). On the basis of these results, Cas12a was found to be preferable over Cas9 for the integration of a transgene (Figure 50). Additionally, Cas12a is particularly well suited for *S. mansoni* due to its preference for AT-rich genomes (328), given its specific PAM motif: 5'-TTTN-3' (190, 258), and is more flexible in its application in schistosomes compared to Cas9, which is more restricted by its PAM 5'-NGG-3' in selecting suitable gRNA binding sites within a target gene (427).

Based on the results built on Cas12a-mediated genome editing and integration of the eGFP reporter-gene, attempts were made to introduce the transgene into the parasitic life cycle. Initially, polymiracidal infection with edited LEs or IVLEs was employed to infect the intermediate snail host. Unfortunately, both approaches failed in snail infection and/or transgene transmission into the following larval stage, the sporocyst. Furthermore, polymiracidial infection by miracidia, hatched from 5 to 7 d old LEs, failed to infect or develop into vital sporocysts *in vivo*. One possible explanation for this developmental deficit could be the influence of GSH1 editing on the GSH1 flanking genes Smp_150460 and Smp_052890 (33), both of which are transcriptional upregulated in sporocysts (62). In particular, Smp_052890 showed a transcriptional peak in sporocysts. It encodes a potential thioredoxin protein (62), which is essential for the antioxidant system and known to control oxidative stress

in mammalian cells (437, 438). Smp_150460 encodes a potential metallo-homeostasis factor, ATX1 (62). For ATX1, an important role in preventing oxidative stress in yeast has been described (439). If these genes were affected by the editing of GSH1, a reduction of vitality of sporocysts within the intermediate host-stage seems likely. However, as the gRNA was designed to process the sequence in the center of GSH1, with a certain distance from the UTRs and coding sequences of these genes (143, 172, 189, 261), it is unlikely that editing of these neighboring genes has occurred. Nevertheless, I cannot exclude an influence of editing on the transcriptional profiles of these genes in sporocytes, which should be investigated in future experiments.

To overcome this potential limitation, miracidia from edited LEs were transformed *in vitro* into sporocysts (223, 224). The number of eGFP-positive sporocysts was comparable to the number of eGFP-positive eggs after 10 d of *in vitro* culture. As expected, some sporocysts showed a mosaic of eGFP-positive cells, with sporocysts containing eGFP-positive cells in the center (Figure 52 B, C). According to previous studies, assessing sporocyst morphology, this structure should harbor germ cells (58, 417), which later develop into daughter sporocysts during asexual reproduction (4, 58, 327). For reintegration into the life-cycle, *in vitro*-generated, eGFP-positive sporocysts were transplanted into snails (222, 227, 228). Cercariognesis occurred in these snails, which released cercariae tested by PCR to be reporter gene-positive, and which were used for final-host infection. This approach resulted in eGFP-positive and thus transgenic sFs (Figure 53). Although the general efficiency of this method was only ~2%, it represents progress of existing protocols. The obtained sFs were probably derived from one single female sporocyst that survived the transplantation process for continuing intra-snail development (440). CLSM analysis of transgenic sFs revealed eGFP expression in various tissues. This included the ovary, which confirms successful germline transgenesis. Furthermore, this result reinforces the predicted constitutive activity of the SmUbi promoter (55, 61, 62) (Figure 53). For additional confirmation, PCR and Sanger sequencing was performed showing the integration of the reporter-gene into the GSH1 locus. Unexpectedly, Sanger sequencing revealed a discrepancy at the 5´-integration site, which exhibited an unexpected large Cas12a-induced deletion (172, 441) of the GSH1 locus followed by imperfect transgene integration (442–445). Given the presence of nearly repetitive, AT-rich sequences within the GSH1 locus (143, 172, 258) and the tendency for HDR-mediated transgene integration to result in imperfect integrations (442–445), it may be possible that the transgene was integrated by partial homology (446)**.** Additionally, by tracking the inheritance of the transgene using fluorescence microscopy and taking Mendel's Law (447) into account, the data obtained suggested heterochromosomal transmission (Supplemental Figure S6). Nonetheless, this result represents the first proof-of-principle that editing GSH1 at the early egg stage is possible as a prerequisite to re-introduced transgenic life stages, here miracidium

and sporocyts, by natural (miracidium - snail infection) or by surgical transplantation (*in vitro*-generated sporocyst into recipient snail) into the life cycle to achieve germ line transformation and transgenic adult *S. mansoni* that are able to inherit the transgene to the following generations. .

In this study, the successful generation of eGFP-positive worms was also observed following monomiracidial infections. Here, hatching of LEs, which were *in vitro*-cultured for 2 d, resulted in a notably increased hatching rate, indicating that the duration of *in vitro* culture also plays a critical role in the survival and development of miracidia. Monomiracidal infection was comparable in efficiency to sporocyst transplantation for obtaining potential transgenic worms. However, this CRISPR/Cas-based method of editing is not yet ready to be considered as a standard method. Further efforts are needed to optimize the *in vitro* culture to make this method a standard procedure in the future (49, 57, 60, 224). In this context, optimizing the *in vitro* culture is an important requirement since it has high potential for improving the production and selection of transgenic larvae. Although some key components, such as human LDL and vitamin-C, were identified during recent years, further research is required to determine the optimal composition of the medium (49, 57, 60)**.** Unlike LEs, IVLEs, that were collected as stage 0 eggs (76), develop entirely *in vitro*. Therefore, there is a high probability that key factors that are essential for the development of the larvae are not present. The addition of 0.25% human LDL, as previously described for adult *S. mansoni* (57), led to a slight improvement in *in vitro* culture of eggs, but other important medium supplements appear to be missing.

Furthermore, the efficiency of germline transmission could be improved by using sporocysts as biological targets for manipulation. Sporocysts are well-suited as they can be maintained *in vitro* for at least four weeks (Supplemental Figure S5). Despite that, sporocysts have a favorable germ cell/somatic cell ratio (327, 448, 449), and the transgene can be inherited and propagated by asexual reproduction. In an independent study, the successful delivery of RNPs in diverse sporocyst cells was demonstrated (170). Finally, due to the low autofluorescence of sporocysts, eGFP-positive individuals can be easily selected for transplantation into snails (222, 227, 227).

Another alternative for the delivery of CRISPR/Cas-material in the zygote of LEs or IVLEs would be the use of the recently established vitellogenin (Vtg) mediated Cas9 RNP delivery in oocytes of the sea star *Patiria minita* (450). For this purpose, the process of endocytosis of Vtg, which is exclusively taken up by oocytes of metazoans, was utilized (450, 451). In this independent study, it was shown that Cas9-enzymes, which were N-terminally fused to the vitellogenin-binding domain, were taken up into the oocyte via a specific vitellogenin receptor (VtgR) (450). This method could also be used for *S. mansoni* to enhance target-directed KI-efficiency. Moreover, the size of the donor DNA template can be optimized, as smaller DNA

fragments have a greater chance of HDR-mediated integration (286, 434–436). Subsequent, this was addressed in initial experimental testing of a 503 bp short potential minimal SmUbi promoter (Supplemental Table S4), which resulted in a significant reduction of ~1500 bp. Following transfection by PB, transgene activity in adult worms was observed (Supplemental Figure S12). This minimal promoter could be used in future studies to increase transgene integration-rates.

In addition to post-genomic research, optimized genome editing for schistosomes would be a valuable tool to decipher the function of certain genes. A previous study that identified multiple GSHs in *S. mansoni* (172), which represented a significant advancement in the application of CRISPR-based functional genomics and transgenesis in *S. mansoni*. In this thesis, existing limitations were overcome by using Cas12a, and by modifying the donor transgene with chemically protected, microhomology arms (286). Along with loss-of-function mutations, these improvements allowed the first gain-of-function approaches by integrating a selectable marker gene into GSH1.

5.4 Outlook – Deciphering the regulatory network of RA-driven gene regulation

Functional analyses of the pairing-specifically and ovary-preferentially transcribed NRs SmRAR, SMRXR-1, and SMTHRβ revealed their key roles in the pairing-induced sexual maturation of the ovary. In particular, SmRAR and SmRXR-1 were found to play an essential role in ovary maturation, but also in early embryogenesis. Initial experiments on paired couples with 9cis-RA or CH-55 revealed an important role for 9cis-RA in the reproductive biology of *S. mansoni*. In light of these results, RARs may even represent potential drug targets for the treatment of schistosomiasis and the suppression of the transmission of vital, infectious eggs. In the recent decades, RAR inhibitors (e.g. BMS-189453, BMS-189532 and BMS-189614), which bind reversibly and specific to human and murine testicular RARα, have been tested as candidates for alternative contraception (452). Furthermore, inhibitors that reversibly inhibit testes-specific RAR-associated proteins like NCoR (453) or an adenylyl cyclase (454), were described. Analysis of the *S. mansoni* proteome (143, 168) for orthologs of these RA signaling-associated proteins (98, 122, 142, 349, 371) identified potential orthologs, transcribed in the bO (Supplemental Figure S9), emphasizing their potential role(s) in oocyte maturation and meiosis (121, 122, 390). Inhibition of these receptors or RAR-associated factors in vertebrate model organisms led to a reversible halt in spermatogenesis (452–455). It would therefore be of great interest to test these inhibitors in *S. mansoni* as potential drugs, but also to further elucidate the regulatory properties of SmRAR. In addition, RARs and RXRs have been described to interact with other RARs and THRs (85, 98, 104, 122). In order to get more insights in the complex interaction of these NR-dimers, potential dimerization partners should be characterized in double KD experiments. Additionally, the effects of TH isoforms (411–413) alone and in any combination with RA isoforms (98, 122, 359, 368) should be tested to get an overview about the regulative roles of these host-derived factors.

NRs act as homo- or heterodimers (85). To narrow down possible interaction partners, Y2H analyses (456), band-shift assays (408) or HEK cell-based NR luciferase reporter systems can be used (457).

Next to this, a CRISPR/Cas12a-based genome editing method was established in the course of this work. This editing method can be used in future studies to edit candidate NRs. KO mutants could be selected by eGFP-signals or, in the best case, by selection on drug resistance. As a potential selection marker, the selectivity for sporocysts and adult schistosomes by oxamniquine was already shown in a recent study (170). According to the findings of this work, the obtained KO worms are expected to show reproductive deficits. In addition, the resulting phenotypes will be free of off-target effects eventually observed upon RNAi, such as the occupation of RISC by siRNAs (151–154). Comparative RNA-Seq

experiments of results from KO versus RNAi experiments could further elucidate the regulatory function of these receptors and help to uncover non-specific RNAi effects (152).

Furthermore, the potential benefits of this new, powerful, CRISPR/Cas12a-based gene editing tool could enable studies of helminth parasites to investigate potential targets for new drugs and vaccine candidates, which are urgently needed as PZQ-alternative for treating schistosomiasis. Additionally, this method could allow the investigation of other genes that are inaccessible to RNAi (150–152, 458). In conclusion, it can be anticipated that this new workflow can serve as a guide for advanced research on individual life stages as well as tissues and contribute to the understanding of the complex biology of *S. mansoni* and other schistosome species

.

6 References

1. WHO (2023) Schistosomiasis: key facts. - https://www.who.int/news-room/fact-sheets/detail/schistosomiasis (12.08.2024)

2. Hotez,P.J. and Kamath,A. (2009) Neglected tropical diseases in sub-saharan Africa: review of their prevalence, distribution, and disease burden. *PLoS Negl. Trop. Dis.*, **3**, e412.

3. Molyneux,D. (2013) Neglected tropical diseases. *Community Eye Health*, **26**, 21–24.

4. McManus,D.P., Dunne,D.W., Sacko,M., Utzinger,J., Vennervald,B.J. and Zhou,X.-N. (2018) Schistosomiasis. *Nat. Rev. Dis. Primer*, **4**, 13.

5. Aula,O.P., McManus,D.P., Jones,M.K. and Gordon,C.A. (2021) Schistosomiasis with a focus on Africa. *Trop. Med. Infect. Dis.*, **6**.

6. Group for Neglected Tropical Diseases. (2012) Accelerating work to overcome the global impact of neglected tropical diseases. - https://iris.who.int/bitstream/handle/10665/338712/WHO-HTM-NTD-2012.5-eng.pdf (13.08.2024)

7. WHO (2023) Schistosomiasis. - https://www.who.int/health-topics/schistosomiasis#tab=tab_1 (12.08.2024)

8. Boissier,J., Grech-Angelini,S., Webster,B.L., Allienne,J.F., Huyse,T., Mas-Coma,S., Toulza,E., Barré-Cardi,H., Rollinson,D., Kincaid-Smith,J., *et al.* (2016) Outbreak of urogenital schistosomiasis in Corsica (France): an epidemiological case study. *Lancet Infect. Dis.*, **16**, 971–979.

9. Salas-Coronas,J., Bargues,M.D., Lozano-Serrano,A.B., Artigas,P., Martínez-Ortí,A., Mas-Coma,S., Merino-Salas,S. and Abad Vivas-Pérez,J.I. (2021) Evidence of autochthonous transmission of urinary schistosomiasis in Almeria (southeast Spain): an outbreak analysis. *Travel Med. Infect. Dis.*, **44**, 102165.

10. Short,E.E., Caminade,C. and Thomas,B.N. (2017) Climate change contribution to the emergence or re-emergence of parasitic diseases. *Infect. Dis.*, **10**, 1178633617732296.

11. Adeyemo,P., Léger,E., Hollenberg,E., Diouf,N., Sène,M., Webster,J.P. and Häsler,B. (2022) Estimating the financial impact of livestock schistosomiasis on traditional subsistence and transhumance farmers keeping cattle, sheep and goats in northern Senegal. *Parasit. Vectors*, **15**.

12. Standley,C.J., Mugisha,L., Dobson,A.P. and Stothard,J.R. (2012) Zoonotic schistosomiasis in non-human primates: past, present and future activities at the human-wildlife interface in Africa. *J. Helminthol.*, **86**, 131–140.

13. Moore,D.V. and Sandground,J.H. (1956) The relative egg producing capacity of *Schistosoma mansoni* and *Schistosoma japonicum*. *Am. J. Trop. Med. Hyg.*, **5**, 831–840.

14. Cheever,A.W., Macedonia,J.G., Mosimann,J.E. and Cheever,E.A. (1994) Kinetics of egg production and egg excretion by *Schistosoma mansoni* and *S. japonicum* in mice infected with a single pair of worms. *Am. J. Trop. Med. Hyg.*, **50**, 281–295.

15. Mason,P.R. and Fripp,P.J. (1977) The reactions of *Schistosoma mansoni* miracidia to light. *J. Parasitol.*, **63**, 240–244.

16. McKerrow,J.H. and Salter,J. (2002) Invasion of skin by *Schistosoma* cercariae. *Trends Parasitol.*, **18**, 193–195.

17. Ingram,J.R., Rafi,S.B., Eroy-Reveles,A.A., Ray,M., Lambeth,L., Hsieh,I., Ruelas,D., Lim,K.C., Sakanari,J., Craik,C.S., *et al.* (2012) Investigation of the proteolytic functions of an expanded cercarial elastase gene family in *Schistosoma mansoni*. *PLoS Negl. Trop. Dis.*, **6**, e1589.

18. Kunz,W. (2001) Schistosome male-female interaction: induction of germ-cell differentiation. *Trends Parasitol.*, **17**, 227–231.

19. LoVerde,P.T. (2019) Schistosomiasis. *Adv. Exp. Med. Biol.*, **1154**, 45–70.

20. Gobbi,F., Tamarozzi,F., Buonfrate,D., van Lieshout,L., Bisoffi,Z., Bottieau,E., and TropNet Schisto Task Force (2020) New insights on acute and chronic schistosomiasis: Do we need a redefinition? *Trends Parasitol.*, **36**, 660–667.

21. Olveda,D.U., Olveda,R.M., McManus,D.P., Cai,P., Chau,T.N.P., Lam,A.K., Li,Y., Harn,D.A., Vinluan,M.L. and Ross,A.G.P. (2014) The chronic enteropathogenic disease schistosomiasis. *Int. J. Infect. Dis.*, **28**, 193–203.

22. Ross,A.G.P., Bartley,P.B., Sleigh,A.C., Olds,G.R., Li,Y., Williams,G.M. and McManus,D.P. (2002) Schistosomiasis. *N. Engl. J. Med.*, **346**, 1212–1220.

23. Gryseels,B., Polman,K., Clerinx,J. and Kestens,L. (2006) Human schistosomiasis. *Lancet Lond. Engl.*, **368**, 1106–1118.

24. Santos,L.L., Santos,J., Gouveia,M.J., Bernardo,C., Lopes,C., Rinaldi,G., Brindley,P.J. and da Costa,J.M.C. (2021) Urogenital schistosomiasis-history, pathogenesis, and bladder cancer. *J. Clin. Med.*, **10**, 205.

25. IARC Working Group on the Evaluation of Carcinogenic Risks to Humans (2012) Biological agents. Volume 100 B. A review of human carcinogens. *IARC Monogr. Eval. Carcinog. Risks Hum.*, **100**, 1–441.

26. von Bülow,V., Lichtenberger,J., Grevelding,C.G., Falcone,F.H., Roeb,E. and Roderfeld,M. (2021) Does *Schistosoma mansoni* facilitate carcinogenesis? *Cells*, **10**, 1982.

27. Peterková,K., Konečný,L., Macháček,T., Jedličková,L., Winkelmann,F., Sombetzki,M., and Dvořák,J.(2024) Winners vs. losers: *Schistosoma mansoni* intestinal and liver eggs exhibit striking differences in gene expression and immunogenicity. *PLoS Pathog.*, **20**.

28. Bustinduy,A.L., Randriansolo,B., Sturt,A.S., Kayuni,S.A., Leustcher,P.D.C., Webster,B.L., Van Lieshout,L., Stothard,J.R., Feldmeier,H. and Gyapong,M. (2022) An update on female and male genital schistosomiasis and a call to integrate efforts to escalate diagnosis, treatment and awareness in endemic and non-endemic settings: the time is now. *Adv. Parasitol.*, **115**, 1–44.

29. Tetteh,C.D., Ncayiyana,J.R., Makhunga,S.E., Manyeh,A.K., Asiamah,E.A. and Ginindza,T.G. (2024) Knowledge and management of female genital schistosomiasis in sub-Saharan Africa: a scoping review protocol. *South. Afr. J. Infect. Dis.*, **39**, 553.

30. Knuhr,K., Langhans,K., Nyenhuis,S., Viertmann,K., Kildemoes,A.M.O., Doenhoff,M.J., Haas,H. and Schramm,G. (2018) *Schistosoma mansoni* egg-released IPSE/alpha-1 dampens inflammatory cytokine responses via basophil interleukin (IL)-4 and IL-13. *Front. Immunol.*, **9**, 2293.

31. Costain,A.H., MacDonald,A.S. and Smits,H.H. (2018) Schistosome egg migration: mechanisms, pathogenesis and host immune responses. *Front. Immunol.*, **9**, 3042.

32. Everts,B., Perona-Wright,G., Smits,H.H., Hokke,C.H., van der Ham,A.J., Fitzsimmons,C.M., Doenhoff,M.J., van der Bosch,J., Mohrs,K., Haas,H., *et al.* (2009) Omega-1, a glycoprotein secreted by *Schistosoma mansoni* eggs, drives Th2 responses. *J. Exp. Med.*, **206**, 1673–1680.

33. Ittiprasert,W., Mann,V.H., Karinshak,S.E., Coghlan,A., Rinaldi,G., Sankaranarayanan,G., Chaidee,A., Tanno,T., Kumkhaek,C., Prangtaworn,P., *et al.* (2019) Programmed genome editing of the *omega-1* ribonuclease of the blood fluke, *Schistosoma mansoni*. *eLife*, **8**, e41337.

34. Andrews,P. (1985) Praziquantel: mechanisms of anti-schistosomal activity. *Pharmacol. Ther.*, **29**, 129–156.

35. Wang,W., Wang,L. and Liang,Y.-S. (2012) Susceptibility or resistance of praziquantel in human schistosomiasis: a review. *Parasitol. Res.*, **111**, 1871–1877.

36. Ismail,M., Botros,S., Metwally,A., William,S., Farghally,A., Tao,L.F., Day,T.A. and Bennett,J.L. (1999) Resistance to praziquantel: direct evidence from *Schistosoma mansoni* isolated from Egyptian villagers. *Am. J. Trop. Med. Hyg.*, **60**, 932–935.

37. Shaw,J.R. and Erasmus,D.A. (1981) *Schistosoma mansoni*: an examination of the reproductive status of females from single sex infections. *Parasitology*, **82**, 121–124.

38. Neves,R.H., de Lamare Biolchini,C., Machado-Silva,J.R., Carvalho,J.J., Branquinho,T.B., Lenzi,H.L., Hulstijn,M. and Gomes,D.C. (2005) A new description of the reproductive system of *Schistosoma mansoni* (Trematoda: Schistosomatidae) analyzed by confocal laser scanning microscopy. *Parasitol. Res.*, **95**, 43–49.

39. Clough,E.R. (1981) Morphology and reproductive organs and oogenesis in bisexual and unisexual transplants of mature *Schistosoma mansoni* females. *J. Parasitol.*, **67**, 535–539.

40. Beckmann,S., Quack,T., Burmeister,C., Buro,C., Long,T., Dissous,C. and Grevelding,C.G. (2010) *Schistosoma mansoni*: signal transduction processes during the development of the reproductive organs. *Parasitology*, **137**, 497–520.

41. Knobloch,J., Kunz,W. and Grevelding,C.G. (2002) Quantification of DNA synthesis in multicellular organisms by a combined DAPI and BrdU technique. *Dev. Growth Differ.*, **44**, 559–563.

42. Ding,H., Liu,F., Zhu,L., Wu,F., Liu,Q., He,S., Shao,W., Du,Y., Ren,C., Shen,J., *et al.* (2017) Tyrosine kinase 4 is involved in the reproduction of the platyhelminth parasite *Schistosoma japonicum*. *Parasit. Vectors*, **10**, 498.

43. Grevelding,C.G. (2004) *Schistosoma. Curr. Biol.*, **14**, R545.

44. LoVerde,P.T., Niles,E.G., Osman,A. and Wu,W. (2004) *Schistosoma mansoni* male–female interactions. *Can. J. Zool.*, **82**, 357–374.

45. Erasmus,D.A. (1973) A comparative study of the reproductive system of mature, immature and ‘unisexual’ female *Schistosoma mansoni*. *Parasitology*, **67**, 165–183.

46. Shaw,M.K. (1987) *Schistosoma mansoni*: vitelline gland development in females from single sex infections. *J. Helminthol.*, **61**, 253–259.

47. Armstrong,J.C. (1965) Maintenance *in vitro* of larval *Schistosoma mansoni* in tissues from the snail, *Australorbis glabratus*. *J. Parasitol.*, **51**, 605–616.

48. Popiel,I. and Basch,P.F. (1984) Reproductive development of female *Schistosoma mansoni* (Digenea: Schistosomatidae) following bisexual pairing of worms and worm segments. *J. Exp. Zool.*, **232**, 141–150.

49. Wang,J., Chen,R. and Collins,J.J. (2019) Systematically improved *in vitro* culture conditions reveal new insights into the reproductive biology of the human parasite *Schistosoma mansoni*. *PLoS Biol.*, **17**, e3000254.

50. Honeycutt,J., Hammam,O., Fu,C.-L. and Hsieh,M.H. (2014) Controversies and challenges in research on urogenital schistosomiasis-associated bladder cancer. *Trends Parasitol.*, **30**, 324–332.

51. Chen,R., Wang,J., Gradinaru,I., Vu,H.S., Geboers,S., Naidoo,J., Ready,J.M., Williams,N.S., DeBerardinis,R.J., Ross,E.M., *et al.* (2022) A male-derived nonribosomal peptide pheromone controls female schistosome development. *Cell*, **185**, 1506-1520.e17.

52. Moczon,T., Swiderski,Z. and Huggel,H. (1992) *Schistosoma mansoni*: the chemical nature of the secretions produced by the Mehlis' gland and ootype as revealed by cytochemical studies. *Int. J. Parasitol.*, **22**, 65–73.

53. Popiel,I. (1986) Male-stimulated female maturation in *Schistosoma*: a review. *J. Chem. Ecol.*, **12**, 1745–1754.

54. Popiel,I., Cioli,D. and Erasmus,D.A. (1984) The morphology and reproductive status of female *Schistosoma mansoni* following separation from male worms. *Int. J. Parasitol.*, **14**, 183–190.

55. Lu,Z., Sessler,F., Holroyd,N., Hahnel,S., Quack,T., Berriman,M. and Grevelding,C.G. (2016) Schistosome sex matters: a deep view into gonad-specific and pairing-dependent transcriptomes reveals a complex gender interplay. *Sci. Rep.*, **6**, 31150.

56. Lu,Z., Spänig,S., Weth,O. and Grevelding,C.G. (2019) Males, the wrongly neglected partners of the biologically unprecedented male–female interaction of schistosomes. *Front. Genet.*, **10**.

57. Li,X., Weth,O., Haeberlein,S. and Grevelding,C.G. (2023) Molecular characterization of *Smtdc-1* and *Smddc-1* discloses roles as male-competence factors for the sexual maturation of *Schistosoma mansoni* females. *Front. Cell. Infect. Microbiol.*, **13**, 1173557.

58. Wang,B., Lee,J., Li,P., Saberi,A., Yang,H., Liu,C., Zhao,M. and Newmark,P.A. (2018) Stem cell heterogeneity drives the parasitic life cycle of *Schistosoma mansoni*. *eLife*, **7**, e35449.

59. Li,T. and Kelly,W.G. (2014) A role for WDR5 in TRA-1/Gli mediated transcriptional control of the sperm/oocyte switch in *C. elegans*. *Nucleic Acids Res.*, **42**, 5567–5581.

60. You,Y., Chen,X., Huo,L., Chen,L., Chen,G., Gu,M., Yi,C., Wang,J. and Hu,W. (2024) An improved medium for *in vitro* studies of female reproduction and oviposition in *Schistosoma japonicum. Parasit. Vectors*, **17**.

61. Wendt,G., Zhao,L., Chen,R., Liu,C., O'Donoghue,A.J., Caffrey,C.R., Reese,M.L. and Collins,J.J. (2020) A single-cell RNA-seq atlas of *Schistosoma mansoni* identifies a key regulator of blood feeding. *Science*, **369**, 1644–1649.

62. Lu,Z., Zhang,Y. and Berriman,M. (2018) A web portal for gene expression across all life stages of *Schistosoma mansoni. bioRxiv.* 10.1101/308213.

63. Li,X., Weth,O., Haimann,M., Möscheid,M.F., Huber,T.S. and Grevelding,C.G. (2024) Rhodopsin orphan GPCR20 interacts with neuropeptides and directs growth, sexual differentiation, and egg production in female *Schistosoma mansoni*. *Microbiol. Spectr.*, **12**, e0219323.

64. Chen,L.L., Rekosh,D.M. and LoVerde,P.T. (1992) *Schistosoma mansoni* p48 eggshell protein gene: characterization, developmentally regulated expression and comparison to the p14 eggshell protein gene. *Mol. Biochem. Parasitol.*, **52**, 39–52.

65. Grevelding,C.G., Sommer,G. and Kunz,W. (1997) Female-specific gene expression in *Schistosoma mansoni* is regulated by pairing. *Parasitology*, **115 (Pt 6)**, 635–640.

66. Michel,A., Knobloch,J. and Kunz,W. (2003) P19: a female and tissue specifically expressed gene in *Schistosoma mansoni*, regulated by pairing with the male. *Parasitology*, **127**, 519–524.

67. Cogswell,A.A., Kommer,V.P. and Williams,D.L. (2012) Transcriptional analysis of a unique set of genes involved in *Schistosoma mansoni* female reproductive biology. *PLoS Negl. Trop. Dis.*, **6**, e1907.

68. Wang,J., Yu,Y., Shen,H., Qing,T., Zheng,Y., Li,Q., Mo,X., Wang,S., Li,N., Chai,R., *et al.* (2017) Dynamic transcriptomes identify biogenic amines and insect-like hormonal regulation for mediating reproduction in *Schistosoma japonicum*. *Nat. Commun.*, **8**, 14693.

69. Fitzpatrick,J.M. and Hoffmann,K.F. (2006) Dioecious *Schistosoma mansoni* express divergent gene repertoires regulated by pairing. *Int. J. Parasitol.*, **36**, 1081–1089.

70. Waisberg,M., Lobo,F.P., Cerqueira,G.C., Passos,L.K.J., Carvalho,O.S., Franco,G.R. and El-Sayed,N.M. (2007) Microarray analysis of gene expression induced by sexual contact in *Schistosoma mansoni. BMC Genomics*, **8**, 181.

71. Leutner,S., Oliveira,K.C., Rotter,B., Beckmann,S., Buro,C., Hahnel,S., Kitajima,J.P., Verjovski-Almeida,S., Winter,P. and Grevelding,C.G. (2013) Combinatory microarray and SuperSAGE analyses identify pairing-dependently transcribed genes in *Schistosoma mansoni* males, including follistatin. *PLoS Negl. Trop. Dis.*, **7**, e2532.

72. Cai,P., Liu,S., Piao,X., Hou,N., Gobert,G.N., McManus,D.P. and Chen,Q. (2016) Comprehensive transcriptome analysis of sex-biased expressed genes reveals discrete biological and physiological features of male and female *Schistosoma japonicum*. *PLoS Negl. Trop. Dis.*, **10**, e0004684.

73. Hahnel,S., Lu,Z., Wilson,R.A., Grevelding,C.G. and Quack,T. (2013) Whole-organ isolation approach as a basis for tissue-specific analyses in *Schistosoma mansoni*. *PLoS Negl. Trop. Dis.*, **7**, e2336.

74. Baran-Gale,J., Chandra,T. and Kirschner,K. (2018) Experimental design for single-cell RNA sequencing. *Brief. Funct. Genomics*, **17**, 233–239.

75. Smyth,J.D. and Clegg,J.A. (1959) Egg-shell formation in trematodes and cestodes. *Exp. Parasitol.*, **8**, 286–323.

76. Jurberg,A.D., Gonçalves,T., Costa,T.A., de Mattos,A.C.A., Pascarelli,B.M., de Manso,P.P.A., Ribeiro-Alves,M., Pelajo-Machado,M., Peralta,J.M., Coelho,P.M.Z., *et al.* (2009) The embryonic development of *Schistosoma mansoni* eggs: proposal for a new staging system. *Dev. Genes Evol.*, **219**, 219–234.

77. Bobek,L., Rekosh,D.M., van Keulen,H. and LoVerde,P.T. (1986) Characterization of a female-specific cDNA derived from a developmentally regulated mRNA in the human blood fluke *Schistosoma mansoni*. *PNAS*, **83**, 5544–5548.

78. Reis,M.G., Kuhns,J., Blanton,R. and Davis,A.H. (1989) Localization and pattern of expression of a female specific mRNA in *Schistosoma mansoni. Mol. Biochem. Parasitol.*, **32**, 113–119.

79. Fitzpatrick,J.M., Hirai,Y., Hirai,H. and Hoffmann,K.F. (2007) Schistosome egg production is dependent upon the activities of two developmentally regulated tyrosinases. *FASEB J.*, **21**, 823–835.

80. deWalick,S., Tielens,A.G.M. and van Hellemond,J.J. (2012) *Schistosoma mansoni*: the egg, biosynthesis of the shell and interaction with the host. *Exp. Parasitol.*, **132**, 7–13.

81. Vogel,H. and Vogel,H. (1942) Über Entwicklung, Lebensdauer und Tod der Eier von *Bilharzia japonica* im Wirtsgewebe. *Dtsch. Tropenmedizinische Z.*, **46**, 57–91.

82. Prata,A. (1957) Biópsia retal na esquistossomose mansoni: bases e aplicações no diagnóstico e tratamento. In *Biópsia retal na esquistossomose mansoni: bases e aplicações no diagnóstico e tratamento*. p. 198-198.

83. Neill,P.J., Smith,J.H., Doughty,B.L. and Kemp,M. (1988) The ultrastructure of the *Schistosoma mansoni* egg. *Am. J. Trop. Med. Hyg.*, **39**, 52–65.

84. Functional characterization of ovary-preferentially or -specifically expressed genes in *Schistosoma mansoni. Justus-Liebig-Univ. Giessen*. - https://www.uni-giessen.de/en/faculties/f10/departments/departments-en/parasitology-en/research-en/schistosoma-en/projects/project-1-signal-transduction-in-the-gonads/functional-

characterization-of-ovary-preferentially-or-specifically-expressed-genes-in-schistosoma-mansoni (06.07.2024)

85. Sever,R. and Glass,C.K. (2013) Signaling by nuclear receptors. *Cold Spring Harb. Perspect. Biol.*, **5**, a016709.

86. Stergiopoulos,A. and Politis,P.K. (2013) The role of nuclear receptors in controlling the fine balance between proliferation and differentiation of neural stem cells. *Arch. Biochem. Biophys.*, **534**, 27–37.

87. Romero,A.A., Cobb,S.A., Collins,J.N.R., Kliewer,S.A., Mangelsdorf,D.J. and Collins,J.J. (2021) The *Schistosoma mansoni* nuclear receptor FTZ-F1 maintains esophageal gland function via transcriptional regulation of *meg-8.3*. *PLoS Pathog.*, **17**, e1010140.

88. Mangelsdorf,D.J., Thummel,C., Beato,M., Herrlich,P., Schütz,G., Umesono,K., Blumberg,B., Kastner,P., Mark,M., Chambon,P., *et al.* (1995) The nuclear receptor superfamily: the second decade. *Cell*, **83**, 835–839.

89. Hollenberg,S.M., Weinberger,C., Ong,E.S., Cerelli,G., Oro,A., Lebo,R., Thompson,E.B., Rosenfeld,M.G. and Evans,R.M. (1985) Primary structure and expression of a functional human glucocorticoid receptor cDNA. *Nature*, **318**, 635–641.

90. Haussler,M.R., Haussler,C.A., Whitfield,G.K., Hsieh,J.-C., Thompson,P.D., Barthel,T.K., Bartik,L., Egan,J.B., Wu,Y., Kubicek,J.L., *et al.* (2010) The nuclear vitamin D receptor controls the expression of genes encoding factors which feed the 'Fountain of Youth' to mediate healthful aging. *J. Steroid Biochem. Mol. Biol.*, **121**, 88–97.

91. Fruchart,J.-C., Santos,R.D., Aguilar-Salinas,C., Aikawa,M., Al Rasadi,K., Amarenco,P., Barter,P.J., Ceska,R., Corsini,A., Després,J.-P., *et al.* (2019) The selective peroxisome proliferator-activated receptor alpha modulator (SPPARMα) paradigm: conceptual framework and therapeutic potential. *Cardiovasc. Diabetol.*, **18**, 71.

92. Bookout,A.L., Jeong,Y., Downes,M., Yu,R.T., Evans,R.M. and Mangelsdorf,D.J. (2006) Anatomical profiling of nuclear receptor expression reveals a hierarchical transcriptional network. *Cell*, **126**, 789–799.

93. Frigo,D.E., Bondesson,M. and Williams,C. (2021) Nuclear receptors: from molecular mechanisms to therapeutics. *Essays Biochem.*, **65**, 847–856.

94. Glass,C.K. (1994) Differential recognition of target genes by nuclear receptor monomers, dimers, and heterodimers. *Endocr. Rev.*, **15**, 391–407.

95. Echeverria,P.C. and Picard,D. (2010) Molecular chaperones, essential partners of steroid hormone receptors for activity and mobility. *Biochim. Biophys. Acta*, **1803**, 641–649.

96. Glass,C.K. and Rosenfeld,M.G. (2000) The coregulator exchange in transcriptional functions of nuclear receptors. *Genes Dev.*, **14**, 121–141.

97. Carroll,J.S., Meyer,C.A., Song,J., Li,W., Geistlinger,T.R., Eeckhoute,J., Brodsky,A.S., Keeton,E.K., Fertuck,K.C., Hall,G.F., *et al.* (2006) Genome-wide analysis of estrogen receptor binding sites. *Nat. Genet.*, **38**, 1289–1297.

98. Li,B., Cai,S.-Y. and Boyer,J.L. (2021) The role of the retinoid receptor, RAR/RXR heterodimer, in liver physiology. *Biochim. Biophys. Acta Mo. Basis Dis.*, **1867**, 166085.

99. Yamamoto,H., Williams,E.G., Mouchiroud,L., Cantó,C., Fan,W., Downes,M., Héligon,C., Barish,G.D., Desvergne,B., Evans,R.M., *et al.* (2011) NCoR1 is a conserved physiological modulator of muscle mass and oxidative function. *Cell*, **147**, 827–839.

100. Chen,J.D. and Evans,R.M. (1995) A transcriptional co-repressor that interacts with nuclear hormone receptors. *Nature*, **377**, 454–457.

101. Hörlein,A.J., Näär,A.M., Heinzel,T., Torchia,J., Gloss,B., Kurokawa,R., Ryan,A., Kamei,Y., Söderström,M. and Glass,C.K. (1995) Ligand-independent repression by the thyroid hormone receptor mediated by a nuclear receptor co-repressor. *Nature*, **377**, 397–404.4.

102. Cohen,R.N., Brzostek,S., Kim,B., Chorev,M., Wondisford,F.E. and Hollenberg,A.N. (2001) The specificity of interactions between nuclear hormone receptors and corepressors is mediated by distinct amino acid sequences within the interacting domains. *Mol. Endocrinol. Baltim. Md*, **15**, 1049–1061.

103. Lee,S. and Privalsky,M.L. (2005) Heterodimers of retinoic acid receptors and thyroid hormone receptors display unique combinatorial regulatory properties. *Mol. Endocrinol.*, **19**, 863–878.

104. Carneiro,V.C., Silva,I.C. de A. da, Torres,E.J.L., Caby,S., Lancelot,J., Vanderstraete,M., Furdas,S.D., Jung,M., Pierce,R.J. and Fantappié,M.R. (2014) Epigenetic changes modulate schistosome egg formation and are a novel target for reducing transmission of schistosomiasis. *PLOS Pathog.*, **10**, e1004116.

105. Watson,P.J., Fairall,L. and Schwabe,J.W.R. (2012) Nuclear hormone receptor co-repressors: structure and function. *Mol. Cell. Endocrinol.*, **348–135**, 440–449.

106. Meester-Smoor,M.A., Janssen,M.J.F.W., ter Haar,W.M., van Wely,K.H.M., Aarnoudse,A.-J.L.H.J., van Oord,G., van Tilburg,G.B.A. and Zwarthoff,E.C. (2011) The ETS family member TEL binds to nuclear receptors RAR and RXR and represses gene activation. *PLoS ONE*, **6**, e23620.

107. Tonk,E.C.M., Pennings,J.L.A. and Piersma,A.H. (2015) An adverse outcome pathway framework for neural tube and axial defects mediated by modulation of retinoic acid homeostasis. *Reprod. Toxicol. Elmsford N*, **55**, 104–113.

108. Bronchain,O.J., Chesneau,A., Monsoro-Burq,A.-H., Jolivet,P., Paillard,E., Scanlan,T.S., Demeneix,B.A., Sachs,L.M. and Pollet,N. (2017) Implication of thyroid hormone signaling in neural crest cells migration: evidence from thyroid hormone receptor beta knockdown and NH3 antagonist studies. *Mol. Cell. Endocrinol.*, **439**, 233–246.

109. Rhinn,M. and Dollé,P. (2012) Retinoic acid signalling during development. *Dev. Camb. Engl.*, **139**, 843–858.

110. Bernal,J. (2007) Thyroid hormone receptors in brain development and function. *Nat. Clin. Pract. Endocrinol. Metab.*, **3**, 249–259.

111. Dawson,M.I. and Xia,Z. (2012) The retinoid X receptors and their ligands. *Biochim. Biophys. Acta*, **1821**, 21–56.

112. Dawson,H.D., Collins,G., Pyle,R., Key,M. and Taub,D.D. (2008) The retinoic acid receptor-α mediates human T-cell activation and Th2 cytokine and chemokine production. *BMC Immunol.*, **9**, 16.

113. Idres,N., Marill,J., Flexor,M.A. and Chabot,G.G. (2002) Activation of retinoic acid receptor-dependent transcription by all-*trans*-retinoic acid metabolites and isomers. *J. Biol. Chem.*, **277**, 31491–31498.

114. Toporova,L., Macejova,D. and Brtko,J. (2016) Radioligand binding assay for accurate determination of nuclear retinoid X receptors: a case of triorganotin endocrine disrupting ligands. *Toxicol. Lett.*, **254**, 32–36.

115. de Urquiza,A.M., Liu,S., Sjöberg,M., Zetterström,R.H., Griffiths,W., Sjövall,J. and Perlmann,T. (2000) Docosahexaenoic acid, a ligand for the retinoid X receptor in mouse brain. *Science*, **290**, 2140–2144.

116. Goldstein,J.T., Dobrzyn,A., Clagett-Dame,M., Pike,J.W. and DeLuca,H.F. (2003) Isolation and characterization of unsaturated fatty acids as natural ligands for the retinoid-X receptor. *Arch. Biochem. Biophys.*, **420**, 185–193.

117. Oliveira,L. de M., Teixeira,F.M.E. and Sato,M.N. (2018) Impact of retinoic acid on immune cells and inflammatory diseases. *Mediators Inflamm.*, **2018**, e3067126

118. Koubova,J., Menke,D.B., Zhou,Q., Capel,B., Griswold,M.D. and Page,D.C. (2006) Retinoic acid regulates sex-specific timing of meiotic initiation in mice. *PNAS*, **103**, 2474–2479.

119. Peer,N.R., Law,S.M., Murdoch,B., Goulding,E.H., Eddy,E.M. and Kim,K. (2018) Germ cell-specific retinoic acid receptor α functions in germ cell organization, meiotic integrity, and spermatogonia. *Endocrinology*, **159**, 3403–3420.

120. Wang,F., Tang,Y., Cai,Y., Yang,R., Wang,Z., Wang,X., Yang,Q., Wang,W., Tian,J. and An,L. (2023) Intrafollicular retinoic acid signaling is important for luteinizing hormone-induced oocyte meiotic resumption. *Genes*, **14**, 946.

121. Gewiss,R.L., Schleif,M.C. and Griswold,M.D. (2021) The role of retinoic acid in the commitment to meiosis. *Asian J. Androl.*, **23**, 549–554.

122. Griswold,M.D. (2016) Spermatogenesis: the commitment to meiosis. *Physiol. Rev.*, **96**, 1–17.

123. Griswold,M.D., Hogarth,C.A., Bowles,J. and Koopman,P. (2012) Initiating meiosis: the case for retinoic acid. *Biol. Reprod.*, **86**, 35.

124. Lin,Y., Gill,M.E., Koubova,J. and Page,D.C. (2008) Germ cell-intrinsic and -extrinsic factors govern meiotic initiation in mouse embryos. *Science*, **322**, 1685–1687.

125. Livera,G., Rouiller-Fabre,V., Pairault,C., Levacher,C. and Habert,R. (2002) Regulation and perturbation of testicular functions by vitamin A. *Reprod. Camb. Engl.*, **124**, 173–180.

126. Hogarth,C.A., Amory,J.K. and Griswold,M.D. (2011) Inhibiting vitamin A metabolism as an approach to male contraception. *Trends Endocrinol. Metab.*, **22**, 136–144.

127. Monaco,H.L. (2000) The transthyretin-retinol-binding protein complex. *Biochim. Biophys. Acta.*, **1482**, 65–72.

128. Berry,D.C., Jacobs,H., Marwarha,G., Gely-Pernot,A., O'Byrne,S.M., DeSantis,D., Klopfenstein,M., Feret,B., Dennefeld,C., Blaner,W.S., *et al.* (2013) The STRA6 receptor is essential for retinol-binding protein-induced insulin resistance but not for maintaining vitamin A homeostasis in tissues other than the eye. *J. Biol. Chem.*, **288**, 24528–24539.

129. Evans,E., Hogarth,C., Mitchell,D. and Griswold,M. (2014) Riding the spermatogenic wave: profiling gene expression within neonatal germ and sertoli cells during a synchronized initial wave of spermatogenesis in mice. *Biol. Reprod.*, **90**, 108.

130. Theodosiou,M., Laudet,V. and Schubert,M. (2010) From carrot to clinic: an overview of the retinoic acid signaling pathway. *Cell. Mol. Life Sci. CMLS*, **67**, 1423–1445.

131. Ishiguro,K.-I., Matsuura,K., Tani,N., Takeda,N., Usuki,S., Yamane,M., Sugimoto,M., Fujimura,S., Hosokawa,M., Chuma,S., *et al.* (2020) MEIOSIN directs the switch from mitosis to meiosis in mammalian germ cells. *Dev. Cell*, **52**, 429-445.e10.

132. Adolfi,M.C., Herpin,A., Regensburger,M., Sacquegno,J., Waxman,J.S. and Schartl,M. (2016) Retinoic acid and meiosis induction in adult versus embryonic gonads of *Medaka*. *Sci. Rep.*, **6**, 34281.

133. Duester,G. (2008) Retinoic acid synthesis and signaling during early organogenesis. *Cell*, **134**, 921–931.

134. Feng,C.-W., Bowles,J. and Koopman,P. (2014) Control of mammalian germ cell entry into meiosis. *Mol. Cell. Endocrinol.*, **382**, 488–497.

135. MacLean,G., Li,H., Metzger,D., Chambon,P. and Petkovich,M. (2007) Apoptotic extinction of germ cells in testes of Cyp26b1 knockout mice. *Endocrinology*, **148**, 4560–4567.

136. Li,H., MacLean,G., Cameron,D., Clagett-Dame,M. and Petkovich,M. (2009) Cyp26b1 expression in murine Sertoli cells is required to maintain male germ cells in an undifferentiated state during embryogenesis. *PloS One*, **4**, e7501.

137. Snyder,E.M., Small,C. and Griswold,M.D. (2010) Retinoic acid availability drives the asynchronous initiation of spermatogonial differentiation in the mouse. *Biol. Reprod.*, **83**, 783–790.

138. Endo,T., Freinkman,E., de Rooij,D.G. and Page,D.C. (2017) Periodic production of retinoic acid by meiotic and somatic cells coordinates four transitions in mouse spermatogenesis. *PNAS.*, **114**, E10132–E10141.

139. Wu,W. and LoVerde,P.T. (2021) Identification and evolution of nuclear receptors in platyhelminths. *PloS One*, **16**, e0250750.

140. Qiu,C., Fu,Z., Shi,Y., Hong,Y., Liu,S. and Lin,J. (2013) A retinoid X receptor (RXR1) homolog from *Schistosoma japonicum*: its ligand-binding domain may bind to 9-cis-retinoic acid. *Mol. Biochem. Parasitol.*, **188**, 40–50.

141. Fantappie,M.R., Freebern,W.J., Osman,A., LaDuca,J., Niles,E.G. and LoVerde,P.T. (2001) Evaluation of *Schistosoma mansoni* retinoid X receptor (*Sm*RXR1 and *Sm*RXR2) activity and tissue distribution. *Mol. Biochem. Parasitol.*, **115**, 87–99.

142. Freebern,W.J., Niles,E.G. and LoVerde,P.T. (1999) RXR-2, a member of the retinoid x receptor family in *Schistosoma mansoni. Gene*, **233**, 33–38.

143. Howe,K.L., Bolt,B.J., Shafie,M., Kersey,P. and Berriman,M. (2017) WormBase ParaSite - a comprehensive resource for helminth genomics. *Mol. Biochem. Parasitol.*, **215**, 2–10.

144. Hu,R., Niles,E.G. and LoVerde,P.T. (2006) DNA binding and transactivation properties of the *Schistosoma mansoni* constitutive androstane receptor homologue. *Mol. Biochem. Parasitol.*, **150**, 174–185.

145. Wu,W., Niles,E.G. and LoVerde,P.T. (2007) Thyroid hormone receptor orthologues from invertebrate species with emphasis on *Schistosoma mansoni*. *BMC Evol. Biol.*, **7**, 150.

146. de Mendonça,R.L., Escriva,H., Bouton,D., Zelus,D., Vanacker,J.-M., Bonnelye,E., Cornette,J., Pierce,R.J. and Laudet,V. (2000) Structural and functional divergence of a nuclear receptor of the RXR family from the trematode parasite *Schistosoma mansoni*. *Eur. J. Biochem.*, **267**, 3208–3219.

147. Bhattacharyya,N., Dey,A., Minucci,S., Zimmer,A., John,S., Hager,G. and Ozato,K. (1997) Retinoid-induced chromatin structure alterations in the retinoic acid receptor β2 promoter. *Mol. Cell. Biol.*, **17**, 6481–6490.

148. Freebern,W.J., Osman,A., Niles,E.G., Christen,L. and LoVerde,P.T. (1999) Identification of a cDNA encoding a retinoid X receptor homologue from *Schistosoma mansoni*. Evidence for a role in female-specific gene expression. *J. Biol. Chem.*, **274**, 4577–4585.

149. Ziniel,P.D., Karumudi,B., Barnard,A.H., Fisher,E.M.S., Thatcher,G.R.J., Podust,L.M. and Williams,D.L. (2015) The *Schistosoma mansoni* Cytochrome P450 (CYP3050A1) is essential for worm survival and egg development. *PLoS Negl. Trop. Dis.*, **9**, e0004279.

150. Geldhof,P., Visser,A., Clark,D., Saunders,G., Britton,C., Gilleard,J., Berriman,M. and Knox,D. (2007) RNA interference in parasitic helminths: current situation, potential pitfalls and future prospects. *Parasitology*, **134**, 609–619.

151. Da'dara,A.A. and Skelly,P.J. (2015) Gene suppression in schistosomes using RNAi. *Methods Mol. Biol. Clifton NJ*, **1201**, 143–164.

152. Moescheid,M.F., Puckelwaldt,O., Beutler,M., Haeberlein,S. and Grevelding,C.G. (2023) Defining an optimal control for RNAi experiments with adult *Schistosoma mansoni. Sci. Rep.*, **13**, 9766.

153. Karunanithi,S., Oruganti,V., Marker,S., Rodriguez-Viana,A.M., Drews,F., Pirritano,M., Nordström,K., Simon,M. and Schulz,M.H. (2019) Exogenous RNAi mechanisms contribute to transcriptome adaptation by phased siRNA clusters in *Paramecium. Nucleic Acids Res.*, **47**, 8036–8049.

154. Gava,S.G., Tavares,N.C., Salim,A.C. de M., Araújo,F.M.G. de, Oliveira,G. and Mourão,M.M. (2017) *Schistosoma mansoni*: Off-target analyses using nonspecific double-stranded RNAs as control for RNAi experiments in schistosomula. *Exp. Parasitol.*, **177**, 98–103.

155. Quack,T., Wippersteg,V. and Grevelding,C.G. (2010) Cell cultures for schistosomes - chances of success or wishful thinking? *Int. J. Parasitol.*, **40**, 991–1002.

156. Weth,O., Haeberlein,S., Haimann,M., Zhang,Y. and Grevelding,C.G. Towards deorphanizing G protein-coupled receptors of *Schistosoma mansoni* using the MALAR yeast two-hybrid system. *Parasitology*, **147**, 865–872.

157. Wilson,R.A., Ashton,P.D., Braschi,S., Dillon,G.P., Berriman,M. and Ivens,A. (2007) 'Oming in on schistosomes: prospects and limitations for post-genomics. *Trends Parasitol.*, **23**, 14–20.

158. Oginuma,M., Nishida,M., Ohmura-Adachi,T., Abe,K., Ogamino,S., Mogi,C., Matsui,H. and Ishitani,T. (2022) Rapid reverse genetics systems for *Nothobranchius furzeri*, a suitable model organism to study vertebrate aging. *Sci. Rep.*, **12**, 11628.

159. Wippersteg,V., Kapp,K., Kunz,W., Jackstadt,W.P., Zahner,H. and Grevelding,C.G. (2002) HSP70-controlled GFP expression in transiently transformed schistosomes. *Mol. Biochem. Parasitol.*, **120**, 141–150.

160. Beckmann,S., Wippersteg,V., El-Bahay,A., Hirzmann,J., Oliveira,G. and Grevelding,C.G. (2007) *Schistosoma mansoni*: germ-line transformation approaches and actin-promoter analysis. *Exp. Parasitol.*, **117**, 292–303.

161. Beckmann,S. and Grevelding,C.G. (2012) Paving the way for transgenic schistosomes. *Parasitology*, **139**, 651–668.

162. Wippersteg,V., Ribeiro,F., Liedtke,S., Kusel,J.R. and Grevelding,C.G. (2003) The uptake of Texas Red-BSA in the excretory system of schistosomes and its colocalisation with ER60 promoter-induced GFP in transiently transformed adult males. *Int. J. Parasitol.*, **33**, 1139–1143.

163. Wippersteg,V., Kapp,K., Kunz,W. and Grevelding,C.G. (2002) Characterisation of the cysteine protease ER60 in transgenic *Schistosoma mansoni* larvae. *Int. J. Parasitol.*, **32**, 1219–1224.

164. Naldini,L., Blömer,U., Gallay,P., Ory,D., Mulligan,R., Gage,F.H., Verma,I.M. and Trono,D. (1996) *In vivo* gene delivery and stable transduction of nondividing cells by a lentiviral vector. *Science*, **272**, 263–267.

165. Rinaldi,G., Eckert,S.E., Tsai,I.J., Suttiprapa,S., Kines,K.J., Tort,J.F., Mann,V.H., Turner,D.J., Berriman,M. and Brindley,P.J. (2012) Germline transgenesis and insertional mutagenesis in *Schistosoma mansoni* mediated by murine leukemia virus. *PLoS Pathog.*, **8**, e1002820.

166. Suttiprapa,S., Rinaldi,G., Tsai,I.J., Mann,V.H., Dubrovsky,L., Yan,H.-B., Holroyd,N., Huckvale,T., Durrant,C., Protasio,A.V., *et al.* (2016) HIV-1 integrates widely throughout the genome of the human blood fluke *Schistosoma mansoni. PLoS Pathog.*, **12**, e1005931.

167. Li,X., Burnight,E.R., Cooney,A.L., Malani,N., Brady,T., Sander,J.D., Staber,J., Wheelan,S.J., Joung,J.K., McCray,P.B., *et al.* (2013) piggyBac transposase tools for genome engineering. *PNAS*, **110**, E2279-2287.

168. Howe,K.L., Bolt,B.J., Cain,S., Chan,J., Chen,W.J., Davis,P., Done,J., Down,T., Gao,S., Grove,C., *et al.* (2016) WormBase 2016: expanding to enable helminth genomic research. *Nucleic Acids Res.*, **44**, D774-780.

169. Ittiprasert,W., Chatupheeraphat,C., Mann,V.H., Li,W., Miller,A., Ogunbayo,T., Tran,K., Alrefaei,Y.N., Mentink-Kane,M. and Brindley,P.J. (2022) RNA-guided AsCas12a- and SpCas9-catalyzed knockout and homology directed repair of the *omega-1* locus of the human blood fluke, *Schistosoma mansoni. Int. J. Mol. Sci.*, **23**, 631.

170. Sankaranarayanan,G., Coghlan,A., Driguez,P., Lotkowska,M.E., Sanders,M., Holroyd,N., Tracey,A., Berriman,M. and Rinaldi,G. (2020) Large CRISPR-Cas-induced deletions in the oxamniquine resistance locus of the human parasite *Schistosoma mansoni. Wellcome Open Res.*, **5**, 178.

171. Du,X., McManus,D.P., French,J.D., Collinson,N., Sivakumaran,H., MacGregor,S.R., Fogarty,C.E., Jones,M.K. and You,H. (2022) CRISPR interference for sequence-specific regulation of fibroblast growth factor receptor A in *Schistosoma mansoni*. *Front. Immunol.*, **13**, 1105719

172. Ittiprasert,W., Moescheid,M.F., Chaparro,C., Mann,V.H., Quack,T., Rodpai,R., Miller,A., Wisitpongpun,P., Buakaew,W., Mentink-Kane,M., *et al.* (2023) Targeted insertion and reporter transgene activity at a gene safe harbor of the human blood fluke, *Schistosoma mansoni. Cell Rep. Methods*, **3**, 100535.

173. Zhang,B. (2021) CRISPR/Cas gene therapy. *J. Cell. Physiol.*, **236**, 2459–2481.

174. Zhang,D., Zhang,Z., Unver,T. and Zhang,B. (2020) CRISPR/Cas: A powerful tool for gene function study and crop improvement. *J. Adv. Res.*, **29**, 207–221.

175. Griffith,A.L., Zheng,F., McGee,A.V., Miller,N.W., Szegletes,Z.M., Reint,G., Gademann,F., Nwolah,I., Hegde,M., Liu,Y.V., *et al.* (2023) Optimization of Cas12a for multiplexed genome-scale transcriptional activation. *Cell Genomics*, **3**.

176. Slaman,E., Kottenhagen,L., de Martines,W., Angenent,G.C. and de Maagd,R.A. (2024) Comparison of Cas12a and Cas9-mediated mutagenesis in tomato cells. *Sci. Rep.*, **14**, 4508.

177. Apostolopoulos,A., Kawamoto,N., Chow,S.Y.A., Tsuiji,H., Ikeuchi,Y., Shichino,Y. and Iwasaki,S. (2024) dCas13-mediated translational repression for accurate gene silencing in mammalian cells. *Nat. Commun.*, **15**, 2205.

178. Kretz,J., Börner,J., Friedrich,T., McIntosh,M., Procida-Kowalski,T., Gerken,F., Wilhelm,J. and Klug,G. (2024) Function of the RNA-targeting class 2 type VI CRISPR Cas system of *Rhodobacter capsulatus*. *Front. Microbiol.*, **15**, 1384543.

179. Pausch,P., Al-Shayeb,B., Bisom-Rapp,E., Tsuchida,C.A., Li,Z., Cress,B.F., Knott,G.J., Jacobsen,S.E., Banfield,J.F. and Doudna,J.A. (2020) CRISPR-CasΦ from huge phages is a hypercompact genome editor. *Science*, **369**, 333–337.

180. Makarova,K.S., Wolf,Y.I., Iranzo,J., Shmakov,S.A., Alkhnbashi,O.S., Brouns,S.J.J., Charpentier,E., Cheng,D., Haft,D.H., Horvath,P., *et al.* (2020) Evolutionary classification of CRISPR-Cas systems: a burst of class 2 and derived variants. *Nat. Rev. Microbiol.*, **18**, 67–83.

181. Pickar-Oliver,A. and Gersbach,C.A. (2019) The next generation of CRISPR-Cas technologies and applications. *Nat. Rev. Mol. Cell Biol.*, **20**, 490–507.

182. Matsumoto,D., Tamamura,H. and Nomura,W. (2020) A cell cycle-dependent CRISPR-Cas9 activation system based on an anti-CRISPR protein shows improved genome editing accuracy. *Commun. Biol.*, **3**, 1–10.

183. Jinek,M., Chylinski,K., Fonfara,I., Hauer,M., Doudna,J.A. and Charpentier,E. (2012) A programmable dual-RNA-guided DNA endonuclease in adaptive bacterial immunity. *Science*, **337**, 816–821.

184. Larson,M.H., Gilbert,L.A., Wang,X., Lim,W.A., Weissman,J.S. and Qi,L.S. (2013) CRISPR interference (CRISPRi) for sequence-specific control of gene expression. *Nat. Protoc.*, **8**, 2180–2196.

185. Cao,H., Wang,Y., Zhang,N., Xia,S., Tian,P., Lu,L., Du,J. and Du,Y. (2022) Progress of CRISPR-Cas13 mediated live-cell RNA imaging and detection of RNA-protein interactions. *Front. Cell Dev. Biol.*, **10**, 866820.

186. Mali,P., Yang,L., Esvelt,K.M., Aach,J., Guell,M., DiCarlo,J.E., Norville,J.E. and Church,G.M. (2013) RNA-guided human genome engineering via Cas9. *Science*, **339**, 823–826.

187. Cong,L., Ran,F.A., Cox,D., Lin,S., Barretto,R., Habib,N., Hsu,P.D., Wu,X., Jiang,W., Marraffini,L.A., *et al.* (2013) Multiplex genome engineering using CRISPR/Cas systems. *Science*, **339**, 819–823.

188. Yang,H., Ren,S., Yu,S., Pan,H., Li,T., Ge,S., Zhang,J. and Xia,N. (2020) Methods favoring homology-directed repair choice in response to CRISPR/Cas9 induced-double strand breaks. *Int. J. Mol. Sci.*, **21**, 6461.

189. Moescheid,M.F., Wisitphongpun,P., Mann,V.H., Quack,T., Grunau,C., Grevelding,C.G., Ittiprasert,W. and Brindley,P.J. (2023) Enhanced efficiency of RNA-guided Cas12a versus Cas9 transgene knock-in and activity at a *Schistosoma mansoni* genome safe harbor. *bioRxiv.* 10.1101/2023.09.12.557428.

190. Paul,B. and Montoya,G. (2020) CRISPR-Cas12a: Functional overview and applications. *Biomed. J.*, **43**, 8–17.

191. Swarts,D.C. and Jinek,M. (2018) Cas9 versus Cas12a/Cpf1: structure-function comparisons and implications for genome editing. *Wiley Interdiscip. Rev. RNA*, **9**, e1481.

192. Svitashev,S., Young,J.K., Schwartz,C., Gao,H., Falco,S.C. and Cigan,A.M. (2015) Targeted mutagenesis, precise gene editing, and site-specific gene insertion in maize using Cas9 and guide RNA. *Plant Physiol.*, **169**, 931–945.

193. Nekrasov,V., Staskawicz,B., Weigel,D., Jones,J.D.G. and Kamoun,S. (2013) Targeted mutagenesis in the model plant *Nicotiana benthamiana* using Cas9 RNA-guided endonuclease. *Nat. Biotechnol.*, **31**, 691–693.

194. Kim,H., Kim,S.-T., Ryu,J., Kang,B.-C., Kim,J.-S. and Kim,S.-G. (2017) CRISPR/Cpf1-mediated DNA-free plant genome editing. *Nat. Commun.*, **8**, 14406.

195. Xu,H., Kita,Y., Bang,U., Gee,P. and Hotta,A. (2021) Optimized electroporation of CRISPR-Cas9/gRNA ribonucleoprotein complex for selection-free homologous recombination in human pluripotent stem cells. *STAR Protoc.*, **2**, 100965.

196. Kim,H.-M. and Colaiácovo,M.P. (2019) CRISPR-Cas9-guided genome engineering in *C. elegans*. *Curr. Protoc. Mol. Biol.*, **129**, e106.

197. Papapetrou,E.P. and Schambach,A. (2016) Gene insertion into genomic safe harbors for human gene therapy. *Mol. Ther.*, **24**, 678–684.

198.A CRISPR primer: Gene editing company leaders talk tech's potential in humans. - https://www.spglobal.com/marketintelligence/en/news-insights/latest-news-headlines/a-crispr-primer-gene-editing-company-leaders-talk-tech-s-potential-in-humans-46820490 (16.07.2024)

199. Li,P., Nanes Sarfati,D., Xue,Y., Yu,X., Tarashansky,A.J., Quake,S.R. and Wang,B. (2021) Single-cell analysis of *Schistosoma mansoni* identifies a conserved genetic program controlling germline stem cell fate. *Nat. Commun.*, **12**, 485.

200. Hahnel,S., Quack,T., Parker-Manuel,S.J., Lu,Z., Vanderstraete,M., Morel,M., Dissous,C., Cailliau,K. and Grevelding,C.G. (2014) Gonad RNA-specific qRT-PCR analyses identify genes with potential functions in schistosome reproduction such as SmFz1 and SmFGFRs. *Front. Genet.*, **5**, 170.

201. Haeberlein,S., Angrisano,A., Quack,T., Lu,Z., Kellershohn,J., Blohm,A., Grevelding,C.G. and Hahnel,S.R. (2019) Identification of a new panel of reference genes to study pairing-dependent gene expression in *Schistosoma mansoni*. *Int. J. Parasitol.*, **49**, 615–624.

202. Brinkman,E.K., Chen,T., Amendola,M. and van Steensel,B. (2014) Easy quantitative assessment of genome editing by sequence trace decomposition. *Nucleic Acids Res.*, **42**, e168.

203. Modi,A., Vai,S., Caramelli,D. and Lari,M. (2021) The Illumina sequencing protocol and the NovaSeq 6000 system. *Methods Mol. Biol. Clifton NJ*, **2242**, 15–42.

204. Sbalzarini,I.F. and Koumoutsakos,P. (2005) Feature point tracking and trajectory analysis for video imaging in cell biology. *J. Struct. Biol.*, **151**, 182–195.

205. Chenouard,N., Smal,I., de Chaumont,F., Maška,M., Sbalzarini,I.F., Gong,Y., Cardinale,J., Carthel,C., Coraluppi,S., Winter,M., *et al.* (2014) Objective comparison of particle tracking methods. *Nat. Methods*, **11**, 281–289.

206. Schneider,C.A., Rasband,W.S. and Eliceiri,K.W. (2012) NIH Image to ImageJ: 25 years of image analysis. *Nat. Methods*, **9**, 671–675.

207. Rueden,C.T., Schindelin,J., Hiner,M.C., DeZonia,B.E., Walter,A.E., Arena,E.T. and Eliceiri,K.W. (2017) ImageJ2: ImageJ for the next generation of scientific image data. *BMC Bioinformatics*, **18**, 529.

208. Schindelin,J., Arganda-Carreras,I., Frise,E., Kaynig,V., Longair,M., Pietzsch,T., Preibisch,S., Rueden,C., Saalfeld,S., Schmid,B., *et al.* (2012) Fiji: an open-source platform for biological-image analysis. *Nat. Methods*, **9**, 676–682.

209. Sievers,F., Wilm,A., Dineen,D., Gibson,T.J., Karplus,K., Li,W., Lopez,R., McWilliam,H., Remmert,M., Söding,J., *et al.* (2011) Fast, scalable generation of high-quality protein multiple sequence alignments using Clustal Omega. *Mol. Syst. Biol.*, **7**, 539.

210. Tamura,K., Stecher,G. and Kumar,S. (2021) MEGA11: Molecular evolutionary genetics analysis version 11. *Mol. Biol. Evol.*, **38**, 3022–3027.

211. Grevelding,C.G. (1995) The female-specific W1 sequence of the Puerto Rican strain of *Schistosoma mansoni* occurs in both genders of a Liberian strain. *Mol. Biochem. Parasitol.*, **71**, 269–272.

212. Dettman,C.D., Higgins-Opitz,S.B. and Saikoolal,A. (1989) Enhanced efficacy of the paddling method for schistosome infection of rodents by a four-step pre-soaking procedure. *Parasitol. Res.*, **76**, 183–184.

213. Duvall,R.H. and DeWitt,W.B. (1967) An improved perfusion technique for recovering adult schistosomes from laboratory animals. *Am. J. Trop. Med. Hyg.*, **16**, 483–486.

214. Basch,P.F. (1981) Cultivation of *Schistosoma mansoni in vitro*. I. Establishment of cultures from cercariae and development until pairing. *J. Parasitol.*, **67**, 179–185.

215. Li,X., Weth,O., Haimann,M., Möscheid,M.F., Huber,T.S. and Grevelding,C.G. (2023) Rhodopsin orphan GPCR20 interacts with neuropeptides and directs growth, sexual differentiation, and egg production in female *Schistosoma mansoni. Microbiol. Spectr.*, **12**, e02193-23.

216. Joyce,K.L., Morgan,W., Greenberg,R. and Nair,M.G. (2012) Using eggs from *Schistosoma mansoni* as an *in vivo* model of helminth-induced lung inflammation. *J. Vis. Exp. JoVE*, **10**.3791/3905.

217. Bge Cell Culture. Biomedical Research Institute (2014). - https://www.afbr-bri.org/schistosomiasis/standard-operating-procedures/biomphalaria-glabrata-embryonic-cell-bge-culture/ (12.08.2024)

218. Wheeler,N.J., Dinguirard,N., Marquez,J., Gonzalez,A., Zamanian,M., Yoshino,T.P. and Castillo,M.G. (2018) Sequence and structural variation in the genome of the *Biomphalaria glabrata* embryonic (Bge) cell line. *Parasit. Vectors*, **11**, 496.

219. Coustau,C., Ataev,G., Jourdane,J. and Yoshino,T.P. (1997) *Schistosoma japonicum: In vitro* cultivation of miracidium to daughter sporocyst using a *Biomphalaria glabrata* embryonic cell line. *Exp. Parasitol.*, **87**, 77–87.

220. Giobbe,G.G., Michielin,F., Luni,C., Giulitti,S., Martewicz,S., Dupont,S., Floreani,A. and Elvassore,N. (2015) Functional differentiation of human pluripotent stem cells on a chip. *Nat. Methods*, **12**, 637–640.

221. StemMACSiPS-Brew XF. - https://www.miltenyibiotec.com/DE-en/products/stemmacs-ips-brew-xf-human.html (04.06.2024)

222. Kapp,K., Coustau,C., Wippersteg,V., Jourdane,J., Kunz,W. and Grevelding,C.G. (2003) Transplantation of *in vitro*-generated *Schistosoma mansoni* mother sporocysts into *Biomphalaria glabrata*. *Parasitol. Res.*, **91**, 482–485.

223. Chernin,E. (1963) Observations on hearts explanted *in vitro* from the snail *Australorbis glabratus*. *J. Parasitol.*, **49**, 353–364.

224. Chernin,E. (1964) Maintenance *in vitro* of larval *Schistosoma mansoni* in tissues from the snail, *Australorbis glabratus*. *J. Parasitol.*, **50**, 531–545.

225. Voge,M. and Seidel,J.S. (1972) Transformation *in vitro* of miracidia of *Schistosoma mansoni* and *S. japonicum* into young sporocysts. *J. Parasitol.*, **58**, 699–704.

226. Yoshino,T.P. and Laursen,J.R. (1995) Production of *Schistosoma mansoni* daughter sporocysts from mother sporocysts maintained in synxenic culture with *Biomphalaria glabrata* embryonic (BGE) cells. *J. Parasitol.*, **81**, 714–722.

227. Jourdane,J. and Theron,A. (1980) *Schistosoma mansoni*: cloning by microsurgical transplantation of sporocysts. *Exp. Parasitol.*, **50**, 349–357.

228. Mouahid,G., Rognon,A., de Carvalho Augusto,R., Driguez,P., Geyer,K., Karinshak,S., Luviano,N., Mann,V., Quack,T., Rawlinson,K., *et al.* (2018) Transplantation of schistosome sporocysts between host snails: a video guide. *Wellcome Open Res.*, **3**, 3.

229. Steffen,H. (2013) Gonadenspezifische Transkriptionsanalysen und erste Charakterisierungen von Transmembranrezeptoren aus *Schistosoma mansoni.* Dissertation. *Justus-Liebig-Univ. Giessen.*

230. Collins,J.J., Wang,B., Lambrus,B.G., Tharp,M.E., Iyer,H. and Newmark,P.A. (2013) Adult somatic stem cells in the human parasite *Schistosoma mansoni. Nature*, **494**, 476–479.

231. Uggeri,J., Gatti,R., Belletti,S., Scandroglio,R., Corradini,R., Rotoli,B.M. and Orlandini,G. (2004) Calcein-AM is a detector of intracellular oxidative activity. *Histochem. Cell Biol.*, **122**, 499–505.

232. White,M.G., Emery,M., Nonner,D. and Barrett,J.N. (2003) Caspase activation contributes to delayed death of heat-stressed striatal neurons. *J. Neurochem.*, **87**, 958–968.

233. Silva,E., Gomes,P. and Soares-da-Silva,P. (2006) Overexpression of Na(+)/K (+)-ATPase parallels the increase in sodium transport and potassium recycling in an *in vitro* model of proximal tubule cellular ageing. *J. Membr. Biol.*, **212**, 163–175.

234. Extraction of DNA using DNAzol Reagent. - https://www.thermofisher.com/de/de/home/references/protocols/nucleic-acid-purification-and-analysis/dna-extraction-protocols/extraction-of-dna-using-reagent.html (12.08.2024)

235. Extraction of RNA using RNAzol RT Reagent. - https://www.genecopoeia.com/wp-content/uploads/2013/06/RNAzol_RT_RNA_Isolation_Reagent_User_Manual.pdf (12.08.2024)

236. Hengen,P.N. (1996) Carriers for precipitating nucleic acids. *Trends Biochem. Sci.*, **21**, 224–225.

237. Untergasser,A., Cutcutache,I., Koressaar,T., Ye,J., Faircloth,B.C., Remm,M. and Rozen,S.G. (2012) Primer3--new capabilities and interfaces. *Nucleic Acids Res.*, **40**, e115.

238. Dorak,M., PFaffl,M.W. (2006) Real-time PCR. Chapter 3: Relative quantification. *Taylor & Francis*. p. 63-80.

239. Pfaffl,M.W. (2001) A new mathematical model for relative quantification in real-time RT-PCR. *Nucleic Acids Res.*, **29**, e45.

240. Lu,Z., Sessler,F., Holroyd,N., Hahnel,S., Quack,T., Berriman,M. and Grevelding,C.G. (2017) A gene expression atlas of adult *Schistosoma mansoni* and their gonads. *Sci. Data*, **4**, 170118.

241. Jumper,J., Evans,R., Pritzel,A., Green,T., Figurnov,M., Ronneberger,O., Tunyasuvunakool,K., Bates,R., Žídek,A., Potapenko,A., *et al.* (2021) Highly accurate protein structure prediction with AlphaFold. *Nature*, **596**, 583–589.

242. Varadi,M., Anyango,S., Deshpande,M., Nair,S., Natassia,C., Yordanova,G., Yuan,D., Stroe,O., Wood,G., Laydon,A., *et al.* (2022) AlphaFold Protein Structure Database: massively expanding the structural coverage of protein-sequence space with high-accuracy models. *Nucleic Acids Res.*, **50**, D439–D444.

243. Letunic,I., Khedkar,S. and Bork,P. (2021) SMART: recent updates, new developments and status in 2020. *Nucleic Acids Res.*, **49**, D458–D460.

244. Kelley,L.A., Mezulis,S., Yates,C.M., Wass,M.N. and Sternberg,M.J.E. (2015) The Phyre2 web portal for protein modeling, prediction and analysis. *Nat. Protoc.*, **10**, 845–858.

245. Sayers,E.W., O'Sullivan,C. and Karsch-Mizrachi,I. (2022) Using GenBank and SRA. *Methods Mol. Biol. Clifton NJ*, **2443**, 1–25.

246. Edgar,R.C. (2004) MUSCLE: a multiple sequence alignment method with reduced time and space complexity. *BMC Bioinformatics*, **5**, 113.

247. Hon,W.-K., Kao,M.-Y., Lam,T.-W., Sung,W.-K. and Yiu,S.-M. (2004) Non-shared edges and nearest neighbor interchanges revisited. *Inf. Process. Lett.*, **91**, 129–134.

248. Goujon,M., McWilliam,H., Li,W., Valentin,F., Squizzato,S., Paern,J. and Lopez,R. (2010) A new bioinformatics analysis tools framework at EMBL-EBI. *Nucleic Acids Res.*, **38**, W695-699.

249. Szklarczyk,D., Gable,A.L., Nastou,K.C., Lyon,D., Kirsch,R., Pyysalo,S., Doncheva,N.T., Legeay,M., Fang,T., Bork,P., *et al.* (2021) The STRING database in 2021: customizable protein-protein networks, and functional characterization of user-uploaded gene/measurement sets. *Nucleic Acids Res.*, **49**, D605–D612.

250. Szklarczyk,D., Franceschini,A., Wyder,S., Forslund,K., Heller,D., Huerta-Cepas,J., Simonovic,M., Roth,A., Santos,A., Tsafou,K.P., *et al.* (2015) STRING v10: protein-protein interaction networks, integrated over the tree of life. *Nucleic Acids Res.*, **43**, D447-452.

251. Wingender,E. (2004) TRANSFAC, TRANSPATH and CYTOMER as starting points for an ontology of regulatory networks. *In Silico Biol.*, **4**, 55–61.

252. Gershenzon,N.I. and Ioshikhes,I.P. (2005) Synergy of human Pol II core promoter elements revealed by statistical sequence analysis. *Bioinforma. Oxf. Engl.*, **21**, 1295–1300.

253. Cartharius,K., Frech,K., Grote,K., Klocke,B., Haltmeier,M., Klingenhoff,A., Frisch,M., Bayerlein,M. and Werner,T. (2005) MatInspector and beyond: promoter analysis based on transcription factor binding sites. *Bioinforma. Oxf. Engl.*, **21**, 2933–2942.

254. Kovács,K.A., Steinmann,M., Magistretti,P.J., Halfon,O. and Cardinaux,J.-R. (2003) CCAAT/enhancer-binding protein family members recruit the coactivator CREB-binding protein and trigger its phosphorylation. *J. Biol. Chem.*, **278**, 36959–36965.

255. Liu,H., Han,H., Li,J. and Wong,L. (2005) DNAFSMiner: a web-based software toolbox to recognize two types of functional sites in DNA sequences. *Bioinforma. Oxf. Engl.*, **21**, 671–673.

256. Nasri,M., Mir,P., Dannenmann,B., Amend,D., Skroblyn,T., Xu,Y., Schulze-Osthoff,K., Klimiankou,M., Welte,K. and Skokowa,J. (2019) Fluorescent labeling of CRISPR/Cas9 RNP for gene knockout in HSPCs and iPSCs reveals an essential role for GADD45b in stress response. *Blood Adv.*, **3**, 63–71.

257. Protasio,A.V., Tsai,I.J., Babbage,A., Nichol,S., Hunt,M., Aslett,M.A., De Silva,N., Velarde,G.S., Anderson,T.J.C., Clark,R.C., *et al.* (2012) A systematically improved high quality genome and transcriptome of the human blood fluke *Schistosoma mansoni*. *PLoS Negl. Trop. Dis.*, **6**, e1455.

258. Berriman,M., Haas,B.J., LoVerde,P.T., Wilson,R.A., Dillon,G.P., Cerqueira,G.C., Mashiyama,S.T., Al-Lazikani,B., Andrade,L.F., Ashton,P.D., *et al.* (2009) The genome of the blood fluke *Schistosoma mansoni*. *Nature*, **460**, 352–358.

259. Roberts,S.B., Segil,N. and Heintz,N. (1991) Differential phosphorylation of the transcription factor Oct1 during the cell cycle. *Science*, **253**, 1022–1026.

260. Jin,V.X., Singer,G.A.C., Agosto-Pérez,F.J., Liyanarachchi,S. and Davuluri,R.V. (2006) Genome-wide analysis of core promoter elements from conserved human and mouse orthologous pairs. *BMC Bioinformatics*, **7**, 114.

261. Labun,K., Montague,T.G., Krause,M., Torres Cleuren,Y.N., Tjeldnes,H. and Valen,E. (2019) CHOPCHOP v3: expanding the CRISPR web toolbox beyond genome editing. *Nucleic Acids Res.*, **47**, W171–W174.

262. Jeon,Y., Choi,Y.H., Jang,Y., Yu,J., Goo,J., Lee,G., Jeong,Y.K., Lee,S.H., Kim,I.-S., Kim,J.-S., *et al.* (2018) Direct observation of DNA target searching and cleavage by CRISPR-Cas12a. *Nat. Commun.*, **9**, 2777.

263. Zetsche,B., Gootenberg,J.S., Abudayyeh,O.O., Slaymaker,I.M., Makarova,K.S., Essletzbichler,P., Volz,S.E., Joung,J., van der Oost,J., Regev,A., *et al.* (2015) Cpf1 is a single RNA-guided endonuclease of a class 2 CRISPR-Cas system. *Cell*, **163**, 759–771.

264. Crooks,G.E., Hon,G., Chandonia,J.-M. and Brenner,S.E. (2004) WebLogo: a sequence logo generator. *Genome Res.*, **14**, 1188–1190.

265. Gibson,D.G., Young,L., Chuang,R.-Y., Venter,J.C., Hutchison,C.A. and Smith,H.O. (2009) Enzymatic assembly of DNA molecules up to several hundred kilobases. *Nat. Methods*, **6**, 343–345.

266. Collins,J.J., Hou,X., Romanova,E.V., Lambrus,B.G., Miller,C.M., Saberi,A., Sweedler,J.V. and Newmark,P.A. (2010) Genome-wide analyses reveal a role for peptide hormones in planarian germline development. *PLoS Biol.*, **8**, e1000509.

267. Agarwal,C., Chandraratna,R.A., Johnson,A.T., Rorke,E.A. and Eckert,R.L. (1996) AGN193109 is a highly effective antagonist of retinoid action in human ectocervical epithelial cells. *J. Biol. Chem.*, **271**, 12209–12212.

268. Chehrehasa,F., Meedeniya,A.C.B., Dwyer,P., Abrahamsen,G. and Mackay-Sim,A. (2009) EdU, a new thymidine analogue for labelling proliferating cells in the nervous system. *J. Neurosci. Methods*, **177**, 122–130.

269. Kellershohn,J., Thomas,L., Hahnel,S.R., Grünweller,A., Hartmann,R.K., Hardt,M., Vilcinskas,A., Grevelding,C.G. and Haeberlein,S. (2019) Insects in anthelminthics research: Lady beetle-derived harmonine affects survival, reproduction and stem cell proliferation of *Schistosoma mansoni*. *PLoS Negl. Trop. Dis.*, **13**, e0007240.

270. Machado-Silva,J.R., Pelajo-Machado,M., Lenzi,H.L. and Gomes,D.C. (1998) Morphological study of adult male worms of *Schistosoma mansoni* Sambon, 1907 by confocal laser scanning microscopy. *Mem. Inst. Oswaldo Cruz*, **93 Suppl 1**, 303–307.

271. Beckmann,S., Buro,C., Dissous,C., Hirzmann,J. and Grevelding,C.G. (2010) The Syk kinase SmTK4 of *Schistosoma mansoni* is involved in the regulation of spermatogenesis and oogenesis. *PLoS Pathog.*, **6**, e1000769.

272. Mughal,M.N., Grevelding,C.G. and Haeberlein,S. (2021) First insights into the autophagy machinery of adult *Schistosoma mansoni*. *Int. J. Parasitol.*, **51**, 571–585.

273. Anthony,B., Mathieson,W., de Castro-Borges,W. and Allen,J. (2010) *Schistosoma mansoni*: Egg-induced downregulation of hepatic stellate cell activation and fibrogenesis. *Exp. Parasitol.*, **124**, 409–420.

274. Truernit,E. and Haseloff,J. (2008) A simple way to identify non-viable cells within living plant tissue using confocal microscopy. *Plant Methods*, **4**, 15.

275. Calcein, AM, Zellfarbstoff. - https://www.thermofisher.com/order/catalog/product/C3099?SID=srch-srp-C3099 (17.04.2024)

276. Latt,S.A., Stetten,G., Juergens,L.A., Willard,H.F., Scher,C.D. (1975) Recent developments in the detection of deoxyribonucleic acid synthesis by 33258 Hoechst fluorescence. *J Histochem Cytochem.* 23(7):493-505.

277. Collins,J.N.R. and Collins,J.J. (2017) Methods for studying the germline of the human parasite *Schistosoma mansoni*. *Methods Mol. Biol. Clifton NJ*, **1463**, 35–47.

278. King,R.S. and Newmark,P.A. (2013) In situ hybridization protocol for enhanced detection of gene expression in the planarian *Schmidtea mediterranea*. *BMC Dev. Biol.*, **13**, 8.

279. King,R.S. and Newmark,P.A. (2018) Whole-mount *in situ* hybridization of planarians. *Methods Mol. Biol. Clifton NJ*, **1774**, 379–392.

280. Ittiprasert,W., Moescheid,M.M., Mann,V.H. and Brindley,P.J. (2024) Multiplexed CRISPR-Cas9 protocol for large transgene integration into the *Schistosoma mansoni* genome. *STAR Protoc.*, **5**, 102886.

281. Montague,T.G., Cruz,J.M., Gagnon,J.A., Church,G.M. and Valen,E. (2014) CHOPCHOP: a CRISPR/Cas9 and TALEN web tool for genome editing. *Nucleic Acids Res.*, **42**, W401-407.

282. Cas9 Nuclease Protein - https://www.abmgood.com/Documents/files/spCas9%20Nuclease%20Protein_K108.pdf (13.07.2024)

283. Renata R.F. Candido, Alessandra L. Morassutti Carlos Graeff-Teixeira Timothy G. St. Pierre, Malcolm K. Jone (2018) Exploring structural and physical properties of schistosome eggs: Potential pathways for novel diagnostics? *Advances in Parasitology*, pp. 211–213.

284. Clement,K., Rees,H., Canver,M.C., Gehrke,J.M., Farouni,R., Hsu,J.Y., Cole,M.A., Liu,D.R., Joung,J.K., Bauer,D.E., *et al.* (2019) CRISPResso2 provides accurate and rapid genome editing sequence analysis. *Nat. Biotechnol.*, **37**, 224–226.

285. Park,J., Lim,K., Kim,J.-S. and Bae,S. (2017) Cas-analyzer: an online tool for assessing genome editing results using NGS data. *Bioinforma. Oxf. Engl.*, **33**, 286–288.

286. Yu,Y., Guo,Y., Tian,Q., Lan,Y., Yeh,H., Zhang,M., Tasan,I., Jain,S. and Zhao,H. (2020) An efficient gene knock-in strategy using 5'-modified double-stranded DNA donors with short homology arms. *Nat. Chem. Biol.*, **16**, 387–390.

287. Yu,Y., Guo,Y., Tian,Q., Lan,Y., Yeh,H., Zhang,M., Tasan,I., Jain,S. and Zhao,H. (2020) Publisher correction: An efficient gene knock-in strategy using 5'-modified double-stranded DNA donors with short homology arms. *Nat. Chem. Biol.*, **16**, 387–390.

288. Buddenborg,S.K., Tracey,A., Berger,D.J., Lu,Z., Doyle,S.R., Fu,B., Yang,F., Reid,A.J., Rodgers,F.H., Rinaldi,G., *et al.* (2021) Assembled chromosomes of the blood fluke *Schistosoma mansoni* provide insight into the evolution of its ZW sex-determination system. *bioRxiv.* 10.1101/2021.08.13.456314.

289. Lu,Z., Sessler,F., Holroyd,N., Hahnel,S., Quack,T., Berriman,M. and Grevelding,C.G. (2016) Schistosome sex matters: a deep view into gonad-specific and pairing-dependent transcriptomes reveals a complex gender interplay. *Sci. Rep.*, **6**, 31150.

290. Camacho,C., Coulouris,G., Avagyan,V., Ma,N., Papadopoulos,J., Bealer,K. and Madden,T.L. (2009) BLAST+: architecture and applications. *BMC Bioinformatics*, **10**, 421.

291. Lazar,M.A. (2003) Nuclear receptor corepressors. *Nucl. Recept. Signal.*, **1**, e001.

292. Sande,S. and Privalsky,M.L. (1996) Identification of TRACs (T3 receptor-associating cofactors), a family of cofactors that associate with, and modulate the activity of, nuclear hormone receptors. *Mol. Endocrinol. Baltim. Md*, **10**, 813–825.

293. Nanes Sarfati,D., Li,P., Tarashansky,A.J. and Wang,B. (2021) Single-cell deconstruction of stem-cell-driven schistosome development. *Trends Parasitol.*, **37**, 790–802.

294. Xu,Y., Greenberg,R.A., Schonbrunn,E. and Wang,P.J. (2017) Meiosis-specific proteins MEIOB and SPATA22 cooperatively associate with the single-stranded DNA-binding replication protein A complex and DNA double-strand breaks. *Biol. Reprod.*, **96**, 1096–1104.

295. Guo,R., Xu,Y., Leu,N.A., Zhang,L., Fuchs,S.Y., Ye,L. and Wang,P.J. (2020) The ssDNA-binding protein MEIOB acts as a dosage-sensitive regulator of meiotic recombination. *Nucleic Acids Res.*, **48**, 12219–12233.

296. Zou,Y., Liu,Y., Wu,X. and Shell,S.M. (2006) Functions of human replication protein A (RPA): from DNA replication to DNA damage and stress responses. *J. Cell. Physiol.*, **208**, 267–273.

297. Hanna,R. (2015) *Fasciola hepatica*: Histology of the reproductive organs and differential effects of Triclabendazole on drug-sensitive and drug-resistant fluke isolates and on flukes from selected field cases. *Pathogens*, **4**, 431–456.

298. Li,X., Weth,O., Haeberlein,S. and Grevelding,C.G. (2023) Molecular characterization of *Smtdc-1* and *Smddc-1* discloses roles as male-competence factors for the sexual maturation of *Schistosoma mansoni* females. *Front. Cell. Infect. Microbiol.*, **13**, 1173557.

299. Attenborough,T., Rawlinson,K.A., Soria,C.L.D., Ambridge,K., Sankaranarayanan,G., Graham,J., Cotton,J.A., Doyle,S.R., Rinaldi,G. and Berriman,M. (2024) A single-cell atlas of the miracidium larva of the human blood fluke *Schistosoma mansoni*: cell types, developmental pathways and tissue architecture. *bioRxiv.* 10.1101/2023.03.27.533868.

300. Anderson,L., Amaral,M.S., Beckedorff,F., Silva,L.F., Dazzani,B., Oliveira,K.C., Almeida,G.T., Gomes,M.R., Pires,D.S., Setubal,J.C., *et al.* (2015) *Schistosoma mansoni* egg, adult male and female comparative gene expression analysis and identification of novel genes by RNA-seq. *PLoS Negl. Trop. Dis.*, **9**, e0004334.

301. Wang,J. and Collins,J.J. (2016) Identification of new markers for the *Schistosoma mansoni* vitelline lineage. *Int. J. Parasitol.*, **46**, 405–410.

302. Huber,T.S. (2022) Charakterisierung der paarungsspezifisch transkribierten Histon-Acetyltransferase SmMyst4 und des nukleären Opsin Rezeptors in weiblichen *Schistosoma mansoni*. Master thesis. *Justus-Liebig-Univ. Giessen.*

303. von Reinersdorff,D., Green,M.H. and Green,J.B. (1998) Development of a compartmental model describing the dynamics of vitamin A metabolism in men. *Adv. Exp. Med. Biol.*, **445**, 207–223.

304. Ross,A.C. and Zolfaghari,R. (2004) Regulation of hepatic retinol metabolism: perspectives from studies on vitamin A status. *J. Nutr.*, **134**, 269S-275S.

305. Jetten,A.M., Anderson,K., Deas,M.A., Kagechika,H., Lotan,R., Rearick,J.I. and Shudo,K. (1987) New benzoic acid derivatives with retinoid activity: lack of direct correlation between biological activity and binding to cellular retinoic acid binding protein. *Cancer Res.*, **47**, 3523–3527.

306. Kim,A.-H., Lee,H.M., Kim,H.-S., Jeong,S.W., Jun,J.K. and Jang,J. (2024) CRISPR/Cas9-mediated knock-in of a fluorescent reporter into the target locus of interest in human pluripotent stem cells. *Methods X*, **13**.

307. Vesuna,F., Winnard,P. and Raman,V. (2005) Enhanced green fluorescent protein as an alternative control reporter to Renilla luciferase. *Anal. Biochem.*, **342**, 345–347.

308. Gao,S., Pan,M., Zheng,Y., Huang,Y., Zheng,Q., Sun,D., Lu,L., Tan,X., Tan,X., Lan,H., *et al.* (2016) Monomer/oligomer quasi-racemic protein crystallography. *J. Am. Chem. Soc.*, **138**, 14497–14502.

309. Silver,C.E., Cusumano,R.J., Fell,S.C. and Strauch,B. (1989) Replacement of upper esophagus: results with myocutaneous flap and with gastric transposition. *The Laryngoscope*, **99**, 819–821.

310. Butler,J.E.F. and Kadonaga,J.T. (2002) The RNA polymerase II core promoter: a key component in the regulation of gene expression. *Genes Dev.*, **16**, 2583–2592.

311. Godbey,W.T. (2021) Biotechnology and its applications: using cells to change the world. *Elsevier Science*.

312. Kozak,M. (1987) At least six nucleotides preceding the AUG initiator codon enhance translation in mammalian cells. *J. Mol. Biol.*, **196**, 947–950.

313. Gruber,A.R., Lorenz,R., Bernhart,S.H., Neuböck,R. and Hofacker,I.L. (2008) The Vienna RNA Websuite. *Nucleic Acids Res.*, **36**, W70–W74.

314. Cheng,S.W., Lynch,E.C., Leason,K.R., Court,D.L., Shapiro,B.A. and Friedman,D.I. (1991) Functional importance of sequence in the stem-loop of a transcription terminator. *Science*, **254**, 1205–1207.

315. Chaudhary,J. and Skinner,M.K. (1999) Basic helix-loop-helix proteins can act at the E-box within the serum response element of the c-fos promoter to influence hormone-induced promoter activation in Sertoli cells. *Mol. Endocrinol. Baltim. Md*, **13**, 774–786.

316. Hess,J., Angel,P. and Schorpp-Kistner,M. (2004) AP-1 subunits: quarrel and harmony among siblings. *J. Cell Sci.*, **117**, 5965–5973.

317. Ohtsuki,S., Levine,M. and Cai,H.N. (1998) Different core promoters possess distinct regulatory activities in the *Drosophila* embryo. *Genes Dev.*, **12**, 547–556.

318. Busek,S.U., Fantappie,M., Malaquias,L.C., Wilson,R.A., Corrêa-Oliveira,R. and Oliveira,G.C. (2002) Cis-acting elements, CArG-, E-, CCAAT- and TATA-boxes may be involved in sexually regulated gene transcription in *Schistosoma mansoni*. *Mem. Inst. Oswaldo Cruz*, **97 Suppl 1**, 85–90.

319. Juven-Gershon,T. and Kadonaga,J.T. (2010) Regulation of gene expression via the core promoter and the basal transcriptional machinery. *Dev. Biol.*, **339**, 225–229.

320. Au,W.-S., Lu,L., Yeung,C.-M., Liu,C.-C., Wong,O.G., Lai,L., Kung,H.-F. and Lin,M.C. (2008) Hepatocyte nuclear factor 1 binding element within the promoter of microsomal triglyceride transfer protein (MTTP) gene is crucial for MTTP basal expression and insulin responsiveness. *J. Mol. Endocrinol.*, **41**, 229–238.

321. Ohler,U., Liao,G., Niemann,H. and Rubin,G.M. (2002) Computational analysis of core promoters in the *Drosophila* genome. *Genome Biol.*, **3**, RESEARCH0087.

322. Arunsan,P., Ittiprasert,W., Smout,M.J., Cochran,C.J., Mann,V.H., Chaiyadet,S., Karinshak,S.E., Sripa,B., Young,N.D., Sotillo,J., *et al.* (2019) Programmed knockout mutation of liver fluke granulin attenuates virulence of infection-induced hepatobiliary morbidity. *eLife*, **8**, e41463.

323. Roquis,D., Taudt,A., Geyer,K.K., Padalino,G., Hoffmann,K.F., Holroyd,N., Berriman,M., Aliaga,B., Chaparro,C., Grunau,C., *et al.* (2018) Histone methylation changes are required for life cycle progression in the human parasite *Schistosoma mansoni. PLoS Pathog.*, **14**, e1007066.

324. Zu,Y., Huang,S., Lu,Y., Liu,X. and Wang,S. (2016) Size specific transfection to mammalian cells by micropillar array electroporation. *Sci. Rep.*, **6**, 38661.

325.Zu,Y., Huang,S., Liao,W.-C., Lu,Y. and Wang,S. (2014) Gold nanoparticles enhanced electroporation for mammalian cell transfection. *J. Biomed. Nanotechnol.*, **10**, 982–992.

326. Peterson,N.A., Hokke,C.H., Deelder,A.M. and Yoshino,T.P. (2009) Glycotope analysis in miracidia and primary sporocysts of *Schistosoma mansoni*: differential expression during the miracidium-to-sporocyst transformation. *Int. J. Parasitol.*, **39**, 1331–1344.

327. Meuleman,E.A., Holzmann,P.J. and Peet,R.C. (1980) The development of daughter sporocysts inside the mother sporocyst of *Schistosoma mansoni* with special reference to the ultrastructure of the body wall. *Z. Für Parasitenkd.*, **61**, 201–212.

328.Tóth,E., Varga,É., Kulcsár,P.I., Kocsis-Jutka,V., Krausz,S.L., Nyeste,A., Welker,Z., Huszár,K., Ligeti,Z., Tálas,A., *et al.* (2020) Improved LbCas12a variants with altered PAM specificities further broaden the genome targeting range of Cas12a nucleases. *Nucleic Acids Res.*, **48**, 3722–3733.

329. Tidman,R., Kanankege,K.S.T., Bangert,M. and Abela-Ridder,B. (2023) Global prevalence of 4 neglected foodborne trematodes targeted for control by WHO: A scoping review to highlight the gaps. *PLoS Negl. Trop. Dis.*, **17**, e0011073.

330. Marchant,J.S. (2024) Progress interrogating TRPMPZQ as the target of praziquantel. *PLoS Negl. Trop. Dis.*, **18**, e0011929.

331. Park,S.-K., Gunaratne,G.S., Chulkov,E.G., Moehring,F., McCusker,P., Dosa,P.I., Chan,J.D., Stucky,C.L. and Marchant,J.S. (2019) The anthelmintic drug praziquantel activates a schistosome transient receptor potential channel. *J. Biol. Chem.*, **294**, 18873–18880.

332. Park,S.-K. and Marchant,J.S. (2020) The journey to discovering a flatworm target of Praziquantel: a long TRP. *Trends Parasitol.*, **36**, 182–194.

333. Xiao,S., Catto,B.A. and Webster,L.T. (1985) Effects of praziquantel on different developmental stages of S*chistosoma mansoni in vitro* and *in vivo*. *J. Infect. Dis.*, **151**, 1130–1137.

334. Ernould,J.-C., Ba,K. and Sellin,B. (1999) Increase of intestinal schistosomiasis after praziquantel treatment in a *Schistosoma haematobium* and *Schistosoma mansoni* mixed focus. *Acta Trop.*, **73**, 143–152.

335. Vale,N., Gouveia,M.J., Rinaldi,G., Brindley,P.J., Gärtner,F. and Correia da Costa,J.M. (2017) Praziquantel for Schistosomiasis: single-drug metabolism revisited, mode of action, and resistance. *Antimicrob. Agents Chemother.*, **61**, 10.1128/aac.02582-16.

336. Alwan,S.N., Taylor,A.B., Rhodes,J., Tidwell,M., McHardy,S.F. and LoVerde,P.T. (2023) Oxamniquine derivatives overcome Praziquantel treatment limitations for schistosomiasis. *PLOS Pathog.*, **19**, e1011018.

337. Spangenberg,T. (2021) Alternatives to Praziquantel for the prevention and control of schistosomiasis. *ACS Infect. Dis.*, **7**, 939–942.

338. Rennar,G.A., Gallinger,T.L., Mäder,P., Lange-Grünweller,K., Haeberlein,S., Grünweller,A., Grevelding,C.G. and Schlitzer,M. (2022) Disulfiram and dithiocarbamate analogues demonstrate promising antischistosomal effects. *Eur. J. Med. Chem.*, **242**, 114641.

339. Moreira-Filho,J.T., Silva,A.C., Dantas,R.F., Gomes,B.F., Souza Neto,L.R., Brandao-Neto,J., Owens,R.J., Furnham,N., Neves,B.J., Silva-Junior,F.P., *et al.* (2021) Schistosomiasis drug discovery in the era of automation and artificial intelligence. *Front. Immunol.*, **12**.

340. Eyayu,T., Zeleke,A.J. and Worku,L. (2020) Current status and future prospects of protein vaccine candidates against *Schistosoma mansoni* infection. *Parasite Epidemiol. Control*, **11**, e00176.

341. Tukahebwa,E.M., Magnussen,P., Madsen,H., Kabatereine,N.B., Nuwaha,F., Wilson,S. and Vennervald,B.J. (2013) A very high infection intensity of *Schistosoma mansoni* in a Ugandan Lake Victoria fishing community is required for association with highly prevalent organ related morbidity. *PLoS Negl. Trop. Dis.*, **7**, e2268.

342. Andrus,P.S., Stothard,J.R. and Wade,C.M. (2023) Seasonal patterns of *Schistosoma mansoni* infection within *Biomphalaria* snails at the Ugandan shorelines of Lake Albert and Lake Victoria. *PLoS Negl. Trop. Dis.*, **17**, e0011506.

343. Chang,C.-C., Sung,L.-Y., Amano,T., Tian,X.C., Yang,X. and Nagy,Z.P. (2009) Nuclear transfer and oocyte cryopreservation. *Reprod. Fertil. Dev.*, **21**, 37–44.

344. Seydoux,G. and Braun,R.E. (2006) Pathway to totipotency: lessons from germ cells. *Cell*, **127**, 891–904.

345. Kanehisa,M., Furumichi,M., Sato,Y., Kawashima,M. and Ishiguro-Watanabe,M. (2023) KEGG for taxonomy-based analysis of pathways and genomes. *Nucleic Acids Res.*, **51**, D587–D592.

346. Kanehisa,M. and Goto,S. (2000) KEGG: Kyoto encyclopedia of genes and genomes. *Nucleic Acids Res.*, **28**, 27–30.

347. Lufkin,T., Lohnes,D., Mark,M., Dierich,A., Gorry,P., Gaub,M.P., LeMeur,M. and Chambon,P. (1993) High postnatal lethality and testis degeneration in retinoic acid receptor alpha mutant mice. *PNAS*, **90**, 7225–7229.

348. Kam,R.K.T., Deng,Y., Chen,Y. and Zhao,H. (2012) Retinoic acid synthesis and functions in early embryonic development. *Cell Biosci.*, **2**, 11.

349. Bowles,J., Knight,D., Smith,C., Wilhelm,D., Richman,J., Mamiya,S., Yashiro,K., Chawengsaksophak,K., Wilson,M.J., Rossant,J., *et al.* (2006) Retinoid signaling determines germ cell fate in mice. *Science*, **312**, 596–600.

350. Takahashi,Y., Moiseyev,G., Chen,Y., Farjo,K., Nikolaeva,O. and Ma,J.-X. (2011) An enzymatic mechanism for generating the precursor of endogenous 13-cis retinoic acid in the brain. *FEBS J.*, **278**, 973–987.

351. Li,X., Long,X., Xie,Y., Zeng,X., Chen,X. and Mo,Z. (2019) The roles of retinoic acid in the differentiation of spermatogonia and spermatogenic disorders. *Clin. Chim. Acta*, **497**, 54–60.

352. Fujiwara,S. (2006) Retinoids and nonvertebrate chordate development. *J. Neurobiol.*, **66**, 645–652.

353. Campo-Paysaa,F., Marlétaz,F., Laudet,V. and Schubert,M. (2008) Retinoic acid signaling in development: tissue-specific functions and evolutionary origins. *Genes.,* **46**, 640–656.

354. Janesick,A., Wu,S.C. and Blumberg,B. (2015) Retinoic acid signaling and neuronal differentiation. *CMLS*, **72**, 1559–1576.

355. Ermakova,O.N., Ermakov,A.M., Tiras,K.P. and Lednev,V.V. (2009) Retinoic acid as a regulator of planarian morphogenesis. *Ontogenez*, **40**, 449–455.

356. Sharma,S., Shen,T., Chitranshi,N., Gupta,V., Basavarajappa,D., Sarkar,S., Mirzaei,M., You,Y., Krezel,W., Graham,S.L., *et al.* (2022) Retinoid X Receptor: cellular and biochemical roles of nuclear receptor with a focus on neuropathological involvement. *Mol. Neurobiol.*, **59**, 2027–2050.

357. Bedo,G., Santisteban,P. and Aranda,A. (1989) Retinoic acid regulates growth hormone gene expression. *Nature*, **339**, 231–234.

358. Kim,C.H. (2018) Control of innate and adaptive lymphocytes by the RAR-retinoic acid axis. *Immune Netw.*, **18**, e1.

359. Meyskens,F.L., Goodman,G.E. and Alberts,D.S. (1985) 13-*cis*-retinoic acid: pharmacology, toxicology, and clinical applications for the prevention and treatment of human cancer. *Crit. Rev. Oncol. Hematol.*, **3**, 75–101.

360. Allenby,G., Bocquel,M.T., Saunders,M., Kazmer,S., Speck,J., Rosenberger,M., Lovey,A., Kastner,P., Grippo,J.F. and Chambon,P. (1993) Retinoic acid receptors and retinoid X receptors: interactions with endogenous retinoic acids. *PNAS.*, **90**, 30–34.

361. Fantappié,M.R., Furtado,D.R., Rumjanek,F.D. and Loverde,P.T. (2008) A unique nuclear receptor direct repeat 17 (DR17) is present within the upstream region of *Schistosoma mansoni* female-specific p14 gene. *Biochem. Biophys. Res. Commun.*, **371**, 689–693.

362. Marmorstein,R. and Zhou,M.-M. (2014) Writers and readers of histone acetylation: structure, mechanism, and inhibition. *Cold Spring Harb. Perspect. Biol.*, **6**, a018762.

363. Kraft,M., Cirstea,I.C., Voss,A.K., Thomas,T., Goehring,I., Sheikh,B.N., Gordon,L., Scott,H., Smyth,G.K., Ahmadian,M.R., *et al.* (2011) Disruption of the histone acetyltransferase MYST4 leads to a Noonan syndrome-like phenotype and hyperactivated MAPK signaling in humans and mice. *J. Clin. Invest.*, **121**, 3479–3491.

364. McGraw,S., Morin,G., Vigneault,C., Leclerc,P. and Sirard,M.-A. (2007) Investigation of MYST4 histone acetyltransferase and its involvement in mammalian gametogenesis. *BMC Dev. Biol.*, **7**, 123.

365. McGraw,S., Robert,C., Massicotte,L. and Sirard,M.-A. (2003) Quantification of histone acetyltransferase and histone deacetylase transcripts during early bovine embryo development. *Biol. Reprod.*, **68**, 383–389.

366. Champagne,N., Bertos,N.R., Pelletier,N., Wang,A.H., Vezmar,M., Yang,Y., Heng,H.H. and Yang,X.J. (1999) Identification of a human histone acetyltransferase related to monocytic leukemia zinc finger protein. *J. Biol. Chem.*, **274**, 28528–28536.

367. Thomas,T. and Voss,A.K. (2007) The diverse biological roles of MYST histone acetyltransferase family proteins. *Cell Cycle Georget. Tex*, **6**, 696–704.

368. Teletin,M., Vernet,N., Ghyselinck,N.B. and Mark,M. (2017) Roles of retinoic acid in germ cell differentiation. *Curr. Top. Dev. Biol.*, **125**, 191–225.

369. Li,H. and Clagett-Dame,M. (2009) Vitamin A deficiency blocks the initiation of meiosis of germ cells in the developing rat ovary in *vivo*. *Biol. Reprod.*, **81**, 996–1001.

370. Wu,W. and LoVerde,P.T. (2019) Nuclear hormone receptors in parasitic Platyhelminths. *Mol. Biochem. Parasitol.*, **233**, 111218.

371. Joseph,P., Everts,H. and Gumienny,T. (2021) Establishing *C. elegans* as a model to study the function of Vitamin A metabolism. *TWU Stud. J.*, **1**, 16–30.

372. Wu,F., Wei,H., Chen,X., Du,Z., Huang,Y., Shi,H., Yang,Y., Du,A. and Ma,G. (2023) Fatty acid- and retinol-binding protein 6 does not control worm fatty acid content in *Caenorhabditis elegans* but might play a role in *Haemonchus contortus* parasitism. *Parasit. Vectors*, **16**, 230.

373. Coutu,D.L. and Galipeau,J. (2011) Roles of FGF signaling in stem cell self-renewal, senescence and aging. *Aging*, **3**, 920–933.

374. Haidar,R., Henkler,F., Kugler,J., Rosin,A., Genkinger,D., Laux,P. and Luch,A. (2021) The role of DNA-binding and ARNT dimerization on the nucleo-cytoplasmic translocation of the aryl hydrocarbon receptor. *Sci. Rep.*, **11**, 18194.

375. Khorram,O., Garthwaite,M. and Golos,T. (2002) Uterine and ovarian aryl hydrocarbon receptor (AHR) and aryl hydrocarbon receptor nuclear translocator (ARNT) mRNA expression in benign and malignant gynaecological conditions. *Mol. Hum. Reprod.*, **8**, 75–80.

376. Shankar,P. and Villeneuve,D.L. (2023) AOP Report: Aryl hydrocarbon receptor activation leads to early–life stage mortality via Sox9 repression-induced craniofacial and cardiac malformations. *Environ. Toxicol. Chem.*, **42**, 2063–2077.

377. Borycki,A., Brown,A.M. and Emerson,C.P. (2000) Shh and Wnt signaling pathways converge to control Gli gene activation in avian somites. *Dev. Camb. Engl.*, **127**, 2075–2087.

378. Mullor,J.L., Dahmane,N., Sun,T. and i Altaba,A.R. (2001) Wnt signals are targets and mediators of Gli function. *Curr. Biol.*, **11**, 769–773.

379. Le Rolle,M., Massa,F., Siggers,P., Turchi,L., Loubat,A., Koo,B.-K., Clevers,H., Greenfield,A., Schedl,A., Chaboissier,M.-C., *et al.* (2021) Arrest of WNT/β-catenin signaling enables the transition from pluripotent to differentiated germ cells in mouse ovaries. *PNAS.*, **118**, e2023376118.

380. von Toerne,C., Bedke,J., Safi,S., Porubsky,S., Gretz,N., Loewe,R., Nelson,P.J. and Gröne,H.-J. (2012) Modulation of Wnt and Hedgehog signaling pathways is linked to retinoic acid-induced amelioration of chronic allograft dysfunction. *Am. J. Transplant.*, **12**, 55–68.

381. Marklund,M., Sjödal,M., Beehler,B.C., Jessell,T.M., Edlund,T. and Gunhaga,L. (2004) Retinoic acid signalling specifies intermediate character in the developing telencephalon. *Development*, **131**, 4323–4332.

382. Mikoláš,P., Kollárová,J., Šebková,K., Saudek,V., Yilma,P., Kostrouchová,M., Krause,M.W., Kostrouch,Z. and Kostrouchová,M. (2013) GEI-8, a homologue of vertebrate nuclear receptor corepressor NCoR/SMRT, regulates gonad development and neuronal functions in *Caenorhabditis elegans*. *PLOS ONE*, **8**, e58462.

383. Jepsen,K., Gleiberman,A.S., Shi,C., Simon,D.I. and Rosenfeld,M.G. (2008) Cooperative regulation in development by SMRT and FOXP1. *Genes Dev.*, **22**, 740–745.

384. Khan,U.W. and Newmark,P.A. (2022) Somatic regulation of female germ cell regeneration and development in planarians. *Cell Rep.*, **38**, 110525.

385. Fan,J. and Pavletich,N.P. (2012) Structure and conformational change of a replication protein A heterotrimer bound to ssDNA. *Genes Dev.*, **26**, 2337–2347.

386. Shimada,R. and Ishiguro,K.-I. (2023) Cell cycle regulation for meiosis in mammalian germ cells. *J. Reprod. Dev.*, **69**, 139–146.

387. Luo,M., Yang,F., Leu,N.A., Landaiche,J., Handel,M.A., Benavente,R., La Salle,S. and Wang,P.J. (2013) MEIOB exhibits single-stranded DNA-binding and exonuclease activities and is essential for meiotic recombination. *Nat. Commun.*, **4**, 2788.

388. Souquet,B., Abby,E., Hervé,R., Finsterbusch,F., Tourpin,S., Le Bouffant,R., Duquenne,C., Messiaen,S., Martini,E., Bernardino-Sgherri,J., *et al.* (2013) MEIOB targets single-strand DNA and is necessary for meiotic recombination. *PLoS Genet.*, **9**, e1003784.

389. Dedukh,D., da Cruz,I., Kneitz,S., Marta,A., Ormanns,J., Tichopád,T., Lu,Y., Alsheimer,M., Janko,K. and Schartl,M. (2022) Achiasmatic meiosis in the unisexual Amazon molly, *Poecilia formosa. Chromosome Res.*, **30**, 443–457.

390. Wang,Y., Liu,L., Tan,C., Meng,G., Meng,L., Nie,H., Du,J., Lu,G.-X., Lin,G., He,W.-B., *et al.* (2022) Novel MEIOB variants cause primary ovarian insufficiency and non-obstructive azoospermia. *Front. Genet.*, **13**.

391.Lawton,S.P., Hirai,H., Ironside,J.E., Johnston,D.A. and Rollinson,D. (2011) Genomes and geography: genomic insights into the evolution and phylogeography of the genus *Schistosoma*. *Parasit. Vectors*, **4**, 131.

392. Oelkrug,R., Harder,L., Pedaran,M., Hoffmann,A., Kolms,B., Inderhees,J., Gachkar,S., Resch,J., Johann,K., Jöhren,O., *et al.* (2023) Maternal thyroid hormone receptor β activation in mice sparks brown fat thermogenesis in the offspring. *Nat. Commun.*, **14**, 6742.

393. Astapova,I. (2016) Role of co-regulators in metabolic and transcriptional actions of thyroid hormone. *J. Mol. Endocrinol.*, **56**, 73–97.

394. Rodrigues,M.S., Tovo-Neto,A., Rosa,I.F., Doretto,L.B., Fallah,H.P., Habibi,H.R. and Nóbrega,R.H. (2022) Thyroid hormones deficiency impairs male germ cell development: A cross talk between hypothalamic-pituitary-thyroid, and -gonadal axes in zebrafish. *Front. Cell Dev. Biol.*, **10**.

395. Vasudevan,N., Ogawa,S. and Pfaff,D. (2002) Estrogen and thyroid hormone receptor interactions: physiological flexibility by molecular specificity. *Physiol. Rev.*, **82**, 923–944.

396. Gao,Y., Lee,W.M. and Cheng,C.Y. (2014) Thyroid hormone function in the rat testis. *Front. Endocrinol.*, **5**, 188.

397. Verma,R. and Haldar,C. (2016) Photoperiodic modulation of thyroid hormone receptor (TR-α), deiodinase-2 (Dio-2) and glucose transporters (GLUT 1 and GLUT 4) expression in testis of adult golden hamster, *Mesocricetus auratus*. *J. Photochem. Photobiol. B*, **165**, 351–358.

398. Zhou,J., Chen,P., Wang,H., Liu,H., Li,Y., Zhang,Y., Wu,Y., Paek,C., Sun,Z., Lei,J., *et al.* (2022) Cas12a variants designed for lower genome-wide off-target effect through stringent PAM recognition. *Mol. Ther.*, **30**, 244–255.

399. Ma,Y., Shen,S., Yan,Y., Zhang,S., Liu,S., Tang,Z., Yu,J., Ma,M., Niu,Z., Li,Z., *et al.* (2023) Adipocyte thyroid hormone β receptor–mediated hormone action fine-tunes intracellular glucose and lipid metabolism and systemic homeostasis. *Diabetes*, **72**, 562–574.

400. Zekri,Y., Guyot,R. and Flamant,F. (2022) An atlas of thyroid hormone receptors' target genes in mouse tissues. *Int J Mol Sci.* 28;23(19):11444.

401. Lin,C., Li,N., Chang,H., Shen,Y., Li,Z., Wei,W., Chen,H., Lu,H., Ji,J. and Liu,N. (2020) Dual effects of thyroid hormone on neurons and neurogenesis in traumatic brain injury. *Cell Death Dis.*, **11**, 1–13.

402. Lee,E.-H., Kim,S.-M., Kim,C.-H., Pagire,S.H., Pagire,H.S., Chung,H.Y., Ahn,J.H. and Park,C.-H. (2019) Dopamine neuron induction and the neuroprotective effects of thyroid hormone derivatives. *Sci. Rep.*, **9**, 13659.

403. Giannocco,G., Kizys,M.M.L., Maciel,R.M. and de Souza,J.S. (2021) Thyroid hormone, gene expression, and central nervous system: Where we are. *Semin. Cell Dev. Biol.*, **114**, 47–56.

404. Bertin,B., Caby,S., Oger,F., Sasorith,S., Wurtz,J.-M. and Pierce,R.J. (2005) The monomeric orphan nuclear receptor *Schistosoma mansoni* Ftz-F1 dimerizes specifically and functionally with the schistosome RXR homologue, SmRXR1. *Biochem. Biophys. Res. Commun.*, **327**, 1072–1082.

405. Brown,J.C. (2020) Involvement of promoter/enhancers in a feedback loop to regulate human gene expression. *Heliyon*, **6**, e04934.

406. Gao,H., Li,Y. and Chen,X. (2022) Interactions between nuclear receptors glucocorticoid receptor α and peroxisome proliferator–activated receptor α form a negative feedback loop. *Rev. Endocr. Metab. Disord.*, **23**, 893–903.

407. Penvose,A., Keenan,J.L., Bray,D., Ramlall,V. and Siggers,T. (2019) Comprehensive study of nuclear receptor DNA binding provides a revised framework for understanding receptor specificity. *Nat. Commun.*, **10**, 2514.

408. Li,C., Schwabe,J.W., Banayo,E. and Evans,R.M. (1997) Coexpression of nuclear receptor partners increases their solubility and biological activities. *PNAS*, **94**, 2278–2283.

409. MacTavish,B., Zhu,D., Shang,J., Shao,Q., Yang,Z.J., Kamenecka,T.M. and Kojetin,D.J. (2024) Ligand efficacy shifts a nuclear receptor conformational ensemble between transcriptionally active and repressive states. *bioRxiv*, 10.1101/2024.04.23.590805.

410. Lazar,M.A. (2003) Thyroid hormone action: a binding contract. *J. Clin. Invest.*, **112**, 497–499.

411. Mullur,R., Liu,Y.-Y. and Brent,G.A. (2014) Thyroid Hormone Regulation of Metabolism. *Physiol. Rev.*, **94**, 355–382.

412. Saule,P., Vicogne,J., Delacre,M., Macia,L., Tailleux,A., Dissous,C., Auriault,C. and Wolowczuk,I. (2005) Host glucose metabolism mediates T4 and IL-7 action on *Schistosoma mansoni* development. *J. Parasitol.*, **91**, 737–744.

413. Saule,P., Adriaenssens,E., Delacre,M., Chassande,O., Bossu,M., Auriault,C. and Wolowczuk,I. (2002) Early variations of host thyroxine and interleukin-7 favor *Schistosoma mansoni* development. *J. Parasitol.*, **88**, 849–855.

414. Stitz,M., Chaparro,C., Lu,Z., Olzog,V.J., Weinberg,C.E., Blom,J., Goesmann,A., Grunau,C. and Grevelding,C.G. (2021) Satellite-like W-elements: repetitive, transcribed, and putative mobile genetic factors with potential roles for biology and evolution of *Schistosoma mansoni. Genome Biol. Evol.*, **13**, evab204.

415. Wang,X., Tang,Y., Lu,J., Shao,Y., Qin,X., Li,Y., Wang,L., Li,D. and Liu,M. (2016) Characterization of novel cytochrome P450 2E1 knockout rat model generated by CRISPR/Cas9. *Biochem. Pharmacol.*, **105**, 80–90.

416. You,H., Mayer,J.U., Johnston,R.L., Sivakumaran,H., Ranasinghe,S., Rivera,V., Kondrashova,O., Koufariotis,L.T., Du,X., Driguez,P., *et al.* (2021) CRISPR/Cas9-mediated genome editing of *Schistosoma mansoni* acetylcholinesterase. *FASEB J.*, **35**, e21205.

417. Pan,S.C. (1980) The fine structure of the miracidium of *Schistosoma mansoni*. *J. Invertebr. Pathol.*, **36**, 307–372.

418. Demaree,R. and Hillyer,G.V. (1981) *Schistosoma* species: Transmission electron microscopy of the circumoval immune precipitin reaction on eggs. *Exp. Parasitol.*, **52**, 77–85.

419. Cao Han-Min, Wang Yun-Fang, and Long So (1982) A study of ultrastructure of egg shell of *Schistosoma japonicum*: I. Transmission electron microscopic observation of *S. japonicum* Egg. *Ann. Parasitol. Hum. Comparée*, **57**, 345–352.

420. Kazemian,P., Yu,S.-Y., Thomson,S.B., Birkenshaw,A., Leavitt,B.R. and Ross,C.J.D. (2022) Lipid-nanoparticle-based delivery of CRISPR/Cas9 genome-editing components. *Mol. Pharm.*, **19**, 1669–1686.

421. Bhandawat,A., Sharma,V., Rishi,V. and K Roy,J. (2020) Biolistic delivery of programmable nuclease (CRISPR/Cas9) in bread wheat. *Methods Mol. Biol. Clifton NJ*, **2124**, 309–329.

422. Hamada,H., Liu,Y., Nagira,Y., Miki,R., Taoka,N. and Imai,R. (2018) Biolistic-delivery-based transient CRISPR/Cas9 expression enables in planta genome editing in wheat. *Sci. Rep.*, **8**, 14422.

423. Heyers,O., Walduck,A.K., Brindley,P.J., Bleiss,W., Lucius,R., Dorbic,T., Wittig,B. and Kalinna,B.H. (2003) *Schistosoma mansoni* miracidia transformed by particle bombardment infect *Biomphalaria glabrata* snails and develop into transgenic sporocysts. *Exp. Parasitol.*, **105**, 174–178.

424. Lu,B., Javidi-Parsijani,P., Makani,V., Mehraein-Ghomi,F., Sarhan,W.M., Sun,D., Yoo,K.W., Atala,Z.P., Lyu,P. and Atala,A. (2019) Delivering SaCas9 mRNA by lentivirus-like bionanoparticles for transient expression and efficient genome editing. *Nucleic Acids Res.*, **47**, e44.

425. Kuppers,D.A., Linton,J., Ortiz Espinosa,S., McKenna,K.M., Rongvaux,A., Paddison,P.J. (2023) Gene knock-outs in human CD34+ hematopoietic stem and progenitor cells and in the human immune system of mice. *PLoS One*. 28;18(6):e0287052.

426. Mazurov,D., Ramadan,L. and Kruglova,N. (2023) Packaging and uncoating of CRISPR/Cas ribonucleoproteins for efficient gene editing with viral and non-viral extracellular nanoparticles. *Viruses*, **15**, 690.

427. Du,Y., Liu,Y., Hu,J., Peng,X. and Liu,Z. (2023) CRISPR/Cas9 systems: delivery technologies and biomedical applications. *Asian J. Pharm. Sci.*, **18**, 100854.

428. Krug,J., Perner,B., Albertz,C., Mörl,H., Hopfenmüller,V.L. and Englert,C. (2023) Generation of a transparent killifish line through multiplex CRISPR/Cas9-mediated gene inactivation. *eLife*, **12**, e81549.

429. Khan,S. and Sallard,E. (2023) Current and prospective applications of CRISPR-Cas12a in pluricellular organisms. *Mol. Biotechnol.*, **65**, 196–205.

430. Moreno-Mateos,M.A., Fernandez,J.P., Rouet,R., Vejnar,C.E., Lane,M.A., Mis,E., Khokha,M.K., Doudna,J.A. and Giraldez,A.J. (2017) CRISPR-Cpf1 mediates efficient homology-directed repair and temperature-controlled genome editing. *Nat. Commun.*, **8**, 2024.

431. Mao,Z., Bozzella,M., Seluanov,A. and Gorbunova,V. (2008) DNA repair by nonhomologous end joining and homologous recombination during cell cycle in human cells. *Cell Cycle Georget. Tex*, **7**, 2902.

432. Byrne,S.M., Ortiz,L., Mali,P., Aach,J. and Church,G.M. (2015) Multi-kilobase homozygous targeted gene replacement in human induced pluripotent stem cells. *Nucleic Acids Res.*, **43**, e21.

433. Zhang,J.-P., Li,X.-L., Li,G.-H., Chen,W., Arakaki,C., Botimer,G.D., Baylink,D., Zhang,L., Wen,W., Fu,Y.-W., *et al.* (2017) Efficient precise knockin with a double cut HDR donor after CRISPR/Cas9-mediated double-stranded DNA cleavage. *Genome Biol.*, **18**, 35.

434. Sakuma,T., Takenaga,M., Kawabe,Y., Nakamura,T., Kamihira,M. and Yamamoto,T. (2015) Homologous recombination-independent large gene cassette knock-in in CHO cells using TALEN and MMEJ-directed donor plasmids. *Int. J. Mol. Sci.*, **16**, 23849–23866.

435. Sakuma,T., Nakade,S., Sakane,Y., Suzuki,K.-I.T. and Yamamoto,T. (2016) MMEJ-assisted gene knock-in using TALENs and CRISPR-Cas9 with the PITCh systems. *Nat. Protoc.*, **11**, 118–133.

436. Li,G., Zhang,X., Wang,H., Mo,J., Zhong,C., Shi,J., Zhou,R., Li,Z., Yang,H., Wu,Z., *et al.* (2019) CRISPR/Cas9-mediated integration of large transgene into Pig CEP112 locus. *GenesGenomesGenetics*, **10**, 467–473.

437. Lee,S., Kim,S.M. and Lee,R.T. (2013) Thioredoxin and thioredoxin target proteins: From molecular mechanisms to functional significance. *Antioxid. Redox Signal.*, **18**, 1165–1207.

438. Sugama,K., Suzuki,K., Yoshitani,K., Shiraishi,K., Miura,S., Yoshioka,H., Mori,Y. and Kometani,T. (2015) Changes of thioredoxin, oxidative stress markers, inflammation and muscle/renal damage following intensive endurance exercise. *Exerc. Immunol. Rev.*, **21**, 130–142.

439. Lin,S.J. and Culotta,V.C. (1995) The ATX1 gene of *Saccharomyces cerevisiae* encodes a small metal homeostasis factor that protects cells against reactive oxygen toxicity. *Proc. Natl. Acad. Sci. U. S. A.*, **92**, 3784–3788.

440. Cobo,F. (2014) Chapter 8: Schistosomiasis (bilharziasis). In *Imported Infectious Diseases. Woodhead Publishing*, p. 115–126.

441. Huang,J., Rowe,D., Subedi,P., Zhang,W., Suelter,T., Valent,B. and Cook,D.E. (2022) CRISPR-Cas12a induced DNA double-strand breaks are repaired by multiple pathways with different mutation profiles in *Magnaporthe oryzae*. *Nat. Commun.*, **13**, 7168.

442. Kirchhoff,J., Schiermeyer,A., Schneider,K., Fischer,R., Ainley,W.M., Webb,S.R., Schinkel,H. and Schillberg,S. (2020) Gene expression variability between randomly and targeted transgene integration events in tobacco suspension cell lines. *Plant Biotechnol. Rep.*, **14**, 451–458.

443. Stevenson,Z.C., Moerdyk-Schauwecker,M.J., Jamison,B. and Phillips,P.C. (2020) Rapid self-selecting and clone-free integration of transgenes into engineered CRISPR safe harbor locations in *Caenorhabditis elegans*. *G3 (Bethesda)*, **10**, 3775–3782.

444. Riesenberg,S., Kanis,P., Macak,D., Wollny,D., Düsterhöft,D., Kowalewski,J., Helmbrecht,N., Maricic,T. and Pääbo,S. (2023) Efficient high-precision homology-directed repair-dependent genome editing by HDRobust. *Nat. Methods*, **20**, 1388–1399.

445. Straume,A.H., Kjærner-Semb,E., Ove Skaftnesmo,K., Güralp,H., Kleppe,L., Wargelius,A. and Edvardsen,R.B. (2020) Indel locations are determined by template polarity in highly efficient in vivo CRISPR/Cas9-mediated HDR in Atlantic salmon. *Sci. Rep.*, **10**, 409.

446. Anderson,R.A., Kato,S. and Camerini-Otero,R.D. (1984) A pattern of partially homologous recombination in mouse L cells. *PNAS.*, **81**, 206–210.

447. Wijsman,E.M. (2005) Mendel's Laws. In *Encyclopedia of Biostatistics*.

448. You,H., Jones,M.K., Whitworth,D.J. and McManus,D.P. (2021) Innovations and advances in schistosome stem cell research. *Front. Immunol.*, **12**, 599014.

449. Diaz Soria,C.L., Attenborough,T., Lu,Z., Fontenla,S., Graham,J., Hall,C., Thompson,S., Andrews,T.G.R., Rawlinson,K.A., Berriman,M., *et al.* (2024) Single-cell transcriptomics of the human parasite *Schistosoma mansoni* first intra-molluscan stage reveals tentative tegumental and stem-cell regulators. *Sci. Rep.*, **14**, 5974.

450. Clarke,D.N., Kane,A., Perillo,M., Lowe,C.J. and Swartz,S.Z. (2024) VitelloTag: a tool for high-throughput cargo delivery into oocytes. *Dev. Camb. Engl.*, 10.1242/dev.202857.

451. Lebouvier,M., Miramón-Puértolas,P. and Steinmetz,P.R.H. (2022) Evolutionarily conserved aspects of animal nutrient uptake and transport in sea anemone vitellogenesis. *Curr. Biol.*, **32**, 4620-4630.e5.

452. Noman,M.A.A., Kyzer,J.L., Chung,S.S.W., Wolgemuth,D.J. and Georg,G.I. (2020) Retinoic acid receptor antagonists for male contraception: current status. *Biol. Reprod.*, **103**, 390–399.

453. Hong,S.-H., Castro,G., Wang,D., Nofsinger,R., Kane,M., Folias,A., Atkins,A.R., Yu,R.T., Napoli,J.L., Sassone-Corsi,P., *et al.* (2024) Targeting nuclear receptor corepressors for reversible male contraception. *PNAS.*, **121**, e2320129121.

454. Balbach,M., Rossetti,T., Ferreira,J., Ghanem,L., Ritagliati,C., Myers,R.W., Huggins,D.J., Steegborn,C., Miranda,I.C., Meinke,P.T., *et al.* (2023) On-demand male contraception via acute inhibition of soluble adenylyl cyclase. *Nat. Commun.*, **14**, 637.

455. Zhao,Y., Deng,S., Li,C., Cao,J., Wu,A., Chen,M., Ma,X., Wu,S. and Lian,Z. (2024) The role of retinoic acid in spermatogenesis and its application in male reproduction. *Cells*, **13**, 1092.

456. Quack,T., Knobloch,J., Beckmann,S., Vicogne,J., Dissous,C. and Grevelding,C.G. (2009) The formin-homology protein SmDia interacts with the Src kinase SmTK and the GTPase SmRho1 in the gonads of *Schistosoma mansoni*. *PloS One*, **4**, e6998.

457. Paguio,A., Stecha,P., Wood,K.V. and Fan,F. (2010) Improved dual-luciferase reporter assays for nuclear receptors. *Curr. Chem. Genomics*, **4**, 43–49.

458. Stefanić,S., Dvořák,J., Horn,M., Braschi,S., Sojka,D., Ruelas,D.S., Suzuki,B., Lim,K.-C., Hopkins,S.D., McKerrow,J.H., *et al.* (2010) RNA interference in *Schistosoma mansoni* schistosomula: selectivity, sensitivity and operation for larger-scale screening. *PLoS Negl. Trop. Dis.*, **4**, e850.

459. Done,B., Khatri,P., Done,A. and Draghici,S. (2010) Predicting novel human gene ontology annotations using semantic analysis. *IEEE ACM Trans. Comput. Biol. Bioinform.,* **7**, 91–99.

460. Pagni,M., Ioannidis,V., Cerutti,L., Zahn-Zabal,M., Jongeneel,C.V., Hau,J., Martin,O., Kuznetsov,D. and Falquet,L. (2007) MyHits: improvements to an interactive resource for analyzing protein sequences. *Nucleic Acids Res.*, **35**, W433–W437.

461. Sigrist,C.J.A., de Castro,E., Cerutti,L., Cuche,B.A., Hulo,N., Bridge,A., Bougueleret,L. and Xenarios,I. (2013) New and continuing developments at PROSITE. *Nucleic Acids Res.*, **41**, D344-347.

462. Skinner,D.E., Rinaldi,G., Suttiprapa,S., Mann,V.H., Smircich,P., Cogswell,A.A., Williams,D.L. and Brindley,P.J. (2012) Vasa-Like DEAD-Box RNA helicases of *Schistosoma mansoni. PLoS Negl. Trop. Dis.*, **6**, e1686.

463. Long,T., Cailliau,K., Beckmann,S., Browaeys,E., Trolet,J., Grevelding,C.G. and Dissous,C. (2010) *Schistosoma mansoni* Polo-like kinase 1: A mitotic kinase with key functions in parasite reproduction. *Int. J. Parasitol.*, **40**, 1075–1086.

464. Long T, Vanderstraete M, Cailliau K, Morel M, Lescuyer A, Gouignard N, Grevelding CG, Browaeys E, Dissous C. 2012- SmSak, the second Polo-like kinase of the helminth parasite *Schistosoma mansoni*: conserved and unexpected roles in meiosis. *PLoS One*. 7(6):e40045. - Google Suche.

465. Kim,M.H., Yuan,X., Okumura,S. and Ishikawa,F. (2002) Successful inactivation of endogenous *oct-3/4* and *c-mos* genes in mouse preimplantation embryos and oocytes using short interfering RNAs. *Biochem. Biophys. Res. Commun.*, **296**, 1372–1377.

466. Roberts,S.B., Segil,N. and Heintz,N. (1991) Differential phosphorylation of the transcription factor Oct1 during the cell cycle. *Science*, **253**, 1022–1026.

467. Julaton,V.T.A. and Reijo Pera,R.A. (2011) NANOS3 function in human germ cell development. *Hum. Mol. Genet.*, **20**, 2238–2250.

468. Wang,X. and Chamberlin,H.M. (2002) Multiple regulatory changes contribute to the evolution of the *Caenorhabditis lin-48 ovo* gene. *Genes Dev.*, **16**, 2345–2349.

469. D'Aurora,M., Budani,M.C., Franchi,S., Sarra,A., Stuppia,L., Tiboni,G.M. and Gatta,V. (2019) Dynactin pathway-related gene expression is altered by aging, but not by vitrification. *Reprod. Toxicol. Elmsford N*, **88**, 48–55.

470. Brandt,J.N. and Kim,Y. (2021) Targeting Polo-like kinase in space and time during *C. elegans* meiosis. *Cell Cycle*, **20**, 1519–1526.

471. Gordon,S.G., Kursel,L.E., Xu,K. and Rog,O. (2021) Synaptonemal Complex dimerization regulates chromosome alignment and crossover patterning in meiosis. *PLoS Genet.*, **17**, e1009205.

472. O'Neil,N. and Rose,A. (2006) DNA repair. *WormBook Online Rev. C elegans Biol.*, 10.1895/wormbook.1.54.1.

473. Lemmens,B.B.L.G. and Tijsterman,M. (2011) DNA double-strand break repair in *Caenorhabditis elegans*. *Chromosoma*, **120**, 1–21.

474. Nepal,M., Che,R., Ma,C., Zhang,J. and Fei,P. (2017) FANCD2 and DNA damage. *Int. J. Mol. Sci.*, **18**, 1804.

475. Wu,Q., Feng,Z. and Hu,W. (2021) Reduction of autofluorescence in whole adult worms of *Schistosoma japonicum* for immunofluorescence assay. *Parasit. Vectors*, **14**, 532.

7 Appendix

7.1 Supplemental Figures

Supplementary Figure S1. Treatment of schistosome couples with non-schistosomal control dsRNA showed no alteration of the ovary structure.

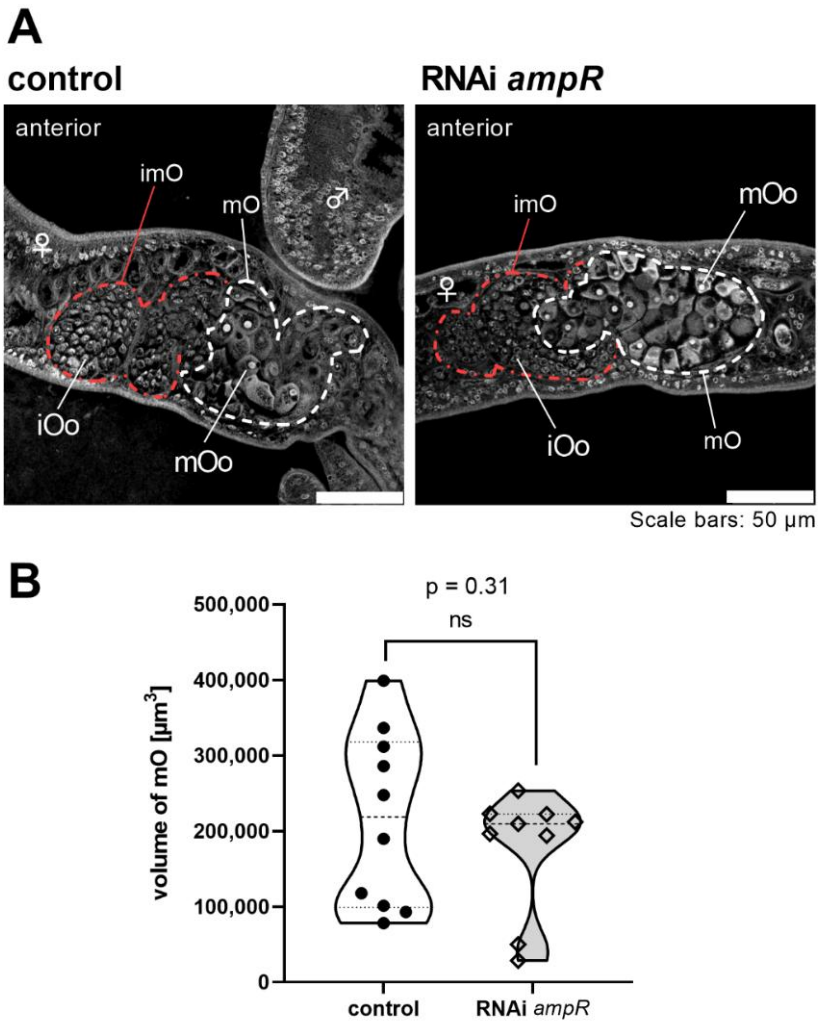

Suppl. Fig. S1.

Results of RNAi experiments using dsRNAs against Sm*rar* and *ampR* (ampicillin resistance gene of *E. coli*) as irrelevant dsRNA control (152), respectively. In each case, worms were treated with 30 µg/mL dsRNA for 22 d. **A**, CLSM showed no obvious differences in ovary morphology between DEPC-treated control worms and *ampR* dsRNA-treated worms. **B**, The volume of the ovary was determined by comparative Z-stack analyses post RNAi at d 22. No effect on the volume of the posterior, mature part of the ovary was observed in the *ampR* RNAi group. The violin plot indicates the range between the minimum and maximum values, with the dashed lines representing the quartiles and the solid line representing the median. The ovaries of worms from three biological replicates were analyzed. The graph shows the pooled results of all analyzed ovaries. Each individual point represents the volume of a single ovary. Abbreviations; iOo, oogonia; imO, immature part of the ovary; mOo, mature oocyte; mO, mature part of the ovary. *P<0.05, **P<0.01, ***P<0.001 by t-test. n=3

Supplemental Figure S2. Treatment with a non-schistosomal dsRNA showed no effects on ovary structure or oocyte differentiation.

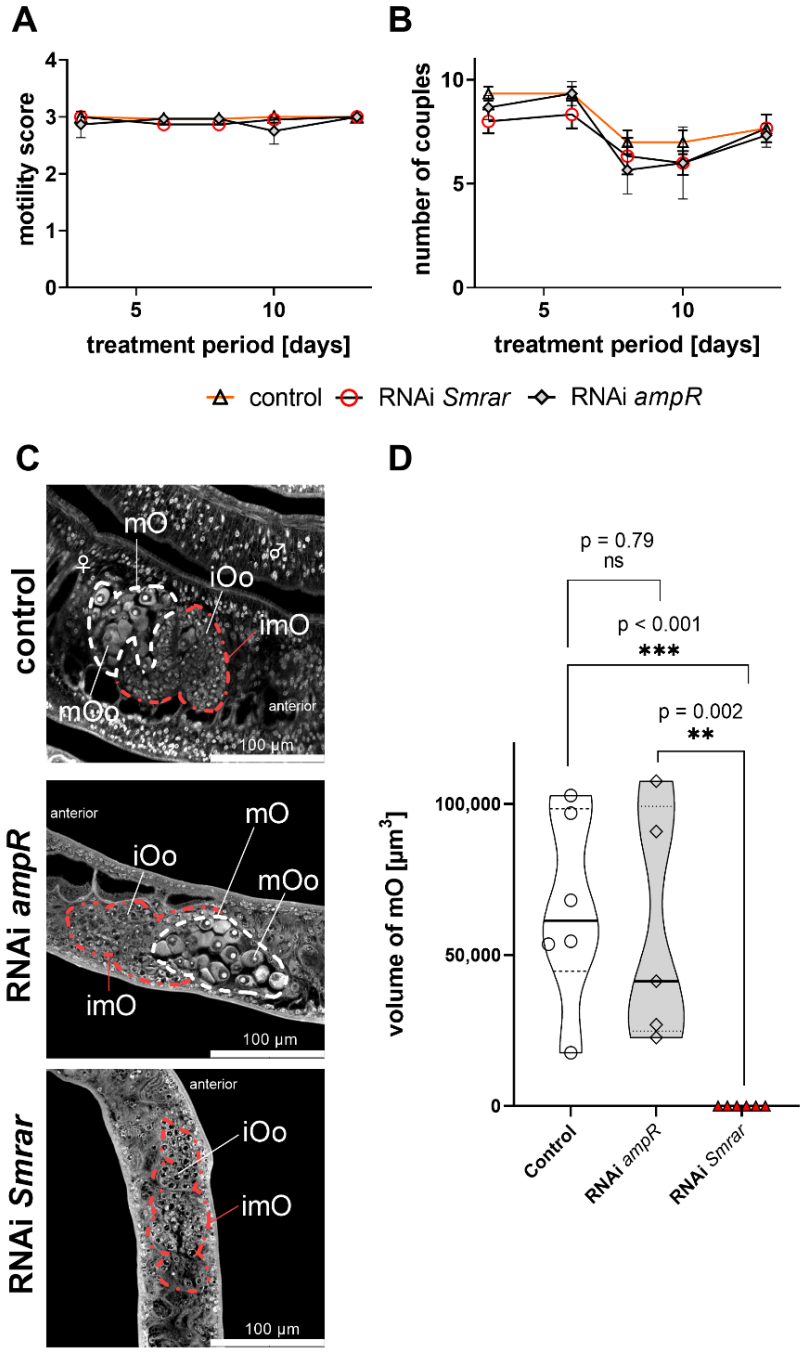

Suppl. Fig. S2.

Results of RNAi experiments using dsRNAs against Sm*rar* or *ampR* (ampicillin resistance gene of *E. coli*) as irrelevant dsRNA control (152), respectively. Physiological parameters such as motility and pairing stability were monitored (Sm*rar*-specific dsRNA, red circles; *ampR* control dsRNA, grey diamonds). Worms treated with DEPC water, but no dsRNA, served as untreated control (orange triangles). **A-B**, RNAi treatment showed no effect on motility (**A**, motility scores: 0 (no motility) to 4

(hyperactive motility). Couples remained stable during the experimental period (**B**). **C**, CLSM showed no obvious differences in ovary morphology between DMSO-treated control worms and *ampR* dsRNA-treated worms, whereas Sm*rar* RNAi showed strong effects on the ovary structure and oocyte differentiation, as described in the main text (4.1.5). **D**, The volume of the mature ovary was determined by comparative Z-stack analyses. No effect on the volume of the posterior, mature part of the ovary was observed in the *ampR* dsRNA-treated control group. The violin plot indicates the range between the minimum and maximum values, with the dashed lines representing the quartiles and the solid line representing the median. The ovaries of worms from three biological replicates were analyzed. The graph shows the pooled results of all analyzed ovaries.Each individual point represents the volume of a single ovary. Abbreviations; iOo, oogonia; imO, immature part of the ovary; mOo, mature oocyte; mO, mature part of the ovary. *P<0.05, **P<0.01, ***P<0.001 by t-test. n=3.

Supplemental Figure S3. Protein structure modelling and alignment analysis of SmMEIOB.

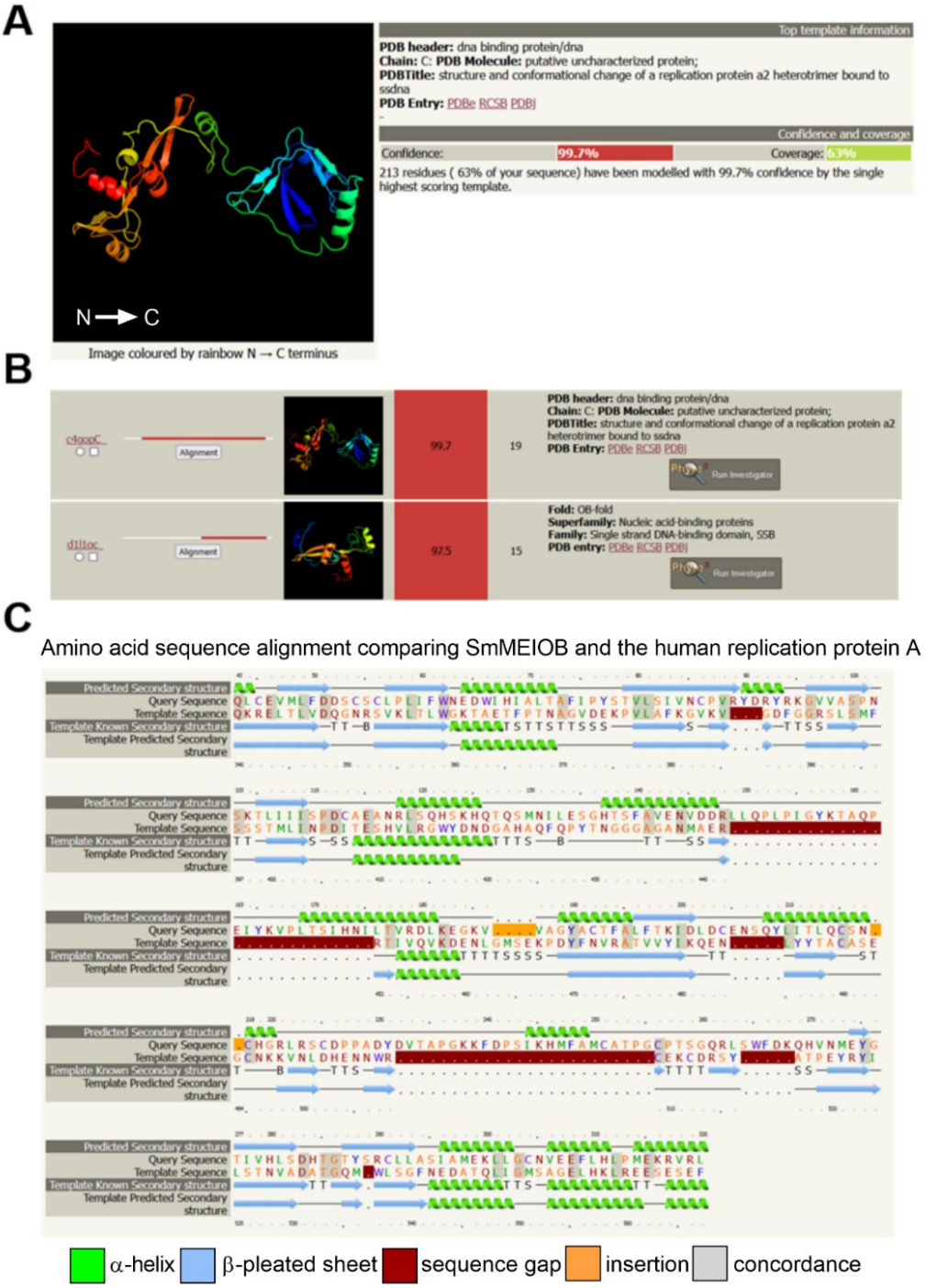

Suppl. Fig. S3.

A, Shown is the protein structure of SmMEIOB according to Phyre2 (244) analysis based on published structures of orthologous proteins in the protein data bank (PDBe). **B**, The amino acid sequence of SmMEIOB showed highest similarities to the human OB-domain containing replication protein A (RPA, (385)). **C**, Phyre2-based results of the protein structure analysis of SmMEIOB in comparison to the human ortholog RPA are presented. Using alignment coverage, SmMEIOB was predicted as an OB-domain-containing, single-strand DNA-binding protein, and highest similarity was assigned to proteins of the replication protein A family.

Supplemental Figure S4. Transcription patterns of Sm*thrβ* and Sm*rxr-1* in adult *S. mansoni*.

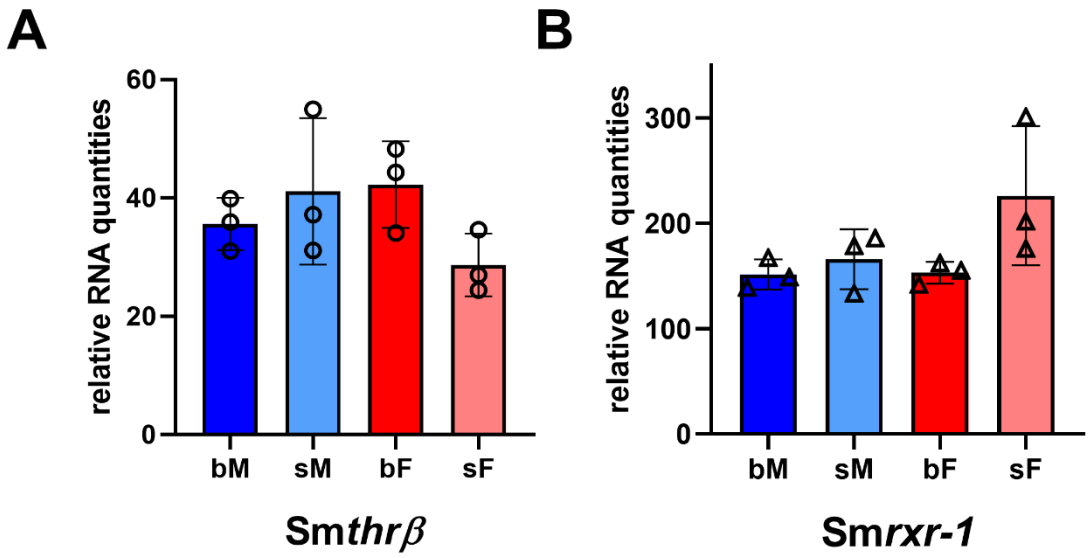

Suppl. Fig. S4.

The transcript profiles of Sm*thrβ* (**A**) und Sm*rxr-1* (**B**) in mature male (bM) and female (bF) and pairing-inexperienced male (sM) and female (sF) *S. mansoni*. No statistically significant sex- or pairing-dependent expression patterns were found. These results confirm the bulk RNA-seq data of Lu *et al.* (289). Whitney-Mann test; n=3.

Supplemental Figure S5. Long-term *in vitro* cultivation of sporocysts.

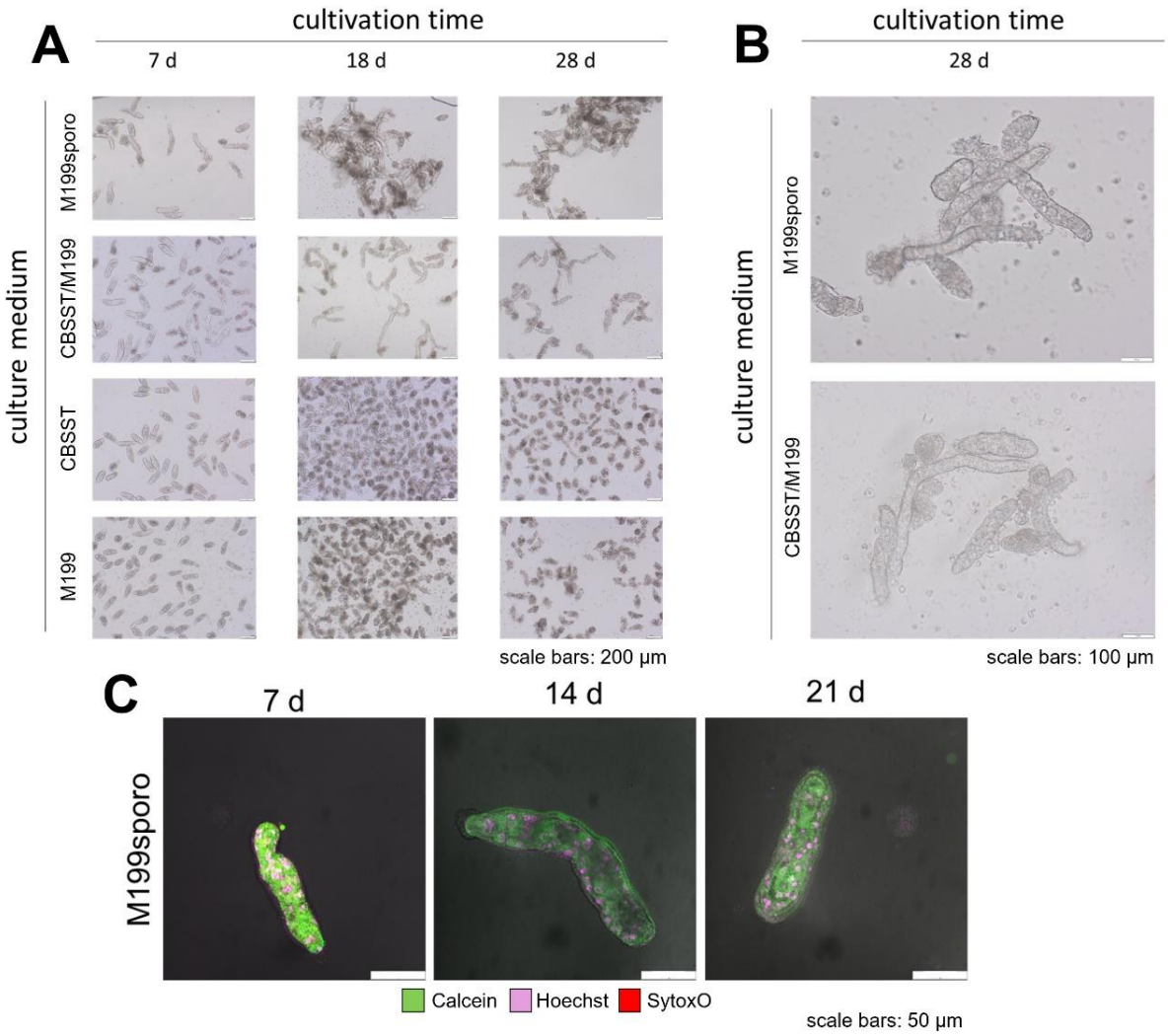

Suppl. Fig. S5.

Miracidia were cultured *in vitro* to induce *in vitro* transformation into sporocysts. Initially, cultivation at low oxygen (5% O2), 5% CO_2, and 26°C was found to be optimal for the intermediate host *B glabrata* (223, 224). **A**, To obtain optimal (Bge-cell-free (226, 326)) *in vitro* conditions for sporocyst cultivation. Different media were used in the present study. The survival and growth of sporocysts were observed over a period of 28 d. Cultivation of sporocysts in M199 without the addition of HEPES and NCS and cultivation in CBSST showed considerably reduced viability after 7 and 18 d respectively. Sporocysts cultured in CBSST/M199 at a 1/1 ratio were still vital after 28 d and showed longitudinally growth. The best conditions in terms of sporocyst viability, morphology, and growth were found for sporocysts cultured in the M199sporo medium. **B**, Detailed image of a vital sporocyst after 28 d. **C**, Sporocysts were cultured in M199sporo and stained with a life death cell stain (HSC stain). Calcein (green) stained vital, esterase-active cells, while SytoxO (red) stained permeabilized, dead cells. Cell nuclei were counterstained with Hoechst 33342 (purple). Sporocytes remained viable throughout the experiment.

Supplemental Figure S6. Tracking of eGFP positive *S. mansoni* up to the F2 generation.

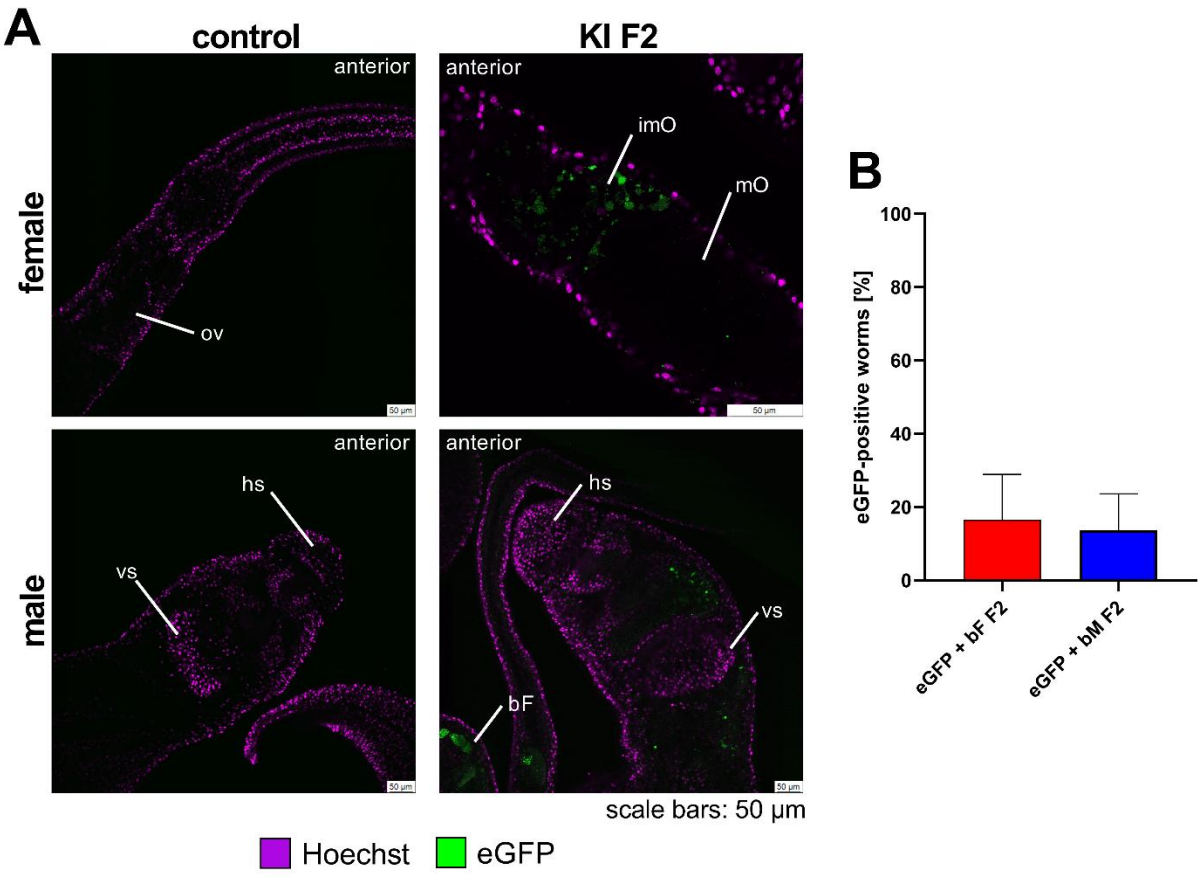

Suppl. Fig. S6.

To propagate the transgene SmUbi-eGFP-SmUbi in subsequent generations, cercariae that tested positive for eGFP-PCR from sporocyst transplantation experiments and unedited wild-type cercariae (control) were utilized to infect hamsters as the final host. The cercariae originated from females from transplantation experiments. **A**, In the F2 generation, green fluorescent cells (eGFP-positive) were observed in both sexes. **B**, The number of eGFP-positive worms was assessed, with worms being considered positive if they displayed green fluorescence in >50% of the tissue or green fluorescence signals in the gonads. Abbreviations: bF, pairing-experienced females; hs, head sucker; F2, filial generation 2; imO, immature ovary; KI, knock-in; mO, mature ovary; ov, ovary; vs, ventral sucker.

Supplemental Figure S7. CRISPR/Cas activity assay showed gRNA directed cleavage of GSH1 by A.s. Cas12a and L.b. Cas12a *in vitro.*

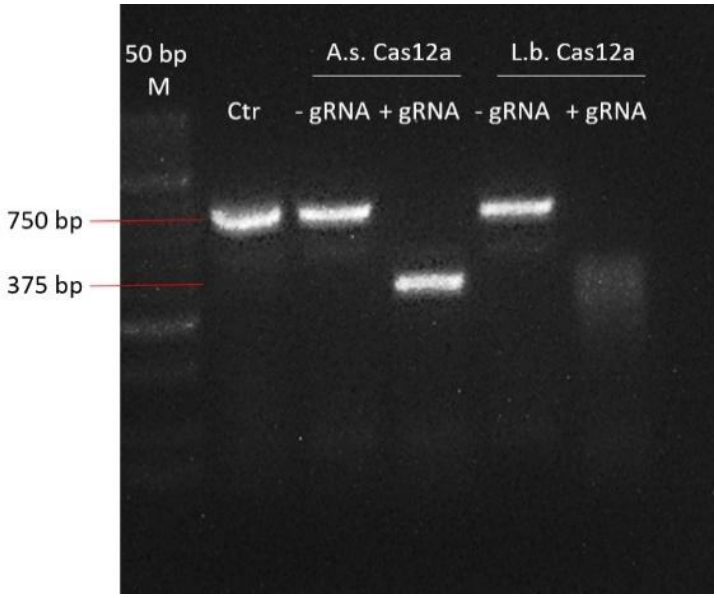

Suppl. Fig. S7.

In vitro CRISPR/Cas-activity assay with A.s. and L.b. Cas12a RNPs targeting GSH1 showed cleavage of a 750 bp DNA GSH1 amplicon (50 ng each) harboring the predicted cleavage site in the middle. The same gRNA sequence was used for both enzymes. PCR amplicons, which were incubated without RNPs, and those, which were incubated wit enzymes without the gRNA, served as control.

Supplemental Figure S8. SmMyst4 is a vitellarium-specific, pairing-dependently transcribed histone actelytransferase.

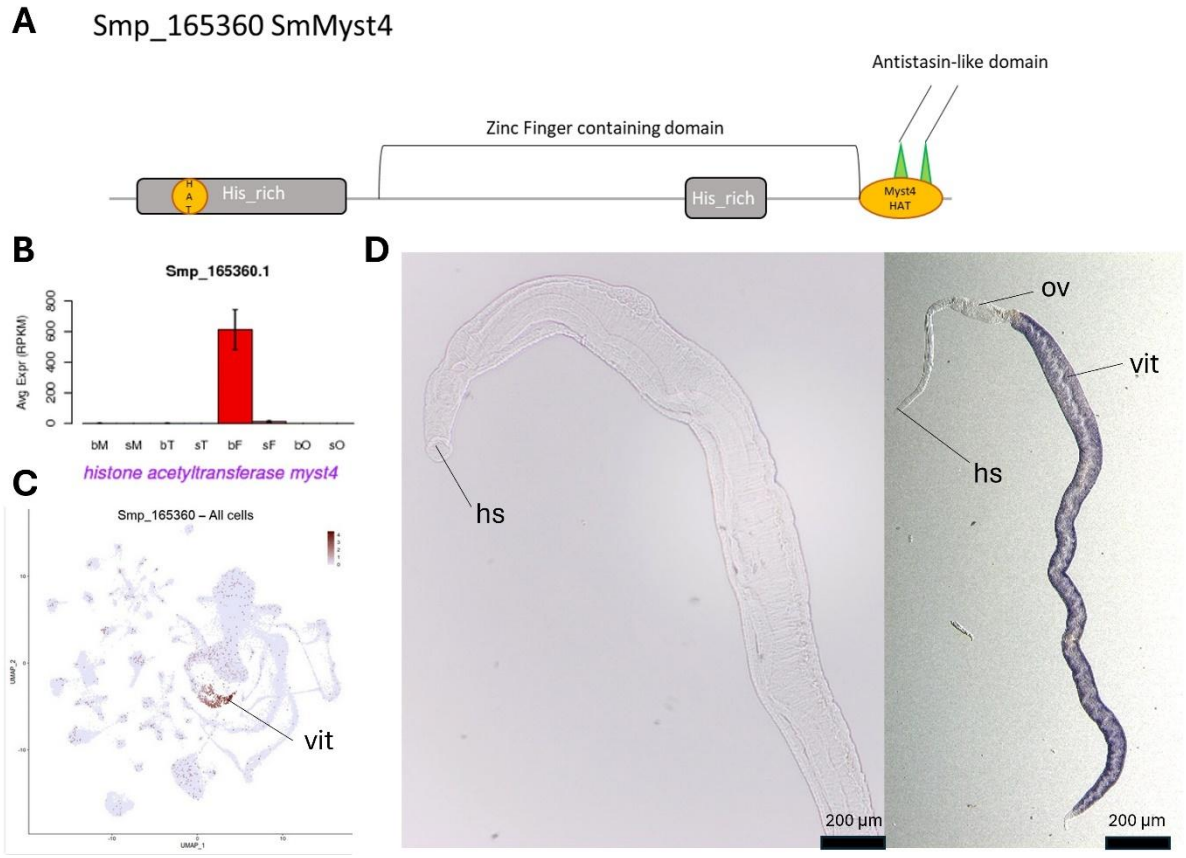

Suppl. Fig. S8.

A, The domain structure of Smp_165360 (SmMyst4). The compiled domain analysis from SMART (243), ProDom (459), MyHits protein structure analyzer (460), PROSITE (461), and AlphaFold (241, 242) of SmMyst4 revealed the characteristic structures of histone acetyltransferases (HATs), like HAT associated domains, zinc finger domains, and a Myst4-associated HAT domain. Additionally shown are transcipt profiles of SmMyst4 in adult schistosomes and their gonads (55) (**B**) and data from the scRNA-Seq atlas of whole worms (61) (**C**), which display specific expression in the vitellarium of mature female schistosomes. **D,** Whole mount *in situ* hybridization revealed confirmed Sm*myst4* transcripts in the vitellarium of mature female schistosomes (right). No specific signals occurred in male schistosomes (left). Abbreviations: **C**, bM, bisex male (pairing-experienced male); sM, single-sex males (pairing-inexperienced male), bT, testes of bM; sT, testes of sM; bF, bisex female (pairing-experienced female); sF, single-sex (pairing-inexperienced female); bO, ovary of bF; sO, ovary of sF. **D**, cg, *canalis gynecophoris*; hs, head sucker; imO, immature ovary; mO, mature ovary; ov, ovary; vit, vitellarium.

Supplemental Figure S9. Identification of meiosis, dsDNA repair and retinoic acid signaling associated genes in the scRNA-Seq atlas of mature ovaries.

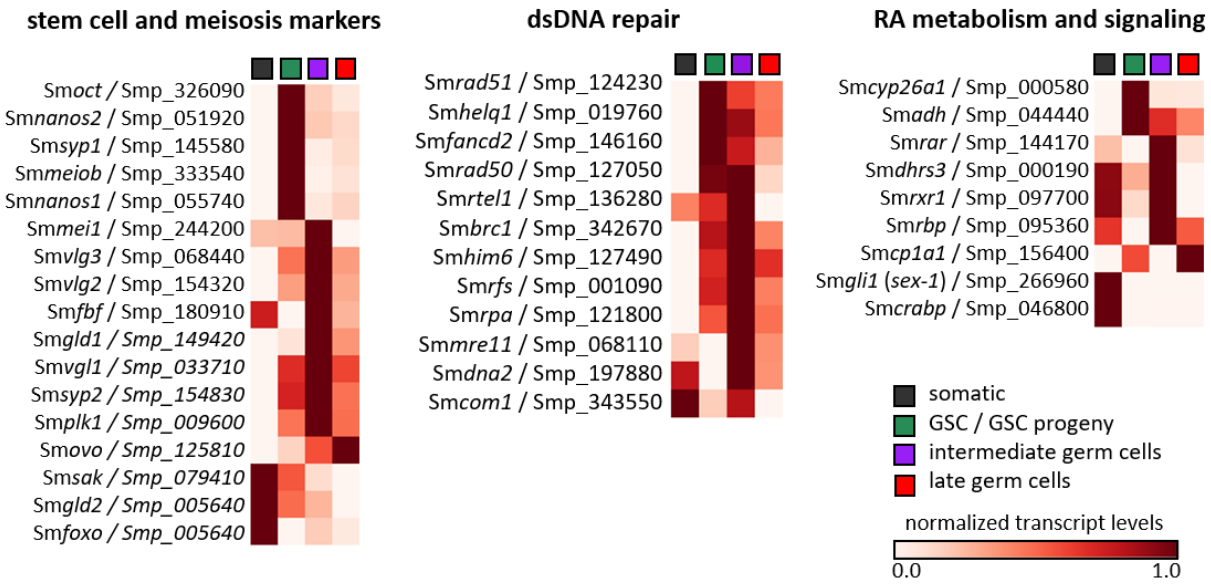

Suppl. Fig. S9.

Heatmap of the oocyte scRNA-Seq cluster-associated transcript amounts of genes coding for orthologs of meiosis (61, 76, 199, 230, 295, 301, 462–471), dsDNA repair (189, 472–474) and RA-metabolism/signaling (51, 122, 371, 372) associated genes. The heatmap illustrates the feature-standardized transcript-levels for each cluster of selected genes (Moescheid and Lu *et al.,* submitted, gonadsc.schisto.xyz).

Supplemental Figure S10. Developmental trajectory of immature oocytes within the GSC/GSC progeny cluster.

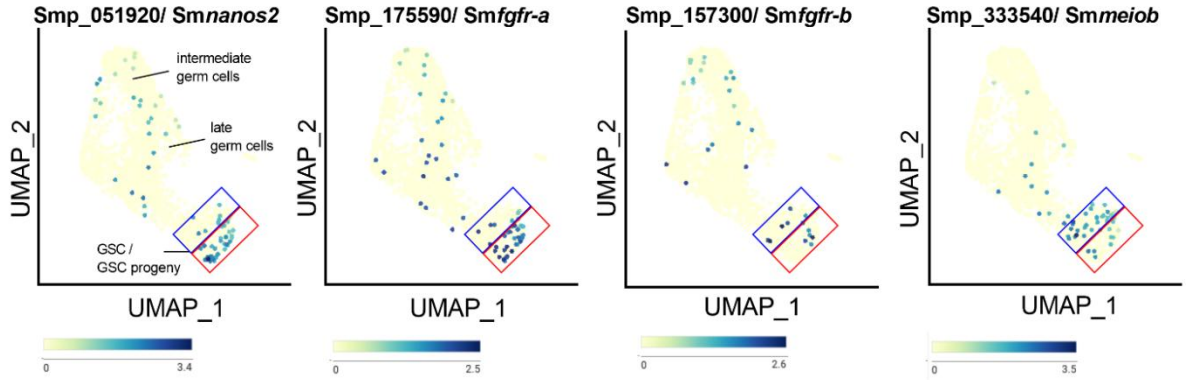

Suppl. Fig. S10.

Analysis of the GSC/GSC progeny cluster showed differences in the expression pattern visualized by UMAP projection. These patterns were assigned to specific stages of development, as indicated by colored boxes. The red box indicates genes with transcriptional peaks, such as Sm*nanos2*, and the blue box indicates genes with transcriptional peaks, such as Sm*meiob*. Sm*nanos2* was found to correlate with S-phase EdU-positive cells, while Sm*meiob* correlates with EdU-negative cells (61). The analysis revealed that the Sm*fgfr-a* transcript profile shares a higher similarity to the transcription pattern of Sm*nanos2*; therefore, both are transcribed very early in oocyte development, probably at the level of the stem cell-like oogonia. Sm*fgfr-b* showed a transcription pattern intermediate between that of Sm*nanos2* and Sm*meiob*. In contrast, the peak of Sm*meiob* transcripts in the other part of the GSC/GSC progeny cluster indicates transcript dominance in an early developmental stage post oogonia cell division (Moescheid and Lu *et al.,* submitted, gonadsc.schisto.xyz).

Supplemental Figure S11. Successful transfection of eggs at an early stage of development using tagged CRISPR/Cas12a RNPs.

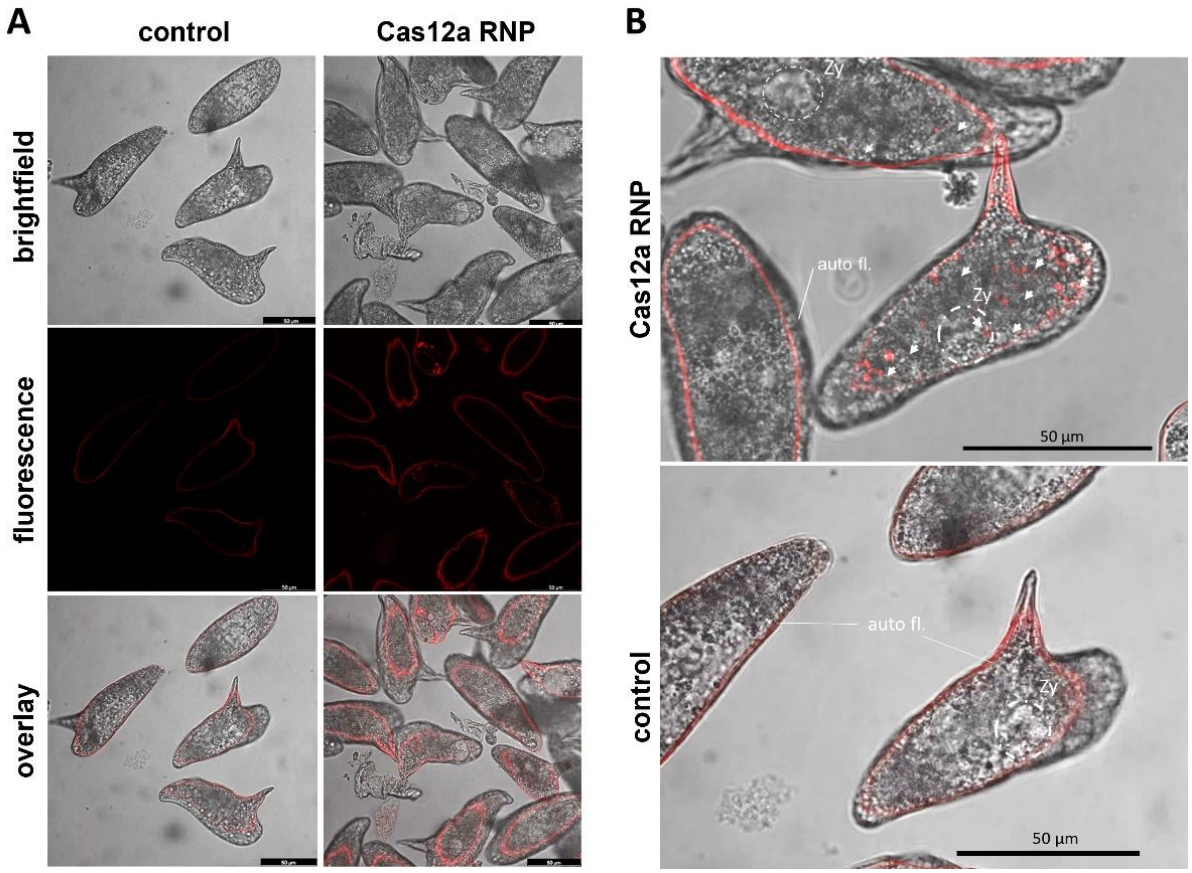

Suppl. Fig. S11.

A, CLSM analysis of early schistosome eggs obtained from *S. mansoni* couples *in vitro* (0-24 h, IVLEs (76)) 2 h after transfection with RNPs containing rhodamine-labelled Cas12a-gRNAs via EPO. The control IVLEs were electroporated in the absence of RNPs. In control IVLEs, only autofluorescence of the eggshell was observed. Fluorescent signals, specific for the rhodamine-labelled RNPs, were detected on the eggshell and in the cells of various RNP treated IVLEs. **B**, Detailed image of IVLEs transfected with rhodamine-labelled Cas12a RNPs 2 h after EPO. Successful delivery of CRISPR/Cas material (arrows) into numerous cells of the IVLEs was observed. In some IVLEs RNPs were detected in the zygote of RNP treated IVLEs (189). Fluorescence spectra were acquired using a Leica TCS SP5 vis confocal laser scanning microscope with Leica LasX software. Scale bars: 50 µm. Abbreviations: auto fl., auto fluorescence; CLSM, confocal laser scanning microscopy; Ctr, control; Zy, Zygote.

Supplemental Figure S12. dsRed transgene activity by SmUbi minimal promoter and terminator.

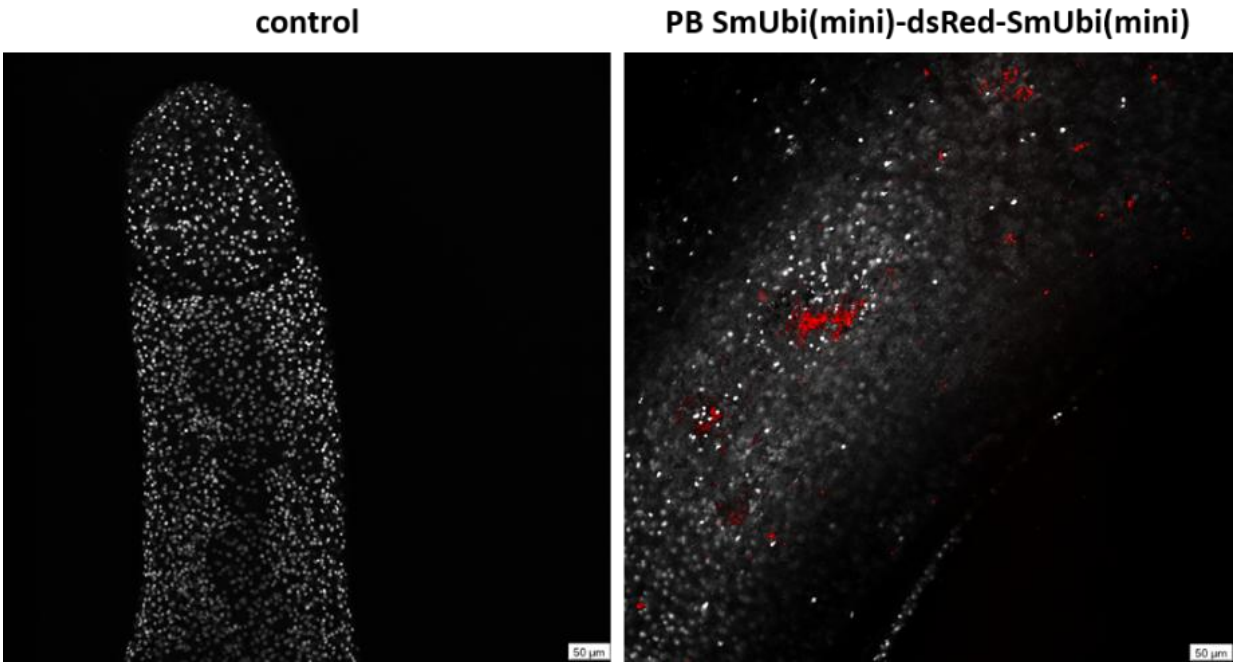

Suppl. Fig. S12.

The activity of the potential SmUbi minimal promoter and terminator (SmUbi(mini), Table 21) was tested in preliminary experiments by ballistic transgene delivery using PB. A dsRed fluorophore driven by SmUbi(mini) (Supplemental Table S4) was used as the transgene to avoid autofluorescence detected in the eGFP channel for eggs and the vitellarium of mature females (475). After 48 h, transfected and untreated control worms were counterstained with Hoechst33342 (white) and analyzed by CLSM. Red fluorescence was observed in the transfected worms, whereas no dsRed-specific signal was found in the control worms. Scale bars: 50 µm.

7.2 Supplemental Tables

Supplemental Table S1. Amino acid sequence of *S. mansoni* NR paralogs and orthologs for phylogenetic analysis

>Smp_144170 SmRAR [*Schistosoma mansoni*]

MSHCPVEYSNPNSQNTISYITSDSVISVSFADCQSSSPSYHSLSSSTALPGVGSFLDKSNHLPHYSPNKYYDTEPTAIPGHSYVEN
TDVFDNNLPYPIKSEAIHETVSGTFITPDAHNESCFTSPLQPLKSLNPSLPVQSSESLLSGFTHPLSMDHTVLEDGGLDLDRVFVAII
NDRNSEHDIFNDNDVNCDSERCKKQLLNNSIQSSVNQSMLTDDSEDKSLLQYYSVIDSEKTTQHQTHPKTSPISEVEQTHKSSGS
SEVSTRMCVVCGDKASGFHYGVSTCEGCKGFFRRAIQRDQSYTCAKNGTCEINKTLRNKCQQCRLLKCIAVGMSRDAVRKRRQ
GKKREQSSCESVTLPSSDSSNKYEGSAYSSCSADVVLTPSKAHLNETTPDPHEMPIKSINFQPSSSIPSSTNISLTLCNNNNNSNN
SNNLTKEDQQTLDKFDRFLNYCKDQAIKYQANNWNISKSDYYHLSGSLSRHLSPIKHTPHELGESLKLLTVDEIFCPAQLKFTHEF
ACHLEQFIRLSQHDQAILLRDCLPELAILMLCRENRNKTHMNSSSTSINYQLNCLFSPWFPNAVVTDSSLDCLHMTCDSITAQSIFQ
FASRLQRLHLTNMEFGPLIGVILFTPERSDLLDIDFVNRTQNLWAELLRRYCESNGSQTRCAHLIMVLSTLRELASKITHNLNAWYK
LSNTPMSNCLKEFLYSSSFNSMDDCF

>Smp_097700 RXR (retinoid-x)-like NR [*Schistosoma mansoni*]

MIMSIFANHDAIHMNHGVSDESVLYTHSYLIPPINQLENDILKPDQDMLTCVQSNRSHSPSQQIYDMLDSTVLSDNPIQTIANSSCK
SQTSLKSSSCDTSNADLGVDIKPSFMYNDNPQVISQSFLTDLHNHTDIHTVSSDTNPNLCPIANSINSTHLQELVYNTPQKFPHML
PPDAHQHTVYSDNVVSEPFTRLLASGNSNETSTSYLPQVTKVETNSLTVSQSPILLFVDPNKTKPESRECFPTQNPSELASQSSS
ATSVNTTNLNPICVICGDKASGKHYGVISCEGCKGFFKRTVRKQLVYVCRESGQCPVDRRKRTRCQHCRFEQCLAKGMKKEAV
QEERHRQPSSNPVPLISKPPKSEKKGPGRRSTFGNKSAESIVTDQPPNINQDSTPNISITPTTTDCVQPNQVKSESSTTCIQSNNV
LLSDETDLPNLTLRCLLSAELSMDPKLAVSERGEAIYEDIPGDDDTGLHPLTIICQSIEQQLPRIVNWARQLPVFSSVYLSFDDQFCL
IKAAWPELVLISSAYHSTVIRDGLLLSIGRHLGREVAKSHGLGPLVDRILHELVARFRDLSLQRTELALLRAIILFNPDANGLSSRHR
VEAVREQLYSALHSYCTTNQPQDTSRFTKLLLRLPPLRSIASKCLEHLVFVKLAAEDPTSCRLINLVEHGVWPIQEKSFELATLPSD
SASTDSVPSQITMVPTPQYIQHQDDNSLPTSSHTDLSYTHTLPNFHTVQNYPF

>Smp_073470 RXR (retinoid-x)-like NR [*Schistosoma mansoni*]

MIPVSIVTPQSVSSAEQIGEHSSSLSLQNVPVQQDSVSYLNSHTTVHMNDGQNEPSSIYLTDQELRLDSSFPNSPLGITRDPHCD
DNGEEQNRISSFELISRLIDAEGLIELGYIPSSCNSAPAIDVASLSDLEEVTSKTLLWSSNCDDVDSFNFDDLSNKINESNTNNADTK
LRSDNKTLEHRSALTTEYISVDFNPLNSTNALVPIISLPSDTNLQTIPSLESNEYENFQAHYKTNTVLENVQSLPSNTVPDDLGPLNI
TSYPMGLVEADIPSITRPSIHQSPVDHHALHPTIKPNHIPYSYSPLTPLSSVQIRSSIHESSFVIDNQVCPIDNICNQQLQTGSFVKNK
YSSDYQEYSGAPECFPTVHTLELFTSHSSDLPHSSSHPSKNVGESPKHLSNDTKPIKYPELLQKIGENCNSNISGPNLPFISHSTY
CSRTQSSSSCSIRQQLATAPSHPQLHVSIPQSPQSIYSVFSCSPNQKVAVSSTVNLPSSDSTSATLIFNGDFPSRPIISSTDNSFWS
HPSIPSGSAVNTQMITNWEHSVPYPAYVPNSQITGFLPENISVTDKAAIYVKDGNSTAIQPVLGSGLVGSFQYLTPTTVLSKPNYTI
LNDQLTFNHPQETLIQPFLPQMSDPIKTTQNLRIPFCQGTQYTLTPGISIPINPEHSFGRLEMNTHRYSSESSKTNPALTSRSSSSR
PFNSPVRRNSAPFQSTYQNCMNFSETAAHQSECSIVVSQLSTKKLTTPVLCCISSNSNNIPIISQQSPNNNNNNNNNNNNVVFKTD
NTKQHIIDQNILTKTATTTSIVQPSELCHIQPILISSPVKNNNNNTHNLGTGSYIDSNCLSNQSNNDKSHSITPSSPLLTNCNSPSTTL
QSSTVCCLLRPSGRSTSTSSGSSCGSSCSGTGGGVSVSSGQYICSICSDRASGKHYGVFSCEGCKGFFKRTVRKELTYICRDSQ
ECQIDKRLRNRCQYCRYQKCLRAGMRREAVQEERQQQQLQSEVQRSPTPPEQNCDLSVNSMIMSDTKITNAMNHSCLAEKQEI
MLKTTNCTSSSSPHLLSNCSDSSINYFYSASNEKSQQPSINDNFNLTVNDAATYPPQELSLIGNKDSNNVTLPLADIHALKLPTTTS
AAIPPPPDALEFIRTAESTISSRRKQWLSAFNKQQCHAEIAKCFQDSMENLKWLENNFEKCTTNHLPLFDLVIWSSKLPYICQLSC
GVHLDLLKSACMQLIIVNLVYWLANDHKPRSLSTSNSTSKLPDTTPTINSTDISNITDDPPENSISDISKDCTIQMKKINKSVPLDEKM
DYYYSNFPEFHLLNNLTKPMDNNNNDSISSKPTNINDNSVDDDMIRKRNTNVYKLIYNLAIKLRMLNLDPVELGCLKLILLLNPDSM
TCLNNIRSLIELLRDQVYAGLEYYCNQVWPNAPHGRMGRLLLKLSNFQSVAARIEKLICSNELNNLLNNLESIFSYLSKKKVDHSNY
ISTTTTTTTTMSSTTTSTSNSIHLEFS

>Smp_105090 SmT19 (vitamin-A-activated NR) [*Schistosoma mansoni*]

MYLHSPITTITSTDSSSTSTITTNTNSTSSLTVTSSPIDPSKLDIMNTMSNPTCCIPSNNIIQPPPIIPNHGLTSLLSNVASNLSAHQNH
QNNFLKPSLVPTGRTSNAQLLQLLRNVTSSLPSSPVSYPISPRNTRNTPVLCDNNHTLSDSTSQVPIISTASSTAIPATDYSSCNND
QTLTLNSQSNRTSSNHPTVNGPSLLPDFETLLANSNPNMSDFIYCLVQSILFNHANTRQKFKSKKETPPLDSAALLSLLSGAGNLN
PSSCSTGSLSNPLNPLSTLSSEIDSANCNIHLRQVLESLISLSVSPAFDQSSPHNLLSNDMLDSGSLSQTFQQLTNLSNRKATTGIQ
KVSPSGQILSNESSNSTNPPGNVSFDLLAQLSAAAAAAAVTPPPSNIVNQLGNLATDGFNPIFPTDENLSSALQNLLFKQMLSINT
GSNAYTSHLGPGRDSVSSISQSGQYTGLKDCRSMSNDESNCSSEKLIPTTYSLASSFLSLHSPNSTNNCSNNNNPRSSFVRPSS
RISPEPITLASSPPSSSSTPSFICPNQSNPPTGEFYPPNETVASSPNSLLLNGCTPVGTSPNTGLNMNQTAVNLSNDNQSWEPCK
VCGDKASGRHYGVVSCEGCKGFFKRSIRGHVSYVCRSEQNCLVNKAYRNRCQYCRLQKCLAVGMRSEAVQNERRPTNTFALN
FLNDNSGNSNCTTTGGSSNMNNGGSPSPSNNCCVSTPSITSTTTTTTTATVTTPTTTSANNSHTSTSGPSVTNVRNSSPQSQQL
PYKIEPNSEELEDDRNNHSEFTTQKSEEGQSSSHSSPSGSSRSVPLTLSGATTVGLLSSSSGGVGSKHLDDNHFTGINKHSALS
DISSSSSSSSYSATIADVEINDPNNASYLQHDIKPPVIQTSLGLKFTPGLCSSPQATSHSLQQPPAICLSTSASSFTRQRSLTSVSSS
IVNNNSTAYASALPAYSNMLEGCHTTNHLDPDCGIANFSRCMNRNPLLSSQLFDIPDNKRGATQESYSRRMTSLSNTPCSSSATV
SNHQDPLSIFDDTGGLNLNELTKLALNNINSLQSSSSASNQQGRSLAALYTYWLAAAAAAGSLNPLHHRHNDNHHHHQQQNHSV
HLSTSNQNFNPLDMKTSLSSLKAGQPSTVTTTSIVGSNQNSTSQFSMKTNPNGLFGQHCNLENQLLINGLNHSSKSSLLSSSSSH
SDALNMLMSIMLNSSDNVGLNNFNTLTDAVNSTTTHLQKAPINHHSHQHHPFMLQHHPHQHQLHMGSSNSHHSSTSPNTLEIPIP

STSSSCLSASLFGLNNTISTNNNTNNNNSNDNNSTMHTTVANNNSPFIPAPPPIKSTNLIQLLCKRTSNSQTSTLTDTDDKSKSGS
CGSMVASTTNVRGRRSSNSSTANNMGENLHESGELIDSYRDANGHLLPKKFELTSSPDVTALRPENELLNPSPKKEETNWSRS
RKRKMHYSFPSDVNNNARSIRRRTQSNNSLQPDTNNSIGLGDTRETCEDDDESRITECISECTKSPDDSRPNSPLVGPVLLNSMF
DLNAHVFKAYQDNNNNRSLSISSELASRVLFLTVDWLRRFDGLKRLPIGVQRDLVAISWSDLFVLGLCQAADQINRSQNHRSNQE
SNDPQSTNSLCAQNDINSTRVKQISGEQQTNSHCSITPTSSFKSNSFDSSSSSHISPMKEPMDTSYLKTNCSSSSAVIELVEQLMK
QFSGAEVDTHEYTYLRCMVILSSGRLCINARDASLAKQITEMESRVLSEFSEFLSTRAASSTTTGSLSSKRTKPIIKRVLILTQLLSTL
RYLDPKDLEEAFFSNLLGSVSIAQILPYLLESNDLFTQSQLVMNSCLPDNSLDYKPGLNHVKLPNKQASRSGLEDSVTNFMGDSL
PNNMTEKIDNLPSSLLLRPDQTSPQSRSASCEITATSIELNNQNTEPANSKSFVDDETNDSA

>RAR-like NR [*Schistosoma rodhaini*]

MSHCPVEYSNPNSQNTISYITSDSVISVSFADCQSSSPSYHSLSSSTALPGVGSFLDKSNHLPHYSPNKYYDTEPTAIPGHSYVEN
TDVFDNNLPYPIKSEAIHEIVSGTFITPDAHNESCFTSPLQPLKSLNPSLPVQSSESLLSGFTHPLSMNHTVLEDGGLDLDRVFVAII
NDRNSEHDIFNDNDVNCDSERCKKQLLNNSIQSSVNQSMLTDDSEDKSLLQYYSVIDSEKTTQHQTHPKTSPVSEVEQTHKSSG
SSEVSTRMCVVCGDKASGFHYGVSTCEGCKGFFRRAIQRDQSYTCAKNGTCEINKTLRNKCQQCRLLKCIAVGMSRDAVRKRR
QGKKREQSSCESVTLPSSDSSNKYEGSAYSSCSANVVLTPSKARLNQTTPDPHEMPIKSINFQPSSSIPSSTNISLTLCSNNNSNN
SNNLTKEDQQTLDKFDRFLNYCKDQAIKYQANNWNISKSDYYHLSGSLSRHLSPIKHTPHELGESLKLLTVDEIFCPAQLKFTHEF
ACHLEQFIRLSQHDQAILLRDCLPELAILMLCRENRNKTHLNSSSTSMNYQLNCLFSPWFPNAVVTDSSLDCLHMTCDSITAQSIF
QFASRLQRLHLTNMEFGPLIGVILFTPERSDLLDIDFVNRTQNLWAELLRRYCESNGSQTRCAHLIMILSTLRELASKITHNLNAWY
KLSNTPMSNCLKEFLYSSSFNSMDDCF

>RAR-like NR [*Schistosoma japonicum*]

MSNCPVEHLAPNCQNPISYIASDSVISVSFADCQSSSPSYHSLSSTTTLPGVGSFLDKSNNLPHYSPNKYYDTETNPLSKHPYVE
ETGFFDNSHPFPTKSECIQDLVSGTFITPATHSHSCFTSSLQPPKSLVPSFPVQSNETALNGSTHLLSVDHTILEDGGLDLDRIFVAI
IGDQSSDHHVFNDADDVNDNGGNCLVDKSNSCNTQLLNNSMQSSVSQSMLTDDSGDKSLLHYYSVVEPEKTTQYQIHSETPVT
EVEQPHKLSGSSEAPVRMCVVCGDKASGFHYGVSTCEGCKGFFRRAIQRDQSYTCAKNGTCEINKTLRNKCQQCRLLKCIAVG
MSRDAVRKRRHGKKRQQSSCSDSAALPSSDSSSKYETATYSSNSTDVFLTPSKTHSNDEITLNSYEMPIKSSNLQSSASSSSLPP
TTNPTLTLSNSSLTKEDQQTLDKFDHFLGYCKDQALKYQTNNWNISKSDHYSLSGSLSRHLSPIKHNSHELGESLLLTVDEIFCPA
QLKFTHEFACHLEQFTRLSQHDQAILLRDCLPELAILMLCLENRNKVPMNSSSTFSSINHQLNCLFSPWFPNAVVTDSSLDCLHMT
CNSITAQSIFQFASRLQRLHLTNMELGPLIGVILFTPERSDLLDIDFVNRTQNLWAELLRRYCESNGSQTRCAHLIMILSTLRELASKI
THNLSGWYKLSQTPISNCLKEFLYSSGFNSADDCF

>RAR-like NR [*Schistosoma haematobium*]

MNPPNIEAAHIDLPIDVNPSTTEEIRMAIRQIKNGKAAGPDNIPAEALKSDIKATTSMLYLLFKKIWGEEQVPMDWKEGHLVKIPKKG
YLSKCENYRGITLLSIPGKVFNRVLLNRMKDAVYAQLRDQQAGFRKDWSCTDQIATLRIIVEQSVEWNSSLYIKFIDYEKAFDSVD
GRTLWKLLRHYGVLEKIVNIIRNSYDGPQCKVVHGGQLTDAFQVRTGVRQGCLLSPFLFLLVVDWITRTSTSEGKHGIQWTAQNQ
LDDLDFADDLALLSHTHEQIQMKKTSVAAVSASVGLNTNEKARSSNTTQRTPSNTITLNGETLEDVESFTYLGIIFDEPGGSDADT
KATIGKMSHCPVEYSNPNSQNTISYITSDSVISVSFADCQSSSPSYHSLSSSTTLPGVGSFLDKSNHLSHYSPNKYYDTEPTVIPG
HSYVENTGVFDNNLPYPIKSEAIHEIVSGTFITPDAHNQSCFTSSQPLKSLNPSLPVQSSESLLTGFTHPLSMDHTVLEDGGLDLD
RVFVAIINDRNSEHDIFNDTDVNCDSERCSIDKSNSCNKQLLNNSIQSSVNQSMLTDDSEDKSLLQYYPVVDTEKTTQHQTHPKT
SPISEVDQTRKSSGSSEVSTRMCVVCGDKASGFHYGVSTCEGCKGFFRRAIQRDQSYTCAKNGTCEINKTLRNKCQQCRLLKCI
AVGMSRDAVRKRRHGKKREQSSCESVTLPSSDSSNKYETSAYSSGSADVVLTPSEAHLNETTLKPHEMPITSTNFQPSSSSIPS
STNISLTLCNNNNSDNSNGLTKEDQQTLDKFDRFLNYCKDQAIKYQANSWNISKSDYYHLSGSLSRHLSPIKHTPYELGESLKLLT
VDEIFCPAQLKFTHEFACHLEQFIRLSQHDQSILLRDCLPELAILMLCRENRNKTHMNFSSTSVNYQLNCLFSPWFPNAVVTDSSL
DCLHMTCDSITSQSIFQFASRLQRLHLTNMEFGPLIGVILFTPERSDLLDIDFVNRTQNLWAELLRRYCESNGSQTRCAHLIMILSTL
RELASKITHNLNAWYKLSNTPMSNCLKEFLYSSSFNSMDDCF

>RXR (retinoid-x)-like NR [*Fasciola hepatica*]

MNINILKSEPDCVDPSLNEDSGLAAAYDLVLEHGDSFGDLTPESKTDLSRSDSFSFDEPRLVLPPVAQTFLRQDSAMPSSTLHYG
VASPTTTSGSAGGVLPMQVCITDTHDSGKQPFEEIIGEHDHLPVVQSQWKFGGSGATVNCETPITNSVQLPTLSSTIQLSSDNSL
KIESNPQTHSQVTTPTSNRKLNSGTSDSRRLAVAQSPAGTPYPSLTQAPMPSFSNLPLALCAICGDTASGRHYGVISCEGCKGFF
KRAVRKQIQFTCRGSGQCPVDRSKRTRCQHCRLEQCLAKGMRREAVQEERHRYFQKTPKSRSKSRKADPLGFQPDLLLSMDS
VSTELNGHTPKSIEHDSTVTTADPLQSSPTTVLCSGRKQNRANQPGRFATTSGTATGELMSASTAPPPLSLASLLTAELSTDAEL
PTTATGERVYVDIGDDGLDPLVVVCQSVEEQLTRLVCWARQLPVFTIPYFSTEDQLWLLRAAWAELLLISASFNSIAVRDGLLLAN
GRHLSRNKARQHGLGPLMDRFLLELVSRFREMSLERIELALLRAIILFNPDANNLCARQHVESVRESLYAGLHSYCTTTHPNDTSR
FTKLLLRLPPLRSIAQKCLEHLVFVKLAAEDPSARRLINLVEHGVWPNDDRAFCPQQSQQQQIQHHHQQLQVKQTSPVGLHPQS
AGPSTSIGPGSSGTVTRFSWPSQGIHNHPVPGTLLPHPMTNTNNNNSNHSHYNSTSGVPTTNTESAPTNGKANIKVDLDSLSQPI
ADNCSVE

>SmRAR-ortholog [*Dicrocoelium dendriticum*]

MNSHSDLLCFENASPSGHEFWNITKGAIETSSSNALGSDCSYHYPSLTPATEFLNDSIGTSHHVTTPCSISTPDHSTTTSEHVTYH
QLQRLTKTSGMSIHAPSELSESLRLGLDCTENYLDINDHSQVPIYPQNHKDSLYIPTSNYQHSNSASPSSAPKEILYDLSHTHQLR
EVFHQPPYHPQASDLPTEGESICLDLDQVFSAIVSPEDESDVDPVKFNENASNSVDFHLKTCIPPAGDSIFPDDILFPLNSAQDAP
RSSDLNPSTLPCIVAGDESLSVTHYPNCPQPLRILCDDREKDVYQRPLLTASHADSSSFPLENRPGFPLLNSSPVSPFSRQILSRS
PRFCSAGPEQLSFSLSPRSALYSSSPMRSKHNSSCSMNTDGSVMTPQPFIHMSSVSSSPRFHQRSPSHLPWPHIQASITDARR
MELAPIIPNLSPNRYLFGNTTRLTASIAEIPVDSTHMDSTVHHAARGSQPLGANVPKESLAHIRPRGAQSVSNPTIRFCEVCGDKS
SGAHYGVYTCEGCKGFFRRAVQRNRTFSCARNGQCEVNRVLRNKCQHCRLHKCLASGMSKDSVRKKFDSDEKVSPLRRAKVR

PTNARTIRKGGPIGVGFQITNPSDLHISRDNDPLPVPQHTTPERPQAPLTPSERPSFTSPTIMPPLSIDDRRMITSLFELFHASRKQ
AIIESGGEGHHVGAKGELTVIGSVEQLFCSAQLQFAHYFASCLGEFNQLSQHDQAVLLRGALVEITFLLLCNNHRCADAPPSIPTIH
SGSVHSTSRCSYLLSPWNKSLILTEESFEHLHLSDNAWTPSRIFQFAERLTQMRLTSDEFGPLLGIVLFTPERANVLDIGAVNQIQ
GTWAELLRRLCESQGSYTRCAQLIMLLATVRELSGRLAHNLARWYRSRGAPFTECLQEFLLPVLSELVYL

>SmRAR-ortholog [*Opisthorchis viverrini*]

MLFVAFRLMSSPSDTAVLQSAISSKADWNYNSSSTNEIQPRAITSFESYLSDVEPVFDHQLSCYTPAIPSCTGSHLSKDTSDARQN
QGCVTGEDLQQEYIPQSIVTNCSLLPTADSINYLPYYLSDRSIGSSVQSPTDTTSLNSRSPTHVTRVASTSDMILPSEPLVLSEGSV
LSQSTVAPDESRSLDLDRVFSAIINPVSDIHFNPASLAVDPRNPVNHCSSLSSFVSSSGNSNVSENVAGSMNLERRRHLSGFPDS
SFSSALSDASESLNSNSVDYVCESSHCRDIRPSFYTKAGTSGAHAPSSLCTIPSEGLSSSCPGTFDRSLHSAPDSLISTRSILSSC
DSQINGVIQHQSNMLDTYSRSDRSVKNNHFTGVDPFTFSPSNESHSWNYQQASTTSCNKFPFATEFQLKRQEFSVDRPAPLSA
QSESPFAADTRSSTENVGQTAQAGVLLRACVVCGDKSTGAHYGVFTCEGCKSRAATVQKSEQPYIRTSTLVTDKSRSVQSCTS
TCTHIHLAVSALDTVRSLPLTAIWMLSSFILRHRSEMAQWLEREFAGWKLDTERVLQLNDFFISLDVLVKAPFPAPCTGWRRHKR
DRPTTSLTAVTSEADFEFTRSMKEVTKRLGAVGATRLPGWGPRDHHCAWLETLQDMTANRCQWRSCCQFLSRLPELSNKSWL
YGSEASMLNTDTYACARNGSCEVNRALRNKCQHCRFLKCLASGMSKDAVRRKQPAGNKKSSKTTGRRRSNKSAHTSSEHPEP
MLPCDVNRSDACSSQTTPRSVYSGTEQSTVGWTAGSSISFPSALTNPLGKLSPTTNFLSPQDRQIIVSLHDLVRASKKHSLAETR
MQMNSCLPESDGKIVITSVEQILCPAQLCFAYQFSGCLAEFAQLSQHDQAILIRGCLMELTFLLMCNNYRLAPEGESALCTGDGTE
ISTSEGECSAYLVSPWNANFLITEASFSHLHLTDNTWTPSRILKFAWRLTQLRLTDEEIGPLLGLVLFTPERADLLEVQAVSRIQGV
WAELLRRLCE

>SMED-HNF4 [*Schmidtea mediterranea*]

MTSTQHPNLNPAFSYQLLTSNSAPISISSNASSMQYPLESEMSSQQHEVYASNASGPEGMENNQLCLICSDKATGKHYGAFSCD
GCKGFFRRSVRKKNNYTCQYNRNCKMDKDKRNQCRYCRLKKCILVGMKRAAVQNERDRISTRRSSFDDIPPNVILSISQLMQAE
QRVAIQKPPNPQEYMNRYADVPDVCESMKNQLFLLVNWAKSLPCFSQLNLSDQISLLKAHAGEILILGVIRRSFQLDEDDVLLLGN
NLIISRNSSDKHFAEIASHILDDLFIPLRELQLDDAEFACLKAIVFFDPRVSESGKEFVRRCRYQIQMDLMNHMNDKQYHKPGRFGE
LLLTIPDLRLVTQLMVKKVEFMKMTGLAEIDSLLSETLLGDNPPGVFSIDPETDGNNNNNQNDSMDIINSHRISSPKYTYQDCYGIP
PFMPDSVLLNINNQNISPEAASKIWSAYLPSSTSMPSGNIYRAFVNQGTEIMQQNSQDNSNFGMIINSDGMMLKNERVGVPSLFS
CVNDSINLYQHSNLSQDTSHFLVNLDQGFPMINQSKYAYNGDANHNCSNSSNSDDLIHPALSVNSTQNVVDPSLLVAYTKSLPNS
PIENCQIQSIANRSSEANQQHNSRSNYSAISSTAHFLTDHPIRIQESESSVFKKEEY

>SMED-TLX-1 [*Schmidtea mediterranea*]

MILSTGRILLDVPCKVCQDHSSGKHYGIYACDGCAGFFKRSIRHSRLYICKNKSIKGDSWIGICKIDKTHRNQCRACRLQKCVDSG
MNKEAVQHERGPRSSTVRKKVAMYFNELSHNILDPSSMLPFTKSFNNANNVKEELLEFSLISAAKLNNFSNKNSFSISSLCDNSE
NSIETFDDCIGTPKSTIYFFQESYFSELSARSLFNTVHWIKSLQLPKEIVSVLLEGNWSQLFLLTAFETKVPFNDRSLMYRICDQVSS
LSTMKQLDLINQCAVLHQHLSKLSLGSSEINILKQIIFLDLKSLNKKLEVAVQDACMDHVSRLCQLFDPTNKIAIEACLLMNIICIDPNF
IHKLFFQKTIGQIPVLNLISDMIA

>RXRb [*Echinococcus granulosus*]

MQVWSNSNNASSVAPPANGDRDPMHSMPVTAESVPPTLNAFDSSIFASLISESDEKPLVDLKSDVISNADLQIGSAMPKPDLGSL
YGGLQSSTQTNNTCDVATTHRTVFPANPQLQTLPCQSSCVSGSLNYPYTPTLYSPVTPVSPQYFQSAPPTVANHRALPHQQQG
SYSLPPLRSYSYNQSFITGAYPKPYNYTIGSDGSISPYHRSVPSTSVKKVTYLCSARNCAICGATATGKHYGALSCDSCRAFFGTA
THLGLRCECSGKSNIHDNNHQLRCHSCRLRKCLAVGMRKEAVRFEKSHAMLLYPNEKDYSSVAPSPASSICSHERADNLVGSRS
SPATEATVKQIRAAEALIFDVPPLDLPESKPIFMDGKDCDSLQTDIQESIINLLLWSQKIPLFSDFSDSDRFILLRAGCIELLLVHFISR
LANSLTESHSSTSLRSSNPPLQESSPSTSVTPIESTTTPPTPLNIPVVVVDVLFPFHSAPKDILFSQQAECDLRNADRWHESRVLM
NILPVDVDHHPISITDVPNELNAQCLSRRLILCRLFDLARLFKRLCLSVEAVGCLRMVILFNPDVPELTEATRERVESRRDEAFICLE
HTFVKADKKTALGRMAQMCLHLADLSFVAERIYSKTSSHPYPSFQCLVDLLECFYKSDPMATVSESST

>RAR-like NHR-23 [*Caenorhabditis elegans*]

MACKVTGPNRHLTSVLEMSSFVYWPRSRQQAHNFPMQAVEQKLADATRTLHAKSSLQPSLSIETPKSKENDESGCESSNCMFH
PHTIKSEPNFCFAREFKSVPDDFRIGGGDLQMGNNSKRLTCVIDTNRVDMAGILPDNMSFRGLPENKSLLVSAQIEVIPCKVCGDK
SSGVHYGVITCEGCKGFFRRSQSSIVNYQCPRQKNCVVDRVNRNRCQYCRLKKCIELGMSRDAVKFGRMSKKQREKVEDEVR
MHKELAANGLGYQAIYGDYSPPPSHPSYCFDQSMYGHYPSGTSTPVNGYSIAVAATPTTPMPQNMYGATPSSTNGTQYVAHQA
TGGSFPSPQVPEEDVATRVIRAFNQQHSSYTTQHGVCNVDPDCIPHLSRAGGWELFARELNPLIQAIIEFAKSIDGFMNLPQETQI
QLLKGSVFELSLVFAAMYYNVDAQAVCGERYSVPFACLIAEDDAEMQLIVEVNNTLQEIVHLQPHQSELALLAAGLILEQVSSSHGI
GILDTATIATAETLKNALYQSVMPRIGCMEDTIHRIQDVETRIRQTARLHQEALQNFRMSDPTSSEKLPALYKELFTADRP

>Eip75B RAR-like [*Drosophila melanogaster*]

MEAVQAAAAATSSGGSSGSVPGSGSGSASKLIKTEPIDFEMLHLEENERQQDIEREPSSSNSNSNSNSLTPQRYTHVQVQTVPP
RQPTGLTTPGGTQKVILTPRVEYVQQRATSSTGGGMKHVYSQQQGTAASRSAPPETTALLTTTSGTPQIIITRTLPSNQHLSRRH
SASPSALHHYQQQQPQRQQSPPPLHHQQQQQQQHVRVIRDGRLYDEATVVVAARRHSVSPPPLHHHSRSAPVSPVIARRGGA
AAYMDQQYQQRQTPPLAPPPPPPPPPPPPPPQQQQQQYISTGVPPPTAAARKFVVSTSTRHVNVIASNHFQQQQQQHQAQQ
HQQQHQQHQQHQQHVIASVSSSSSSSAIGSGGSSSSHIFRTPVVSSSSSSNMHHQQQQQQQQSSLGNSVMRPPPPPPPPKVK
HASSSSSGNSSSSNTNNSSSSSNGEEPSSSIPDLEFDGTTVLCRVCGDKASGFHYGVHSCEGCKGFFRRSIQQKIQYRPCTKNQ
QCSILRINRNRCQYCRLKKCIAVGMSRDAVRFGRVPKREKARILAAMQQSTQNRGQQRALATELDDQPRLLAAVLRAHLETCEF
TKEKVSAMRQRARDCPSYSMPTLLACPLNPAPELQSEQEFSQRFAHVIRGVIDFAGMIPGFQLLTQDDKFTLLKAGLFDALFVRLI

CMFDSSINSIICLNGQVMRRDAIQNGANARFLVDSTFNFAERMNSMNLTDAEIGLFCAIVLITPDRPGLRNLELIEKMYSRLKGCLQ
YIVAQNRPDQPEFLAKLLETMPDLRTLSTLHTEKLVVFRTEHKELLRQQMWSMEDGNNSDGQQNKSPSGSWADAMDVEAAKSP
LGSVSSTESADLDYGSPSSSQPQGVSLPSPPQQQPSALASSAPLLAATLSGGCPLRNRANSGSSGDSGAAEMDIVGSHAHLTQ
NGLTITPIVRHQQQQQQQQQIGILNNAHSRNLNGGHAMCQQQQQHPQLHHHLTAGAARYRKLDSPTDSGIESGNEKNECKAVS
SGGSSSCSSPRSSVDDALDCSDAAANHNQVVQHPQLSVVSVSPVRSPQPSTSSHLKRQIVEDMPVLKRVLQAPPLYDTNSLMD
EAYKPHKKFRALRHREFETAEADASSSTSGSNSLSAGSPRQSPVPNSVATPPPSAASAAAGNPAQSQLHMHLTRSSPKASMAS
SHSVLAKSLMAEPRMTPEQMKRSDIIQNYLKRENSTAASSTTNGVGNRSPSSSSTPPPSAVQNQQRWGSSSVITTTCQQRQQS
VSPHSNGSSSSSSSSSSSSSSSSSTSSNCSSSSASSCQYFQSPHSTSNGTSAPASSSSGSNSATPLLELQVDIADSAQPLNLSK
KSPTPPPSKLHALVAAANAVQRYPTLSADVTVTASNGGPPSAAASPAPSSSPPASVGSPNPGLSAAVHKVMLEA

>RXRa [*Homo sapiens*]

MDTKHFLPLDFSTQVNSSLTSPTGRGSMAAPSLHPSLGPGIGSPGQLHSPISTLSSPINGMGPPFSVISSPMGPHSMSVPTTPTL
GFSTGSPQLSSPMNPVSSSEDIKPPLGLNGVLKVPAHPSGNMASFTKHICAICGDRSSGKHYGVYSCEGCKGFFKRTVRKDLTY
TCRDNKDCLIDKRQRNRCQYCRYQKCLAMGMKREAVQEERQRGKDRNENEVESTSSANEDMPVERILEAELAVEPKTETYVEA
NMGLNPSSPNDPVTNICQAADKQLFTLVEWAKRIPHFSELPLDDQVILLRAGWNELLIASFSHRSIAVKDGILLATGLHVHRNSAHS
AGVGAIFDRVLTELVSKMRDMQMDKTELGCLRAIVLFNPDSKGLSNPAEVEALREKVYASLEAYCKHKYPEQPGRFAKLLLRLPA
LRSIGLKCLEHLFFFKLIGDTPIDTFLMEMLEAPHQMT

>RARa [*Homo sapiens*]

MASNSSSCPTPGGGHLNGYPVPPYAFFFPPMLGGLSPPGALTTLQHQLPVSGYSTPSPATIETQSSSSEEIVPSPPSPPPLPRIY
KPCFVCQDKSSGYHYGVSACEGCKGFFRRSIQKNMVYTCHRDKNCIINKVTRNRCQYCRLQKCFEVGMSKESVRNDRNKKKKE
VPKPECSESYTLTPEVGELIEKVRKAHQETFPALCQLGKYTTNNSSEQRVSLDIDLWDKFSELSTKCIIKTVEFAKQLPGFTTLTIAD
QITLLKAACLDILILRICTRYTPEQDTMTFSDGLTLNRTQMHNAGFGPLTDLVFAFANQLLPLEMDDAETGLLSAICLICGDRQDLEQ
PDRVDMLQEPLLEALKVYVRKRRPSRPHMFPKMLMKITDLRSISAKGAERVITLKMEIPGSMPPLIQEMLENSEGLDTLSGQPGG
GGRDGGGLAPPPGSCSPSLSPSSNRSSPATHSP

>RARg [*Homo sapiens*]

MATNKERLFAAGALGPGSGYPGAGFPFAFPGALRGSPPFEMLSPSFRGLGQPDLPKEMASLSVETQSTSSEEMVPSSPSPPPP
PRVYKPCFVCNDKSSGYHYGVSSCEGCKGFFRRSIQKNMVYTCHRDKNCIINKVTRNRCQYCRLQKCFEVGMSKEAVRNDRNK
KKKEVKEEGSPDSYELSPQLEELITKVSKAHQETFPSLCQLGKYTTNSSADHRVQLDLGLWDKFSELATKCIIKIVEFAKRLPGFTG
LSIADQITLLKAACLDILMLRICTRYTPEQDTMTFSDGLTLNRTQMHNAGFGPLTDLVFAFAGQLLPLEMDDTETGLLSAICLICGDR
MDLEEPEKVDKLQEPLLEALRLYARRRRPSQPYMFPRMLMKITDLRGISTKGAERAITLKMEIPGPMPPLIREMLENPEMFEDDSS
QPGPHPNASSEDEVPGGQGKGGLKSPA

> RXR [*Xenopus laevis*]

MVGSAMTSSVNSPLGSIGSPFPVINCSVGSPGIPGTPSIGYGPVSSPQINSTVNLSGLHSVSSSEDVKPPLGMRSMPSHPNGGA
VSGKRLCAICGDRSSGKHYGVYSCEGCKGFFKRTIRKDLTYTCRDSKDCIVDKRQRNRCQYCRYQKCLATGMKREAVQEERQR
GKERDGEAELSGAINEEMPVEKILEAELAVEQKSDQSLEGGGSPSDPVTNICQAADKQLFTLVEWAKRIPHFSELALDDQVILLRA
GWNELLIASFSHRSISVKDGILLATGLHVHRNSAHSAGVGAIFDRVLTELVSKMRDMRMDKTELGCLRAIILFNPDAKGLSNPGDV
EVLREKVYASLESYCKQKYPDQQGRFAKLLLRLPALRSIGLKCLEHLFFFKLIGDTPIDTFLMEMLEAPHQLS

>RARa [*Mus musculus*]

MASNSSSCPTPGGGHLNGYPVPPYAFFFPPMLGGLSPPGALTSLQHQLPVSGYSTPSPATIETQSSSSEEIVPSPPSPPPLPRIY
KPCFVCQDKSSGYHYGVSACEGCKGFFRRSIQKNMVYTCHRDKNCIINKVTRNRCQYCRLQKCFDVGMSKESVRNDRNKKKKE
APKPECSESYTLTPEVGELIEKVRKAHQETFPALCQLGKYTTNNSSEQRVSLDIDLWDKFSELSTKCIIKTVEFAKQLPGFTTLTIAD
QITLLKAACLDILILRICTRYTPEQDTMTFSDGLTLNRTQMHNAGFGPLTDLVFAFANQLLPLEMDDAETGLLSAICLICGDRQDLEQ
PDKVDMLQEPLLEALKVYVRKRRPSRPHMFPKMLMKITDLRSISAKGAERVITLKMEIPGSMPPLIQEMLENSEGLDTLSGQSGG
GTRDGGGLAPPPGSCSPSLSPSSHRSSPATQSP

>RXRg [*Mus musculus*]

MYGNYSHFMKFPTGFGGSPGHTGSTSMSPSVALPTGKPMDSHPSYTDTPVSAPRTLSAVGTPLNALGSPYRVITSAMGPPSGA
LAAPPGINLVAPPSSQLNVVNSVSSSEDIKPLPGLPGIGNMNYPSTSPGSLVKHICAICGDRSSGKHYGVYSCEGCKGFFKRTIRK
DLIYTCRDNKDCLIDKRQRNRCQYCRYQKCLVMGMKREAVQEERQRSRERAESEAECASSSHEDMPVERILEAELAVEPKTES
YGDMNVENSTNDPVTNICHAADKQLFTLVEWAKRIPHFSDLTLEDQVILLRAGWNELLIASFSHRSVSVQDGILLATGLHVHRSSA
HSAGVGSIFDRVLTELVSKMKDMQMDKSELGCLRAIVLFNPDAKGLSNPSEVETLREKVYATLEAYTKQKYPEQPGRFAKLLLRL
PALRSIGLKCLEHLFFFKLIGDTPIDSFLMEMLETPLQIT

>E 1-like NR [*Acropora millepora*]

MDSDYRIQAVDRKPIILCRVCGDRSSGKHYGVFTCDGCRGFFKRSIRRNLTYQCKERGNCTVDVTRRNQCQACRLKKCFAVKM
NKDAVQHERAPRSSQVVPVVPACSMLSGMYDQPPGQASEQQLVYHKSDSSAEAKRQCSPDSEADHTTPENHKRCFSPPASLS
QYHGQNNNQSPESSKKRSFLSIESLIETKNDVRQASVGNAHPSQNHVKDDNTDGPSAVYPHSPETLYESAVHLLYMSVTWARNI
PTFLDLPFRDQAILLEEGWSELFVLSAAQFSLPVEMGPLLSAAGLQVDKAPTDKIVAGMADIRLLQNIIARFRRVQIDSTEYACLKAI
VLFKPDLRGLRAPHMVERLQDQAQGMLGEYCRSKNPEQQVRFGKLLLMLPSLRSVSPKTIEDLFFRGALDNVPIERMLCDMFKS
S

>E 1-like NR [*Stylophora pistillata*]

MADADVLGARRGKSAKQTVLCKVCGDRASGKHYGVLTCDGCRGFFKRSIRRDLAYQCKENNSCPIDVARRNQCQACRLKKCF
EVRMNRDAVQHERAPRTNQFKQASNEEIRCKPLKRKHNSYEQENMDLPPGQIHVTPKKEKLLDSPVTPEPIFYRNSPPRYSMEH
KSLFLVGYSKAESPKDVPVAVSVPTATAMTPPHTPQHGQQVPYSIMYFSSPEMLHESAVRILFMTVKWVRNIPTFFDLPFRDQAIL
LEEGWSELFILSVAQWNLPVEIGTLLAAAGLNPERDNSDKSVCGTGEIKAMKNIVERFKAANIDQTEYACLKAILLFKPDIRGLRAP
GHVEQLQDQAQGMLGEYDRQTYPNQQVRFGRLLLILPGLRVLSAKCIEQMFFRGTLDNIPMERLLSDMFKSA

>Smp_174260 SmTHR-β [*Schistosoma mansoni*]

MKYKQLLSKHINLESSQHGNLVSLNHTTLDNDIQSVQLEYHTNSPLKPTESQTSYPPLPPPITHVTESLVFVTENKLKEDIRAFNIE
NTQTSTFQVNTASQLLSSPSRNSNITNKCQIKLSTLSNPPKIKKREPYIPSYMDPLAGPEPCVVCGDNATGFHYRAMTCEGCKGF
FRRSVQKKLIYTCKFQGRCSVSDKQNRNSCQKCRFDRCISGGMAKDLVLDEDKRLAKRRLIEANRARKRAEAIEASTAVYVTDPS
INIPNITNPNSVSKYHIIHNQPISTSNTISSTPVIMSTIPYHSTIHSNIHFTNQFALNSTTRSQFNCNPIQTRYLEVTNNDIHSFVNPKTP
DATYSPANEAKLIVQPIQTIDKLQPTTMPNNMCWNPICGAPYTQCFMNDASNHDNHNSKTPLSFKESINRIQLSSVSMQINKNPLF
PSEDGYCNLLSKYSNFNSQQSVYTKAVDNNRINHSNANNVQINTHYEPQQYSPVTPEKCQTLSCDQPAITDNLSFSYPKHVSIMD
SNDTVHNDCPWTTEDQNMVDSIVQAYSNMLNPSFKRKMDNGDVDKEPEKAFYSSTDSRITSLIEPMIASLVAFARLVPGFELLDA
NDQTRLLRGCCLDIITLRAAYLLSRIAVSLGIVDSNGHNKPQFTTSPLDSADIFVQNVPSHQHNVASVIPNNIYPQLGTSDVKCAQM
IRAVALKLARLEIDQTEVALMTSILLMSPDRFGLTDCETVEHTQDILLETFNRYANRIRKIRFNRMNHNNMSSRSININGISQQQQQY
WPRILMALTELRSITLCNQGLFVEKAYGNTTEQLPWYFHELFTGDFILQETNISSFESGNNNDNNNLC

>Smp_134490 SmTHR-α like NR [*Schistosoma mansoni*]

MNLPITTNLTNIWSSVTTTNLSQLPVQQQQQQQQHQQTTDMQQPFIGNYNNSNPPVTELVNLISTPSSSSSLSASSSSSSSSSSS
SSSSSSSSGRRINDSQSYWNGITLLRETIPSYYSNSIGSSILCPIINPSIVSQSSINNCTMNYSNVPNSLHGSSSSSSSSGNVSSTT
GNGTTKVPRQRKKDPYIPSYMDPANGPEPCVVCGDNATGFHYRAMTCEGCKGFFRRSVQKKLVYTCKYNGRCSVSDKQNRNS
CQKCRFDRCIKGGMAKDLVLDEEKRLAKRRLIEANRARKRAESDNAIQQSQINSGPSPPKQTSYLPPTPSSISSAVSPLHRSPLM
SQQNVISAQIRQSQIKPPMVTTNQSRSVLHNYPSIAQTGVMNFTNLSPTDGNSTQLHISTNLSPTIQSSTNNLDQHNSTSIQPTIYD
PNCAMLPLLQTSPTRNNLIYSDGNSPINQHSHYVSTNHHQPHHHQHHQHHHQQHPTGHPLQVPTTDLMPNNTLHSSSLVNISSS
IPLDESNQLYWSNNSTIENTFHHHHPLTTIHSGINPIHQHHQLPLQQHQNNFIQPIVTDQSWNNEQFTQSIIDTGNNISQYCPVSLIN
DTLSYDQHQRNQHPHHHHQHHHHDHHHHQQQQQQQQQQQQPSSMSHQTHDVNLVMKQTNPMNIFHFDPLIKNDDVSGMKI
AKLDERKFTMPITSINTPSTINSFSNTDYSSSLSSSSSSSSCSLSSSSSLSLSSSSSSVTLTKNTEDQLQLNSKNDDTLNVTDELFV
WTVDDQNLINSICNAYESTYFDKDSPNNKTIQNQLSGTNNKDVTQSGDNSQQNSGEFVIKSIVDSHLDEVEQEDIQHARTFYMTT
FHDLAYLIEPAITRLVKFAKQIQGFDTLEADDQIRLLCGCCIDLITLRAYCLSKSAKIQGLVDHSLLIRGPITTATTPPTTTSTSRPSNN
QSNLTHQYNTITPPYIPNNQYPKLGISDEKCAQLIRGVALKMARLNIDQTDVAMMAAILLMSPDRSDLLDVESIENNQNNLLETFNR
YVNRTRGQIKQSGLYPVSSSQCWPRIIMTLTELRSVTMCAQDLFSQTYGMSDNNNNNNQLPWYLHELFLADEKINTME

>THR-α like EgrG [*Echinococcus granulosus*]

MKAKIEPDEVLEEGLKTSLPSSSSSTSVSNTSSSSSGVTIPAPADSNVYTQFNYLYPVTTASSSSADNNDSGAPSSSSFIGLPYWS
MPSASAASTIPGNGGGLDIPRYEQYPASGYYQQPTDASRSPYTPMIIPQQLNPGYYGQTTSMPLPPQQPRPQTSQMHLTPKYP
QPQAKSSVKRRVHDTIATSSANPTPTRQRKKEPYIPSYMDTTNGPEPCVVCGDNATGFHYRAMTCEGCKGFFRRSVQKKLEYT
CKFNGNCSVGDKQNRNSCQKCRFDRCIKGGMAMDLVLDEDKRLAKRRLIEANRARKQAEAAMAAPQQPPPPQPLPQPRQTLIP
STFSPTTSYLPHKPETINPSDFLSSSPSSSSANSSLYWNSAGVSHNLPHQQYPSSSSTSMVQYQQSQQQPQPDANFHILEQVSQ
LMPSKEAAIMAAIAAAAASASTSASPQKCDTPTNTITTTTTITRPSTSSEAKVRNTSAATSATSMASVAPATAVAAAASSSDEVPQP
APGLESSAAIVTPSVSAAASAAVSMGSASYNGIAKALTEAYKSMSITAVKIGDAMKKISENNDADQSEKMNTLLEVVSNVIKSRILD
VLSFAKFVPGFLLLSVRDQTRLLQSSLLDILTLRAVEALSRKMARSTINREEDDSESDNQSVTTSKAYAFIARSADGNSKAIRDLAR
KVLLWKLDVTELALVANRSDVSDPGAVVAIETLLTNVLVSHVMKGNMDGVKLRRLFSMFSEIHSITIRNKEEFVEHLHDEVDTNEH
KYLSEILLAGSEDEESVMVKSEEVASTSTSNNQQLGAPLSYLRVVPAIPKAYSVLPKRILSKCYIFSSLHGNGEGLQM

>THR-β [*Fasciola hepatica*]

MKFQLLNKRAVFHEYNQTEDNNTSWNPISIIPLEPTSSSSYSFGRANLTGHTANTDQSDLHFKPPILSVPTPLERRSLEPISDRQD
YGGLPALSAPCLTLPSGVSEQMVLSVQGTSSSSSAPTTPSKAVCLGNPPIRPRKKEPYIPSYMDPTSGPEPCVVCGDNATGFHY
RAMTCEGCKGFFRRSIQKKLVYTCKFQGRCSVSDKQNRNSCQKCRFDRCIRGGMAKDLVLDEDKRLAKRRLIEANRARKRAEV
DAISPTSSGNVIQSSLNSAPTMFANPTYMTSQLTELQTTPHGPGHSIPMVHSLVETLGPHLYAVEQSGQPVPQPTIEVPRTVYWS
RMVAPNSMQQVQSTGFTAAVSAPSSMAASQYPPILQPYGAHSFEPIVGKEDTDVSFLMIPQSTPSVETKRVCFNLKPQSPPPPV
SVTPSISGAADSSSRLMVLSVPSEQTSSSQLIQPMSAPSGSRVDPISHEQSLKPVSRVQPPSTECAWTKDDEAMVDSIRQAYRE
MLVPCDKSMIHADNDDAGSAFRSIPPSTNISTLIEPIIARLVAFAKLIPGFGLLGADDQTRLLRGCCLDVITLRAAYVLSLSARQKGLV
ESSSLAGNESNANHANGTLVIANSTYPQLGVSDAKCAQMIRAVALKLARLEIDQTEVALMAAILLMSPDRGQLVDVDTVEHTQDLL
LETFNRYANWSRKHSGAQLTRSHSICTRPTPSSFQSQYWPRIFMALTELRSITLCNQGLFVERAFNATCDQLPWYFHELFHGSQ
LSVGADIESANDRTDGPSACLK

>THR-α [*Fasciolopsis buski*]

MKFQLLNKRAVFHGSKQTEDNNNSSPNDAPWNPTFDLASTSGRISLPGHVVDVEQSVPLSDQDLRPPTLSTPTPLERRSSEPIP
HRPIYNNLPIMSTSFLAPHNTVSEQTSVQRTSSCSSYTPTTPIKSVSSGNQPIRPRKKEPYIPSYMDPASGPEPCVVCGDSATGFH
YRAMTCEGCKGFFRRSIQKKLVYTCKFQDRCSVSDKQNRNSCQKCRFDRCIRGGMAKDLVLDEDKRLAKRRLIEANRARKRAE
AEATSSTPSMNNIHSSLTGAPTMFVSPTCMTPQLPELQTTPRDTDHSVTVAPPLVETIGQHLYATEQPWQSFTQSTFEAPNTIYW
SRMVAPHPIQQVQSTGFTAVVNTTTPPPYQPLLQPFAAHSFDPVTMKEDPNISILMIPQTAPVVEAKRVCFSLTPQNAQSPTGVA
NPIQSMSEPSGRLMLPPAPPEPVNSSQLTGPAPVPSRPPEPPVKHQAPIKPIARVQPPNVEYAWTKDDEKMVDSIRQAYREMLL
PSEKSKVHADIDDAGTAFRSIPSSSNISTLIEPIIARLVAFAKLVPGFGLLGADDQTRLLRGCCLDVITLRAAYVMSLDARQKGLIEST

SGSSNESSGNHGSVALGIPNSTYPQLGVSDAKCAQMIRAVALKLARLEIDQTEVALMAAILLMSPDRGQLVDVDTVEHTQDLLLE
TFNRYANWSRKHSNTQLTRSLSSCTRQTPSSVQTQYWPRIFMALTELRSITLCNQGLFVERAFSATCDQLPWYFHELFQGSQVS
LGVETESDVSIPINDRPGS

>THR-β ortholog [*Schistosoma japonicum*]

MKYKQMLSKHINHYSSQLDDCISVTCMTIDKNDAQSVQLECNTTLPLKSTGTQRFHTLATESLLTVTENNLKENIQTANTQYTQSS
AHQVLSPDTQLSPPSTSHNPHKCHTKINASHNPPKVKKREPYIPSYMDPLTGPEPCVVCGDNATGFHYRAMTCEGCKGFFRRSI
QKKLVYTCKFQGRCSVSDKQNRNSCQKCRFDRCISGGMAKDLVLDEDKRLAKRRLIEANRARKKAEAVAAATSVTDSLTTTPGII
NPDTTTNYHITNNQPISMSNTISTPVVMSSLPHHSTFHAYNSFTN
QFTVSSAPTGQLNYNLIKAYPLEVPNSSSHSIVSTSTSVIHLPENEPKSVVQSSQTTDKLQQPTVPNNICWHPVYGIPYAQCLANA
KTGNRNNTSSISISYEESMNRIQLLNVSNQITNYPSLSSEVDHCNLLSELKNLKNQQTTNAKTIDDNHISANTVNSNGKNNNHVHL
TTDYAPQQYSPITPEKCSTSSCDKQIKFTDNSLSVTYPKHINIMDSIETVYNDCPWTKEDQNMVDSIVQAYGNMLNPNFKLKTANE
DIDKDPEKAFYSSTDSKITSLIEPMIASLVAFARLVPEFELL
DANDQTRLLRGCCLDVITLRAAYLLSRIAMSLGIVEPNAYNKSQLASSSDSVDAFVQHMPSHQQENVTSNIPNNIYPQLGTSDTKC
AQMIRAVALKLARLEIDQTEVALMTAILLMSPDRPGLTDCETVEHTQDALLETFNRYANRIRKIRSNRTNHNNVTSSQQQYWPRIL
MALTELRSITLCNQGLFLEKAYGSANEQLPWYFRELFTGDFMIQQTDRLTFQYDSNSNSNNNYSY

>THR-β ortholog [*Schistosoma rodhaini*]

MKYKQLLSKHINLESSQHSNLVSLNHTTLDSDKQSVQLEYHTNSPLKPTESETSYPPLLAPIIRVTESLVFVTENKLKEDIRAFNIEN
TQTSTVQVNKASQLLSSPSRNSNITHKCQIKLSTLSNPPKIKKREPYIPSYMDPLAGPEPCVVCGDNATGFHYRAMTCEGCKGFF
RRSVQKKLIYTCKFQGRCSVSDKQNRNSCQKCRFDRCISGGMAKDLVLDEDKRLAKRRLIEANRARKRAEAIEASTAVYVTDPSI
NIPNITNPNSVSKYHIIHNQPISTSNTISSTPVIMSTIPYHSTIHSNIHFTNQFALNSTTRSQFNCNPIQTRYLEVTNNDIHSLVNPKTP
DATYSPANEAKLIVQPIQTIDKLQPTTMPNNMCWNPICGAPYTQCFMNDASNHDNQNSKIPLSYKESINRIQLSNVSMQINKNPLF
PSEDGYCNLLSKYSNFNSQQSVYTKAVDNNRINHSNVNNVQINTHYEPQQYSPVTPEKCQTSCDQPAITDNLSFSYPKHVSIMD
SNDTVHNDCPWTTEDQNMVDSIVQAYSNMLNPSFKRKMDNEDVDKEPEKAFYSSTDSRITSLIEPMIASLVAFARLVPGFELLDA
NDQTRLLRGCCLDIITLRAAYLLSRIAVSLGIVDSNGHNKPQFTTSPLDSADIFVQNVPSHQHNVASAIPNNIYPQLGTSDVKCAQM
IRAVALKLARLEIDQTEVALMTSILLMSPDRFGLTDCETVEHTQDILLETFNRYANRIRKIRFNRMNHNNMSSRSININGISQQQQQ
QYWPRILMALTELRSITLCNQGLFVEKAYGNTTEQLPWYFHELFTGDFILQETNISSFEGGNNNDNNNLC

>THR-α [*Mus musculus*]

MEQKPSKVECGSDPEENSARSPDGKRKRKNGQCPLKSSMSGYIPSYLDKDEQCVVCGDKATGYHYRCITCEGCKGFFRRTIQK
NLHPTYSCKYDSCCVIDKITRNQCQLCRFKKCIAVGMAMDLVLDDSKRVAKRKLIEQNRERRRKEEMIRSLQQRPEPTPEEWDLI
HVATEAHRSTNAQGSHWKQRRKFLPDDIGQSPIVSMPDGDKVDLEAFSEFTKIITPAITRVVDFAKKLPMFSELPCEDQIILLKGCC
MEIMSLRAAVRYDPESDTLTLSGEMAVKREQLKNGGLGVVSDAIF
ELGKSLSAFNLDDTEVALLQAVLLMSTDRSGLLCVDKIEKSQEAYLLAFEHYVNHRKHNIPHFWPKLLMKEREVQSSILYKGAAAE
GRPGGSLGVHPEGQQLLGMHVVQGPQVRQLEQQLGEAGSLRGPVLQHQSPKSPQQRLLELLHRSGILHSRAVCGEDDSSEAS
SLSSSSDTEDTEVCEDQAGKAASP

>THR-α-a [*Danio rerio*]

MENTEQEHNLPEGDETQWPNGVKRKRKNSQCSMNSTSDKSISVPGYVPSYLEKDEPCVVCGDKATGYHYRCITCEGCKGFFR
RTIQKNLHPSYSCKYDSCCIIDKITRNQCQLCRFRKCISVGMAMDLVLDDSKRVAKRRLIEENREKRKKEEIVKTLHNRPEPTVSE
WELIRMVTEAHRHTNAQGPHWKQKRKFLPEDIGQSPAPTSDNDKVDLEAFSEFTKIITPAITRVVDFAKKLPMFSELPCEDQIILLK
GCCMEIMSLRAAVRYDPESETLTLSGEMAVSREQLKNGGLGVVSDAIFDLGKSLSQFNLDDSEVALLQAVLLMSSDRSGLTCVE
KIEKCQEMYLLAFEHYINHRKHNISHFWPKLLMKVTNLRMIGACHASRFLHMKVECPTELFPPLFLEVFEDQEGSTGVAAQEDGS
CLR

>THR-β [*Danio rerio*]

MSEQADKCNSRWKDEAMQNGYIPSYLDKDELCVVCGDKATGYHYRCITCEGCKGFFRRTIQKNLNPTYACKYEGKCVIDKVTR
NQCQECRFKKCIAVGMATDLVLDDSKRLAKRKLIEENRERRRREELQKTVWDRPEPTQEEWEMIRVVTEAHMATNAQGNHWK
QKRKFLSAVGVKEAKPEDIGSAPIVNAPEGNKVDIEAFSQFTKIITPAITRVVDFAKKLPMFCELPCEDQIILLKGCCMEIMSLRAAV
RYDPESDTLTLNGEMAVTRGQLKNGGLGVVSDAIFDLGVSLSSFNLDDSEVALLQAVILLSSDRPGLTSVERIERCQEEFLLAFEH
YINYRKHKVAHFWPKLLMKVTDLRMIGACHASRFLHMKVECPTELFPPLFLEVFED

>THR-β [*Mus musculus*]

MTPNSMTENGLPAWDKQKPRPDRGQDWKLVGMSEACLHRKSHVERRGALKNEQTSPHLIQATWTSSIFHLDPDDVNDQSISSA
QTFQTEEKKCKGYIPSYLDKDELCVVCGDKATGYHYRCITCEGCKGFFRRTIQKSLHPSYSCKYEGKCIIDKVTRNQCQECRFKK
CIYVGMATDLVLDDSKRLAKRKLIEENREKRRREELQKSIGHKPEPTDEEWELIKTVTEAHVATNAQGSHWKQKRKFLPEDIGQA
PIVNAPEGGKVDLEAFSHFTKIITPAITRVVDFAKKLPMFCELPCEDQIILLKGCCMEIMSLRAAVRYDPDSETLTLNGEMAVTRGQ
LKNGGLGVVSDAIFDLGMSLSSFNLDDTEVALLQAVLLMSSDRPGLACVERIEKYQDSFLLAFEHYINYRKHHVTHFWPKLLMKVT
DLRMIGACHASRFLHMKVECPTELFPPLFLEVFED

>Nhr-2 [*Caenorhabditis elegans*]

MVPMNPELMHYPNQPHMMPGYPMINAYQQSYLQNPAQWTPEMLLCMQMQMQQMVPGTATNSTYMPPQSKNTVTPNATSPL
SQISDRDSGNDTISPPLTSQNSATTPNYHNQPQMQLTPLQQAKPEKEEISPYAINNILSSTQSSPDNGNEADDKENSSVRRNTFP
ASSASTKKPRGTPYDRTNTPMTVVPQMPQFAPDFSNYNLTMNAWSEFFKKDRCMVCGDNSTGYHYGVQSCEGCKGFFRRSV
HKNIAYVCTKGENCTFSYENCAANRGVRTRCQACRFAKCLAVGMNRDNVRVNKETDKDVKPSVASPNFEMTSQVKELTAAFVA

NMPCSTHLTSGTHAIGAIKKFIESVPALSSLLPKDEKALEMSIQKVMSGILAIRAAFTFDPITFYSCENPVNLLRGGIRNTVFNDCEV
ALLSGIHILQIVNGGVAEIFTSYCQGLRHQLSQTHLQEIGLCDRLLMRLGPYLNQ

>THR-β [*Homo sapiens*]

MTPNSMTENGLTAWDKPKHCPDREHDWKLVGMSEACLHRKSHSERRSTLKNEQSSPHLIQTTWTSSIFHLDHDDVNDQSVSSA
QTFQTEEKKCKGYIPSYLDKDELCVVCGDKATGYHYRCITCEGCKGFFRRTIQKNLHPSYSCKYEGKCVIDKVTRNQCQECRFK
KCIYVGMATDLVLDDSKRLAKRKLIEENREKRRREELQKSIGHKPEPTDEEWELIKTVTEAHVATNAQGSHWKQKRKFLPEDIGQ
APIVNAPEGGKVDLEAFSHFTKIITPAITRVVDFAKKLPMFCELPCEDQIILLKGCCMEIMSLRAAVRYDPESETLTLNGEMAVTRG
QLKNGGLGVVSDAIFDLGMSLSSFNLDDTEVALLQAVLLMSSDRPGLACVERIEKYQDSFLLAFEHYINYRKHHVTHFWPKLLMK
VTDLRMIGACHASRFLHMKVECPTELFPPLFLEVFED

Supplemental Table S2. Sequencing results of A.s. Cas12a-mediated SmUbi-eGFP-SmUbi integration into GSH1 of sporocysts from transplantation experiments

1. 3´-integration side sequence (5´- 3´): CATGGACGAGCTGTACAAGTGAGAGGTTAACTTTAATTTTGTTCATTTAACTTAATAAACGTTTA ATTTAACTTATTAAAATGTTTTCTTCCTAATTTGTAGCGTATCTTAGTGTAACTGTGCTTCCTATT AGATTGAAATTCTATCGTAATCTGCAATTAGGCTCATGGGGATATGTTATGCCAATTTTCCGAAA ATTGTTAGCACTTAGGTTTCGGTGTTTTTTTACTAGGATGTCATGTTTTATTCATATTTGCGTCCT TGCTCTTGTGTGTGGTATGCGTCGCTATGTGGAACTCGTAA **Sequencing primer: GSH1primer rev (5´-3):** GTG TAT TTC CTA TGC TAT GAA AAT ACC T
2. 3´-integration side sequence (5´- 3´): CATGGACGAGCTGTACAAGTGAGAGGTTAACTTTAATTTTGTTCATTTAACTTAATAAACGTTTA ATTTAACTTATTAAAATGTTTTCTTCCTAATTTGTAGCGTATCTTAGTGTAACTGTGCTTCCTATT AGATTGAAATTCTATCGTAATCTGCAATTAGGCTCATGGGGATATGTTATGCCAATTTTCCGAAA ATTGTTAGCACTTAGGTTTCGGTGTTTTTTTACTAGGATGTCATGTTTTATTCATATTTGCGTCCT TGCTCTTGTGTGTGGTATGCGTCGCTA **Sequencing primer: GSH1 primer rev (5´-3):** GTG TAT TTC CTA TGC TAT GAA AAT ACC T

Supplemental Table S3. Sequencing results of A.s. Cas12a-mediated SmUbi-eGFP-SmUbi integration into GSH1 of adult worms from transplantation experiments

1. 3´-integration side sequence (5´- 3´):

AACGTTTAATTTAACTTATTAAAATGTTTTCTTCCTAATTTGTAGCGTATCTTAGTGTAACTGTGC
TTCCTATTAGATTGAAATTCTATCGTAATCTGCAATTAKGCTCATGGGGATATGTTATGCCAATT
TTCCGAAAATTGTTAGCACTTAGGTTTCGGTGTTTTTTTACTAGGATGTCATGTTTTATTCATATT
TGCGTCCTTGCTCTTGTGTGTGGTATGCGTCGCTATGGTCTCAGCTTTGGGCTGCATTGTTAAG
TTTAAGGAAACTGCATAGTATGGAACCAAGGCAGTGGTCACAGAGTAGTATAAYAARATTYTCC
TTCAGGCTGCCCACCAGCACAAARAATGACATAATCGATAGKTACRTCCCCTCMGYTGGAGGG
TTTGACCTACGACAGCATGATYTAATATATTTTCRAGAAAAGYCTAWGATGAAATCGAMCGAAT
GATGTTAAATCMWACAGGAAAACATTGTTTCGAAGGGGAGAATAAWAGGAGGGGCTTTWCTM
TKAAGGTCCATTAAAGATTTCCTGGATATGCACCACTGCATGTGGCTAATATTTTRTCTCCTGC
GACCCTCAATMARGAGTCTCAATACKGCTAACCCAWAAGTCTATAATWTCAGYACTAATAGCA
TATCTTGMTCTGACTTCCAACATCATTCTTATCRTTCTACTTGCAAGTCRCCCAACATAWAGGC
GCTGKATGRRTAGATCCTTACATMSCCCAACCACCTGTGATGTTTACAAATTCATTCKKCCTAAT
ACCATCTGTATGTAGGACTTTTCTTAACATCATTGT

Sequencing primer: eGFP-Ubi-Ter fw (5´-3):

CAT GGA CGA GCT GTA CAA GTG AGA GGT TAAC

2. 3´-integration side sequence (5´- 3´):

YCTAAATGTTTTCTTCCTAATTTGTAGCGTATCTTAGTGTAACTGTGCTTCCTATTAGATTGAAAT
TCTATCGTAATCTGCAATTAGGCTCATGGGGATATGTTATGCCAATTTTCCGAAAATTGTTAGCA
CTTAGGTTTCGGTGTTTTTTTACTAGGATGTCATGTTTTATTCATATTTGCGTCCTTGCTCTTGTG
TGTGGTATGCGTCGCTATGTGGAACTCGGTAGATGAAGGCTGGTTCAATAGCTGGAATTGGGA
TGGTGTGCCACAAGTGTTTAAGGAAACTGCATAGTATGGAACCAGCCTTCATCTACCGAGTTCC
ACATAGCGACGCATACCACACACAAGAGCAAGGACGCAAATATGAATAAAACATGACATCCTA
GTAAAAAAACACCGAAACCTAAGTGCTAACAATTTTCGGAAAATTGGCATAACATATCCCCATG
AGCCTAATTGCAGATTACGATAGAATTTCAATCTAATAGGAAGCACAGTTACACTAAGATACGC
TACAAATTAGGAAGAAAACATTTTAATAAGTTAAATTAAACGTTTATTAAGTTAAATGAACAAAAT
TAAAGTTAACCTCTCACTTGTACAGCTC

Sequencing primer: GSH1 primer rev (5´-3):

GTG TAT TTC CTA TGC TAT GAA AAT ACC T

3. 3´-integration side sequence (5´- 3´):

ARCGKATCTTAGTGTAACTGTGCTTCCTATTAGATTGAAATTCTATCSTAATCTGCAATTAKGCT
CATGGGGATATGTTATGCCAATTTTCCGAAAATTGTTAGCACTTAGGTTTCGGTGTTTTTTTACT
AGGATGTCATGTTTTATTCATATTTGCGTCCTTGCTCTTGTGTGTGGWATGCGTCGCTATGGTC
TCASCTTTGGGCTGCATTGTTAAGTTTAAGGAAACTGCATAGTATGGAACCAGAG

Sequencing primer: eGFP-Ubi-Ter fw (5´-3): CAT GGA CGA GCT GTA CAA GTG AGA GGT TAAC
1. 5´-integration side sequence (5´- 3´): TTGAGATAAGTGAAATCAATCGGAGACAATCTGGAAAGGTCAGATAATTGATCTCGAGGTATTT TCATAGCATAGGAAATACACAATCCG **Sequencing primer: Ubi-Prom HA left rev (5´-3´):** ATT GAG GAC CGT TCA GAT CGT GTC
2. 5´-integration side sequence (5´- 3´): GCGTATCTTAKTGTAACTGTGCTTCCTATTAGATWGAAATTCTATCSKAATCTGCAATTAKGCTC ATGGGGATATGTTATGCCAATTTTCCKAAAATTGTTASCACTTAGGTTTCGGTGTTTTTTTACTA GGATGTCATGTTTTATTCATATTTGCGTCCTTGCTCYTGTGTGTGGWATGCGTCGCTATGTGR **Sequencing primer: Ubi-Prom HA left rev (5´-3´):** ATT GAG GAC CGT TCA GAT CGT GTC
3. 5´-integration side sequence (5´- 3´): CTTATCTCAATCACCACCAGATTGTGTCTTCTCACTTGGACACGATCTGAACGGTCCTCAATAA TG **Sequencing primer: GSH1 primer fw (5´-3´):** GTG TAT TTC CTA TGC TAT GAA AAT ACC T

Supplemental Table S4. Sequence information of the potential SmUbi minimal promoter/terminator-driven dsRed reporter-gene construct

Sequence of the Smp_335990 (SmUbi) minimal promoter 5´- 3´
TCAGAGACAAACTAGTGAGACATTTTCAAGGTCTTCACAATTGTTTTCTGTTGATTTAGATGTGA AAAATCATTCATATGATGCACTTGGAGATGTTTAAGTTCCGATCTAACGAAGCATATCTCCAACA GTTAACTGCTCTAATAAATTGATGACTTCACGTGAACTAAAACCCATAAAGATAAAATGGCAAAC TTTATTTTACATTATTACCTAAACTTTTGTCATCTTGAAACTCGAAAAATGTGGCACTTGAATGAG AAGTTGCTGACTAACAAAAACGTTTCATAATGAATTAGGAGGTTCAGACTGTAACAAGTTATTTT CTGAAAGTAAATGTGACTAGAATGTGGTTTGAGTAAGTAACAATCACCTCGACGAATACCTTGT TTTACTGCCCTGAATTGAAGGTAGCGCTAAATAAACGTAGTATAGACTATATATAGCCAGCAAA ATCGAAAGGCTGCCATACTTGTTCGTTAGTGTAAACGATAGACCTTACG
Sequence of the dsRed reporter-gene 5´- 3´
ATGGCCTCCTCCGAGGACGTCATCAAGGAGTTCATGCGCTTCAAGGTGCGCATGGAGGGCTC CGTGAACGGCCACGAGTTCGAGATCGAGGGCGAGGGCGAGGGCCGCCCCTACGAGGGCACC CAGACCGCCAAGCTGAAGGTGACCAAGGGCGGCCCCCTGCCCTTCGCCTGGGACATCCTGTC

CCCCCAGTTCCAGTACGGCTCCAAGGTGTACGTGAAGCACCCCGCCGACATCCCCGACTACA
AGAAGCTGTCCTTCCCCGAGGGCTTCAAGTGGGAGCGCGTGATGAACTTCGAGGACGGCGGC
GTGGTGACCGTGACCCAGGACTCCTCCCTGCAGGACGGCTCCTTCATCTACAAGGTGAAGTTC
ATCGGCGTGAACTTCCCCTCCGACGGCCCCGTAATGCAGAAGAAGACTATGGGCTGGGAGGC
CTCCACCGAGCGCCTGTACCCCCGCGACGGCGTGCTGAAGGGCGAGATCCACAAGGCCCTG
AAGCTGAAGGACGGCGGCCACTACCTGGTGGAGTTCAAGTCCATCTACATGGCCAAGAAGCC
CGTGCAGCTGCCCGGCTACTACTACGTGGACTCCAAGCTGGACATCACCTCCCACAACGAGG
ACTACACCATCGTGGAGCAGTACGAGCGCGCCGAGGGCCGCCACCACCTGTTCCTGTAG

Sequence of the Smp_335990 (SmUbi) minimal terminator 5´- 3´

TGAGAGGTTAACTTTAATTTTGTTCATTTAACTTAATAAACGTTTAATTTAACTTATTAAAATGTTT
TCTTCCTAATTTGTAGCGTATCTTAGTGTAACTGTGCTTCCTATTAGATTGAAATTCTATCGTAAT
CTGCAATTAGGCTCATGGGGATATGTTATGCCAATTTTCCGAAAATTGTTAGCACTTAGGTTTC
GGTGTTTTTTTACTAGGATGTCATGTTTTATTCATATT

Plasmid map

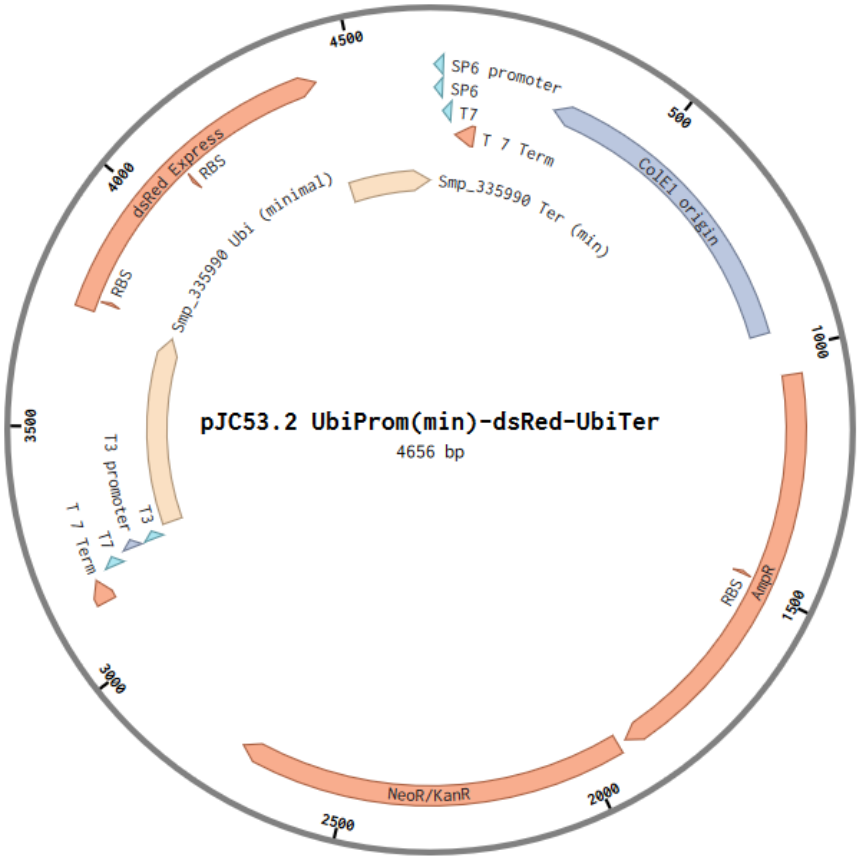

8 Contributions

8.1 Publications and published abstracts

Publications

Moescheid MF, Lu Z, Diaz Soria C, Quack T, Holroyd N, Holzaepfel P, Puckelwaldt O, Haeberlein S, Rinaldi G, Berriman M, Grevelding CG. The retinoic acid family-like nuclear receptor SmRAR identified by single-cell transcriptomics of ovarian cells controls oocyte differentiation in *Schistosoma mansoni. Nucleic Acids Res.* In revision. 2024.

Ittiprasert W, **Moescheid M**, Mann VH, Brindley PJ. Multiplexed CRISPR-Cas9 protocol for large transgene integration into the *Schistosoma mansoni* genome. *STAR Protoc*. 2024 Mar 15;5(1):102886. doi: 10.1016/j.xpro.2024.

Li X, Weth O, Haimann M, **Möscheid MF**, Huber TS, Grevelding CG. Rhodopsin orphan GPCR20 interacts with neuropeptides and directs growth, sexual differentiation, and egg production in female *Schistosoma mansoni*. *Microbiol Spectr.* 2024 Jan 11;12(1):e0219323. doi: 10.1128/spectrum.02193-23.

Papaiakovou M, Maclean K, Zwanenburg L, Ajakaye OG, Chakraborty S, Costain A, Souza COS, Cunningham K, Cobb SA, **Moescheid MF**, Mora J, Amaral MS. Hydra at 21, key to the door for helminth researchers. *Trends Parasitol*. 2023 Dec;39(12):973-981. doi: 10.1016/j.pt.2023.09.013.

Moescheid MF, Wisitphongpun P, Mann VH, Quack T, Grunau C, Grevelding CG, Ittiprasert W, Brindley PJ. Enhanced efficiency of RNA-guided Cas12a versus Cas9 transgene knock-in and activity at a *Schistosoma mansoni* genome safe harbor. *bioRxiv* 2023.09.12.557428; doi: https://doi.org/10.1101/2023.09.12.557428.

Ittiprasert W, **Moescheid MF**, Chaparro C, Mann VH, Quack T, Rodpai R, Miller A, Wisitpongpun P, Buakaew W, Mentink-Kane M, Schmid S, Popratiloff A, Grevelding CG, Grunau C, Brindley PJ. Targeted insertion and reporter transgene activity at a gene safe harbor of the human blood fluke, *Schistosoma mansoni. Cell Rep Methods.* 2023 Jul 24;3(7):100535. doi: 10.1016/j.crmeth.2023.100535.

Moescheid MF, Puckelwaldt O, Beutler M, Haeberlein S, Grevelding CG. Defining an optimal control for RNAi experiments with adult *Schistosoma mansoni. Sci Rep*. 2023 Jun 16;13(1):9766. doi: 10.1038/s41598-023-36826-6.

Abstracts

Sölter R, von Bülow V, Dreizler D, Stampa G, Quack T, Grevelding CG, **Möscheid M**, Tschuschner A, Müller H, Roderfeld M, Roeb E. *Schistosoma mansoni* eggs can be destroyed by Myeloperoxidase (MPO)-producing cells. *Z Gastroenterol.* 2023; 61(01): e7. doi: 10.1055/s-0042-1759910

8.2 Conferences

14th Hydra Conference. Parasitic Helminths: New Perspectives in Biology and Infection 2023, 1-6 September, Hydra, Greece.

Poster: **Max F. Möscheid**, Prapakorn Wistiphongpun, Wannaporn Ittiprasert, Thomas Quack, Victoria H. Mann, Christoph Grunau, Paul J. Brindley, Christoph G. Grevelding (2023). Chromosomal integration of a reporter-gene by RNA-guided Cas-enzymes into a genomic safe-harbor site of *Schistosoma mansoni.*
This poster was awarded with a price for the best poster of this international conference**.**

30th Annual meeting of the German Society for Parasitology 2023, 15-17 March 2023, Giessen, Germany.

Talk: **Max F. Möscheid**, Prapakorn Wistiphongpun, Wannaporn Ittiprasert, Thomas Quack, Victoria H. Mann, Paul J. Brindley, Christoph Grunau, Christoph G. Grevelding (2023). Chromosomal integration of a reporter-gene by RNA-guided Cas-enzymes into a genomic safe-harbor site of *Schistosoma mansoni*

15th Annual GGL Conference 2022, 29-30 September 2022, Giessen, Germany.

Poster: **Max F. Möscheid**, Prapakorn Wistiphongpun, Wannaporn Ittiprasert, Paul J. Brindley, Christoph Grunau, Christoph G. Grevelding (2022). Chromosomal integration of a reporter-gene by RNA-guided Cas-enzymes into a genomic safe-habor site of *Schistosoma mansoni.*

15th International Conference of Parasitology (ICOPA) 2022, 21-26 August 2022, Copenhagen, Denmark.

Talk: **Max F. Möscheid**, Thomas Quack, Christoph G. Grevelding (2022). Insights in the role of the pairing-dependently and ovary-preferentially expressed thyroid hormone receptor (TRB) of *Schistosoma mansoni.*

14th Annual GGL Conference 2021, 29-30 September 2021, Giessen, Germany.

Talk: **Möscheid, MF**, Quack, T, Grevelding, CG (2021). First insights in the role of the pairing-dependently and ovary-preferentially expressed thyroid hormone receptor (THRB) of *Schistosoma mansoni* in the development of vital eggs.

13th Annual GGL Conference 2020, 29-30 September 2020, Giessen, Germany.

Talk: **Möscheid, MF**, Quack, T, Grevelding, CG (2020). Role of ovary-preferentially expressed nuclear receptors in egg and larval development of *Schistosoma mansoni.*

9 Acknowledgments

The realization of this project would not have been possible without a good team, cooperation partners, and scientific exchange, both in discussion and in laboratory practice. I would like to thank everyone involved in the realization of this project.

Credits:

Justus Liebig University Giessen

Grevelding Lab

Prof. Dr. Christoph G. Grevelding
Dr. Thomas Quack
Dr. Xuesong Li
Sophie Welsch
Monique Überall
Theresa Huber
Pauline Holzäpfel
Dr. Mandy Beutler
Saranya Geetha, PhD
Benedikt Wiebach
Georgette Stovall
Christina Scheld
Bianca Kulik
Dr. Oliver Weth
Martin Haimann

Haeberlein Lab

PD. Dr. Simone Häberlein
Oliver Puckelwaldt
Svenja Gramberg
Tobias Schmitt
Sagar Ajmera
Rashmi Nakate
Dr. Hicham Houhou
Lennart Schulte

Falcone Lab

Dr. Pia Naujack

Roeb Lab

Dr. Martin Roderfeld

Cooperations:

George Washington University

Prof. Paul J. Brindley, PhD
Victoria H. Mann, PhD
Wannaporn Ittiprasert, PhD
Jom Wistiphongpun, PhD
Anastas Popratiloff, PhD

Université de Perpignan

Prof. Dr. Christoph Grunau
Anne Rognon

Wellcome Sanger Institute

Dr. Zhigang Lu

University of Aberystwyth

Prof. Matthew Berriman, PhD
Gabriel Rinaldi, PhD

10 Funding

This work was funded by the post-graduate scholarship of the JLU Giessen, through funding from the JLU Giessen, the Flatworm Functional Genomics Initiative (FUGI, Wellcome Trust), the TransMIT GmbH, the travel grand of the German society of parasitology (DFG). Experiments, which were carried out in the laboratory of Prof. Paul Brindley (GW University, Washington DC) during a scientific exchange, were funded by the US Defense Advanced Research Projects Agency (DARPA) and FUGI.

I would like to express my gratitude to the funding partners/organizations mentioned above for their support of this project.

11 Declaration

Selbstständigkeitserklärung

Ich (Max F. Möscheid) erkläre, dass die vorgelegte Dissertation selbständig und ohne unerlaubte fremde Hilfe und nur mit den in der Dissertation angegebenen Hilfsmitteln angefertigt worden ist. Alle Stellen, die veröffentlichten Schriften wörtlich oder sinngemäß entnommen sind, sowie alle Angaben, die auf mündlichen Auskünften beruhen, habe ich als solche kenntlich gemacht. Ich bin mit einer eventuellen Überprüfung meiner Dissertation durch eine Plagiatssoftware einverstanden. Bei den von mir durchgeführten und in der Dissertation erwähnten Untersuchungen habe ich die Grundsätze guter wissenschaftlicher Praxis beachtet, wie sie in der „Satzung der Justus-Liebig-Universität Gießen zur Sicherung guter wissenschaftlicher Praxis“ niedergelegt sind.

_____ _____

Datum **Unterschrift**